Cyclodextrin Nanomachines at Work

Roger James Coulston

October, 2009

A thesis submitted for the degree of Doctor of Philosophy of

The Australian National University

ANU
THE AUSTRALIAN NATIONAL UNIVERSITY

Research School of Chemistry
Canberra, Australia

Authors Statement

This is to declare that the work that is presented herein represents original work that I have carried out during my PhD candidature from February 2006 to October 2009, except for the following.

Presented in Chapter 2: Figure 2.1.3 was generated by Dr. Hideki Onagi.

Presented in Chapter 4: Ms. Jing Zhang assisted with the synthesis, characterisation and operation of the hermaphrodite **4.7**. Ms. Hwi-Young Lee provided technical assistance with the ITC binding experiments.

To the best of my knowledge, this thesis does not contain material that has been previously published or accepted for the award of any other degree or diploma in any university or other tertiary institution. Published or written work by another person has been acknowledged by citation throughout the text.

I give consent for a copy of my thesis to be deposited in the University library and be available for loan and photocopying.

Roger Coulston
October 2009

Acknowledgements

First and foremost, I would like to express my sincere gratitude to my supervisor, Prof. Chris Easton, for his support, guidance and time, all of which made this PhD project possible. I also thank him for providing me with the opportunity to gain such a valuable experience in research and in life.

I am very thankful to Dr Hideki Onagi for his support, technical assistance and general advice throughout this project, and in particular his supervision during the first six months. I would like to acknowledge Dr Allan Gamble for his technical advice and excellent support during the writeup. I also wish to thank Daniel Bartkus for his technical support and for being a good bloke.

I would also like to thank the people that helped make my time in the Easton group so enjoyable; Susan Riches, Dr Alex Buchan, Dr Amy Philbrook, Amy Zhang, Ashley Bartelson, Dr Candace Tsai, Dr Dan Stigers, Darshana Padmakshan, David Brittain, Georgina Statham, Dr Hye-Kyung Kim, Junming Ho, Dr Ken Robinson, Dr Lorna Barr, Dr Mary Gresser, Hwi-Young Lee, Dr Iris Li, Isaac Arthur, James Hennesy, Prof. Jeff Keillor, Kathryn Sedgewick, Kelly Morris, Lucy (Feihua) Cao, Dr Marta Cieslinski, Dr Ryan Dawson, Saara Bowen, Dr Satish Chand, Dr Subashni Maniam and Dr Zac Watts. Also, the good people of the Research School of Chemistry.

A very special thank you to all of my family: Mum, Dad, Ma and Ba for their guidance and support over the past three and a half years. Erica, Liam, Sarah, Jason, Zara, Darcy and Evy, thanks for being you guys.

And finally to my beautiful wife, Jing, I could not have done this without you and I cannot wait to spend the rest of my life with you.

Abstract

In this thesis, several types of cyclodextrin based artificial molecular machines have been developed where the output energy of molecular recognition is harnessed to do quantifiable mechanical work and constrain the geometry of an amide bond. The performance and unharnessed potential of their operation are determined using ^{1}H NMR spectroscopy and isothermal titration calorimetry. Importantly, this is one of the few demonstrations of synthetic nanomachines that perform quantifiable work at the molecular level.

In Chapter 1 the field of supramolecular chemistry is introduced and its importance towards the "bottom-up" development of molecular devices discussed. This Chapter also contains a brief summary of the relevant literature for the progression of molecular machines. Also introduced are the host-guest properties of cyclodextrins and their potential as the building blocks for molecular machines. Isothermal titration calorimetry is described and its use for measuring the thermodynamic parameters of host-guest binding interactions discussed.

The work in Chapter 2 describes the preparation of propionamido- and cinnamido-cyclodextrin based hermaphrodites with a tertiary amide group that serves as a "torsion bar" to harness the mechanical work output resulting from the intramolecular encapsulation of the aryl substituent by the cyclodextrin in aqueous solution. The displacement of the *trans*-cinnamido "piston" from the cyclodextrin "cylinder" using 1-adamantanol "fuel" alters the Z/E-amide isomer ratio from 1:100 to 1:2.6. Consequently, in this mode the machine is turned "ON" and the work harnessed by the amide bond is 2.1 kcal mol^{-1}. In contrast, the *cis*-cinnamido "piston" has little interaction with the CD "cylinder", so the machine is turned "OFF" and the work output is a negligible -0.2 kcal mol^{-1}. On this basis, the alkene moiety of the aryl "piston" serves as the molecular machine's photochemical "ON/OFF" switch.

In Chapter 3 the thermodynamic parameters for the operation of the propionamido- and cinnamido-cyclodextrins, developed in Chapter 2, are measured against the "fuel" using isothermal titration calorimetry. By determining the uncaptured work energy, as quantified with isothermal titration calorimetry, and comparing this to the work energy harnessed in the amide bond, based on ^{1}H NMR spectroscopy, the energy harnessing efficiency of the cinnamido molecular machines can be quantified as 30% and -3% in the "ON" and "OFF" states, respectively. It is demonstrated that these

artificial molecular machines are operating with the comparable efficiency of their macroscopic counterparts and have a maximum working potential of 6-8 kcal mol^{-1}.

Presented in Chapter 4 is the synthesis and conformational analysis of several cyclodextrin based hermaphrodites developed to investigate the effects of various substituents upon the work output and performance of the molecular machines studied in the preceding Chapters. These results show that a cyclodextrin is capable of harnessing 0.9 kcal mol^{-1} of work in a secondary amide bond, while the energy harnessed by an N,α-dimethylcinnamido cyclodextrin is 3.7 kcal mol^{-1} with its operation causing a greater than three hundred-fold change in the Z/E-amide isomer ratio in the absence and presence of 1-adamantanol "fuel".

The successful preparation of a horizontally opposed molecular pump that harnesses the strain energy of intermolecular complexation to bias the Z/E-amide isomer ratio is described in Chapter 5. A combined ^{1}H NMR spectroscopic and isothermal titration calorimetric strategy is used to measure the work output as 1.9 kcal mol^{-1} and a performance of 25% for a *trans*-stilbenylamido-α-cyclodextrin hermaphrodite that forms an intermolecular complex to favor the Z-amide isomer. The reversible *trans*- and *cis*-photoisomerisation of the stilbene "piston" sees a greater than forty-fold modulation in the stability of the intermolecular complex and again allows the work output to be switched "ON" and "OFF".

As an alternative to the photochemical systems studied in Chapters 2-5, the work described in Chapter 6 details the synthesis and conformational analysis of a new type of molecular machine that is controlled *via* a pH stimulus. Through the addition of a nitrogen donor group to the aryl "piston", these systems having pK_as of around 4.5 exhibit up to an eight-fold change in the Z/E-amide isomer ratio just by changing the pH from 9 to 2.

Chapter 7 discusses the operation and performance of the pH dependent molecular machines that were developed in Chapter 6. ^{1}H NMR spectroscopic analysis shows that up to 1.2 kcal mol^{-1} of energy can be harnessed by these systems which can be switched "ON" and "OFF" by protonation/deprotonation. The best of these pH dependent molecular machines is demonstrated to operate with an efficiency of 20% and -2% in the "ON" and "OFF" states, respectively. These pH dependent systems provide a fast, clean and efficient alternative to the photochemical systems from the earlier Chapters.

Publications and Conference Presentations

Coulston, R. J., Onagi, H., Lincoln, S. F., Easton, C. J., Harnessing the Energy of Molecular Recognition in a Nanomachine Having a Photochemically Dependent On/Off Switch, *J. Am. Chem. Soc.*, **2006**, *128*, 14750-14751.
Highlighted in *Chem. Aust.*, April, **2007.**

Easton, C. J., Onagi, H., Dawson, R. E., Maniam, S., Coulston, R. J., Zhang, J., Cyclodextrin Nanoscale Devices, *Chem. Aust.*, **2009**, *76*, 8-12.
Article and front cover.

Coulston, R. J., Gamble, A., Zhang, J., Lee, H., Onagi, H., Lincoln, S. F., Easton, C. J., Molecular Recognition Energy Harnessing Efficiency in a Nanomachine Having a Photochemical On/Off Switch, Poster presentation, *The 5th Asian Cyclodextrin Conference* (ACC09), May **2009**, Busan, Korea.

Coulston, R. J., Gamble, A., Zhang, J., Lee, H., Onagi, H., Lincoln, S. F., Easton, C. J., Molecular Recognition Energy Harnessing Efficiency in a Nanomachine Having a Photochemical On/Off Switch, Poster presentation, *Joint International Symposium on Macrocyclic & Supramolecular Chemistry* (ISMSC 2008), Jul **2008**, Las Vegas, U.S.A..

Coulston, R. J., Gamble, A., Zhang, J., Lee, H., Onagi, H., Lincoln, S. F., Easton, C. J., Molecular Recognition Energy Harnessing Efficiency in a Nanomachine Having a Photochemical On/Off Switch, Poster presentation, *Sino-Australia Organic Chemistry Symposium*, Oct **2008**, Canberra, Australia.

Coulston, R. J., Gamble, A., Zhang, J., Lee, H., Onagi, H., Lincoln, S. F., Easton, C. J., Molecular Recognition Energy Harnessing Efficiency in a Nanomachine Having a Photochemical On/Off Switch, Poster presentation, *Royal Australian Chemical Institute Organic Division Conference*, Dec **2008**, Hobart, Australia.
*Student Poster Presentation Prize.

Coulston, R. J., Onagi, H., Spilman, N., Lincoln, S. F., Easton, C. J., Harnessing the Energy of Molecular Recognition in a Nanomachine Having a pH Dependent On/Off Switch, Poster presentation, *Royal Australian Chemical Institute Organic and Physical Chemistry Conference* (OPC07), Jan **2007**, Adelaide, Australia.

Coulston, R. J., Onagi, H., Spilman, N., Lincoln, S. F., Easton, C. J., Harnessing the Energy of Molecular Recognition in a Nanomachine Having a pH Dependent On/Off Switch, Poster presentation. *Australian Research Council Centre of Excellence for Free Radical Chemistry and Biotechnology Spring Carnival*, Sep **2007**, Melbourne, Australia.

Glossary

AcOH	acetic acid
AU	absorbance unit
BOC	di-*tert*-butyl dicarbonate
BOP	benzotriazole-1-yloxy-tris(dimethylamino)phosphonium hexafluorophosphate
br	broad
BuOH	butanol
°C	degree Celcius
ca.	circa (approximately)
CD	cyclodextrin
D_2O	deuterium oxide
DCM	dichloromethane
dec.	decomposition
DMF	*N,N*-dimethylformamide
DMSO	dimethylsulfoxide
EI	electron impact
ESI	electrospray ionization
et al.	*et alia*
EtOAc	ethyl acetate
EtOH	ethanol
g	gram
h	hour(s)
HMBC	heteronuclear multiple bond correlation
HMQC	heteronuclear multiple quantum coherence
HPLC	high performance liquid chromatography
HRMS	high resolution mass spectrometry
hv	photon of light
Hz	hertz
ITC	isothermal titration calorimetry
J	coupling constant
L	litre
LRMS	low resolution mass spectrometry
m.p.	melting point
mg	milligram
mL	milliliter

|	
min	minute(s)
m/z	mass-to-charge ratio
M	moles per litre
M^+	molecular ion
MeCN	acetonitrile
MeOH	methanol
MHz	megahertz
NaOH	sodium hydroxide
nm	nanometer
NMP	N-methyl-2-pyrrolidinone
NMR	nuclear magnetic resonance
NOE	nuclear overhauser effect
PPh_3	triphenylphosphine
ppm	parts per million
PrOH	propanol
R_f	retention factor
ROESY	rotating-frame overhauser effect spectroscopy
rpm	revolutions per million
RT	room temperature
sec	second(s)
TEA	triethylamine
THF	tetrahydrofuran
TLC	thin layer chromatography
t_R	retention time (HPLC)
TsCl	p-toluene sulfonyl chloride
UV	ultraviolet
v	volume
w	weight
δ	chemical shift
ε	molar extinction coefficient
λ_{max}	wavelength absorption maximum
μL	microliter

Table of Contents

CHAPTER 1

Introduction

1.1 Supramolecular Chemistry

Synthetic organic chemists engineer complex structures by covalently linking collections of molecular subunits together. Molecules can also interact *via* a combination of weak non-covalent bonds to form highly ordered structures that have interesting physical properties.[1] The field of chemistry that studies these intermolecular assemblies is supramolecular chemistry which is defined as the "chemistry beyond the molecule".[2] The foundations for supramolecular chemistry were laid in the late 1960's by Cram,[3] Lehn[2] and Pederson[4] who introduced a range of macrocyclic hosts that were synthesised for the selective molecular recognition of ions and small organic guests using non-covalent interactions. This early work was inspired by the understanding and imitation of substrate-receptor recognition processes that are an important part of biological functions.[5] The current-generation of supramolecular assemblies are not limited to understanding the processes of biological systems,[2] but have evolved towards the development of molecular-level devices and machines.[6]

1.2 Molecular Machines

The literal definition of a machine is an apparatus consisting of interrelated parts with separate functions, and used to perform some kind of work.[7] The miniaturisation of machines has the potential for advancing the functional properties of everyday materials,[8] however the limitations of a scaling down approach have been realised.[9] In 1959, a physicist by the name of Richard Feynman introduced in a famous presentation entitled, "there is plenty of room at the bottom",[10,11] the concept of using a "bottom-up" strategy for developing artificial molecular-level machines. The advent of supramolecular chemistry provided chemists with a viable approach to the "bottom-up" development of artificial molecular machines that mimic their macroscopic counterparts.[12]
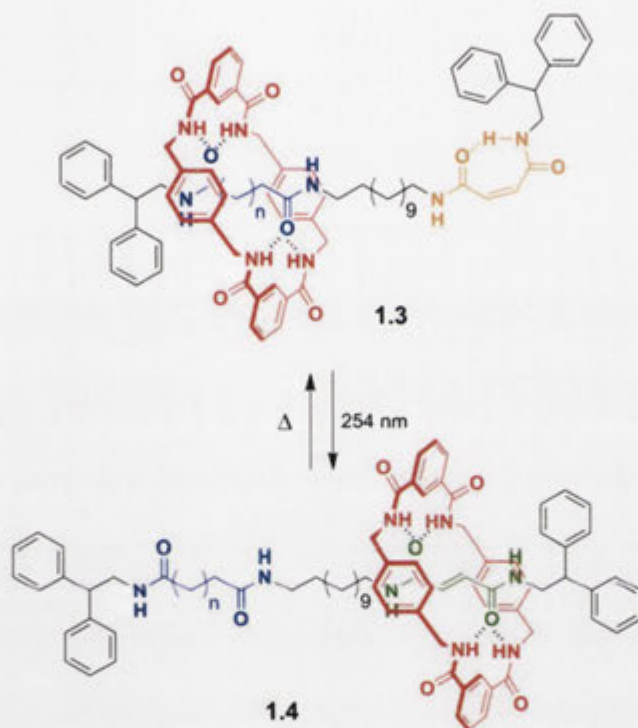
The first-generation of artificial molecular machines were simple multicomponent structures that respond to external stimuli and perform a supramolecular operation. Early examples were the photoresponsive azacrown ethers developed by Shinkai and co-workers[13,14] in the 1980's (Figure 1.2.1). When the azobenzene-bridged crown ether **1.1** was exposed to UV and visible light, the resulting *trans-cis* photoisomerisation of the azobenzene moiety lead to a conformational change in the molecule which altered its molecular recognition of certain ionic guests. In a similar system, the reversible *trans-cis* photoisomerisation of an azobenzene incorporated between two crown ether subunits, as with the bis-(crown ether) **1.2**, resulted in the molecule performing a butterfly-like operation. This motion controlled the selectivity of the bis-(crown ether) **1.2** for alkali metal cations and thus the system behaves as a molecular tweezer.

1.1 **1.2**
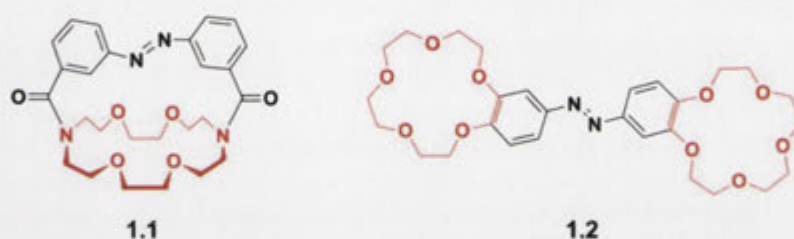
Figure 1.2.1. Azobenzene-bridged crown ether **1.1** and azobenzene linked bis-(crown ether) **1.2** as photoresponsive molecular machines for guest selective binding.

Over time molecular machines have been developed to operate with either photochemical, chemical or electrochemical stimuli and most commonly draw on inspiration from the operation of shuttles, muscles and switches.[15] The first molecular shuttle was reported in 1991 by Stoddart *et al.*,[16] which demonstrated the concept of shuttling a mechanically entrapped macrocycle between two binding stations along an axle that is capped at either end with bulky stopper groups. Stimuli-responsive binding stations can also be incorporated into the axle as illustrated by the photochemically dependent molecular shuttle reported by Leigh and coworkers[17] (Scheme 1.2.1). For this system, the [2]-rotaxane **1.3** contains an axle having both *cis*-maleamide (orange) and succinamide (blue) binding stations. A benzylic amide macrocycle (red) is mechanically interlocked onto the axle and preferentially forms hydrogen bonds with the succinamide

site (blue). Photochemical isomerisation of the *cis*-maleamide to the *trans*-fumaramide (green) with 254 nm light to give the [2]-rotaxane **1.4** sees the macrocyclic ring shuttle to the *trans*-fumaramide (green) station while heating induces the reverse process. The molecular shuttling concept has been further developed with the directed transport of the macrocyclic unit based on its position on the axle[18] and the autonomous sunlight driven shuttling operation of an artificial molecular motor.[19]

Scheme 1.2.1. Photochemically induced translocation of a benzylic amide macrocycle (red) on a molecular shuttle **1.3** that has both *cis*-maleamide (orange) and succinamide (blue) binding stations.

An important development of artificial molecular machines was the incorporation of the features of molecular shuttles into doubly interlocked dimers by Sauvage and coworkers[20] (Scheme 1.2.2). This system forms the basis of a molecular muscle through its expansion and contraction that are reminiscent of the elongation and shrinking of a biological muscle fibre. Each monomer contains a macrocyclic ring (red) that incorporates a phenanthroline chelating unit and appended to the ring is an axle with both phenanthroline (blue) and terpyridine (green) chelating subunits and capped at the end with bulky stoppers. Coordination of the phenanthroline units in the rings and

axles with Cu^I allows the muscle **1.5** to adopt an extended state. Coordination of the phenanthroline units of the rings with the terpyridine chelating subunits of the axles using Zn^{II} allows the muscle **1.6** to form the contracted state. Recently, the molecular muscle concept has been extended with Easton's[21] light driven device and Stoddart's[22] acid-base system.
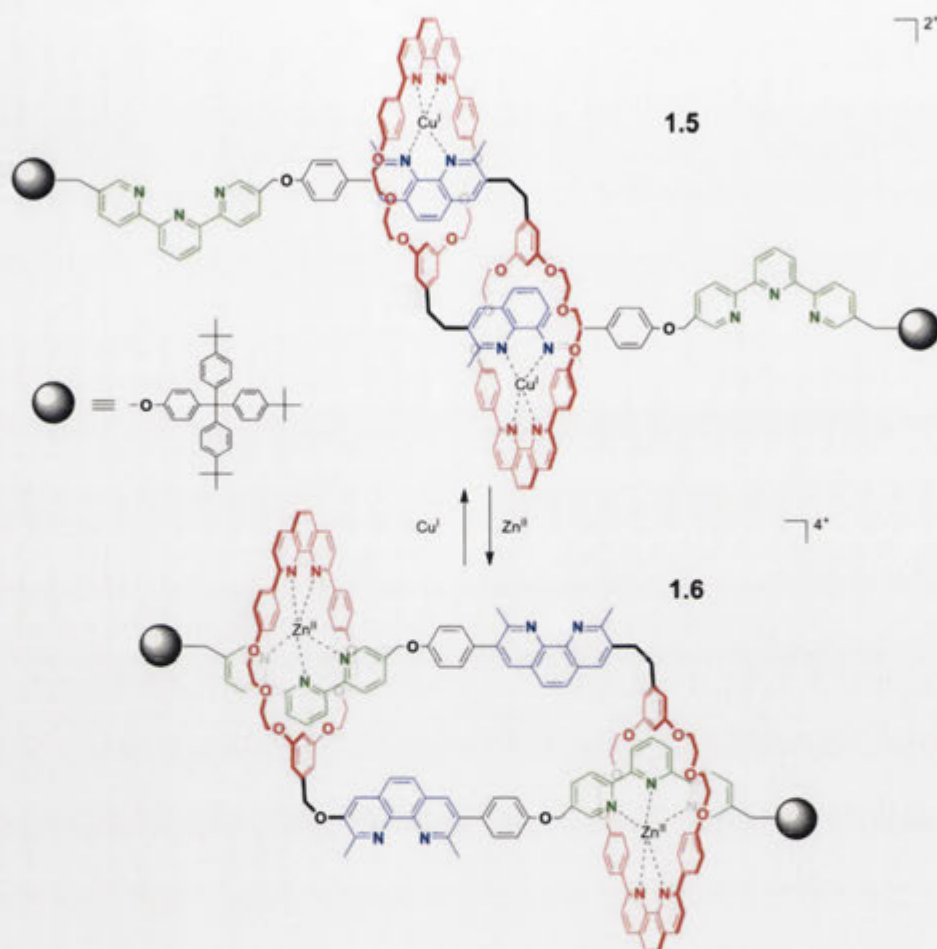
Scheme 1.2.2. Chemically induced reversible expansion **1.5** and contraction **1.6** of a molecular muscle with metal ions.[20]

Self-inclusion complexes are another interesting class of compounds that have been developed as molecular switches. Intramolecular complexation of a pendant group that is covalently linked by a flexible linkage group to a macrocyclic host occurs through non-covalent interactions. An early example of a self-included molecular switch was reported by Stoddart *et al.*,[23] in 1997 (Scheme 1.2.3). The molecular switch contains a tetracationic cyclophane host (red) appended to a π-electron rich 1,5-dioxynaphthalene (blue) binding station through

a polyether linkage group. Hydrogen bonding and π-π charge-transfer interactions stabilise the intramolecular complex **1.7** while electrochemical reduction to the cyclophane host (green) switches "OFF" these non-covalent interactions and the machine adopts a non-included conformation **1.8**.

1.7   **1.8**
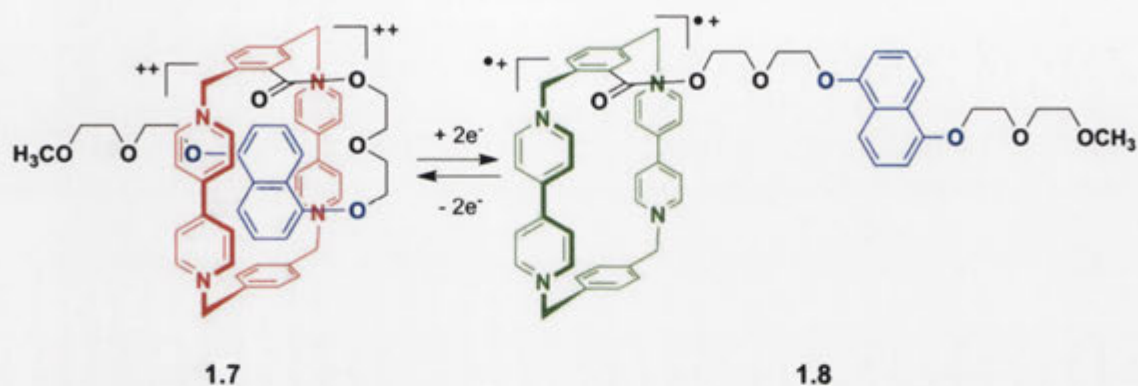
**Scheme 1.2.3.** Electrochemically controlled self-inclusion molecular switch.[23,24]

There are many examples of supramolecular based molecular machines in the literature that perform highly controlled operations in response to different external stimuli.[25-31] However at the outset of this work there were no examples of synthetic molecular machines that perform quantifiable work at the molecular level. Knowing the amount of work that a molecular machine can actually perform is likely to indicate the current limitations and future possibilities for working molecular machines in everyday society. With this in mind, a suitable building block for developing a molecular level machine is a cyclodextrin (CD).

1.3 Cyclodextrins

In 1891, Villiers[32] first reported the isolation of crystalline substances, now known as cyclodextrins (CDs), from the digestion of starch with *Bacillus amylobacter*.[33] These isolated CDs were later characterised as cyclic oligosaccharides by Schardinger[34,35] and determined to be constructed from α-1,4-linked glycosidic bonds as reported by Freudenberg.[36] Of the naturally occurring CDs the most widely studied contain six, seven or eight D-glucopyranose subunits and have the nomenclature of α-, β- or γ-CD, respectively (Figure 1.3.1).[37] The glucupyranose units of these cyclic oligosacharides adopt a $^4C_1$ chair conformation which results in the primary hydroxy

5

groups being at the narrow end of the cavity and the secondary hydroxy groups at the wider end.[38] Intramolecular hydrogen bonding between the C2 and C3 secondary hydroxy groups of adjacent glucopyranose units results in CDs adopting a rigid truncated cone shape.[39]

α-CD **1.9** n = 1
β-CD **1.10** n = 2
γ-CD **1.11** n = 3
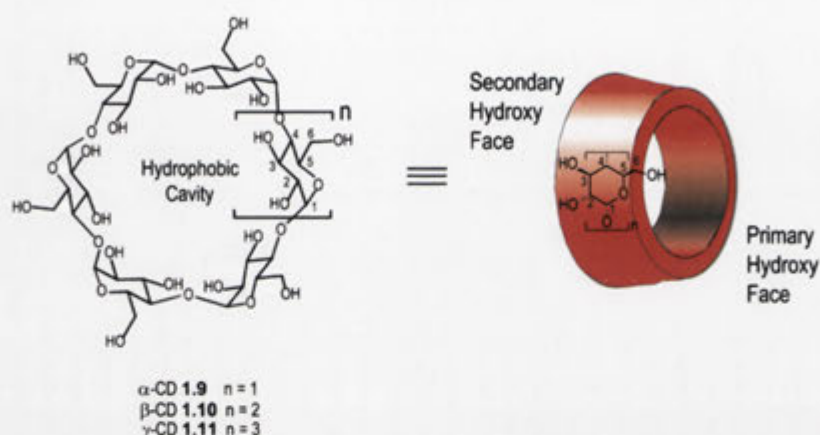
Figure 1.3.1. Molecular structure of α-CD **1.9**, β-CD **1.10** and γ-CD **1.11** (left). Schematic representation of CD as a truncated cone (right). Secondary hydroxy groups are at the wider end of the cavity while the primary hydroxy groups are at the narrow end.

CDs have found uses in various fields, including pharmaceuticals, agrochemicals, food science and cosmetics due to their unique physical properties.[40-43] CDs have hydrophilic ends due to the exposed C2, C3 and C6 hydroxy groups and hydrophobic interiors due to the O4 ether oxygen and C3, C5 and C6 protons which extend toward the centre of the annulus. This amphiphilic character enables CDs to form inclusion complexes with appropriately sized apolar guests in aqueous solutions (Figure 1.3.2).[33] The equilibrium that is established for the 1:1 complex between CD and guest is expressed by the association constant K_A as shown in Equation 1.3.1. The major driving forces for the CD guest binding interaction are van der Waals and hydrophobic interactions, however hydrogen bonding and electronic effects also contribute to the overall stability.[44,45] On this basis the structural and electronic properties of the guest can determine the overall complex stability and accordingly association constant (K_A).[46]
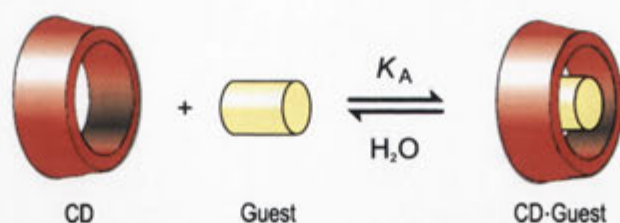
Figure 1.3.2. Equilibrium established between CD and guest in aqueous solution with association constant K_A.

$$K_A = \frac{[CD \cdot Guest]}{[CD] + [Guest]} \qquad (1.3.1)$$

A wide variety of analytical techniques have been employed to determine the association constants and thermodynamic parameters of CD and guest binding interactions which include isothermal titration calorimetry,[47] UV/visible spectroscopy,[48] circular dichroism,[49] ^{1}H NMR spectroscopy,[50] fluorescence spectroscopy[51] and HPLC.[52] Of these techniques, isothermal titration calorimetry remains the most powerful and sensitive method available for measuring the molecular interactions between CDs and guests.[53]

1.4 Isothermal Titration Calorimetry of CDs

Isothermal titration calorimetry (ITC) allows the direct measurement of the enthalpy (ΔH), association constant (K_A) and stoichiometry (n) of a CD binding interaction with a guest.[54] A typical experiment involves the stepwise addition of a guest into a calorimetric cell maintained at constant temperature that contains a rapidly stirred solution of CD (Figure 1.4.1).
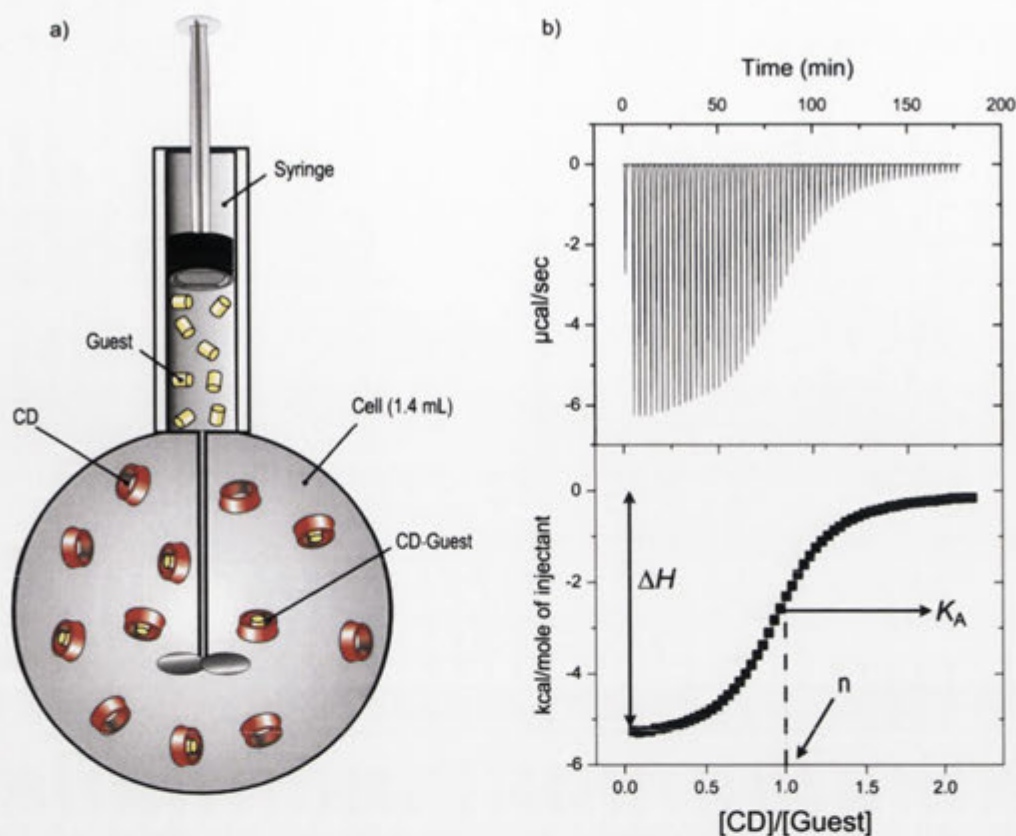
Figure 1.4.1. a) Schematic representation of an ITC cell. The cell (1.4 mL) contains a known concentration of CD and the syringe contains a known concentration of guest in identical buffer. b) Typical ITC enthalpogram for an exothermic binding interaction between a CD and guest (top) and integrated peak areas (bottom) from the above enthalpogram with line of best fit used to calculate ΔH, K_A and n.

The binding interaction releases (exothermic) or absorbs (endothermic) a certain quantity of heat which results in the power (μcal/sec) that is applied to maintain constant cell temperature being adjusted accordingly.[55] The deviation in power to restore the steady state is recorded as a differential peak. At the point where there is an excess of CD the peak area reflects, after correcting for the heat of dilution and mechanical effects, the molar enthalpy of binding (ΔH).[56] With each consecutive injection of guest the concentration of unbound CD decreases until it reaches saturation thus the peak areas become smaller and reach the heat of dilution. It is from this section of the enthalpogram that the association constant (K_A) can be derived while the stoichiometry (n) is determined from the inflection point of the curve.[56] Knowing the enthalpy (ΔH) and association constant (K_A) for a binding interaction the change in

Gibbs free energy (ΔG) can be determined from Equation 1.4.1 and thus the entropy change (ΔS) from Equation 1.4.2. By conducting the titration experiment at different temperatures, the change in heat capacity (ΔC_p) can be determined from Equation 1.4.3. From this, ITC permits the thermodynamic parameters of a particular CD and guest binding interaction to be measured.

$$\Delta G = -RT \ln K_A \qquad (1.4.1)$$

$$\Delta G = \Delta H - T\Delta S \qquad (1.4.2)$$

$$\Delta C_p = \frac{\Delta H_{T2} - \Delta H_{T1}}{T_2 - T_1} \qquad (1.4.3)$$

1.5 The Development of Cyclodextrin Based Molecular Machines

The molecular recognition properties of CDs can be utilised for both the template-directed construction[57] and integration of machine-like function into molecular-level shuttles, muscles and switches.[58] An important milestone towards the early generation of CD based molecular machines was the use of CDs for the template-directed synthesis of an interlocked rotaxane by Ogino in 1981.[59] Since Ogino's pioneering work many CD-based rotaxanes have been prepared, however it remained some time until systems that performed stimuli responsive supramolecular operations were synthesised. The first CD based molecular shuttle that was responsive to a photochemical stimulus was reported in 1997 by Nakashima and coworkers[60,61] (Scheme 1.5.1). This system was prepared by mechanically entrapping an α-CD **1.9** macrocyclic ring (red) onto an axle having both *trans*-azobenzene (blue) and methylene (green) binding stations using 2,4-dinitroflurobenzene in aqueous solution. The α-CD **1.9** ring (red) is interlocked by the 2,4-dinitrophenyl stopper groups and preferentially binds the *trans*-azobenzene binding site (blue) in water to give the [2]-rotaxane **1.12**. Photochemical irradiation of the solution with 360 nm light sees the *trans*-azobenzene isomerise to the *cis*-azobenzene (orange) and the macrocyclic ring is displaced to one of the methylene (green) spacers to produce the [2]-rotaxane **1.13**. The development of CD based molecular shuttles has since progressed with the unidirectional stilbene system of

Anderson *et al.*,[62] the lockable shuttle by Tian and coworkers,[63] and more recently the redox-responsive α-CD [2]-rotaxane of Stoddart.[64]
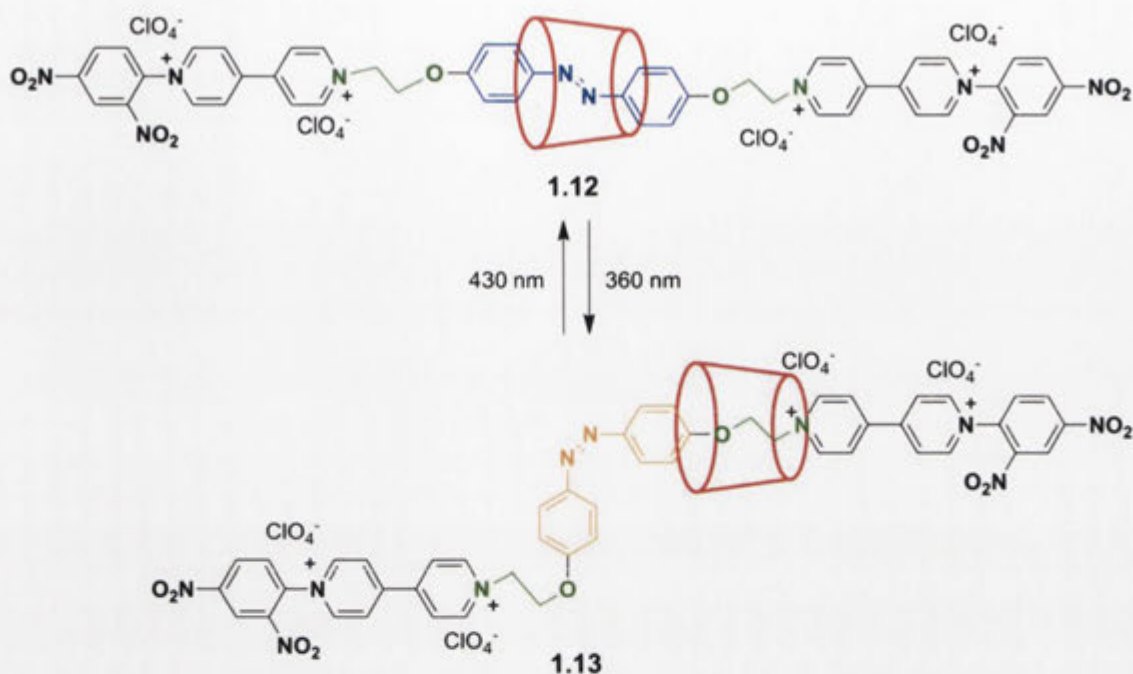
Scheme 1.5.1. Photochemically induced translocation of α-CD **1.9** (red) on a molecular shuttle **1.12** that has both *trans*-azobenzene and methylene (green) binding stations.

A different range of artificial molecular machines can be accessed by changing the physical properties of the CDs *via* chemical modification. New functional groups can be introduced into the cyclic ring through the substitution of the primary C6 and secondary C2 and C3 hydroxy groups.[65-67] Modified CDs can be covalently attached to appropriately sized apolar guests to develop hermaphroditic species that can form intermolecular[68-78] inclusion complexes in water. An early example of such an intermolecular species was by Ueno *et al.*[68] in 1988, who reported the formation of dimeric complexes in concentrated aqueous solutions of anthracene-appended CDs. The utility of such an intermolecular complex for building molecular machines was later realised through the integration of electrochemically[72] or photochemically[75] stimuli responsive groups into the guest, to enable the formation of the polymeric species to be controlled. Similarly, the intermolecular complex can also be incorporated as the foundations of molecular machines through the template-directed synthesis of doubly threaded and interlocked rotaxanes.[73,76] This has been shown by Easton and

coworkers[21] through their preparation of a photochemically driven CD based molecular muscle (Scheme 1.5.2). In this system, each monomer contains a CD ring (red) that is appended to an axle having both stilbene (blue) and methylene (green) binding stations and capped at the end with 3,5-dimethoxytriazine blocking groups. In aqueous solution, the CDs preferentially bind the *trans*-stilbene (blue) stations allowing the muscle **1.14** to adopt an extended state. Photochemical irradiation of the solution with 350 nm light results in the isomerisation of the *trans*-stilbene (blue) to the *cis*-stilbene (orange) and the CDs shuttle to the methylene (green) station to give the muscle **1.15** in the contracted state. This CD based molecular muscle has since been extended by incorporating an azobenzene moiety into the device to permit both photochemical and thermal control.[79]

1.14

254 nm   350 nm

1.15
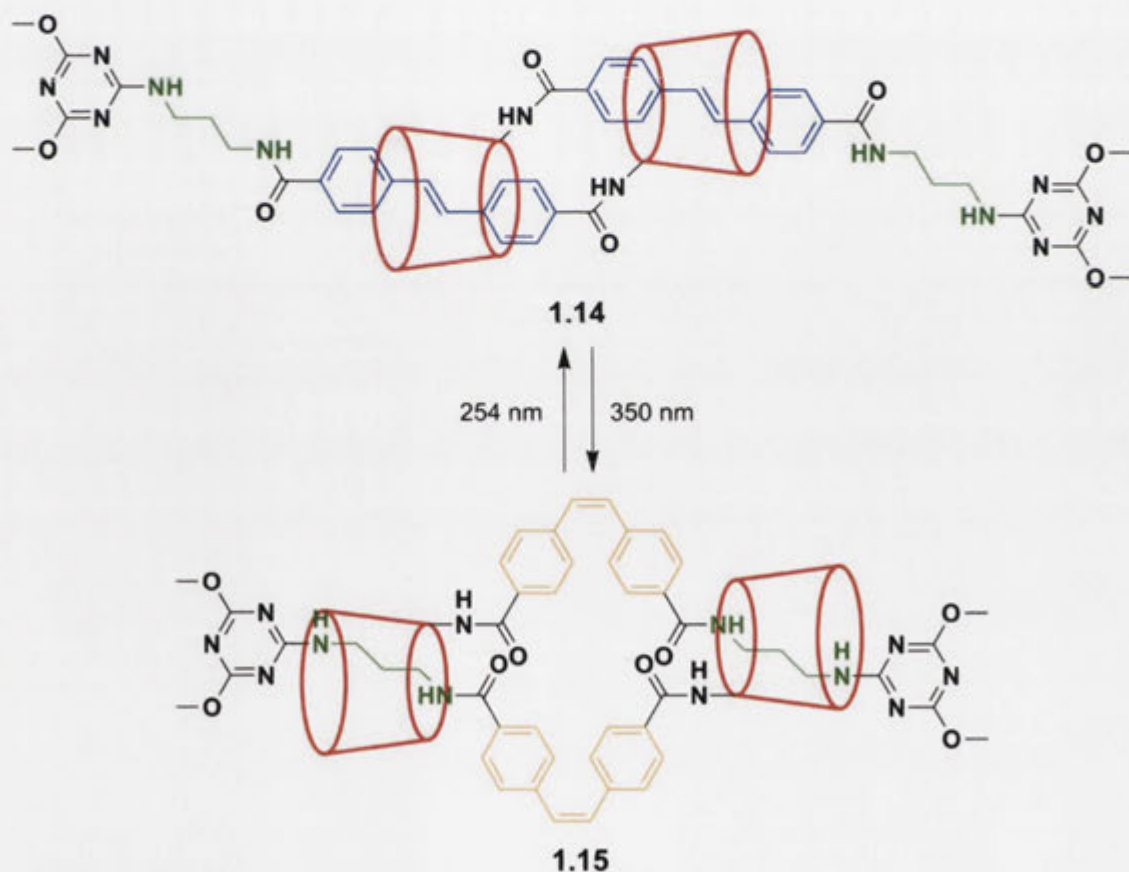
Scheme 1.5.2. Photochemically induced reversible expansion **1.14** and contraction **1.15** of a CD based molecular muscle.[21]

Apart from intermolecular complexes, CDs covalently attached to apolar guests through flexible linkage groups can be developed that form intramolecular structures.[80-

[92] In the early 1980's Ueno *et al.*,[80] reported that anthracene-appended γ-CDs were capable of forming self-included complexes which exhibited induced-fit binding affinities for small molecules. Over time, Ueno[81,82] further developed these intramolecular complexes for use as chemosensors. Alternatively, Inoue[91,92] explored the use of the CD based intramolecular complexes as templates for photochemical catalysis, while Harada[89] studied the formation of self-threaded CD polymers. More recently, a molecular machine based on the formation of a self-inclusion complex has been reported by Harada and coworkers[90] (Scheme 1.5.3). The molecular switch contains a β-CD (red) that is covalently attached to a pendant group that incorporates both azobenzene (green) and phenyl (blue) binding stations. At low temperature the CD preferentially binds to the phenyl (blue) station as the self-included species **1.16**. Photochemical isomerisation of the *trans*-azobenzene (green) to the *cis*-azobenzene (orange) with 340 nm light to give the self-included species **1.17** sees the β-CD ring shuttle to the *cis*-azobenzene (orange) station while heating or 420 nm light causes the reverse process.


1.16

420 nm, Δ ↑↓ 340 nm

1.17
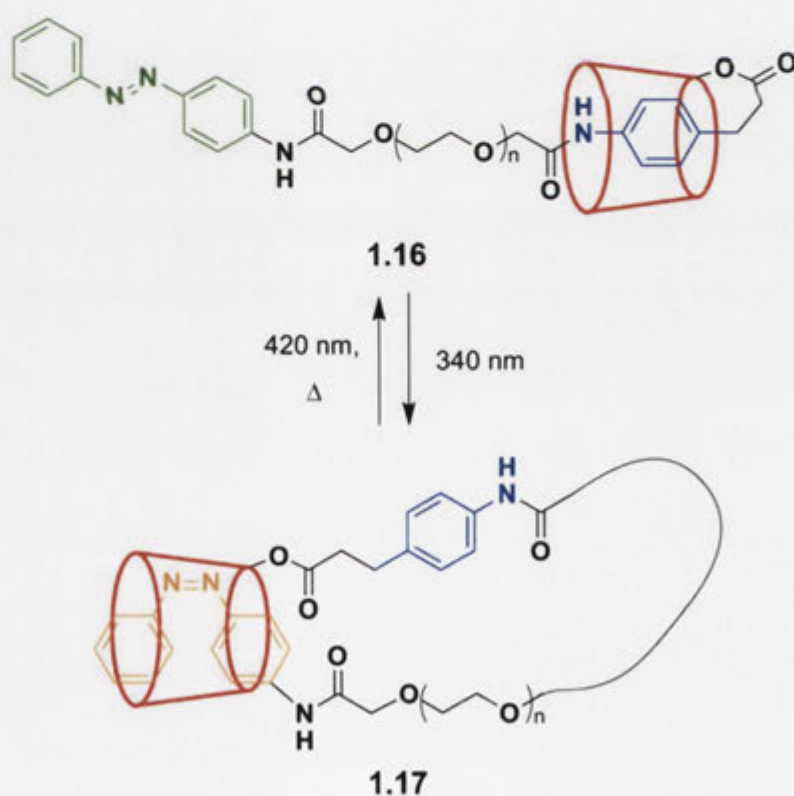
Scheme 1.5.3. Thermal and photochemical switching of self-inclusion conformations of a modified β-CD.

There are many examples of CD based molecular machines in the literature that are operated in aqueous solutions in response to different external stimuli.[93] However, at the beginning of this project none of these supramolecular systems that perform machine-like functions had yet been demonstrated to carry out quantifiable work at the molecular level. It was envisaged that the formation of CD based inclusion complexes in aqueous solutions could be harnessed for work provided that a suitable handle for measuring output was integrated into the molecular device. For this purpose, a suitable candidate for a molecular handle that can be readily incorporated into a CD based compound is an amide bond.

1.6 Amides

One strategy for the installation of pendant groups into CDs is through an amide bond. The amide moiety is planar with the nitrogen atom sp^2 hybridised which allows the lone pair electrons to conjugate with the π bond of the carbonyl group. Electron delocalisation gives the amide group partial double-bond character which restricts the free rotation around the C-N bond.[94] This barrier to rotation permits only two geometrical isomers which have the *Z/E*-nomenclature as depicted in Figure 1.6.1. The interconversion around the C-N bond is slow on the NMR timescale giving rise to a separate set of resonances for the *Z/E*-substituents on nitrogen yet fast enough to allow equilibrium to be established.[95] Under any particular set of conditions, the ratio of *Z/E*-amide isomers reflects the difference in their ground state free energies (ΔG) according to the relationship shown in Equation 1.6.1.[96] On this basis, *Z/E*-amide ratios can be quantified using ^{1}H NMR spectroscopic analysis.
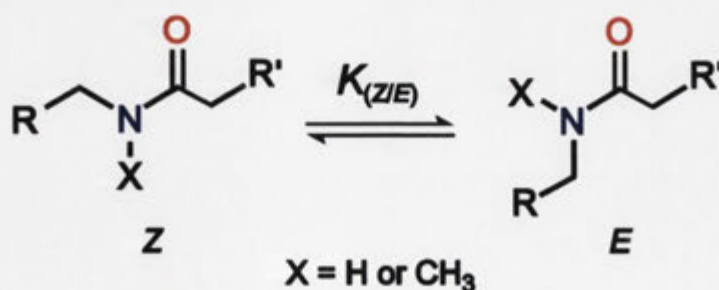
Figure 1.6.1. Schematic representation of *Z/E*-amide isomers

$$\Delta G = -RT \ln K_{(Z/E)} \qquad (1.6.1)$$

1.7 Aim

The aim of the research described in this thesis was to develop CD based species that act as artificial molecular machines to constrain the geometry of amide bonds. Using ^{1}H NMR spectroscopy, the *Z/E*-amide isomer ratios under various conditions were to be established and the amount of molecular level work performed by the molecular machines was to be quantified. To demonstrate that artificial molecular machines can be developed to perform work outputs at the molecular level, the performance of their operation was to be measured with ITC.

CHAPTER 2

Harnessing the Energy of Molecular Recognition in a Nanomachine Having a Photochemical On/Off Switch

2.1 Introduction

As outlined in Chapter 1, the aim of this research was to develop artificial molecular machines where the work output resulting from molecular recognition is harnessed to constrain the geometry of an amide bond. In view of this, a suitable building block for constructing such an artificial molecular machine is a hermaphroditic compound comprising a guest covalently appended to a host.[76,97] This duality permits the hermaphrodite to adopt monomeric acyclic [*a*1] and cyclic [*c*1] conformations as illustrated in Figure 2.1.1.[98,99] Formation of the [*c*1] conformation has been observed for β-CD hosts linked to non-rigid hydrophobic guests.[100-103] One such example was reported by Corradini *et al.*,[100] where a β-CD host encapsulated a dansyl group through molecular recognition to form a [*c*1] complex in both solution and the solid state. During the molecular recognition process the linkage group must experience some conformational constraint. It is the harnessing of this strain energy from the formation of a CD [*c*1] complex that forms the basis of the research described in this Chapter.

[*a*1]   [*c*1]
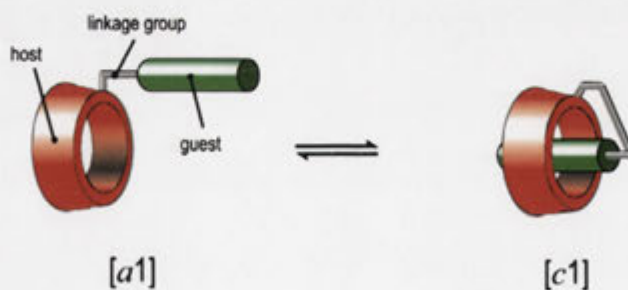
Figure 2.1.1. Schematic representation of unimolecular hermaphrodite conformations. (*a*: acyclic, *c*: cyclic, 1: monomer No.).

One of the features of a CD based [*c*1] complex, as demonstrated by Miyauchi and Harada in 2004,[104] is that a competitive guest such as an adamantane derivative can be added to preferentially include in the host in aqueous solution. The result is an equilibrium shift away from the [*c*1] CD complex toward the competitive guest [*a*1] CD

complex as illustrated in Figure 2.1.2. This bias towards the formation of the adamantane [*a*1] CD complex should in principle change the extent of conformational constraint of the linkage group. For the purpose of quantifying the change in strain energy an amide linkage group was chosen where the *Z/E* ratio reflects the difference between the isomer ground state free energies (ΔG) under a particular set of conditions. Any difference in the *Z/E* ratios and ground state free energies between the [*c*1] CD and competitive guest [*a*1] CD complex reflects the work performed by the molecular recognition process. This difference is the focus of the investigation with the aim to harness the previously uncaptured work output of molecular recognition.
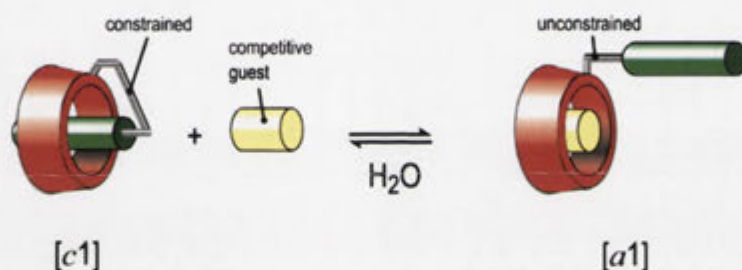
Figure 2.1.2. Schematic representation of the effect of a competitive guest.

With this in mind the desired molecular analogue of a macroscopic mechanical pump is illustrated in Figure 2.1.3 and Scheme 2.2.2. For the purpose of replicating the "piston" and "cylinder" of a mechanical pump an aryl guest was to be attached to β-CD **1.10** to produce the target phenylpropionamido hermaphrodite **2.3**. The intended purpose was for molecular recognition of the aryl "piston" by the CD "cylinder" to create the [*c*1] complex in water, then to form the [*a*1] conformation by adding 1-adamantanol as the "fuel". In the absence and presence of the "fuel" the ratio of amide isomers was to be measured with the difference ($\delta\Delta G$) reflecting the work output. Knowing that hosts based on β-CD **1.10** are also capable of distinguishing between guests,[46] the properties of a different "piston" could affect the work output. For this reason the cinnamido hermaphrodite **2.4** having a *trans*-olefinic moiety adjacent to the aryl substituent was also to be studied.
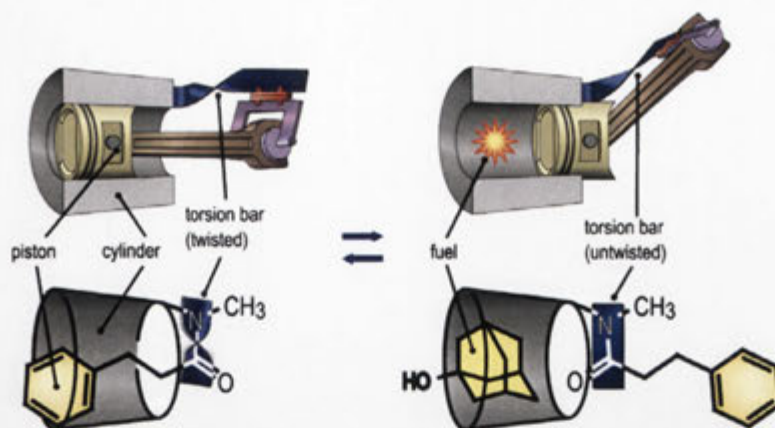
Figure 2.1.3. Schematic representation of a mechanical machine and its molecular counterpart.

A large amount of this work has been published in the form of a communication[105] which appears later in this Chapter. In this thesis *Z*- and *E*-amide assignments are based on the substituent priorities on amide nitrogen and carbon, though sometimes and in the communication the assignment is based on the priority of the *N*-substituents relative to that of the substituent on the carbonyl carbon. Additional research that was not covered in detail in the paper but has relevance to the understanding of this project is discussed in the following sections.

2.2 Synthesis of Propionamido- and Cinnamido-substituted β-Cyclodextrins

The synthesis of the hermaphrodites **2.3** and **2.4** started with the preparation of 6^A-deoxy-6^A-methylamino-β-CD **2.2** as detailed in Scheme 2.2.1. This involved converting a C6 primary hydroxy group of β-CD **1.10** to a methylamino group using established methodology.[106] To begin natural β-CD **1.10** was treated with *p*-toluenesulfonyl chloride to yield 6^A-*O*-toluenesulfonyl-β-CD **2.1**.[107] The tosyl group of the sulfonate **2.1** was then substituted with methylamine to access, after chromatography, the amino-CD **2.2**.
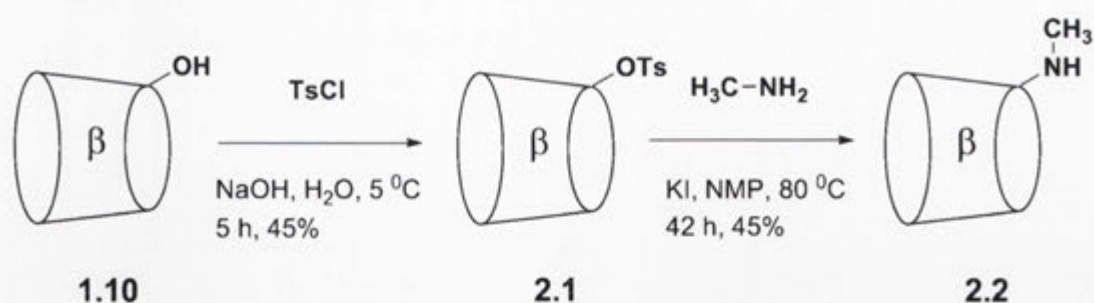
Scheme 2.2.1. Synthesis of 6^A-deoxy-6^A-methylamino-β-CD **2.2**.

After modifying the CD "cylinder", the hermaphrodites **2.3** and **2.4** could be prepared (Scheme 2.2.2). The aryl "pistons" were installed onto the amino-CD **2.2** through an amide "torsion bar". The crude mixtures were applied to anionic (DEAE) then cationic (SP) exchange resins, followed by reverse-phase HPLC, to isolate the hermaphrodites **2.3** and **2.4** in yields of 60% and 30%, respectively. TLC analysis of the hermaphrodites **2.3** and **2.4** identified both a UV responsive aromatic group and a "positively staining" CD component.[108] In addition, the hermaphrodites **2.3** and **2.4** were characterised by elemental analysis and showed, using ESI HRMS, [M+H]$^+$ ions at 1280.467 and 1278.452, respectively.
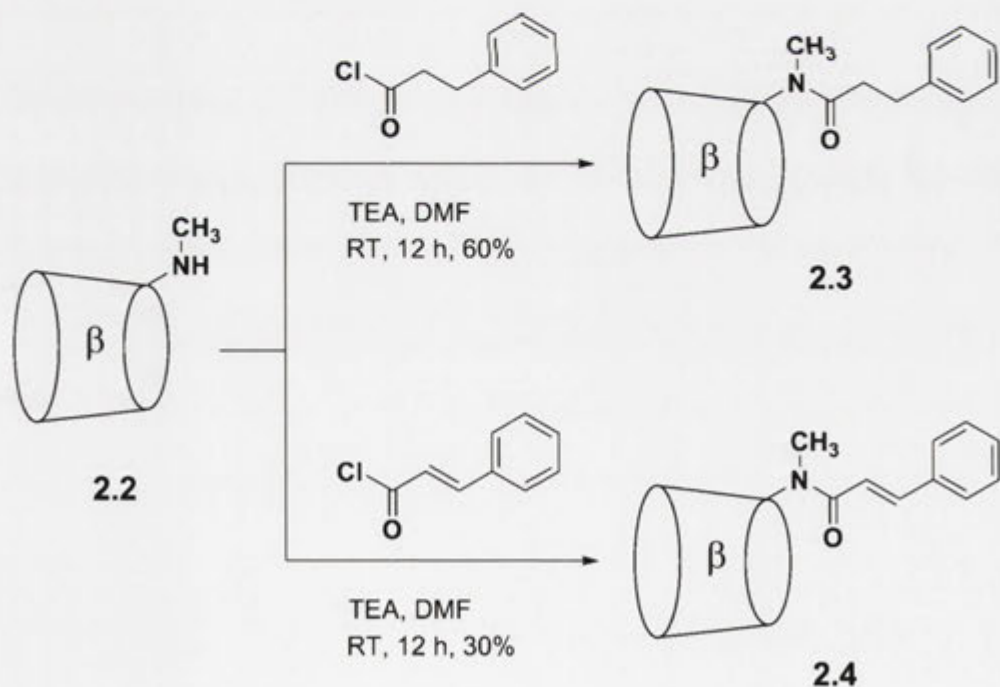
Scheme 2.2.2. Synthesis of 6^A-deoxy-6^A-(*N*-methyl-3-phenylpropionamido)-β-CD **2.3** and *trans*-6^A-deoxy-6^A-(*N*-methylcinnamido)-β-CD **2.4**.

Photolysis of the *trans*-hermaphrodite **2.4** provided the opportunity of preparing the *cis*-isomer **2.5**, as illustrated in Scheme 2.2.3. Accordingly, an aqueous solution of the hermaphrodite **2.4** was irradiated with 300 nm light for 2.5 h. Chromatography of the crude mixture afforded, after reverse-phase HPLC, the hermaphrodite **2.5** in 32% yield. The hermaphrodite **2.5** was characterised by elemental analysis and was shown using ^{1}H NMR spectroscopy to be the *cis*-isomer by the coupling constant between the olefinic protons ($J = 13$ Hz).[109]


2.4 hv 300 nm, H$_2$O   RT, 2.5 h, 32%   **2.5**
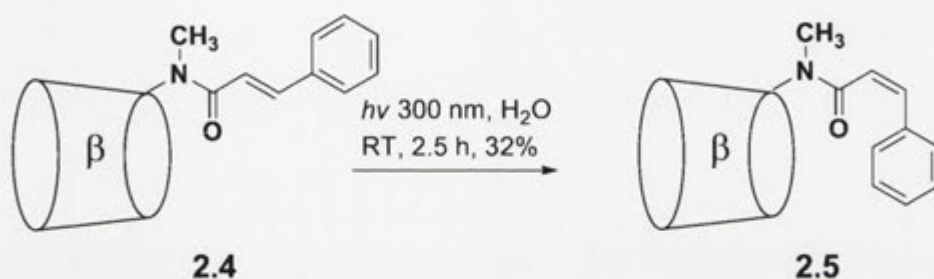
Scheme 2.2.3. Synthesis of *cis*-6^A-deoxy-6^A-(*N*-methylcinnamido)-β-CD **2.5**.

2.3 Conformational Analysis of Cyclodextrin Based Hermaphrodites

Having prepared the hermaphrodites **2.3**, **2.4** and **2.5**, their function as machines as illustrated in Figure 2.1.3 is dependent upon their conformational behaviors in the organic solvent d_6-DMSO, D$_2$O with 1-adamantanol and D$_2$O alone. The conformations of non-symmetrically modified CDs can be investigated using an established protocol[110] of 2D NMR spectroscopic techniques. The conformational behaviors of the hermaphrodites **2.3**, **2.4** and **2.5** were studied with the aim of distinguishing between the *Z*/*E*-amide isomers and determining the position accordingly of the aryl "piston" with respect to the CD "cylinder".

A section of the 1D ^{1}H NMR spectrum of the hermaphrodite **2.3** in d_6-DMSO is shown in Figure 2.3.1. Two major proton signals are observed at δ 2.93 and 2.79 ppm which integrate to a ratio of approximately 1:1.2, respectively. In the ROESY spectrum (Figure 2.3.2), these signals show negative exchange cross-peaks indicating the corresponding species are in equilibrium and hence the peaks are assigned to the methyl groups of the amide isomers. The less intense proton signal at δ 2.93 ppm (F2 axis) shows an NOE interaction with the methylene proton signal at δ 2.60 ppm (F1 axis) and therefore is assigned to be the *Z*-amide isomer. The larger signal at δ 2.79 ppm shows

no NOE with the methylene signal and is assigned to the *E*-amide isomer. The aryl "piston" showed no interaction with the CD "cylinder" (Figure 2.3.3), consistent with the fact that organic solvent does not provide driving force for inclusion.[111] It was concluded that in d_6-DMSO the hermaphrodite **2.3** adopts a non-included [*a*1] conformation with two amide isomers in an *Z*/*E* ratio of 1:1.2.
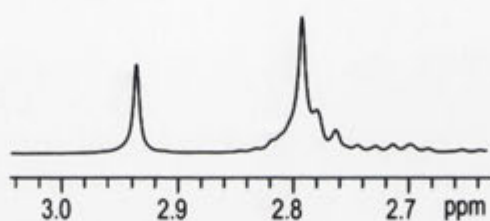
Figure 2.3.1. Section of the ^{1}H NMR spectrum (500 MHz) of the hermaphrodite **2.3** in d_6-DMSO at 25 °C.
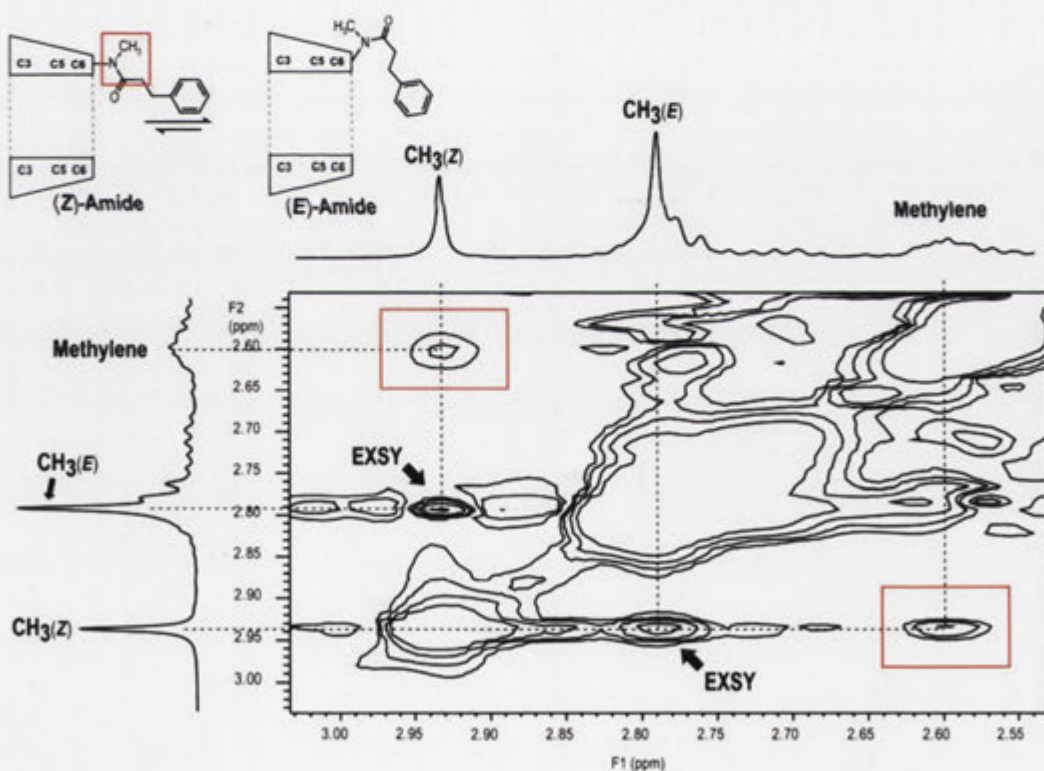
Figure 2.3.2. Section of the ROESY NMR spectrum (500 MHz) of the hermaphrodite **2.3** in d_6-DMSO (25 °C) with 0.250 ms mixing time.

20
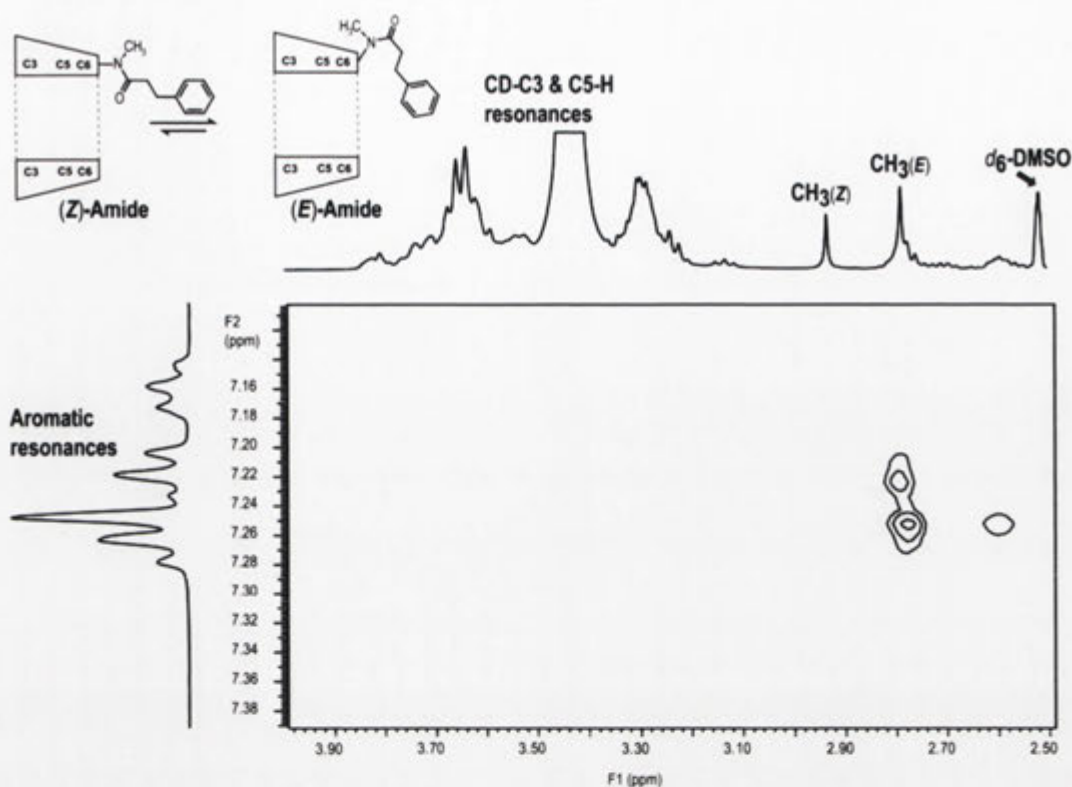
Figure 2.3.3. Section of the ROESY NMR spectrum (500 MHz) of the hermaphrodite **2.3** in d_6-DMSO (25 °C) with 0.250 ms mixing time.

In D_2O, the hermaphrodite **2.3** appears to exist as one dominant species as shown by its ^{1}H NMR spectrum in Figure 2.3.4. Nevertheless, the methylene region of the spectrum is not typical of the standard A_2B_2 resonance pattern, presumably due to the presence of a mixture of methylene conformations in solution. In spite of this, one strong proton singlet at δ 3.09 ppm is observed in the *N*-methyl region of the spectrum. From ROESY analysis (Figure 2.3.5) this signal shows no NOE interactions with the signals for the methylene protons and is therefore assigned to the methyl group of the *E*-amide isomer. The aromatic resonances show cross-peaks with the CD proton signals, therefore the aryl "piston" is included within the CD "cylinder". On this basis the predominant structure of the hermaphrodite **2.3** in D_2O is the included [*c*1] complex which is expected as there is a driving force for inclusion.[111] The *E*-amide predominates however, there also is a relatively low intensity singlet at δ 2.98 ppm that can be assigned to the *Z*-amide isomer, in an *Z*/*E*-amide ratio of 1:25, for reasons demonstrated later in this Chapter from titrations with 1-adamantanol "fuel" (Figure S1).[105]
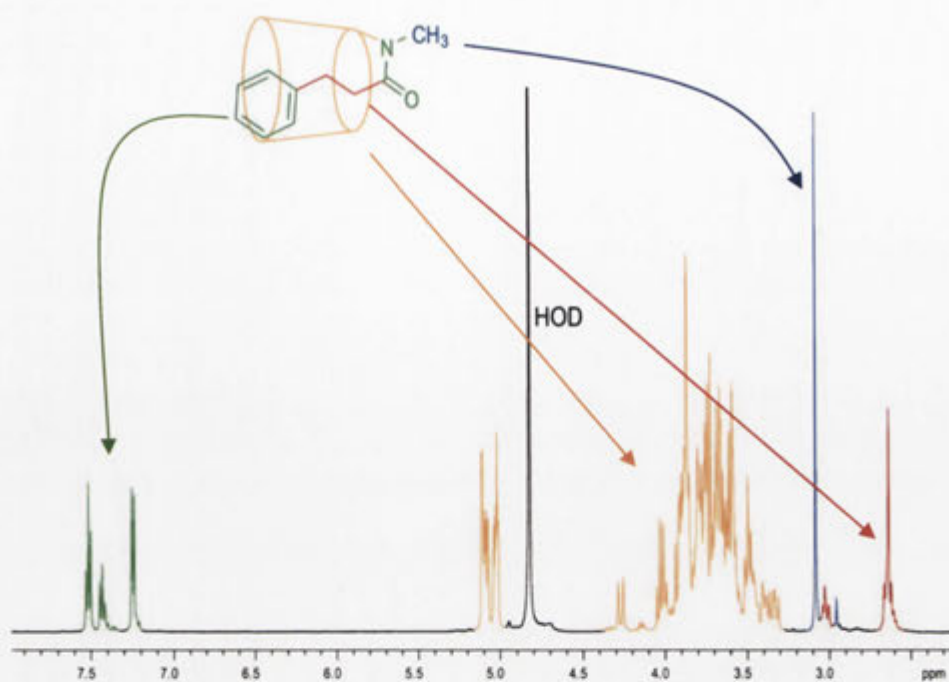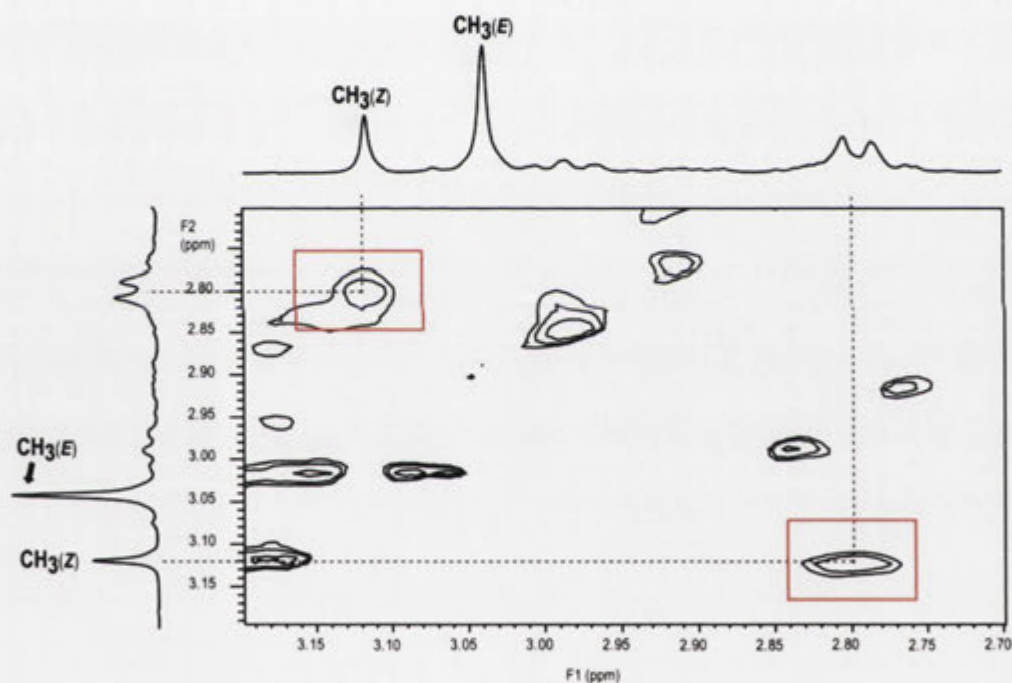
Figure 2.3.4. ^1H NMR spectrum (500 MHz) of the hermaphrodite **2.3** in D_2O at 25 °C.
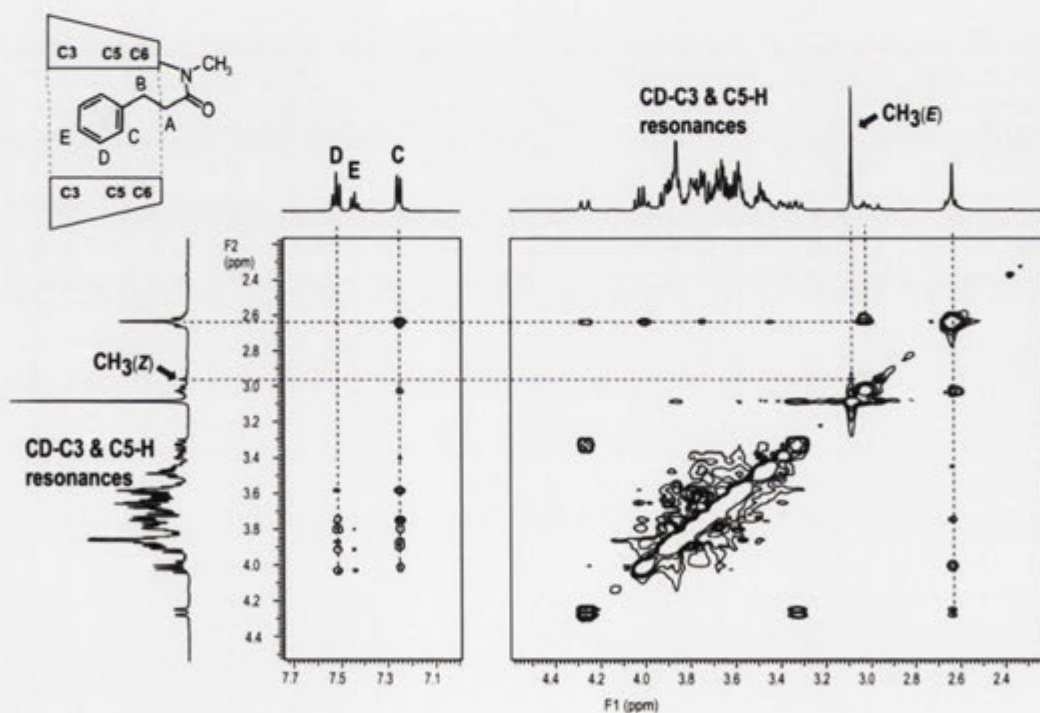
Figure 2.3.5. ROESY NMR spectrum (500 MHz) of the hermaphrodite **2.3** in D_2O (25 °C) with 0.250 ms mixing time.

Figure 2.3.6 shows the ROESY NMR spectrum for the hermaphrodite **2.3** in D_2O with 3 equivalents of 1-adamantanol "fuel". Two proton signals are observed in the *N*-methyl region of the spectrum at δ 3.12 and 3.04 ppm which integrate to a ratio of about 1:2.4, respectively. The less intense signal at δ 3.12 ppm (F2 axis) shows an NOE interaction with the methylene proton signal at δ 2.80 ppm (F1 axis) and is therefore assigned to the methyl group of the *Z*-amide isomer. Both the 1-adamantanol "fuel" and the aryl "piston" interact with the CD "cylinder" based on ROESY NMR analysis (Figure 2.3.7), which is indicative of an equilibrium between species such as those illustrated. On this basis, the hermaphrodite **2.3** with 1-adamantanol "fuel" interconverts between [*a*1] and [*c*1] complexes with two amide conformations in an overall *Z/E* ratio of about 1:2.4.

Figure 2.3.6. Section of the ROESY NMR spectrum (500 MHz) of 1-adamantanol (3-equivalents) and the hermaphrodite **2.3** in D_2O (25 °C) with 0.250 ms mixing time.
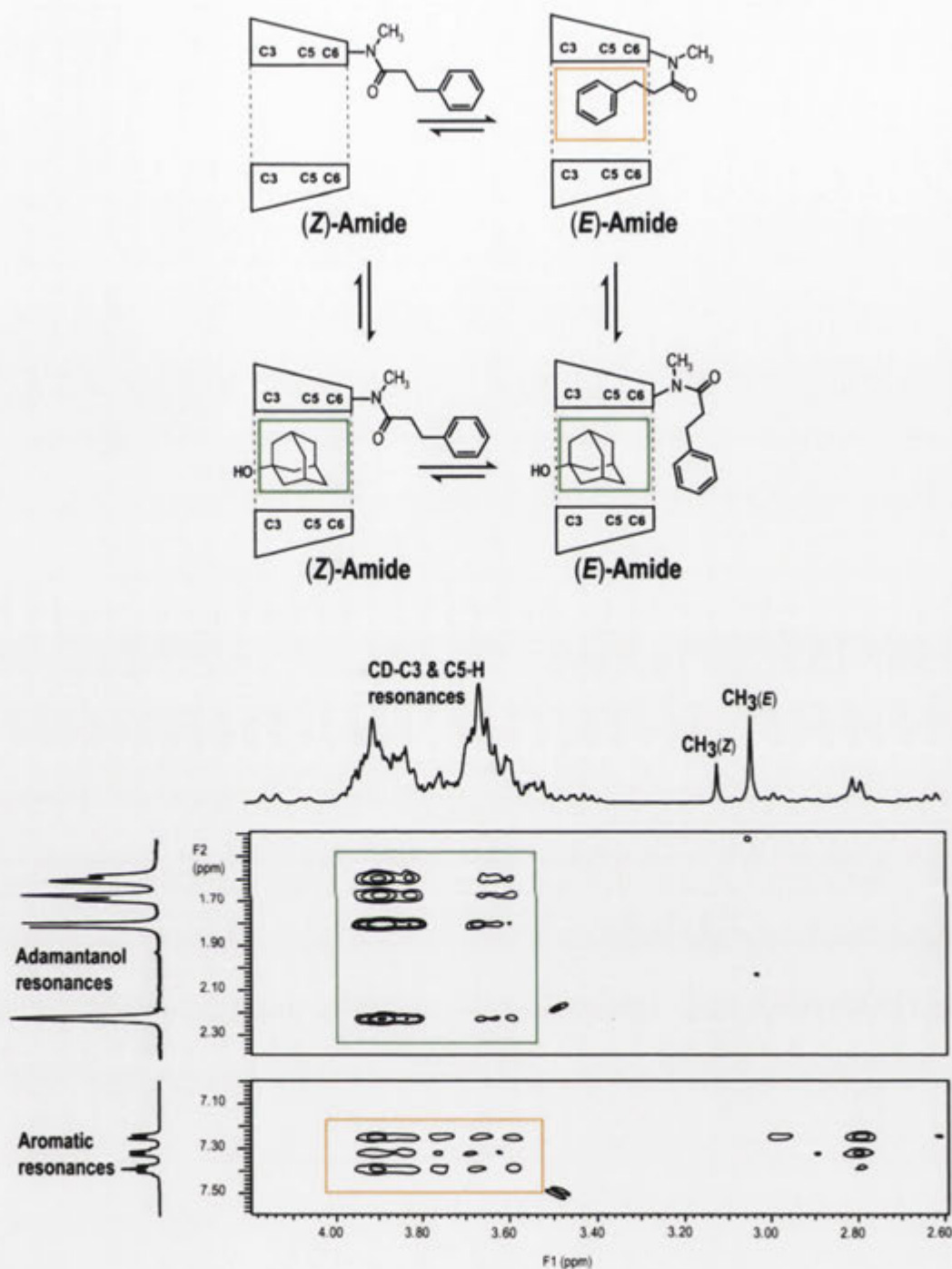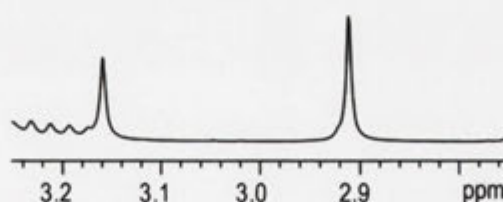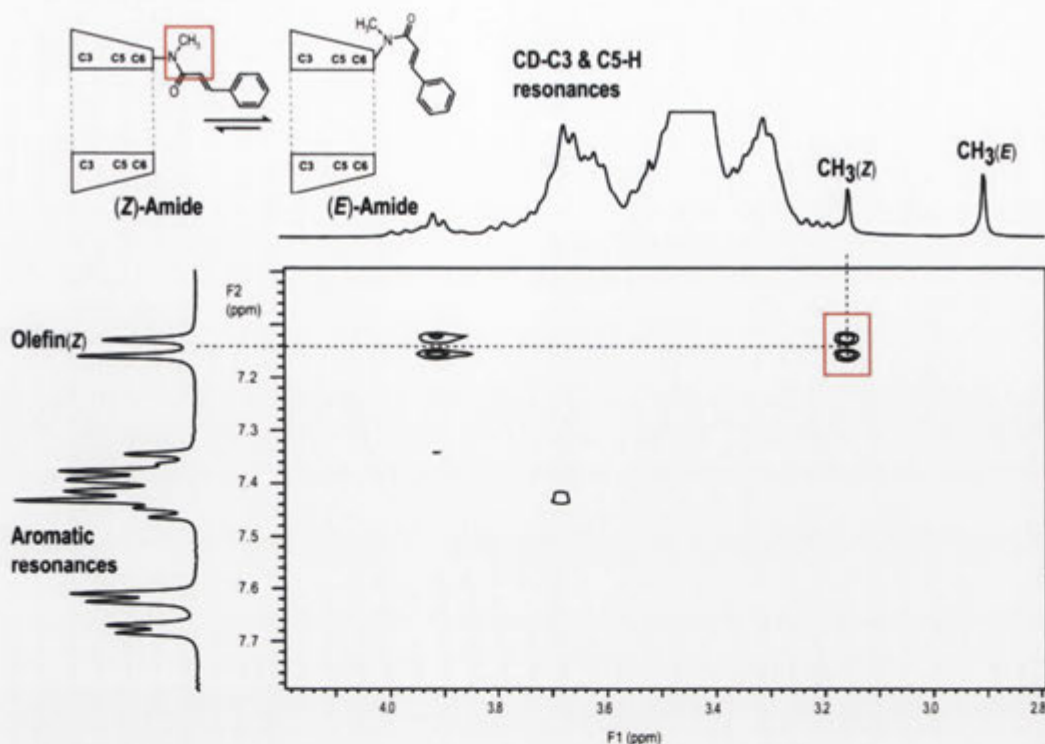
Figure 2.3.7. Sections of the ROESY NMR spectrum (500 MHz) of 1-adamantanol (3-equivalents) and the hermaphrodite **2.3** in D_2O (25 °C) with 0.250 ms mixing time.

To summarise the conformational behavior of the hermaphrodite **2.3**, in d_6-DMSO the aryl "piston" is not included and the observed Z/E-amide ratio is 1:1.6. In D_2O the aryl "piston" is included and the E-amide isomer predominates. In D_2O in the presence of 1-adamantanol "fuel", the "fuel" and the aryl "piston" compete for inclusion within the CD "cylinder" and the Z/E ratio is 1:2.4. In d_6-DMSO the aryl "piston" is not included so there isn't any constraint upon the amide bond. However, in D_2O in the presence of 1-adamantanol "fuel" the aryl "piston" is mostly not included but there still is some interaction because the [c1] complex is in equilibrium with [a1] guest complex and therefore there is residual constraint on the amide bond. This is the reason for the difference observed between the Z/E-amide ratios in d_6-DMSO and D_2O with 1-adamantanol.

With the conformational behavior of the hermaphrodite **2.3** investigated in d_6-DMSO, D_2O with 1-adamantanol and D_2O alone, the focus shifted toward investigating the hermaphrodite **2.4**. The ^1H NMR spectrum of the hermaphrodite **2.4** in d_6-DMSO shows two major proton signals at δ 3.16 and 2.91 ppm which integrate to a ratio of about 1:1.8 (Figure 2.3.8). From the ROESY spectrum (Figure 2.3.9) the weaker proton signal is assigned to the Z-amide isomer because of the NOE interaction with the olefinic proton signal at δ 7.14 ppm (F2 axis). In this solvent the aryl "piston" shows no interaction with the CD "cylinder" which indicates that the dominant species is the [a1] conformation. Overall, the hermaphrodite **2.4** forms the non-included [a1] conformation in d_6-DMSO with two amide isomers in an Z/E ratio of 1:1.8.

Figure 2.3.8. Section of the ^1H NMR spectrum (500 MHz) of the hermaphrodite **2.4** in d_6-DMSO at 25 °C.

Figure 2.3.9. Section of the ROESY NMR spectrum (500 MHz) of the hermaphrodite **2.4** in d_6-DMSO (25 °C) with 0.250 ms mixing time.

The hermaphrodite **2.4** in D_2O exists in one major form as seen from the ^{1}H NMR spectrum shown in Figure 2.3.10. In the *N*-methyl region of the ROESY spectrum (Figure 2.3.11), the methyl singlet at 3.15 ppm shows no NOE interaction with the olefinic proton signals and is accordingly assigned to the *E*-amide isomer. The aromatic and olefinic proton signals show cross-peaks with the CD resonances so the aryl "piston" is included within the CD "cylinder". These results suggest that the major structure of the hermaphrodite **2.4** in D_2O is the [*c*1] complex with a dominant *E*-amide conformation. Nevertheless, a low intensity singlet at δ 3.36 ppm can be assigned to the *Z*-amide isomer, in an *Z/E*-amide ratio of 1:100, from evidence shown later in the Chapter from titrations with 1-adamantanol "fuel" (Figure S2).[105]
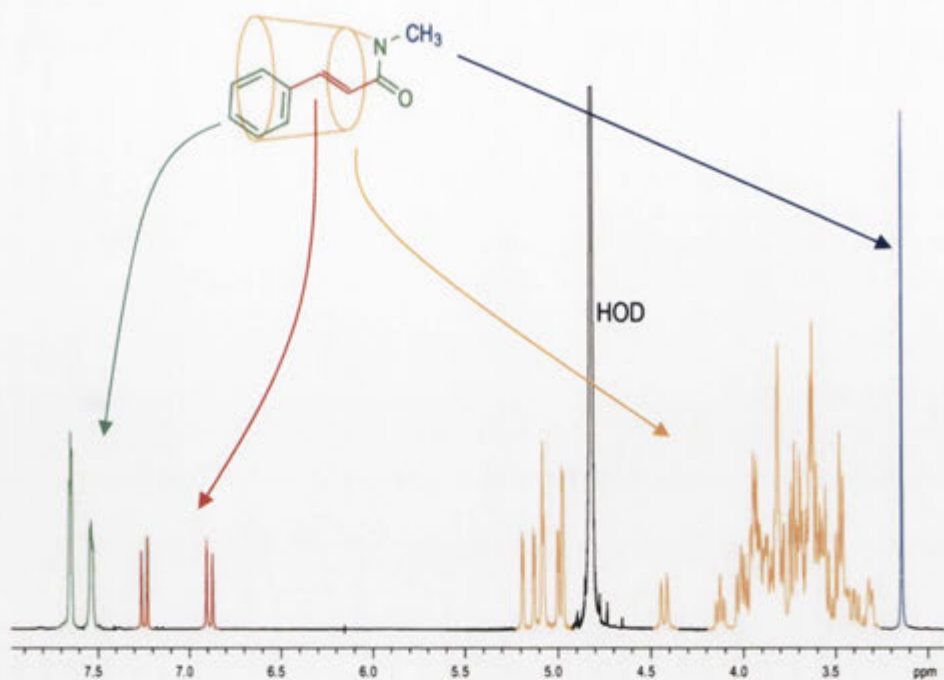
Figure 2.3.10. ^{1}H NMR spectrum (500 MHz) of the hermaphrodite **2.4** in D_2O at 25 °C.

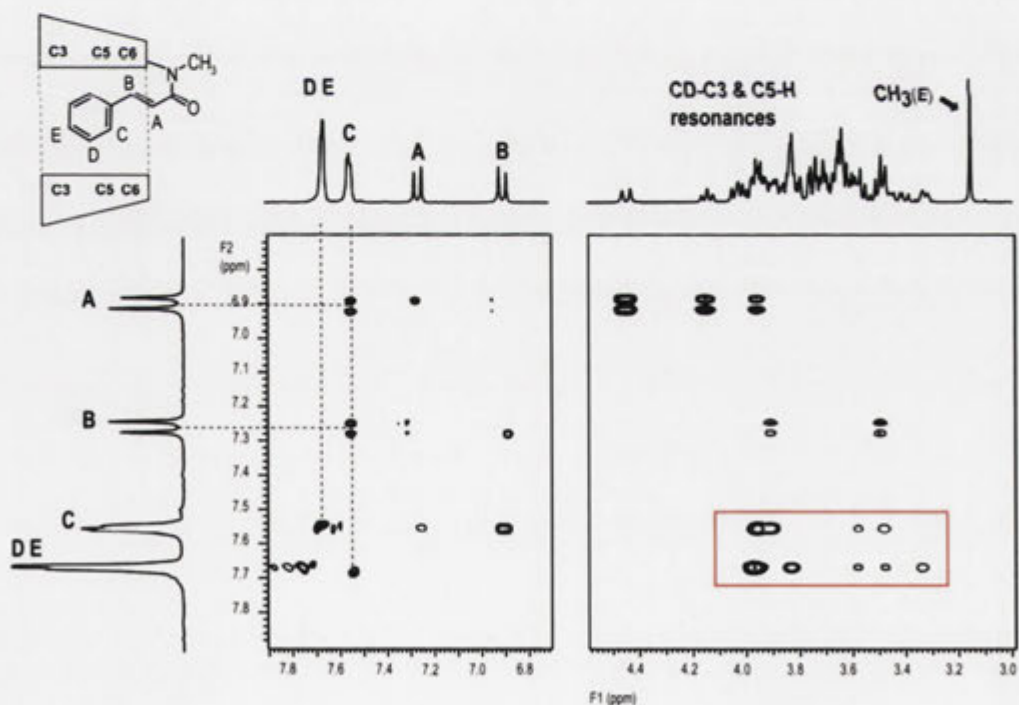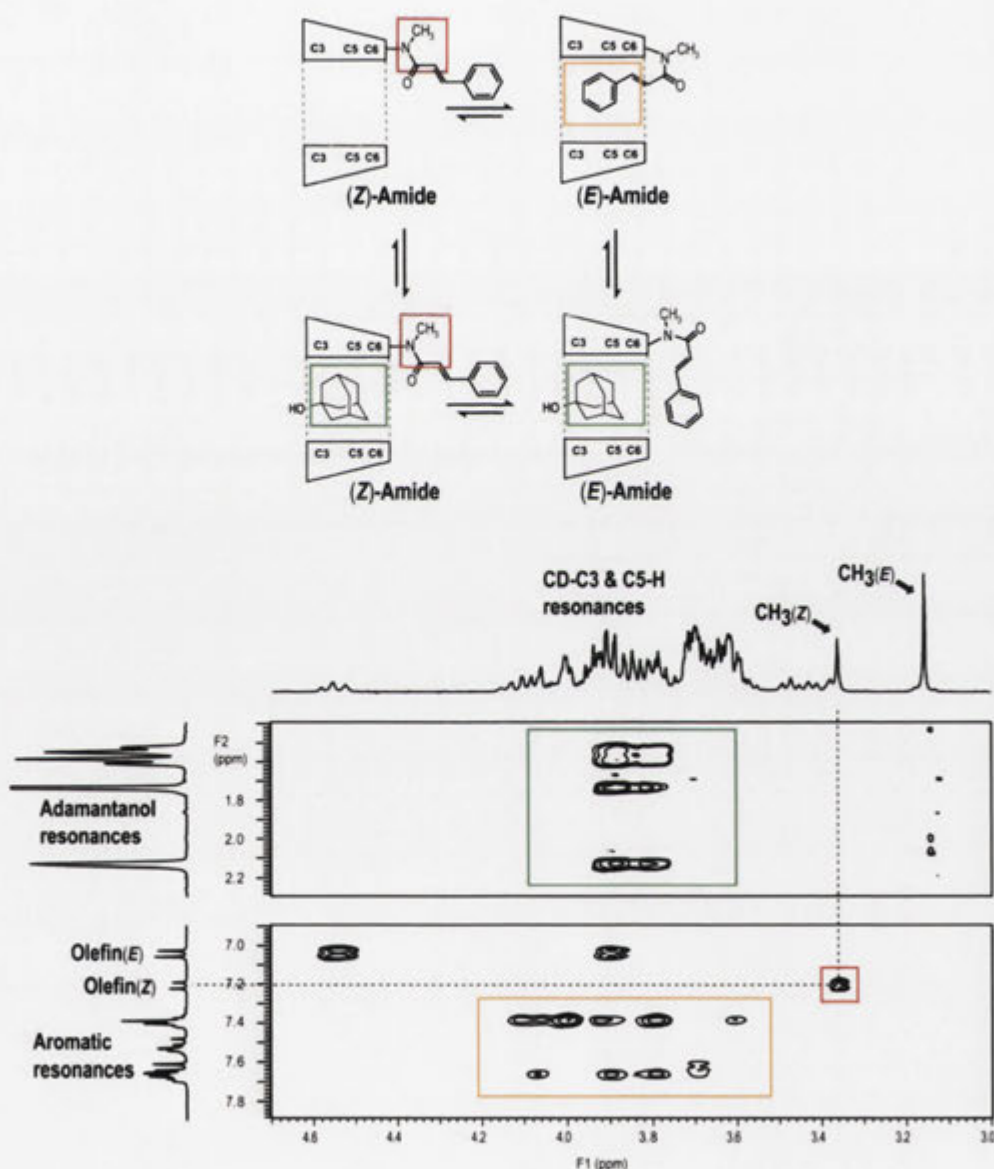

Figure 2.3.11. ROESY NMR spectrum (500 MHz) of the hermaphrodite **2.4** in D_2O (25 °C) with 0.250 ms mixing time.

27

The ROESY spectrum of the hermaphrodite **2.4** in the presence of 1-adamantanol "fuel" in D_2O is shown in Figure 2.3.12. In the *N*-methyl region of the spectrum, two major proton signals are observed at δ 3.34 and 3.14 ppm that integrate in a ratio of about 1:2.6, respectively. The less intense proton signal at δ 3.34 ppm (F1 axis) shows an NOE interaction with the olefinic proton signal at δ 7.22 ppm (F2 axis) and is therefore assigned to the *Z*-amide isomer. The ratio of the olefinic signals is consistent with the ratio of the *N*-methyl proton signals and accordingly acts as an alternative handle for quantifying the *Z/E*-amide ratio. The olefinic resonance at δ 7.22 ppm (F2 axis) that interacts with the *Z*-amide methyl signal shows no NOE interactions with the CD "cylinder" suggesting that this aryl group is not included. The NOE interactions of both the aryl "piston" and the 1-adamantanol "fuel" with the CD "cylinder" suggest that multiple species are in equilibrium as illustrated. In the presence of 1-adamantanol "fuel" the hermaphrodite **2.4** in D_2O appears to alternate between [*a*1] and [*c*1] conformations with an overall *Z/E*-amide ratio of 1:2.6.

To summarise the conformational behavior of the hermaphrodite **2.4**, in d_6-DMSO the aryl "piston" does not include and the *Z/E*-amide ratio is 1:1.8. In D_2O the aryl "piston" is included and the *E*-amide is dominant. In D_2O in the presence of 1-adamantanol, the aryl "piston" competes with the guest for the CD "cylinder" and the *Z/E*-amide ratio is 1:2.6. In d_6-DMSO without the driving force for inclusion the aryl "piston" is not included within the CD "cylinder" and there isn't any constraint upon the amide bond. However, in D_2O in the presence of 1-adamantanol "fuel" the [*c*1] complex is in equilibrium with [*a*1] guest complex and therefore the small amount of interaction results in residual constraint upon the amide bond. This is the reason for the difference observed in the *Z/E*-amide ratio between d_6-DMSO and D_2O in the presence of 1-adamantanol.

With the conformational behavior of the hermaphrodite **2.4** determined under the various conditions, its *cis*-isomer **2.5** was examined accordingly. In d_6-DMSO, the ¹H NMR spectrum (Figure 2.3.13) of the hermaphrodite **2.5** shows two major proton signals at δ 2.93 and 2.91 ppm which appear in an approximate ratio of 1.6:1. From the ROESY NMR analysis (Figure 2.3.14), the smaller signal interacts with the olefinic proton signal at δ 6.18 ppm (F2 axis) and is therefore assigned to the *Z*-amide isomer. Two sets of olefinic signals are observed that integrate in a 1.6:1 ratio which is consistent with the relative intensities of the *N*-methyl signals. The larger olefinic

proton signals correspond to the *E*-amide conformation and show interactions with the opening of the annulus, while the less intense olefinic proton signals of the *Z*-amide isomer do not. The aromatic signals show very weak NOE interactions with the CD "cylinder" and are presumably due to shallow inclusion of the "piston" of the *E*-amide structure at the CD rim. In summary, the hermaphrodite **2.5** in d_6-DMSO forms two conformations, which are illustrated in the top of Figure 2.3.14. The major species weakly interacts with the primary face of the CD and the *Z*/*E*-amide ratio is 1:1.6.

Figure 2.3.12. Sections of the ROESY NMR spectrum (500 MHz) of 1-adamantanol (3-equivalents) and the hermaphrodite **2.4** in D_2O (25 °C) with 0.250 ms mixing time.

29
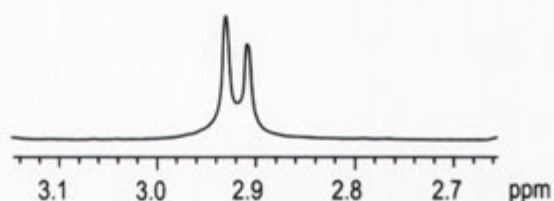
Figure 2.3.13. Section of the ^{1}H NMR spectrum (500 MHz) of the hermaphrodite **2.5** in d_6-DMSO at 25 $^\circ$C.
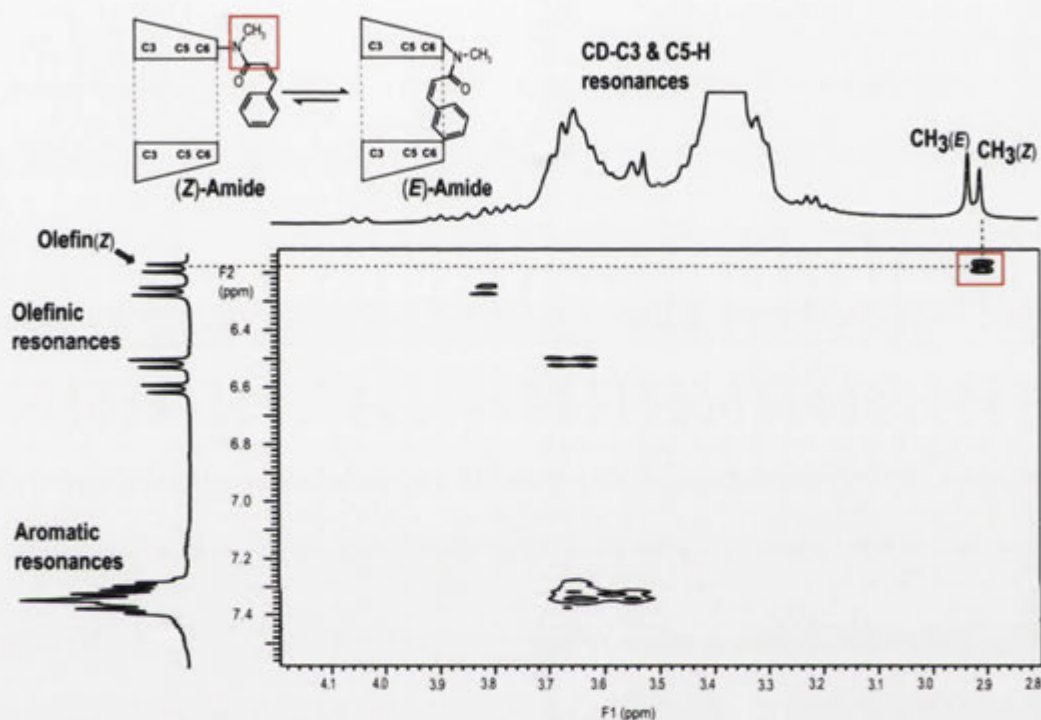
Figure 2.3.14. Section of the ROESY NMR spectrum (500 MHz) of the hermaphrodite **2.5** in d_6-DMSO (25 $^\circ$C) with 0.250 ms mixing time.

Shown in Figure 2.3.15 is the ^{1}H NMR spectrum of the hermaphrodite **2.5** in D$_2$O. In this solvent, the *N*-methyl region of the spectrum shows two methyl proton signals at δ 3.13 and 2.87 ppm in a ratio of about 3.2:1, respectively. In the olefinic region two sets of signals are observed, with the major set of resonances at δ 6.62 and 6.24 ppm and the minor set at δ 6.90 and 6.25 ppm. Also observed are two sets of signals in the aromatic region, with the major set of resonances at δ 7.54 and 7.40 ppm and the minor set at δ 7.49 and 7.25 ppm. The two sets of olefinic and aromatic signals integrate in a ratio consistent with the relative intensities of the *N*-methyl signals and show that two species are present. From the ROESY spectrum (Figure 2.3.16) the less intense methyl signal at δ 2.87 ppm (F1 axis) interacts with the minor olefinic

30

resonance at δ 6.25 ppm (F2 axis) and is therefore assigned to the Z-amide isomer. The minor set of olefinic signals associated with this isomer show no NOE interactions with the CD "cylinder" which suggests they protrude away from the cavity. In contrast the major set of olefinic signals assigned to the E-amide show limited interactions with the CD "cylinder" and therefore extend into the annulus. As the aromatic proton signals of the E-amide also show NOE interactions with the CD "cylinder" these are thought to be interacting at the CD rim as illustrated in the top of Figure 2.3.16. The weak NOE interactions observed between the minor set of aromatic proton signals and the CD resonances suggest that the aryl "piston" also interacts at the rim of the CD "cylinder". In conclusion, the hermaphrodite **2.5** in D$_2$O comprises two species where the aryl "pistons" partially include within the CD "cylinder" and the Z/E-amide ratio is 1:3.2.
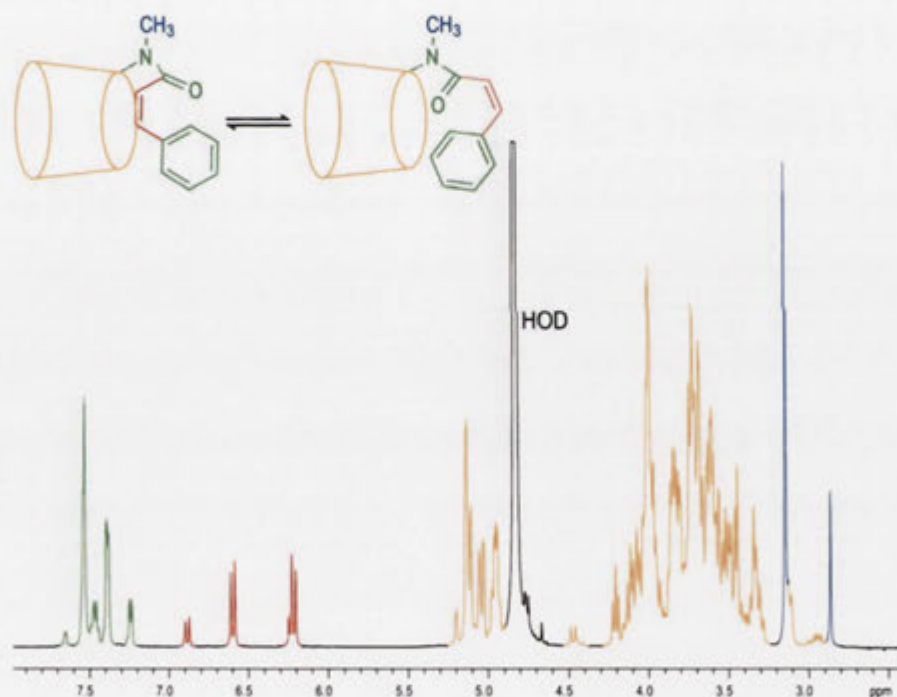
Figure 2.3.15. ^{1}H NMR spectrum (500 MHz) of the hermaphrodite **2.5** in D$_2$O at 25 °C.
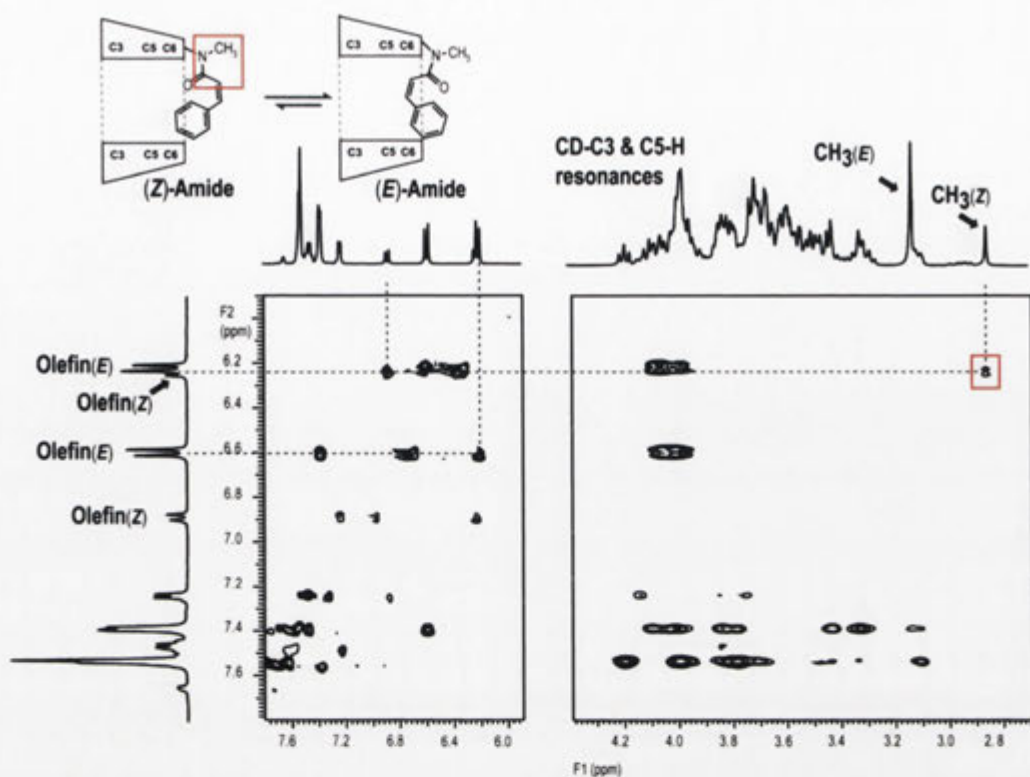
Figure 2.3.16. ROESY NMR spectrum (500 MHz) of the hermaphrodite **2.5** in D₂O (25 °C) with 0.250 ms mixing time.

The ROESY NMR spectrum (Figure 2.3.17) of the hermaphrodite **2.5** in D_2O in the presence of 1-adamantanol "fuel" shows two major proton signals at δ 3.15 and 3.09 ppm that integrate to a ratio of approximately 5.6:1. Neither of the *N*-methyl proton singlets shows NOE interactions with the olefinic signals and accordingly cannot be assigned to an amide isomer on this basis. Nevertheless, the low intensity singlet at δ 3.09 ppm can be assigned to the *Z*-amide from evidence shown later in the Chapter derived through titrations with 1-adamantanol "fuel" (Figure S2).[105] The major set of olefinic protons show NOE interactions with the CD "cylinder" and accordingly extend within the cavity. However, interactions between the aryl "piston" and the 1-adamantanol "fuel" with the CD "cylinder" suggests that more than one species are in equilibrium as illustrated. In summary, the hermaphrodite **2.5** in D_2O with 1-adamantanol "fuel" adopts several conformations with an *Z/E*-amide ratio of 1:5.6, respectively.

To review the conformational analysis of the hermaphrodite **2.5**, in d_6-DMSO the aryl "piston" weakly interacts with the CD "cylinder" and the *Z/E*-amide ratio is 1:1.6.

In D_2O, the aryl "piston" shows interactions with the CD "cylinder" and the Z/E-amide ratio is 1:3.2, respectively. In the presence of 1-adamantanol "fuel" multiple species are in equilibrium and the Z/E-amide ratio is 1:5.6. In d_6-DMSO the aryl "piston" only weakly includes within the CD "cylinder" and there isn't any constraint upon the amide bond. However, in D_2O in the presence of 1-adamantanol "fuel" multiple species are in equilibrium and the aryl "piston" can still interact with the CD "cylinder" to result in some constraint upon the amide bond. This is the reason for the difference observed in the Z/E-amide ratio between d_6-DMSO and D_2O in the presence of 1-adamantanol. However, the similarities between the Z/E-amide ratios for the D_2O and D_2O with 1-adamantanol "fuel" suggest that the inclusion of the aryl group within the CD "cylinder" must be shallow as the competitive guest has little effect upon the orientation of the "piston".
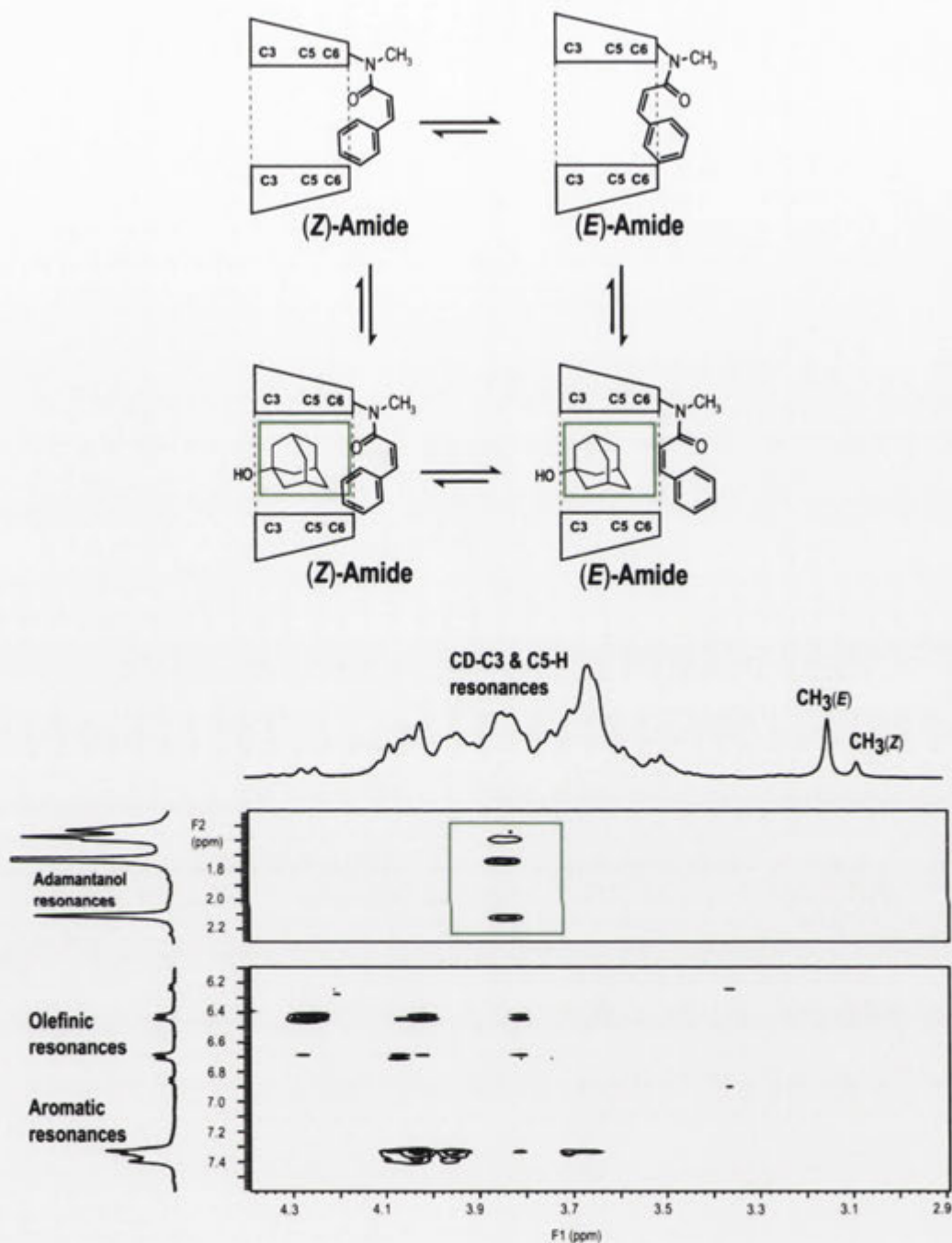
Figure 2.3.17. Sections of the ROESY NMR spectrum (500 MHz) of 1-adamantanol (3-equivalents) and the hermaphrodite **2.5** in D_2O (25 °C) with 0.250 ms mixing time.

## 2.4 Photochemical Switching of Cyclodextrin Based Hermaphrodites

Having prepared the hermaphrodites **2.4** and **2.5**, their conformational properties under various conditions, determined using ^{1}H NMR spectroscopy, showed that the conversion from the hermaphrodite **2.4** to its *cis*-isomer **2.5** resulted in a distinct change in conformational behavior. This is an attribute reminiscent of a molecular machine. On this basis the photochemically induced switching between the hermaphrodites **2.4** and **2.5** was studied (Scheme 2.4.1). Accordingly, the photochemical process was investigated using a combined UV/visible spectroscopic and reverse-phase HPLC strategy, in order to monitor the progression of the photolysis and quantify the resulting products.

In Figure 2.4.1 is the UV/visible spectrum for an aqueous solution of the hermaphrodite **2.4** in H_2O (5.87 x 10^{-5} M) showing a maximum absorption (λ_{MAX}) at 278 nm. This is typical for a *trans*-cinnamic acid[112] and signifies the wavelength of light required for the photochemical isomerisation to its *cis*-isomer with maximum yield. However, the typical λ_{MAX} for a *cis*-cinnamic acid is 258 nm[112] thus its absorption band has considerable overlap with that of the *trans*-isomer at 278 nm. In order to maximise the product yield of *cis*-isomer by selectively irradiating the absorption band of the *trans*-isomer, a light of wavelength > 278 nm was required. Accordingly, a solution of the hermaphrodite **2.4** was irradiated with light of 300 nm wavelength in order to obtain the hermaphrodite **2.5**. Over the course of the photochemical treatment, shown in Figure 2.4.1, the maximum absorbance at 278 nm decreased which corresponded to an increase in the absorption band at lower wavelengths. The photostationary state was reached at approximately 6 minutes however the exposure was continued for an additional two minutes to ensure completion. The photostationary mixture was applied to reverse-phase HPLC monitored at the isosbestic point of 258 nm, which is where the individual components of the mixture have the same molar absorptivity. Analysis of the photostationary mixture showed that the hermaphrodite **2.4** and the *cis*-isomer **2.5** were present in a ratio of 49:51. In order to complete the photoisomerisation cycle and restore the hermaphrodite **2.4**, the photostationary mixture was irradiated with light of 254 nm wavelength. After irradiation for 1 minute the photostationary ratio was 92:8 for the hermaphrodite **2.4** and the *cis*-isomer **2.5**, respectively. The percentage of the hermaphrodite **2.4** present in the solution over three consecutive photoisomerisation

cycles using 300 nm and 254 nm light is shown in Figure 2.4.2. Little decomposition was observed, demonstrating that the hermaphrodite **2.4** is robust enough to undergo multiple cycles of photochemical switching.

i) *hv* 300 nm, H_2O, RT, 6-8 min
ii) *hv* 350 nm, H_2O, RT, 300 min
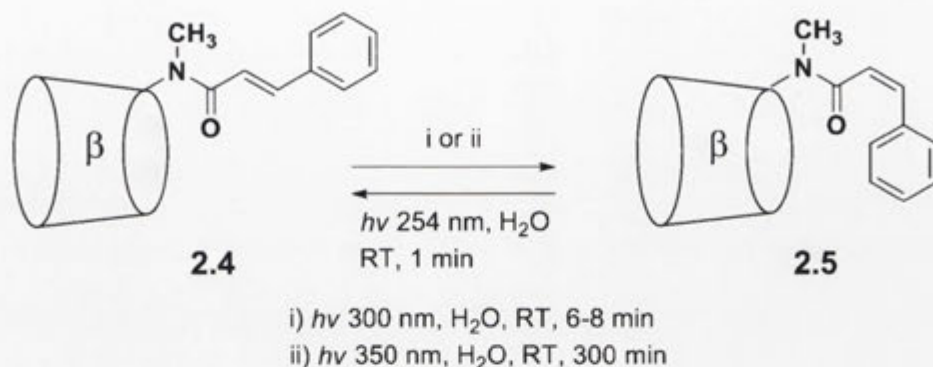
Scheme 2.4.1. Reversible photochemical isomerisation of the hermaphrodite **2.4** and its *cis*-isomer **2.5**.
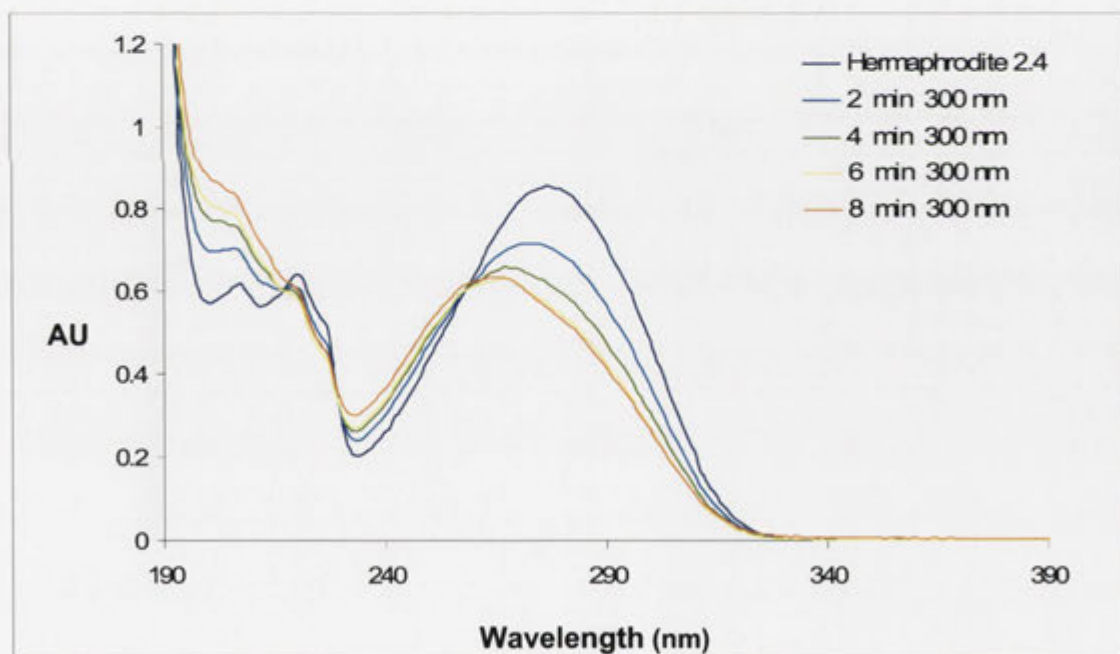
Figure 2.4.1. UV/visible spectra of the hermaphrodite **2.4** (5.87×10^{-5} M) in H_2O and after irradiation with 300 nm light.
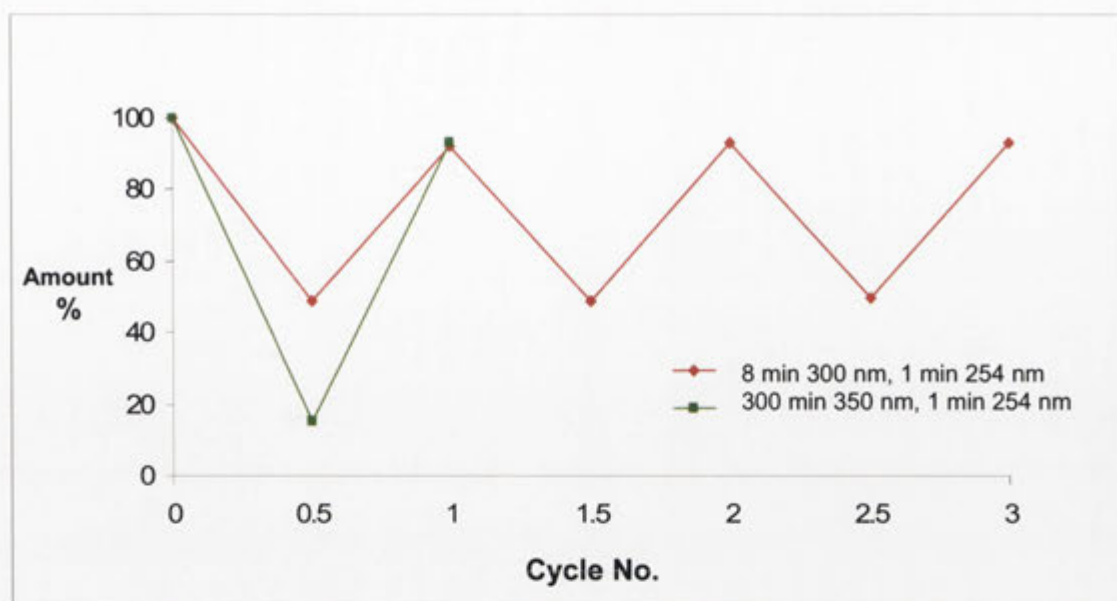
Figure 2.4.2. Amount (%) of the hermaphrodite **2.4** present after photoirradiation as determined by reverse-phase HPLC (258 nm). Each cycle consists of irradiation at 300 nm or 350 nm followed by 254 nm.

In order to improve the yield of the *cis*-isomer **2.5** from the photochemical treatment of the hermaphrodite **2.4**, use of different wavelength light was considered. Accordingly broad spectrum light centered at wavelength 350 nm was used. Shown in Figure 2.4.3 is the UV/visible spectra for the hermaphrodite **2.4** in H_2O (5.87 x 10^{-5} M) upon irradiation using 350 nm light. In this case, the photostationary state was obtained after 300 mins. Using reverse-phase HPLC and monitoring at the isosbestic point of 258 nm, the photostationary mixture contained the hermaphrodite **2.4** and the *cis*-isomer **2.5** in a ratio of 15:85. To restore the hermaphrodite **2.4** and complete the photoisomerisation cycle this photostationary mixture was irradiated with 254 nm light for 1 min, resulting in a photostationary ratio of 92:8 for the hermaphrodite **2.4** and the *cis*-isomer **2.5**. From this, irradiation with 350 nm followed by 254 nm light improved the photochemical switching cycle between the hermaphrodite **2.4** and its *cis*-isomer **2.5** over that using 300 nm light.

In summary, having developed the hermaphrodites **2.3**, **2.4** and **2.5**, their conformational behaviors were found to be different in d_6-DMSO, D_2O and D_2O with 1-adamantanol. These analyses identified conformational differences between the hermaphrodite **2.4** and its *cis*-isomer **2.5**. The photochemical properties of these two

systems were investigated using a combined UV/visible spectroscopic and reverse-phase HPLC strategy in order to establish if their conversion was switchable. The hermaphrodite **2.4** was treated using 300 nm light to obtain its *cis*-isomer **2.5** in a photostationary ratio of 49:51. By comparison, the 350 nm light source afforded an improved photostationary ratio of 15:85 at the expense of an increased exposure time. The reverse process from the hermaphrodite **2.5** to its *trans*-isomer **2.4** using a 254 nm light source afforded the photostationary mixture of 8:92, respectively. It can be concluded that the interconversion between the hermaphrodite **2.4** and its *cis*-isomer **2.5** is photochemically switchable.

Figure 2.4.3. UV/visible spectra of the hermaphrodite **2.4** (5.87×10^{-5} M) in H_2O and after irradiation with 350 nm light.

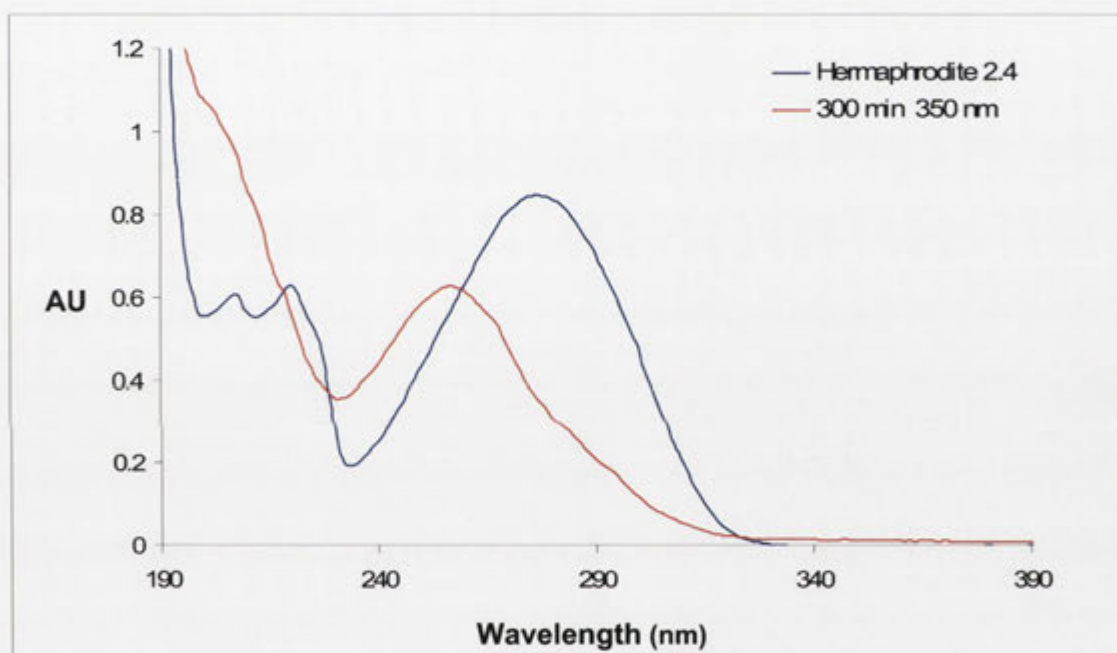## 2.5 Operation of Cyclodextrin Based Hermaphrodites by Changing the Solvent

Having studied the hermaphrodites **2.3**, **2.4** and **2.5**, in d_6-DMSO, D_2O and D_2O with 1-adamantanol distinct differences in their conformational behavior were identified under the various conditions. Described earlier the Z/E-amide ratio reflects the difference between the isomer ground state free energies (ΔG) under a particular set of conditions. The differences in the amide isomer ratios and ground state free energies between the [c1] complex formed in aqueous solution and [a1] complex formed in organic solvent would reflect the work output performed by the molecular recognition process. Accordingly, the operation of the hermaphrodites **2.3**, **2.4** and **2.5** could be investigated by quantifying the work outputs resulting from a change in the solvent from D_2O to d_6-DMSO.

In D_2O the hermaphrodite **2.3** aryl "piston" includes within the CD "cylinder" and the Z/E-amide ratio is 1:25 (Figure 2.5.1, Figure S1).[105] When this amide isomer ratio is applied to the equation $\Delta G = -RT \ln K_{Z/E}$, where ΔG is the ground state free energy difference (kcal mol^{-1}), R is the universal gas constant (1.9872 cal K^{-1} mol^{-1}) and T is the temperature (298 K), a ΔG of 1.9 kcal mol^{-1} is obtained. In d_6-DMSO little interaction was observed between the aryl "piston" and the CD "cylinder" and the Z/E-amide ratio is 1:1.2 resulting in a ΔG of 0.1 kcal mol^{-1}. On this basis, the work performed on the amide bond by changing the solvent is 1.8 kcal mol^{-1} (Figure 2.5.1).
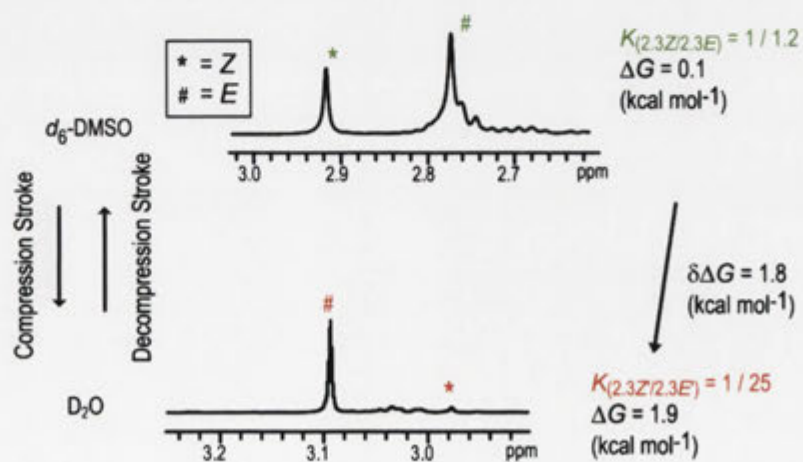
Figure 2.5.1. 500 MHz ^{1}H NMR spectra of the hermaphrodite **2.3** in D_2O and d_6-DMSO.

The hermaphrodite **2.4** in D_2O affords an *Z/E*-amide ratio of 1:100 (Figure 2.5.2, Figure S2)[105] representing a ΔG of 2.7 kcal mol^{-1}. In d_6-DMSO the *Z/E*-amide ratio is 1:1.8, which affords a ΔG of 0.4 kcal mol^{-1}. Hence by changing the polarity of the solvent the hermaphrodite **2.4** performs 2.3 kcal mol^{-1} of work upon the amide bond (Figure 2.5.2).
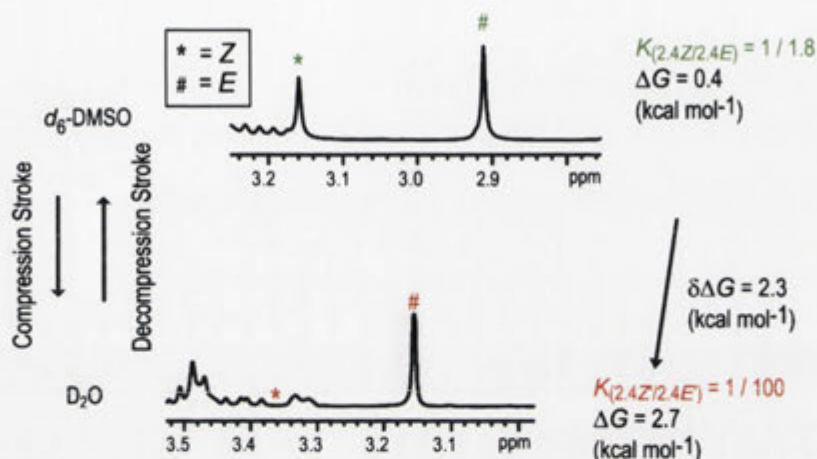
Figure 2.5.2. 500 MHz ^{1}H NMR spectra of the hermaphrodite **2.4** in D_2O and d_6-DMSO.

Finally, the hermaphrodite **2.5** in D_2O affords an *Z/E*-amide ratio of 1:3.2 representing a ground state free energy difference (ΔG) of 0.7 kcal mol^{-1}. In d_6-DMSO the ratio is 1:1.6 for the *Z*-amide and its *E*-isomer affording a ground state free energy difference (ΔG) of 0.3 kcal mol^{-1}. In this case the work performed on the amide bond by the change in solvent polarity is 0.4 kcal mol^{-1} (Figure 2.5.3).
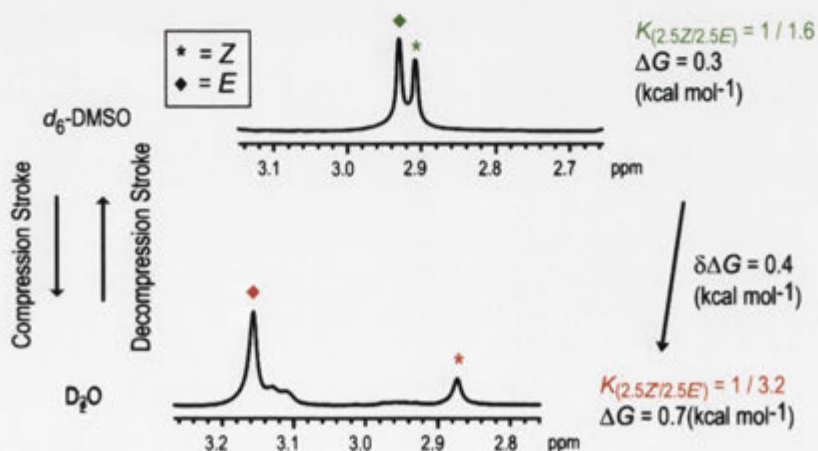
Figure 2.5.3. 500 MHz ^{1}H NMR spectra of the hermaphrodite **2.5** in D_2O and d_6-DMSO.

2.6 Summary of Published Work

The D_2O and d_6-DMSO ^1H NMR spectroscopy results demonstrate from the different conformations and ratios of amide isomers that changing the solvent polarity can drive the operation of the hermaphrodites **2.3**, **2.4** and **2.5**. Alternatively, a better method that doesn't require the solvent to be changed to operate the hermaphrodites **2.3**, **2.4** and **2.5** is with 1-adamantanol "fuel", for which the results are presented in the following paper.[105] The research described demonstrates that an artificial molecular machine can perform a quantifiable work output resulting from molecular recognition which was harnessed to constrain the geometry of an amide bond. The hermaphrodite **2.3** operates as a molecular machine, where the amide group serves as a "torsion bar" to harness the work output resulting from complexation of the aryl substituent by the CD, which behave as the "piston" and "cylinder" of a molecular pump. At 25 °C, after removing the "fuel" 1-adamantanol, the [*c*1] CD complex changes the ratio of the *Z/E*-amide isomers from 1:2.4 to 1:25, on which basis the work performed on the amide bond is calculated to be 1.4 kcal mol^{-1}. The hermaphrodite **2.4** and its *cis*-isomer **2.5** function as a more sophisticated version of the machine, with the alkene moiety fortuitously serving as a photochemical "ON/OFF" switch. Irradiation at 300 nm converts the *trans*-cinnamide **2.4** to the *cis*-isomer **2.5**, while the reverse process occurs at 254 nm. For the *cis*-isomer **2.5** there is little interaction of the aryl "piston" with the CD "cylinder", so the machine is turned "OFF". By contrast, complexation of the aryl substituent by the CD occurs with the *trans*-hermaphrodite **2.4** and changes the ratio of the *Z/E*-amide isomers from 1:2.6 to 1:100. Consequently, in this mode the machine is turned "ON" and the work harnessed by the amide bond is 2.1 kcal mol^{-1}. Importantly, this is one of the few examples where the work output of an artificial molecular machine has been quantified. Having discussed the preparation of the hermaphrodites **2.3**, **2.4** and **2.5**, their conformational behaviors in d_6-DMSO, D_2O with 1-adamantanol and D_2O alone, their photochemical switching properties and their operation by a change the solvent in the preceding sections **2.2-2.5**, all of the research necessary for the understanding of this paper has been discussed. Following is the Communication and Supplementary Information as it appeared in published form.

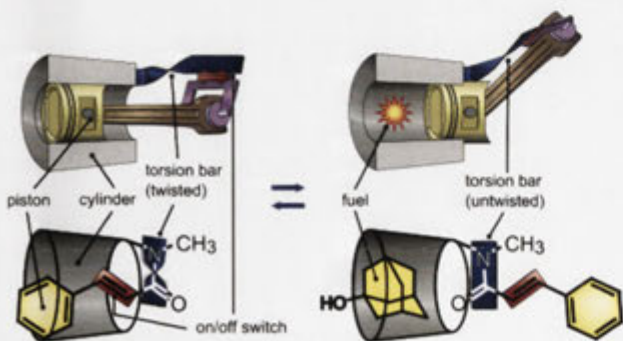# Harnessing the Energy of Molecular Recognition in a Nanomachine Having a Photochemical On/Off Switch

Roger J. Coulston,[†] Hideki Onagi,[†] Stephen F. Lincoln,[‡] and Christopher J. Easton[*,†,§]

Research School of Chemistry, Australian National University, Canberra ACT 0200, Australia, School of Chemistry and Physics, University of Adelaide, Adelaide SA 5005, Australia, and ARC Centre of Excellence in Free Radical Chemistry and Biotechnology

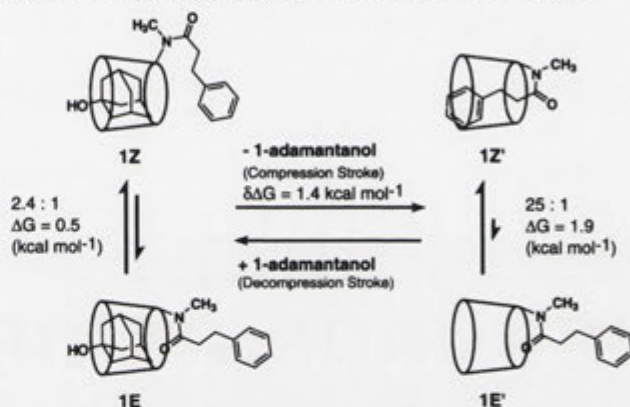Received July 19, 2006; E-mail: easton@rsc.anu.edu.au

The literal definition of a machine is an apparatus consisting of interrelated parts with separate functions and used in the performance of some kind of work. With molecular machines, the work involves regulating molecular motions and occurs in response to external stimuli which may be either chemical, thermal, or photochemical.[1–4] A stimulus initially produces a system that is out of equilibrium and, as equilibration occurs, work is done.[3] This is illustrated by molecular shuttles,[4] where a stimulus changes the balance of the molecular recognition events to destabilize the original conformation and cause the components to move. Here we report a molecular machine where the work output resulting from molecular recognition is harnessed to constrain the geometry of an amide bond, and the apparent work performed in this process is quantified. Further, a more advanced form of the device exists as two isomers that are interconverted photochemically. Only one of the isomers exhibits the molecular recognition and performs the work, so the photoisomerization turns the machine on and off.

The molecular machine is illustrated in Figure 1 and its operation is shown in Schemes 1 and 2. The basic form **1** (Scheme 1) comprises an aryl substituent attached to β-cyclodextrin. These behave as the piston and cylinder, respectively, of a molecular pump. The pump is fueled by 1-adamantanol. The compression stroke of the piston involves intramolecular complexation of the aryl substituent within the cyclodextrin annulus in water, in response to using hexane to extract the competitive guest, 1-adamantanol, from the aqueous solution and therefore from the cyclodextrin cavity. This molecular recognition process provides strain energy to alter the ratio of the (E)- and (Z)-isomers of the amide group linking the cyclodextrin to the phenyl substituent, which therefore serves as a torsion bar. The decompression piston stroke simply involves the addition of 1-adamantanol with the reverse consequences.

Figure 1. Schematic representation of a mechanical machine and its molecular counterpart.

† Australian National University.
‡ University of Adelaide.
§ ARC Centre of Excellence in Free Radical Chemistry and Biotechnology.

Scheme 1. Operation of 6^A-Deoxy-6^A-(N-methyl-3-phenylpropionamido)-β-cyclodextrin **1** as a Molecular Machine

The conformations of the machine **1** were determined in D_2O at 25 °C, primarily using 2D ^{1}H NMR spectroscopy. This included distinguishing between the amide (Z)- and (E)-isomers **1Z** and **1E**, and **1Z′** and **1E′**, and the phenyl substituent when free and included in the cyclodextrin, as well as precluding the formation of dimeric Janus complexes.[5] The methyl group was incorporated into the machine as a convenient handle for analysis, and the isomer ratios were calculated by integrating the corresponding signals for those protons in 1D ^{1}H NMR spectra. In the presence of 1-adamantanol, when the phenyl substituent is not complexed, the (Z)-isomer **1Z** is in excess only by a ratio of 2.4:1. Complexation of the aryl group by the cyclodextrin through removal of the 1-adamantanol causes a more than 10-fold increase in the proportion of the (Z)-isomer **1Z′**, to a ratio of 25:1.

Under any particular set of conditions, the ratio of amide isomers reflects the difference in their ground state free energies (ΔG),[6] and the alteration in the ratio resulting from a change in conditions reflects the work performed on the amide bond ($\delta\Delta G$).[7] The difference between the ratios of the isomers **1Z** and **1E**, and **1Z′** and **1E′**, in water containing 1-adamantanol, and in water alone, is directly attributable to the cyclodextrin–phenyl group host–guest interaction. These ratios correspond to ΔG values of 0.5 and 1.9 kcal mol^{-1}, respectively, on which basis the energy apparently harnessed by the amide torsion bar as a result of the extraction of 1-adamantanol and the consequent inclusion complex formation is $\delta\Delta G = 1.4$ kcal mol^{-1}.

In the more advanced version of the machine, shown in Scheme 2, the alkene moiety between the phenyl substituent and the amide group serves as a photochemical on/off switch. Irradiation at 300 nm converts the trans cinnamide **2** to the cis isomer **3**, while the reverse process occurs at 254 nm.[8] The ratios of the amide isomers of **2** and **3** were determined under the conditions and in the manner described above for **1**. The ratio of the isomers **3Z** and **3E** of

Scheme 2. Operation of *trans*-6^A^-Deoxy-6^A^-(N-methylcinnamido)-β-cyclodextrin **2** and the Cis Isomer **3** as a Molecular Machine Having a Photochemical On/Off Switch

different conformations and ratios of the amide isomers in DMSO and water without 1-adamantol, that changing the solvent in this way, and vice versa, drives these molecular machines in a similar manner to the addition and removal of 1-adamantanol to aqueous solutions.

In summary, the apparatus illustrated in Figure 1 and exemplified by the cyclodextrin derivatives **1–3** constitutes a molecular machine where the output energy of molecular recognition is harnessed to do work and constrain the geometry of an amide bond. In the case of the cinnamides **2** and **3**, their photoisomerization provides the machine's on/off switch. The apparent work performed on the amide bond is 1.4, 2.1, and −0.2 kcal mol^{-1}, with the propionamide **1**, and the cinnamides **2** and **3**, respectively. This demonstration that work output can be harnessed and quantified in such molecular devices takes us one step closer to their practical application.

Supporting Information Available: Details for the synthesis of **1–3** and their operation as molecular machines. This material is available free of charge via the Internet at http://pubs.acs.org.

References

(1) For reviews on molecular machines, see (a) Stoddart, J. F. *Acc. Chem. Res.* **2001**, *34*, 409–522. (b) *Molecular Switches*; Feringa, B. L., Ed.; Wiley-VCH: Weinheim, Germany, 2001. (c) Feringa, B. L.; Koumura, N.; van Delden, R. A.; ter Wiel, M. K. J. *Appl. Phys. A* **2002**, *75*, 301–308. (d) Balzani, V.; Venturi, M.; Credi, A. *Molecular Devices and Machines: A Journey into the Nanoworld*; Wiley-VCH: Weinheim, Germany, 2003. (e) Easton, C. J.; Lincoln, S. F.; Barr, L.; Onagi, H. *Chem.—Eur. J.* **2004**, *10*, 3120–3128. (f) Kelly, T. R. *Top. Curr. Chem.* **2005**, *262*, 1–227. (g) Khuong, T.-A. V.; Nunez, J. E.; Godinez, C. E.; Garcia-Garibay, M. A. *Acc. Chem. Res.* **2006**, *39*, 413–422.

(2) For some recent examples of molecular machines, see (a) Morin, J.-F.; Shirai, Y.; Tour, J. M. *Org. Lett.* **2006**, *8*, 1713–1716. (b) Eelkema, R.; Pollard, M. M.; Vicario, J.; Katsonis, N.; Ramon, B. S.; Bastiaansen, C. W. M.; Broer, D. J.; Feringa, B. L. *Nature* **2006**, *440*, 163. (c) Berná, J.; Leigh, D. A.; Lubomska, M.; Mendoza, S. M.; Pérez, E. M.; Rudolf, P.; Teobaldi, G.; Zerbetto, F. *Nat. Mater.* **2005**, *4*, 704–710. (d) Carella, A.; Rapenne, G.; Launay, J.-P. *New J. Chem.* **2005**, *29*, 288–290. (e) Scarso, A.; Onagi, H.; Rebek, J., Jr. *J. Am. Chem. Soc.* **2004**, *126*, 12728–12729. (f) Onagi, H.; Blake, C. J.; Easton, C. J.; Lincoln, S. F. *Chem.—Eur. J.* **2003**, *9*, 5978–5988.

(3) For detailed discussions of such processes in the context of supramolecular chemistry, see (a) Chatterjee, M. N.; Kay, E. R.; Leigh, D. A. *J. Am. Chem. Soc.* **2006**, *128*, 4058–4073. (b) Kay, E. R.; Leigh, D. A. *Nature* **2006**, *440*, 286–287. (c) Balzani, V.; Clemente-León, M.; Credi, A.; Ferrer, B.; Venturi, M.; Flood, A. H.; Stoddart, J. F. *Proc. Natl. Acad. Sci. U.S.A.* **2006**, *103*, 1178–1183.

(4) (a) Anelli, P. L.; Spencer, N.; Stoddart, J. F. *J. Am. Chem. Soc.* **1991**, *113*, 5131–5133. (b) Murakami, H.; Kawabuchi, A.; Kotoo, K.; Kunitake, M.; Nakashima, N. *J. Am. Chem. Soc.* **1997**, *119*, 7605–7606. (c) Lane, A. S.; Leigh, D. A.; Murphy, A. *J. Am. Chem. Soc.* **1997**, *119*, 11092–11093. (d) Armaroli, N.; Balzani, V.; Collin, J.-P.; Gaviña, P.; Sauvage, J.-P.; Ventura, B. *J. Am. Chem. Soc.* **1999**, *121*, 4397–4408. Also see the extensive list of references cited in 3a.

(5) (a) Onagi, H.; Easton, C. J.; Lincoln, S. F. *Org. Lett.* **2001**, *3*, 1041–1044. (b) Miyauchi, M.; Takashima, Y.; Yamaguchi, H.; Harada, A. *J. Am. Chem. Soc.* **2005**, *127*, 2984–2989. (c) Miyauchi, M.; Hoshino, T.; Yamaguchi, H.; Kamitori, S.; Harada, A. *J. Am. Chem. Soc.* **2005**, *127*, 2034–2035.

(6) Thomas, K. M.; Naduthambi, D.; Zondlo, N. J. *J. Am. Chem. Soc.* **2006**, *128*, 2216–2217.

(7) The work performed to stabilize the amide (Z)-isomer is the inverse of the apparent stability and increase in proportion of that isomer. Therefore the ΔG and $\delta\Delta G$ values are calculated from the inverse of the amide (Z)-/(E)-isomer ratios.

(8) Irradiation of the trans alkene **2** at 300 nm affords a 1:9 mixture of **2** and **3** in the photostationary state, from which the cis isomer **3** was isolated using HPLC. Irradiation of the cis isomer at 254 nm affords a 1:1 mixture of **2** and **3**. The efficiency of the photoreversion is limited by the overlapping absorptions of **2** and **3** at this wavelength. Sources of lower wavelength light that might be more effective are not readily available.

(9) Easton, C. J.; Lincoln, S. F. *Modified Cyclodextrins: Scaffolds and Templates for Supramolecular Chemistry*; Imperial College Press: London, 1999.

JA0651761

5.6:1, found when 1-adamantanol is present in the mixture, is very similar to that of **3Z'** and **3E'** of 4.2:1, measured in the absence of the competitive guest. This is consistent with the NMR spectra recorded for this system, which show little interaction of the phenyl group with the cyclodextrin cavity, irrespective of the presence of 1-adamantanol. The small difference between the ΔG values for the isomers **3Z** and **3E** (1.0 kcal mol^{-1}), and **3Z'** and **3E'** (0.8 kcal mol^{-1}), shows a corresponding lack of work on the amide bond ($\delta\Delta G = -0.2$ kcal mol^{-1}). Thus the cis double bond prevents the host–guest interaction and in that mode the machine is turned off. By contrast, the ratio of the trans cinnamide amide isomers **2Z'** and **2E'** in water alone (100:1) is much greater than that of **2Z** and **2E** in water containing 1-adamantanol (2.6:1). The increase is attributable to removal of 1-adamantanol causing complexation of the aryl substituent by the cyclodextrin, as observed in NMR spectra. In this case the energy harnessed by the amide bond, as calculated from the difference between the ΔG values for the isomers in the presence of 1-adamantanol (0.6 kcal mol^{-1}) and in its absence (2.7 kcal mol^{-1}), is $\delta\Delta G = 2.1$ kcal mol^{-1}. It follows that the trans alkene moiety allows complexation, and in this mode the machine is turned on.

The conformations of the cyclodextrin derivatives **1–3** were also examined in d_6-DMSO. The NMR spectra show that in this solvent there is little interaction of the aryl substituent with the cyclodextrin cavity, consistent with there being no driving force for the inclusion.[9] As expected on this basis, the ratios of the (Z)- and (E)-amide isomers in DMSO were found to be remarkably similar to those in water containing 1-adamantanol. It follows from the

Harnessing the Energy of Molecular Recognition in a Nanomachine Having a Photochemical On/Off Switch

Roger J. Coulston,[1] Hideki Onagi,[1] Stephen F. Lincoln[2] and Christopher J. Easton[1,3]*

[1]Research School of Chemistry, Australian National University, Canberra ACT 0200, Australia, [2]School of Chemistry and Physics, University of Adelaide, Adelaide SA 5005, Australia and [3]ARC Centre of Excellence in Free Radical Chemistry and Biotechnology

E-mail: easton@rsc.anu.edu.au

Supporting Information

1. GENERAL EXPERIMENTAL

^{1}H NMR spectra were recorded using a Varian Inova 500 spectrometer. d_6-Dimethyl sulfoxide (d_6-DMSO) with an isotopic purity of 99.9% and deuterium oxide (D_2O) with an isotopic purity of 99.75% were purchased from Cambridge Isotope Laboratories Inc., MA. Electrospray ionization (ESI) low-resolution mass spectra (LRMS) were recorded using a Micromass VG Quattro II triple quadrupole mass spectrometer. ESI high-resolution mass spectra (HRMS) were obtained with a Bruker Apex 4.7T FTICR-MS mass spectrometer. The Microanalytical Laboratory of The Australian National University carried out the elemental analyses. Ultraviolet spectra were recorded using a Shimadzu UV-2101PC UV-VIS scanning spectrophotometer. Thin-layer chromatography (TLC) was performed on Kieselgel 60 F_{254} coated plates (Merck Chemical Co.). Developed plates were visualized using ultraviolet light and/or by dipping into a solution of 0.1% naphthalene-1,3-diol in 200:157:43 v/v/v EtOH–water–H_2SO_4 followed by heating with a heat-gun. HPLC was carried out using a Waters Alliance Separation Module 2690 with a Waters 996 photodiode array detector. HPLC grade mobile phase solvents were purchased from LabScan Asia, Bangkok, Thailand. Ultrapure water (resistivity >15 MΩ cm^{-1}) was prepared using a Milli-Q$^{®}$ reagent system. Photochemical experiments were performed using a Luzchem LZC-ORG photolysis reactor (Luzchem Research Inc., Ottawa, Canada). Melting points were determined on a Kofler hot stage melting point apparatus under a Reichert microscope. β-Cyclodextrin (99.1% purity) was purchased from Nihon Shokuhin Kako Co., Japan, and recrystallized from water then dried *in vacuo* over P_2O_5 to constant weight before use. (*E*)-Cinnamoyl chloride (>98%), hydrocinnamoyl chloride (>98%), methylamine (2 M in THF), anhydrous 1-methyl-2-pyrrolidinone (NMP) and anhydrous *N,N*-dimethylformamide (DMF) were purchased from Sigma-Aldrich Chem. Co. Toyopearl SP-650M cation-exchange and DEAE-650M anion-exchange resins were purchased through Supelco, PA.

2. SYNTHETIC PROCEDURES

2.1 Synthetic schemes

Scheme S1. Preparation of the amino-substituted β-cyclodextrin **S2**
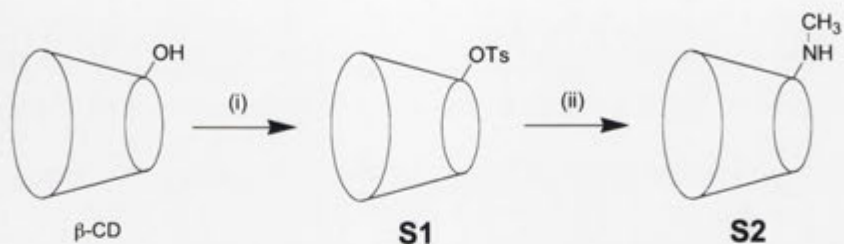
i) *p*-Toluenesulfonyl chloride, NaOH, water, RT, 5 h, 45%; ii) 2M Methylamine in THF, KI, dry NMP, 80 °C, 42 h, 23%.

Scheme S2. Preparation of the molecular machines **1-3**
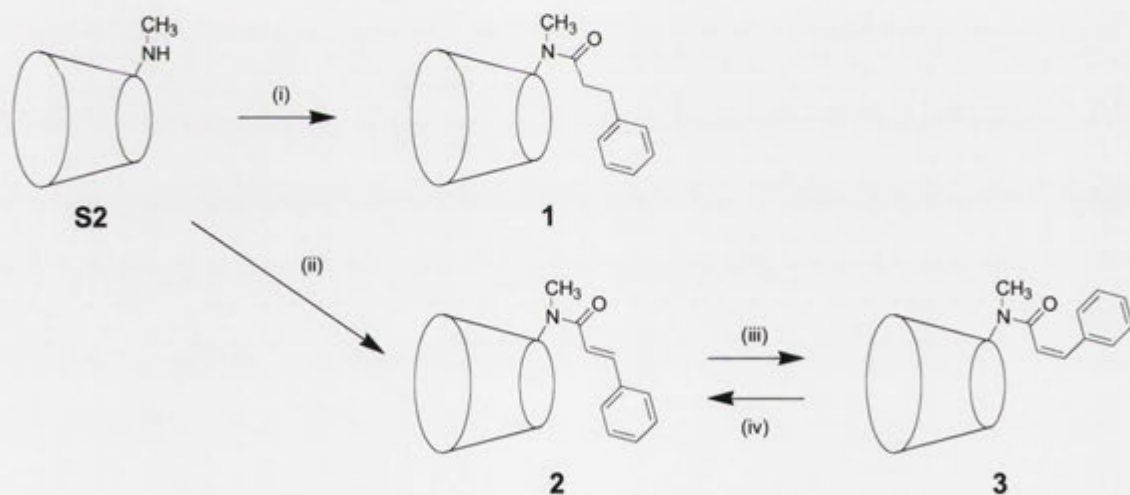
i) Hydrocinnamoyl chloride, triethylamine, dry DMF, –5 °C then RT, 6 h, 60%; ii) (*E*)-Cinnamoyl chloride, triethylamine, dry DMF, –5 °C then RT, 6 h, 12%; iii) *hv* 300 nm, water, RT, 2.5 h, 32%; iv) *hv* 254 nm, water, RT.

2.2 Syntheses

6^A-O-p-Toluenesulfonyl-β-cyclodextrin (S1)

Prepared as described by Byun, Zhong and Bittman,[S1] with physical and spectral properties consistent with those reported.

TLC R_f: 0.55, n-BuOH/EtOH/H$_2$O 5:4:3.

^{1}H NMR (500 MHz, d_6-DMSO) δ: 7.78 (d, 2H, J = 8.5 Hz, Ar), 7.46 (d, 2H, J = 8.5 Hz, Ar), 5.82–5.68 (m, 14H), 4.86 (br s, 4H), 4.78 (br s, 2H), 4.55–4.47 (m, 5H), 4.40 (m, 2H), 4.33 (m, 1H), 4.20 (m, 1H), 3.67–3.23 (m), 2.45 (s, 3H, CH$_3$) ppm.

LRMS (ESI) m/z (%): 1311 (100) [M+Na]$^+$.

6^A-Deoxy-6^A-methylamino-β-cyclodextrin (S2)

6^A-O-p-Toluenesulfonyl-β-cyclodextrin **S1** (3.0 g, 2.32 mmol), KI (41 mg, 0.25 mmol) and a solution of methylamine in THF (2M, 5.8 mL, 11.6 mmol) were combined in anhydrous NMP[S2] (8 mL), and the mixture was heated at 80 °C for 42 h, with the periodic addition of further 3 mL aliquots of the methylamine solution at 6, 19 and 24 h. The resulting solution was cooled and added dropwise to vigorously stirred acetone (360 mL). The resultant precipitate was separated and washed with acetone, before it was applied to Toyopearl SP-650M cation exchange resin. The eluant was concentrated to dryness to give the title compound **S2** as a colorless solid (0.61 g, 23%), with physical and spectral properties consistent with those reported.[S3]

TLC R_f: 0.42, i-PrOH/EtOH/H$_2$O/AcOH 5:4:3:2.

^{1}H NMR (500 MHz, d_6-DMSO) δ: 5.80–5.66 (m, 14H), 4.82–4.80 (m, 7H), 4.51–4.43 (m, 6H), 3.67–3.55 (m, 28H), 3.34–3.29 (m, 14H), 2.83–2.63 (m, 2H), 2.24 (s, 3H, CH$_3$) ppm.

LRMS (ESI) m/z (%): 1148 (100) [M+H]$^+$.

6^A-Deoxy-6^A-(N-methyl-3-phenylpropionamido)-β-cyclodextrin (1)

The amine **S2** (100 mg, 87 μmol) and triethylamine (50 μL) were dissolved in anhydrous DMF (3 mL) at –5 °C. Hydrocinnamoyl chloride (18 mg, 0.10 mmol) was

then added and the mixture was allowed to warm to room temperature and stirred for 6 h. H_2O (2 mL) was then added and the resulting solution was added dropwise to vigorously stirred acetone (150 mL). The resultant precipitate was separated and applied to Toyopearl DEAE-650M anion-exchange resin, and then Toyopearl SP-650M cation-exchange resin. The eluant was concentrated to dryness to give the title compound **1** as a colorless powder (67 mg, 60%).

mp 295–297 °C decomposed.

TLC R_f: 0.38, *n*-BuOH/EtOH/H_2O 5:4:3.

^{1}H NMR (500 MHz, D_2O) δ: 7.54 (t, 2H, J = 7.5 Hz, Ar), 7.46 (t, 1H, J = 7.5 Hz, Ar), 7.26 (d, 2H, J = 7.5 Hz, Ar), 5.11–5.01 (m, 7H), 4.28 (m, 1H), 4.05–3.31 (m, 41H), 3.09 (s, 3H, CH_3), 3.03 (m, 1H), 2.64 (m, 3H) ppm. In addition a low intensity singlet was observed at δ 2.98 ppm for the methyl group of the amide (*E*)-isomer.

LRMS (ESI) *m/z* (%): 1303 (100) $[M+Na]^+$, 1281 (20) $[M+H]^+$; **HRMS (ESI)** found 1280.4672. Calculated *m/z* for $C_{52}H_{82}NO_{35}$ (M+H) 1280.4667.

Elemental analysis Found C, 43.91; H, 6.78; N, 0.88%. $C_{52}H_{81}NO_{35}\cdot 8H_2O$ requires C, 43.85%; H, 6.86%; N, 0.98%.

HPLC t_R 3.8 min. [Column: YMC ODS-AQ, 250 × 10 mm; MeCN/H_2O (15/85), flow rate: 3 mL min^{-1}].

trans-6^A-Deoxy-6^A-(*N*-methylcinnamido)-β-cyclodextrin (2)

The amine **S2** (150 mg, 0.13 mmol) and triethylamine (30 μL) were dissolved in anhydrous DMF (10 mL) at –5 °C. *trans*-Cinnamoyl chloride (30 mg, 0.17 mmol) was then added and the mixture was allowed to warm to room temperature and stirred for 6 h. H_2O (1 mL) was then added and the resulting solution was added dropwise to vigorously stirred acetone (150 mL). The resultant precipitate was separated and washed with acetone (3 × 50 mL) and diethyl ether (2 × 50 mL), before it was applied to Toyopearl DEAE-650M anion-exchange resin, and then Toyopearl SP-650M cation-exchange resin. The eluant was concentrated to dryness to give the title compound **2** as a colorless powder (20 mg, 12%). This procedure has not been optimized.

mp 288–290 °C decomposed.

TLC R_f: 0.34, *n*-BuOH/EtOH/H$_2$O 5:4:3.

^{1}H NMR (500 MHz, D$_2$O) δ: 7.67–7.65 (m, 3H, Ar), 7.55–7.49 (m, 2H, Ar), 7.27 (d, 1H, J = 16.0 Hz, CH), 6.91 (d, 1H, J = 16.0 Hz, CH), 5.20 (d, 1H, J = 3.5 Hz), 5.14 (d, 1H, J = 3.2 Hz), 5.09 (m, 2H), 5.01 (d, 1H, J = 3.3 Hz), 4.98 (m, 2H), 4.45–3.31 (m, 42H), 3.15 (s, 3H, CH$_3$) ppm. In addition a very low intensity singlet was observed at δ 3.36 ppm for the methyl group of the amide (*E*)-isomer.

LRMS (ESI) *m/z* (%): 1301 (60) [M+Na]$^+$, 1279 (20) [M+H]$^+$; **HRMS (ESI)** found 1278.4521. Calculated *m/z* for C$_{52}$H$_{80}$NO$_{35}$ (M+H) is 1278.4510.

Elemental analysis Found C, 41.48; H, 6.69; N, 1.06%. C$_{52}$H$_{79}$NO$_{35}$·12H$_2$O requires C, 41.79%; H, 6.95%; N, 0.94%.

λ_{MAX}: 278 nm; ε: 15,825 M^{-1} cm^{-1} (H$_2$O).

HPLC t_R 10.8 min. [Column: Alltech Alltima C18, 250 × 10 mm; MeCN/H$_2$O (10/90), flow rate: 3 mL min^{-1}].

cis-6^A-Deoxy-6^A-(*N*-methylcinnamido)-β-cyclodextrin (3)

trans-6^A-Deoxy-6^A-(*N*-methylcinnamido)-β-cyclodextrin **2** (19 mg, 15 µmol) was dissolved in H$_2$O (20 mL), in a quartz round-bottom flask, and the solution was irradiated at 300 nm for 2.5 h, then it was concentrated to dryness. HPLC of the residue afforded the title compound **3** as a colorless solid (6 mg, 32%).

mp 279–285 °C decomposed.

TLC R_f: 0.30, *n*-BuOH/EtOH/H$_2$O 5:4:3.

^{1}H NMR (500 MHz, D$_2$O) δ: 7.67 (m, 0.2 × 1H, Ar), 7.54 (m, 0.8 × 3H, Ar), 7.49 (m, 0.2 × 2H, Ar), 7.40 (m, 0.8 × 2H, Ar), 7.25 (m, 0.2 × 2H, Ar), 6.90 (d, 0.2 × 1H, J = 11.0 Hz, CH), 6.60 (d, 0.8 × 1H, J = 13.0 Hz, CH), 6.25 (d, 0.2 × 1H, J = 11.0 Hz, CH), 6.23 (d, 0.8 × 1H, J = 13.0 Hz, CH), 5.2–4.5 (m), 4.2–3.3 (m), 3.16 (s, 0.8 × 3H, CH$_3$), 3.13 (m), 2.87 (s, 0.2 × 3H, CH$_3$) ppm.

LRMS (ESI) *m/z* (%): 1301 (50) [M+Na]$^+$; **HRMS (ESI)** found 1278.4506. Calculated *m/z* for C$_{52}$H$_{80}$NO$_{35}$ (M+H) is 1278.4510.

Elemental analysis Found C, 42.86; H, 6.52; N, 1.08%. C$_{52}$H$_{79}$NO$_{35}$·10H$_2$O requires C 42.83; H, 6.84; N, 0.96%.

λ_{MAX}: 255 nm; ε: 5,167 M^{-1} cm^{-1} (H_2O).

**HPLC** t_R 16.1 min. [Column: Alltech Alltima C18, 250 × 10 mm; MeCN/H_2O (10/90), flow rate: 3 mL min^{-1}].

3. OPERATION OF THE MOLECULAR MACHINES 1–3

3.1. Operation of 6^A-deoxy-6^A-(*N*-methyl-3-phenylpropionamido)-β-cyclodextrin 1 as a molecular machine

Figure S1 illustrates the operation of 6^A-deoxy-6^A-(*N*-methyl-3-phenylpropionamido)-β-cyclodextrin **1** (3 mg, 2.3 µmol) as a molecular machine in D$_2$O (700 µL) at 25 °C. In the absence of 1-adamantanol, the ^{1}H NMR spectrum shows that the amide (*E*)- and (*Z*)-isomers **1E'** and **1Z'** are present in the ratio 1:25. The difference in their ground state free energies, calculated according to equation 1, is therefore ΔG = 1.9 kcal mol^{-1}.

$$\Delta G = -RT \ln K_{(E/Z)} \qquad \qquad \text{(Equation 1)}$$

Sequential addition of aliquots (5 × 20 µL, 5 × 0.46 µmol, to 1 equiv., and then 4 × 50 µL, 4 × 1.15 µmol, to 3 equiv.) of a solution of 1-adamantanol (3.5 mg, 23 µmol) in D$_2$O (1 mL) afforded spectra showing that the ratio of the isomers changes with increasing concentration of 1-adamantanol. In the final solution, the ratio of the amide isomers **1E** and **1Z** is 1:2.4, corresponding to ΔG = 0.5 kcal mol^{-1}. On this basis the work performed on the amide bond equals δΔG = 1.9 – 0.5 = 1.4 kcal mol^{-1}.
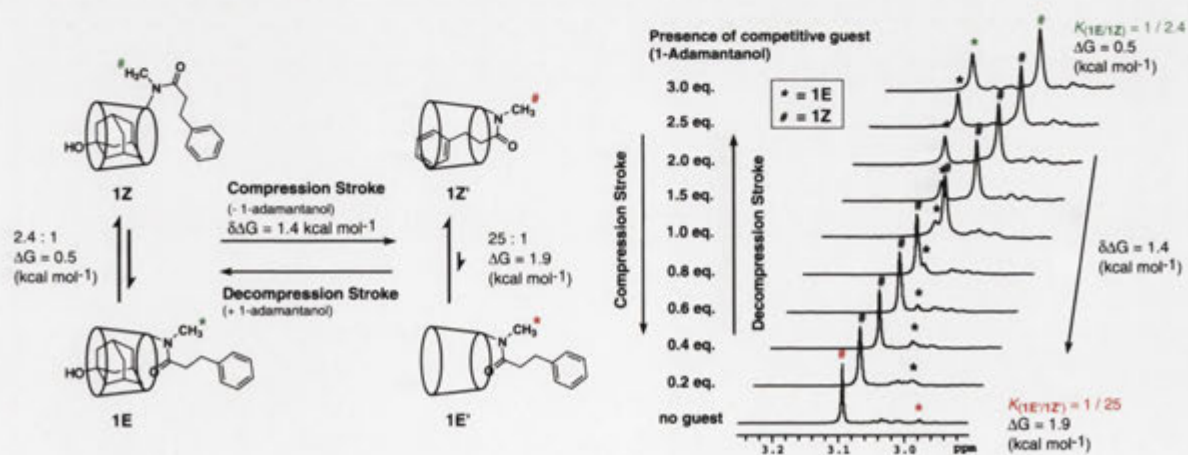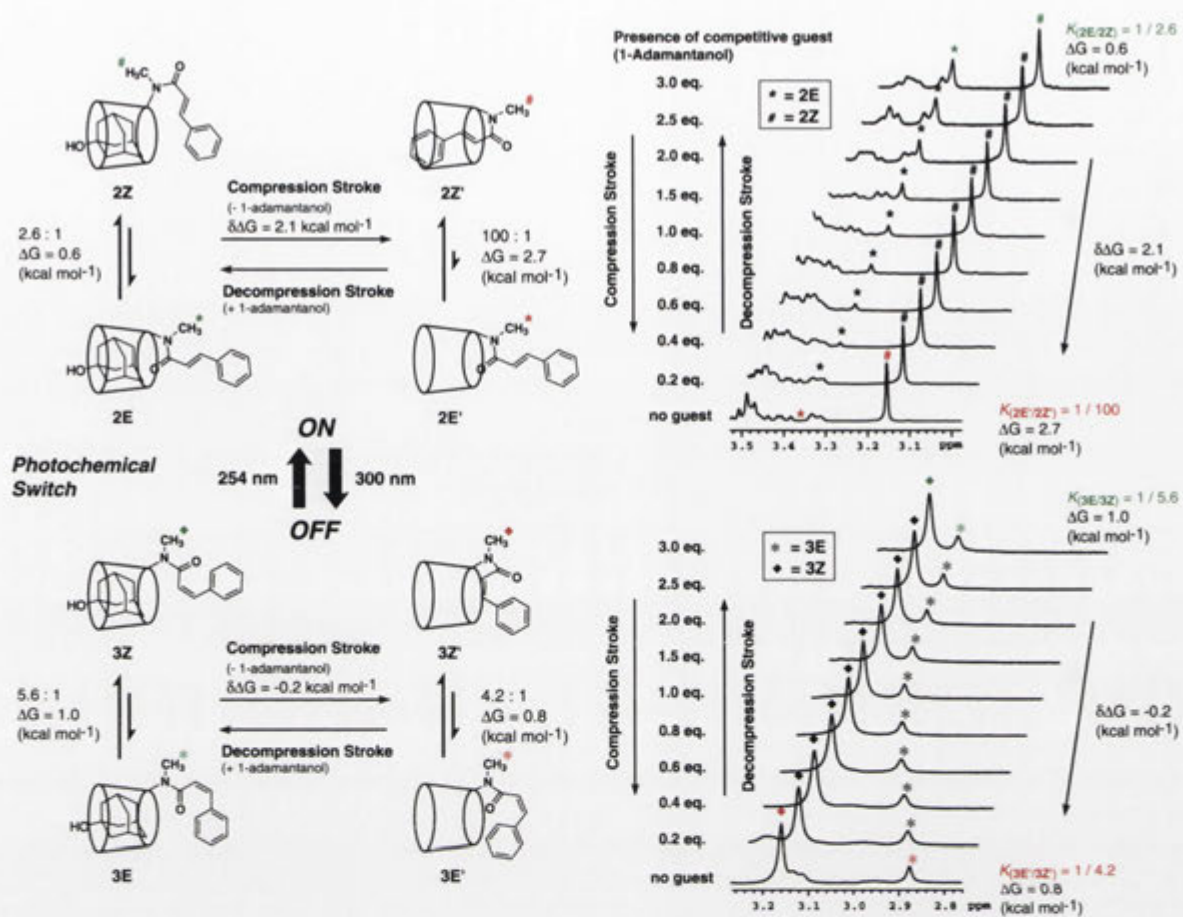

Figure S1. Operation of 6^A-deoxy-6^A-(*N*-methyl-3-phenylpropionamido)-β-cyclodextrin **1** as a molecular machine in D$_2$O at 25 °C (left) and 500 MHz ^{1}H NMR spectra of aqueous solutions of **1** containing various concentrations of 1-adamantanol (right). Sequential spectra are offset for clarity.

The process is completely reversible. Washing solutions containing 1-adamantanol with *n*-hexane (7 × 1 mL) and then removing the residual *n*-hexane under reduced pressure affords the original 1:25 mixture of the amide (*E*)- and (*Z*)-isomers **1E'** and **1Z'**. The steps can then be repeated. The isomeric mixtures formed in the presence and absence of the adamantanol are quite distinct and are generated independently, although the contributing species coexist when relatively low concentrations of the adamantanol are present. Then the ^{1}H NMR spectra show averaged signals reflecting the distribution of the contributing species that are rapidly interconverting.

An alternative way to operate the machine **1** is to exchange the solvent D_2O with d_6-DMSO and *vice versa*. In the latter solvent the amide (*E*)- and (*Z*)-isomers **1E** and **1Z** are present in the ratio 1:1.2, corresponding to ΔG = 0.1 kcal mol^{-1}, and on which basis the work performed on the amide bond as a result of the solvent exchange equals $\delta\Delta G$ = 1.9 – 0.1 = 1.8 kcal mol^{-1}.

3.2. Operation of *trans*-6^A-deoxy-6^A-(*N*-methylcinnamido)-β-cyclodextrin 2 and the cis-isomer 3 as a molecular machine having a photochemical on/off switch.

Figure S2 illustrates the operation of the cinnamides **2** and **3** as a molecular machine according to the same protocols as described above for the propionamide **1**. The interconversion of the cinnamides **2** and **3** was carried out photochemically, by irradiation at either 300 or 254 nm of a solution of the substrate (2.5 mg, 2 mmol) in Milli-Q water (1 mL) contained in a quartz tube. In d_6-DMSO the ratios of the amide (*E*)- and (*Z*)-isomers **2E** and **2Z**, and **3E** and **3Z**, were found to be 1:1.8 and 1:1.6, corresponding to ΔG = 0.4 and 0.3 kcal mol^{-1}. Allowing for the ratios of those isomers formed in D_2O in the absence of 1-adamantanol, the work performed on the amide bonds of the cinnamides **2** and **3** as a result of the change in solvent corresponds to $\delta\Delta G$ = 2.7 – 0.4 = 2.3 and 0.8 – 0.3 = 0.5 kcal mol^{-1}, respectively.

Figure S2. Operation of *trans*-6^A-deoxy-6^A-(*N*-methylcinnamido)-β-cyclodextrin **2** and the *cis*-isomer **3** as a molecular machine in D_2O at 25 °C (left) and 500 MHz ^1H NMR spectra of solutions of **2** and **3** containing various concentrations of 1-adamantanol (right). Sequential spectra are offset for clarity.

4. REFERENCES

S1.   Byun, H.-S.; Zhong, N.; Bittman, R. *Org. Synth.* **2000**, *77*, 225.

S2.   May, B. L.; Kean, S. D.; Easton, C. J.; Lincoln, S. F. *J. Chem. Soc., Perkin Trans. 1* **1997**, 3157.

S3.   Šebesta, R.; Sališová, M. *Enantiomer* **1999**, *4*, 271.

CHAPTER 3

Measuring the Efficiency of Harnessing the Energy of Molecular Recognition in a Nanomachine Having a Photochemical On/Off Switch

3.1 Introduction

The work described in the previous Chapter demonstrated that the energy of molecular recognition could be harnessed to perform quantifiable work output at the molecular level. This was achieved by measuring the difference in strain energy between a [c1] complex and a competitive guest [a1] complex associated with a change in the conformation of an amide group. Not all of the energy available from the molecular recognition process is likely to be harnessed in the amide bond. Rather, an unknown quantity of energy is expected to be exchanged with the surroundings from the molecular reorganisation that occurs from the host-guest binding interaction (Figure 3.1.1).[53] This is reminiscent of the radiant heat energy produced from the operation of a petroleum fuelled motor, which leads to only 15-30% of the input energy being harnessed for useable work output.[113] On this basis, the quantity of waste energy reflects the performance and the true potential of the system in regards to harnessing work output. It is the measurement of this uncaptured energy from molecular recognition that forms the basis of the research described in this Chapter.
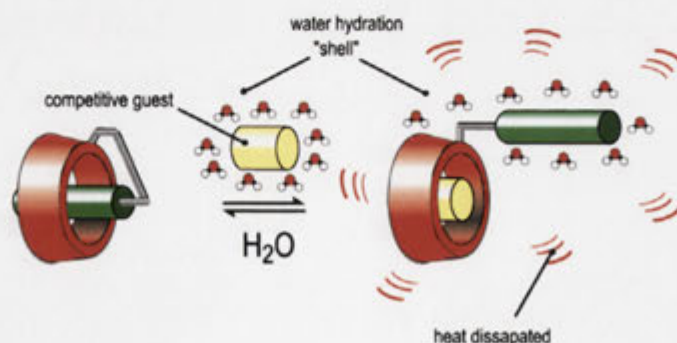
Figure 3.1.1. Schematic representation of the heat transfer effect of a competitive guest.

As outlined in Chapter 1, the most sensitive technique available for measuring the thermodynamics of host-guest interactions is isothermal titration calorimetry (ITC).[56] ITC has been used extensively to investigate the binding interactions between CDs and guests in aqueous solutions.[46] From a single ITC experiment the enthalpy change (ΔH) representing the radiant energy dissipated upon host-guest binding can be directly measured, as well as providing the association constant (K_A) and stoichiometry (n) of interaction. This data can be used to derive the entropy change (ΔS) and importantly Gibbs free energy (ΔG) which reflects the work energy released to the surroundings. On this basis, the thermodynamic properties of a binding interaction detail the energy released from the molecular recognition process and accordingly these can be quantified using ITC.

In this context, the hermaphrodites **2.3**, **2.4** and **2.5** were to be analysed using ITC upon addition of 1-adamantanol "fuel". If the energy released during this process could be measured using ITC and by knowing the amount of work harnessed in the amide bond as quantified in Chapter 2, then the energy harnessing efficiency and any unharnessed potential of the hermaphrodites **2.3**, **2.4** and **2.5** would be determined.

3.2 Isothermal Titration Calorimetry of Cyclodextrin Based Hermaphrodites

In order to investigate the hermaphrodites **2.3**, **2.4** and **2.5** using ITC, an experimental method needed to be developed. While 1-adamantanol "fuel" was suitable for the ^{1}H NMR spectroscopic analysis, this guest was too insoluble at the higher concentrations required to obtain accurate ITC data. For this purpose, 1-adamantanecarboxylate was chosen which has a relatively higher solubility under the ITC experimental conditions of 25 °C in pH 6.9 phosphate buffer (0.05 M). ^{1}H NMR titrations with the 1-adamantanecarboxylate reproduced the same $\delta \Delta G$ values that were obtained with 1-adamantanol for the hermaphrodites **2.3**, **2.4** and **2.5** and so data with 1-adamantanol and 1-adamantanecarboxylate can be directly compared. Although, the ITC and ^{1}H NMR spectroscopic data were obtained in H_2O and D_2O solvents, respectively, the isotope effects on K_A (< 20%) are too small to substantially alter ΔG.[114,115]

The thermodynamic analyses involved titrating aliquots of the 1-adamantanecarboxylate "fuel" (pH 6.9) into the ITC cell containing buffer with a known concentration of the chosen hermaphrodite. Accordingly the stepwise changes in heat from the resulting binding interaction are recorded as isotherms. Shown in Figure 3.2.1 are the ITC enthalpograms (top) and integrated peak areas (bottom) typical of the binding interaction between the 1-adamantanecarboxylate "fuel" and the hermaphrodite **2.4** and its *cis*-isomer **2.5**. The negative heat changes indicate that an exothermic process between the "fuel" and the hermaphrodites is occurring. Also, both the hermaphrodites **2.4** and **2.5** afford curves with inflection points at molar ratios of 1.0 characteristic of a stoichiometric 1:1 complex with the "fuel". The scale of the integrated peaks (bottom) indicates the magnitude of the enthalpic changes is smaller for the hermaphrodite **2.4** than its *cis*-isomer **2.5**. Also, the hermaphrodites **2.4** and **2.5** show a difference between their binding interactions for the 1-adamantanecarboxylate "fuel" as observed by the shape of the curves. The shape of the isotherm is described by the c value from the relationship, $c = K_A[M]_t$, where K_A is the association for the "fuel" and $[M]_t$ is the CD "cylinder" concentration within the cell.[116] Optimal thermodynamic data can be obtained from binding isotherms where the c value is between 10-500. Thus, for each of the CD based hermaphrodites a preliminary ITC experiment was conducted in order to obtain an approximate value for K_A. The concentration of both the chosen hermaphrodite and the "fuel" could then be adjusted accordingly so that binding isotherms having suitable c values were generated. In doing this the nonlinear least-squares fitting of these curves then provides accurate and reliable thermodynamic parameters.
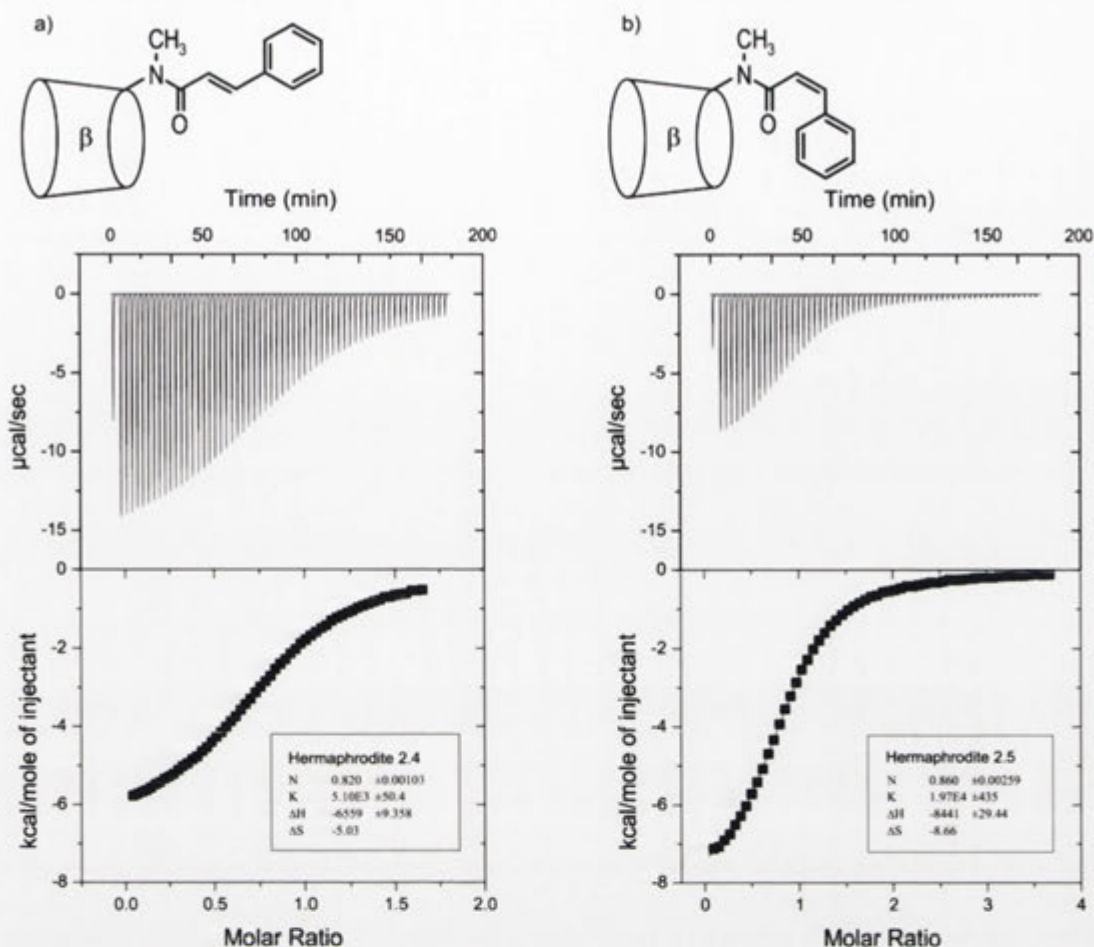
Figure 3.2.1. ITC thermograms for 60 successive injections (5 µl) of 1-adamantanecarboxylate (13.28 mM) in 0.05 M NaH$_2$PO$_4$/Na$_2$HPO$_4$ buffer (pH 6.9) into cells containing the hermaphrodites **2.4**(a) or **2.5**(b) in identical buffer.

For each of the hermaphrodites **2.3**, **2.4** and **2.5**, two independent titrations with 1-adamantanecarboxylate "fuel" were conducted the results of which were averaged to obtain the thermodynamic parameters reported in Table 3.2.1. The Table shows the association constant (K_A), work output ($\delta\Delta G$), free energy change (ΔG), enthalpy change (ΔH) and entropy change ($T\Delta S$) for each of the CDs which are organised in decreasing order of affinity for 1-adamantanecarboxylate "fuel". To establish the reliability of the experiment the results for the β-CD **1.10** control were compared against reported values for β-CD[117,118] and 1-adamantanecarboxylate and found to be satisfactory within experimental error.

CD	K_A (M^{-1})	$\delta\Delta G$ (kcal mol^{-1})[a]	ΔG (kcal mol^{-1})[b]	ΔH (kcal mol^{-1})	$T\Delta S$ (kcal mol^{-1})
β-CD	42050 ± 50	N/A	-6.3	-5.5 ± 0.0	0.8 ± 0.001
β-CD[c]	39500 ± 150	N/A	-6.3	-5.2 ± 0.05	1.1
2.5	19500 ± 200	-0.2	-5.9	-8.3 ± 0.2	-2.4 ± 0.2
2.4	5130 ± 30	2.1	-5.0	-6.5 ± 0.02	-1.5 ± 0.02
2.3	5065 ± 85	1.4	-5.1	-6.4 ± 0.03	-1.3 ± 0.02

Table 3.2.1. ITC and NMR experimental data for the binding of 1-adamantanecarboxylate "fuel" (pH 6.9) with the hermaphrodites **2.3**, **2.4** and **2.5**. [a]$\delta\Delta G$ values reported are amide strain energy stored from the decompression stroke of the piston with 1-adamantanecarboxylate as measured by ^{1}H NMR spectroscopy. [b]ΔG values calculated from ΔH-$T\Delta S$. [c]Data from Zhang and Breslow, 1993.[118]

The unhindered annulus of β-CD **1.10** afforded the highest affinity (K_A = 42050 M^{-1}) for the "fuel" and largest ΔG of -6.3 kcal mol^{-1}. Also, from the equation of ΔG = ΔH-$T\Delta S$, the binding interaction between β-CD **1.10** and the "fuel" is enthalpically driven with a ΔH of -5.5 kcal mol^{-1} and a smaller entropic contribution of 0.8 kcal mol^{-1}.

Of the molecular machines, the hermaphrodite **2.5** with the *cis*-cinnamido "piston" had the highest affinity for the 1-adamantanecarboxylate "fuel" with a K_A of 19500 M^{-1}. The relatively high association constant suggests that the aryl "piston" does not effectively hinder the CD "cylinder" which is consistent with the conformational analysis from Chapter 2. For this reason the addition of the 1-adamantanecarboxylate "fuel" has little effect upon the amide isomer ratio and as a consequence the amount of work harnessed ($\delta\Delta G$) is only -0.2 kcal mol^{-1}. The ΔG of -5.9 kcal mol^{-1} is similar to that observed for the β-CD **1.10** control. As little work ($\delta\Delta G$) is being harnessed in the amide bond therefore the work energy (ΔG) released into the surroundings is similar to the β-CD control **1.10**. The decompression stroke is driven by enthalpic contributions (ΔH) of -8.3 kcal mol^{-1} with only a minor entropic change ($T\Delta S$) of -2.4 kcal mol^{-1}.

In contrast, the hermaphrodite **2.4** having the *trans*-cinnamido "piston" afforded a K_A of 5130 M^{-1}. In this case the association for the "fuel" is eight-fold lower than the unhindered β-CD **1.10** control. This is presumably a result of the aryl "piston" strongly including within the CD "cylinder" as was observed in the ^{1}H NMR conformational

analysis from Chapter 2. The addition of the "fuel" results in the transition from the [*c*1] complex to the [*a*1] complex and accordingly 2.1 kcal mol^{-1} of work is harnessed ($\delta\Delta G$) in the amide bond. Interestingly, the magnitude of ΔG has decreased to -5.0 kcal mol^{-1} in comparison to the -6.3 kcal mol^{-1} for β-CD **1.10**. This suggests that the more work that is harnessed in the amide bond ($\delta\Delta G$), the less work energy (ΔG) that is released into the surroundings. Finally, the binding interaction is enthalpically driven with a ΔH of -6.5 kcal mol^{-1} and smaller entropic change of -1.5 kcal mol^{-1}.

Similarly, the hermaphrodite **2.3** which has the phenylpropionamido "piston" affords a K_A for the "fuel" of 5065 M^{-1}. This is consistent with the aryl "piston" including within the CD "cylinder" to hinder the 1-adamantanecarboxylate "fuel" as identified from the conformational analysis in Chapter 2. The addition of "fuel" therefore alters the *Z*/*E*-amide ratio with the $\delta\Delta G$ being 1.4 kcal mol^{-1}. This is also reflected in the ΔG of -5.1 kcal mol^{-1} which is different than that for β-CD **1.10** and is due to the work energy being harnessed in the amide bond. The binding interaction is also enthalpically driven by -6.4 kcal mol^{-1} with an entropic contribution of -1.3 kcal mol^{-1}.

To summarise these results, the lower the molecular machine's K_A for the "fuel", the stronger the "piston" includes within the "cylinder" and the more work is done ($\delta\Delta G$) on the amide bond as demonstrated by the hermaphrodites **2.3** and **2.4**. These molecular machines are "ON". Alternatively, the higher the K_A of the "fuel" for the "cylinder", the less the "piston" hinders the cavity, and the less energy is harnessed as output ($\delta\Delta G$) as demonstrated by the hermaphrodite **2.5**. This demonstrates that the molecular machine can be switched "OFF". As the K_A from binding increases the ΔG becomes more negative which is expected at the constant temperature from the relationship $\Delta G = -RT\ln K_A$. Importantly, this decrease in ΔG is matched by an increase in the work output ($\delta\Delta G$) and therefore suggests that the more work harnessed by the molecular machine in the amide bond the less work energy that is released into the surroundings. The decompression stroke is enthalpy driven with the ΔG component of Equation 1.4.2 ($\Delta G = \Delta H - T\Delta S$) being dominated by ΔH contributions ($|\Delta H| \gg |T\Delta S|$).

Having successfully obtained the thermodynamic properties for the operation of the hermaphrodites **2.3**, **2.4** and **2.5**, it is possible to make assessments about their energy harnessing efficiency. By comparing the work energy not harnessed in the amide bond (ΔG) to the work energy harnessed in the amide bond ($\delta\Delta G$), the efficiency can

then be calculated using Equation 3.2.1. However, considering that ΔG is equal to $\Delta H - T\Delta S$, then an unavoidable energy cost from molecular reorganisation ($T\Delta S$) is also incurred and in this sense the energy that is truly wasted is ΔH. Thus, Equation 3.2.2 may also be used to assess the energy efficiency. The energy efficiency of the work harnessed in the amide bond in relation to the uncaptured work energy and to the heat energy dissipated for the hermaphrodites **2.3**, **2.4** and **2.5** at 25 °C is accordingly shown in Table 3.2.2.

$$\text{Eff}_{\Delta G} \, (\%) = \frac{|\, \delta\Delta G \,|}{|\delta\Delta G + \Delta G|} \qquad (3.2.1)$$

$$\text{Eff}_{\Delta H} \, (\%) = \frac{|\, \delta\Delta G \,|}{|\delta\Delta G + \Delta H|} \qquad (3.2.2)$$

Nanomachine	$\text{Eff}_{\Delta G}$ (%)[a]	$\text{Eff}_{\Delta H}$ (%)[b]
2.5	-3	-2
2.3	22	18
2.4	30	24

Table 3.2.2. Efficiency of harnessing the energy of molecular recognition in the hermaphrodites **2.3**, **2.4** and **2.5** at 25 °C. [a]Calculated from Equation 3.2.1. [b]Calculated from Equation 3.2.2.

The hermaphrodite **2.5** shows the lowest energy harnessing efficiencies which are -3% and -2% as calculated from the uncaptured work energy and the heat dissipated, respectively. The thermodynamic properties of this system for 1-adamantanecarboxylate "fuel" are similar to that of natural β-CD **1.10** and unambiguously this molecular machine is switched "OFF". In comparison, the energy efficiency of the hermaphrodite **2.3** is 22% when determined from the uncaptured work energy and 18% when the favorable entropic contribution is removed from the equation. For both results this system has the comparable energy harnessing efficiency to that of a petroleum-fueled macroscopic motor.[113] Next, the *trans*-hermaphrodite **2.4** having the cinnamido "piston"

affords an even greater energy efficiency of 30% when calculated from the ΔG and 24% using the ΔH. Therefore, photochemically switching between the *trans*-hermaphrodite **2.4** and its *cis*-isomer **2.5** can modulate the energy harnessing efficiency. The important message from this research is that even with enhancements, synthetic molecular machines of this type will really only ever be capable of work that requires energy inputs up to 6-8 kcal mol^{-1}.

3.3 Temperature Effects on the Operation of the Cyclodextrin Based Hermaphrodites

Having successfully measured the energy released from the binding interactions between 1-adamantanecarboxylate and the hermaphrodites **2.3**, **2.4** and **2.5**, their operating efficiencies were able to be assessed. On the basis that the work energy released to the surroundings (ΔG) is equal to $\Delta H - T\Delta S$ then the operation of the molecular machines should be temperature dependent. Using a combined ITC and NMR strategy the temperature dependence of the binding interaction between the hermaphrodite **2.4**, which was chosen for its superior efficiency, and 1-adamantanecarboxylate "fuel" was investigated.

Figure 3.3.1 shows the ITC enthalpograms and integrated peaks for the decompression stroke between 1-adamantanecarboxylate "fuel" (13.28 mM) and the hermaphrodite **2.4** (1.84 mM) at 10 °C, 25 °C, 40 °C and 55 °C. Over the chosen temperature range the binding of the "fuel" by the hermaphrodite **2.4** remains an exothermic process as shown by the negative enthalpograms. As the temperature increases the binding isotherms become less sigmoidal in appearance which is characteristic of a relatively lower affinity for the "fuel". Although the c value drops below 10 for the 55 °C temperature isotherm, the fitted thermodynamic data is consistent with the linear trend established over the entire temperature range as discussed later in the Chapter.
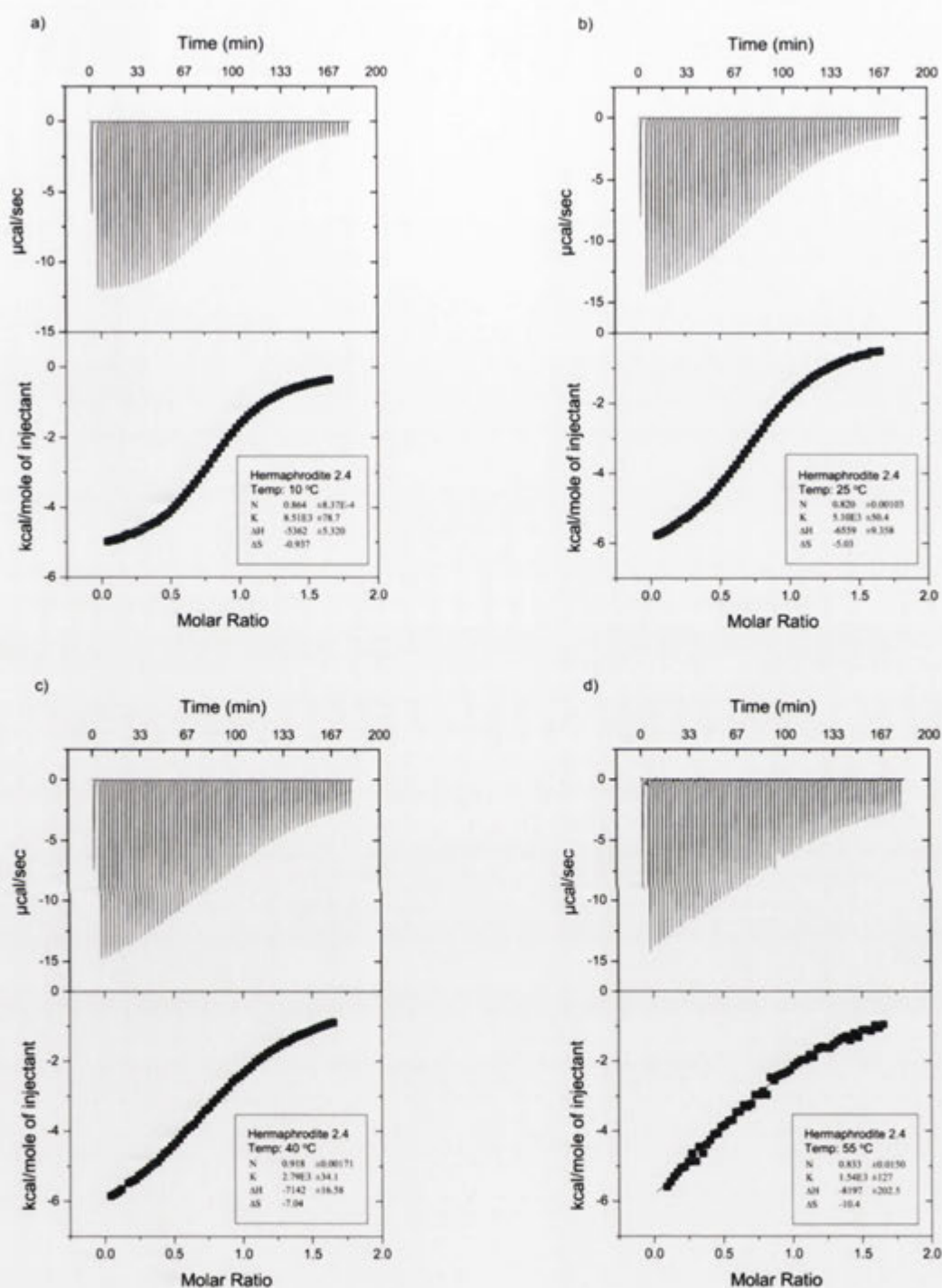
Figure 3.3.1. ITC enthalpograms for 60 successive injections (5 μl) of 1-adamantanecarboxylate (13.28 mM) in 0.05 M NaH$_2$PO$_4$/Na$_2$HPO$_4$ buffer (pH 6.9) into cells containing the hermaphrodite **2.4** at (a) 10 °C; (b) 25 °C; (c) 40 °C; (d) 55 °C.

For the hermaphrodite **2.4** at each temperature, two independent titrations with 1-adamantanecarboxylate "fuel" were conducted and the results were averaged to obtain

the thermodynamic parameters reported in Table 3.3.1. The Table shows the association constant (K_A), free energy change (ΔG), enthalpy change (ΔH) and entropy change ($T\Delta S$) which are organised in increasing order of temperature beginning at 10 °C. Firstly, the association of the 1-adamantanecarboxylate "fuel" for the hermaphrodite **2.4** weakens from 8545 M^{-1} to 1575 M^{-1} as the temperature increases from 10 to 55 °C. At lower temperature the adamantane based "fuel" binds the hermaphrodite **2.4** with higher affinity and on this basis, less "fuel" is required to perform the decompression stroke. Next, the ΔG appears to remain almost invariant to temperature, which from $\Delta G = \Delta H - T\Delta S$ suggests that enthalpy-entropy compensation must be occurring. This is supported by the linear increase in the magnitude of both ΔH and $T\Delta S$ with increasing temperature. Figure 3.3.2 illustrates the compensatory effect between ΔH and ΔS to afford the relatively unchanged ΔG with raising temperature.

Temperature (°C)	K (M^{-1})	ΔG (kcal mol^{-1})[a]	ΔH (kcal mol^{-1})	$T\Delta S$ (kcal mol^{-1})
10	8545 ± 135	-5.1	-5.4 ± 0.07	-0.3 ± 0.07
25	5130 ± 30	-5.0	-6.5 ± 0.02	-1.5 ± 0.02
40	2780 ± 25	-4.9	-7.2 ± 0.2	-2.3 ± 0.2
55	1575 ± 91	-4.8	-8.1 ± 0.2	-3.3 ± 0.2

Table 3.3.1. ITC experimental data for the decompression stroke of 1-adamantanecarboxylate (pH 6.9) and the hermaphrodite **2.4** at various temperatures. ITC experiments at 10 °C, 25 °C, 40 °C and 55 °C were performed in duplicate. [a]ΔG values calculated from ΔH-$T\Delta S$.
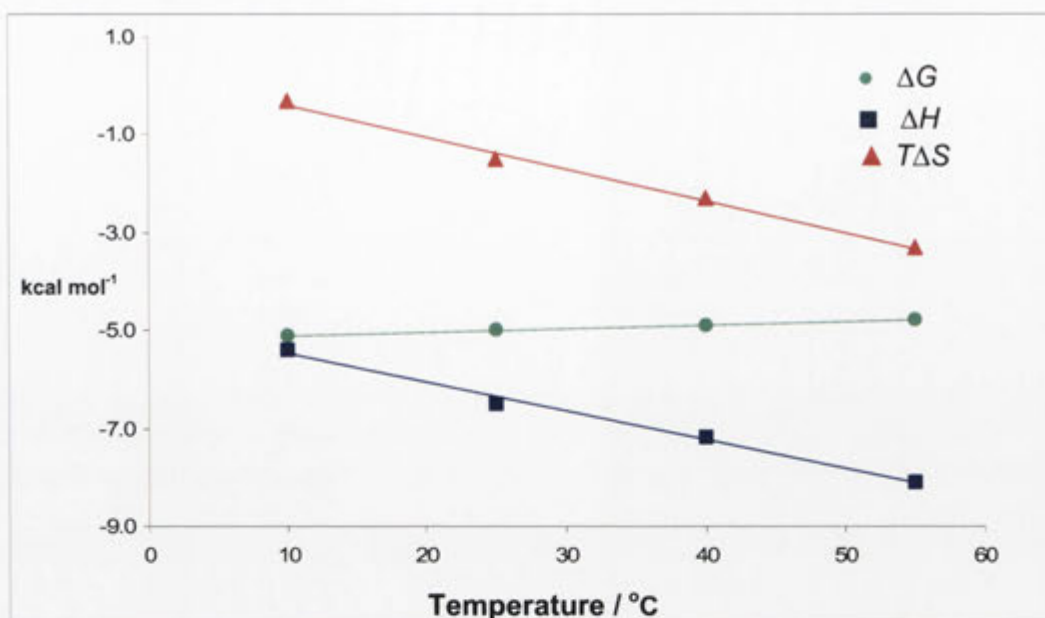
Figure 3.3.2. Effect of temperature upon thermodynamic properties of the binding interaction between 1-adamantanecarboxylate (pH 6.9) and the hermaphrodite **2.4** (10 °C to 55 °C).

Although the enthalpy-entropy compensatory effect is not well understood it is commonly observed over small temperature ranges as a consequence of a change in heat capacity (ΔC_p).[119] Having measured the temperature dependence of ΔH the change in heat capacity (ΔC_p) can be determined from Equation 1.4.3.

$$\Delta C_p = \frac{\Delta H_{T2} - \Delta H_{T1}}{T_2 - T_1}$$

(1.4.3)

The negative change in heat capacity (ΔC_p) of -0.07 kcal mol^{-1} °C^{-1} for the "fuel" with the hermaphrodite **2.4** indicates that significant hydrophobic interactions are involved.[120] These forces are expected for an adamantyl guest binding in the cavity of a CD in water and the magnitude is typical of such a complex.[46] Interestingly, if ΔG remains invariant to temperature while the heat energy dissipated (ΔH) changes, then the efficiencies can in principle be different between Equation 3.2.1 and Equation 3.2.2. However, before this can be established the temperature effects on the work harnessed in the amide bond ($\delta\Delta G$) must be determined using ^{1}H NMR spectroscopy.

The $\delta\Delta G$ values were determined from the amide ratios for the hermaphrodite **2.4** in the presence and absence of 1-adamantanecarboxylate "fuel" over the chosen temperature range (10 to 55 °C). The $\delta\Delta G$'s remained unchanged with no significant effect on the amide ratios observed by varying the temperature. On this basis the energy efficiency of the hermaphrodite **2.4** remains constant (~30%) showing no temperature dependence if calculated using ΔG (Equation 3.2.1). This can be attributed to enthalpy-entropy compensation. However, if the energy efficiency of the hermaphrodite **2.4** is calculated using ΔH from Equation 3.2.2, then the efficiency decreases from 28% to 21% from 10 °C to 55 °C. This suggests that the operation of the machine is more efficient in colder temperatures.

In summary, as the association of the "fuel" becomes stronger for the "cylinder" at lower temperatures, and the $\delta\Delta G$'s remain unchanged, the molecular machine does the same amount of work with less "fuel" than at higher temperatures. The energy harnessing efficiency is either invariable or variable with changing temperature depending on whether determined against ΔG or ΔH which is caused by enthalpy-entropy compensation. Thus, by measuring the dissipated energy for the operation of the hermaphrodite **2.4** at various temperatures it can be concluded that a temperature dependency exists.

3.4 Conclusion

In this Chapter ITC was used to analyse the thermodynamic properties of the decompression stroke of the hermaphrodites **2.3**, **2.4** and **2.5** due to the 1-adamantanecarboxylate "fuel". This research showed that the nature of the "piston" could alter the association of the "fuel" for the CD "cylinder" for the enthalpically driven binding interaction. By measuring the uncaptured work energy, as quantified with ITC, and comparing this to the energy harnessed in the amide bond, from ^{1}H NMR spectroscopy, the efficiency of the work output could be examined. The hermaphrodite **2.3** operates with an $Eff_{\Delta G}$ of 22% and $Eff_{\Delta H}$ of 18%. Photochemically switching from the hermaphrodite **2.4** ($Eff_{\Delta G}$: 30%, $Eff_{\Delta H}$: 24%) to its *cis*-isomer **2.5** ($Eff_{\Delta G}$: -3%, $Eff_{\Delta H}$: -2%) modulates the efficiency. Also the decompression stroke of the hermaphrodite **2.4** was shown to be temperature dependent and required less 1-adamantanecarboxylate "fuel" to operate in colder temperatures. The efficiency from the work energy released

to the surroundings was temperature independent while the efficiency from the dissipated heat energy was temperature dependent. Importantly, it was demonstrated that artificial molecular machines can be developed to perform work outputs at the molecular level with the comparable efficiency of their macroscopic counterparts. This research shows that synthetic molecular machines in this form are capable of harnessing energy of around 6-8 kcal mol^{-1}.

CHAPTER 4

Effect of Substituents on the Harnessed Energy of Molecular Recognition in a Nanomachine

4.1 Introduction

The work described in Chapters 2 and 3 demonstrated that artificial molecular machines can be developed to perform work outputs at the molecular level with the comparable efficiency of their macroscopic counterparts. Importantly, this research shows that the work performed upon the amide bond ($\delta\Delta G$) is governed by the ΔH, ΔS, ΔG and K_A of the binding interaction between the 1-adamantanecarboxylate "fuel" and the hermaphrodite. These thermodynamic parameters are dependent on the properties of the molecular machine's components. With this in mind, several structural variations of the hermaphrodites developed in the preceding Chapters were prepared with the aim of investigating the substituent effects on the energy harnessed from molecular recognition.

An important component of the hermaphrodites **2.3**, **2.4** and **2.5** is the tertiary amide bond of the linkage group. The conformation of this group permits the strain energy difference between a [c1] complex and a competitive guest [a1] complex to be measured. From the findings in Chapter 2, in d_6-DMSO the relative populations of the *E*-amide isomer were between 55% and 64%. In contrast, the expected proportion of the *E*-isomer of a secondary amide bond in organic solvent is only about 1%.[121] It was decided to investigate whether a hermaphroditic [c1] complex could also constrict the geometry of a secondary amide bond. For this, the secondary amide hermaphrodite **4.3** was to be prepared and its operation investigated.

In addition to changing the amide linkage group, the aryl "piston" could also be modified to investigate the effect on the operation of the hermaphrodites. CD complexes can be stabilised through hydrophobic interactions that are dependent on the hydrophobic surface area of the guest.[46] This is demonstrated by the addition of methylene substituents to alkyl chains which result in a decrease of about 0.7 kcal mol^{-1} in the Gibbs free energy (ΔG) of the binding interaction for the CD.[122] It therefore seemed likely that by increasing the hydrophobic surface area of the aryl "piston" the hermaphrodite's operation would be altered. To investigate this, the α-methylcinnamido

hermaphrodite **4.7** was prepared and its operation studied using a combined ^{1}H NMR spectroscopic and ITC analysis.

The focus of the research described in this Chapter was therefore to prepare and then analyse the operation of various structural analogues of the hermaphrodites discussed in Chapters 2 and 3. Comparisons between the energy harnessed in the amide bond ($\delta\Delta G$), as quantified with ^{1}H NMR spectroscopy, to the work available (ΔG) and energy dissipated (ΔH), as determined with ITC analysis, were to establish the effects of these different modifications. The research herein aimed to expand the understanding of the operation of synthetic molecular machines of this type.

4.2 Synthesis of Secondary Cinnamido- and *N*,α-Dimethylcinnamido- Substituted β-Cyclodextrins

The synthesis of the hermaphrodites **4.3** and **4.4** proceeded through the preparation of 6^A-amino-6^A-deoxy-β-CD **4.2** as detailed in Scheme 4.2.1. The tosyl group of the earlier prepared sulfonate **2.1** was substituted with sodium azide to access the azido-CD **4.1**. The azido-CD **4.1** was then reduced to the amino-CD **4.2** using triphenylphosphine and ammonia *via* a Staudinger reaction.[123,124] The crude reaction mixture was applied to cationic (SP) exchange resin to isolate 6^A-amino-6^A-deoxy-β-CD **4.2** in a yield of 35%.
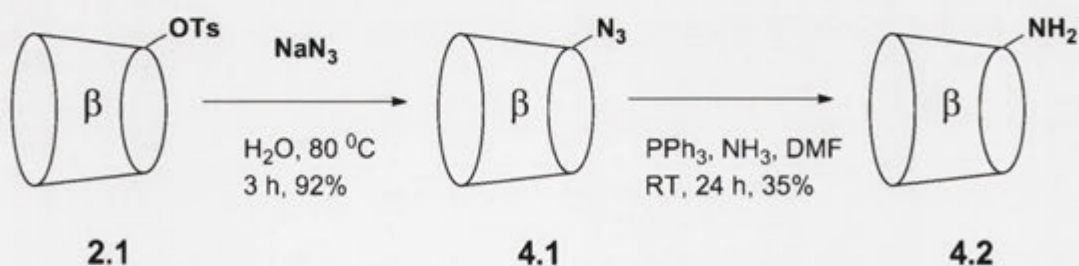
Scheme 4.2.1. Synthesis of 6^A-amino-6^A-deoxy-β-CD **4.2**.

After obtaining the amino-CD **4.2**, the hermaphrodite **4.3** could be prepared (Scheme 4.2.2). Accordingly the aryl "piston" was installed onto the amino-CD **4.2** through an amide "torsion bar". The crude mixture was applied to anionic (DEAE) then cationic (SP) exchange resins, followed by reverse-phase HPLC, to isolate the hermaphrodite **4.3** in a yield of 28%. The hermaphrodite **4.3** was pure by elemental

analysis and showed, using ESI HRMS, an $[M+H]^+$ ion at 1264.436. TLC analysis identified both the UV active aromatic group and a "positively staining" CD component. The hermaphrodite **4.3** was also found to be relatively non-polar (R_f: 0.52) and has a lower water solubility than the earlier hermaphrodites **2.3**, **2.4** and **2.5**.
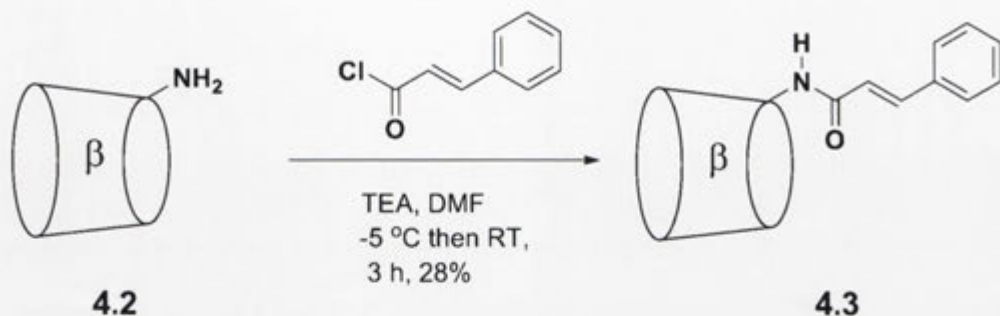
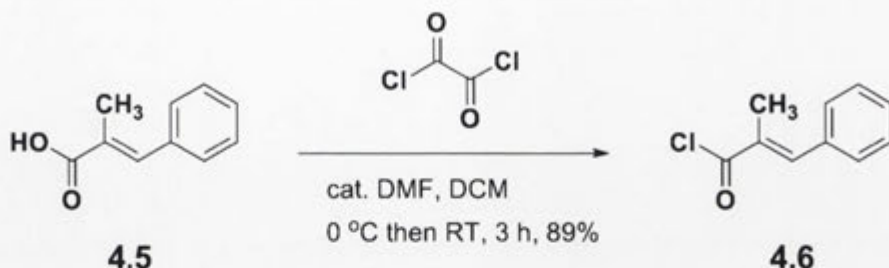**Scheme 4.2.2.** Synthesis of *trans*-6^A-deoxy-6^A-cinnamido-β-CD **4.3**.

Photolysis of the *trans*-hermaphrodite **4.3** was performed to provide access to its *cis*-isomer **4.4**, as illustrated in Scheme 4.2.3. An aqueous solution of the hermaphrodite **4.3** was irradiated with 300 nm light for 2 h. The crude reaction mixture was applied to reverse-phase HPLC to isolate the hermaphrodite **4.4** in a yield of 35%. The hermaphrodite **4.4** was pure by elemental analysis and was characterised using ^{1}H NMR spectroscopy to be the *cis*-isomer by the coupling constant between the olefinic protons (J = 12 Hz). The hermaphrodite **4.4** was slightly more polar (R_f: 0.42) than the hermaphrodite **4.3** (R_f: 0.52) by TLC.
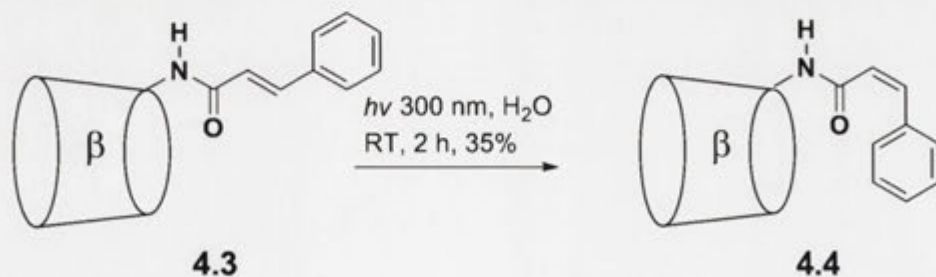
Scheme 4.2.3. Synthesis of *cis*-6^A-deoxy-6^A-cinnamido-β-CD **4.4**.

After preparing the secondary amide hermaphrodite **4.3** and its *cis*-isomer **4.4**, the hermaphrodite **4.7** was synthesised. This involved converting the acid **4.5** to the acyl chloride **4.6** as shown in Scheme 4.2.4. The acyl chloride **4.6** was then treated with the amino-CD **2.2** to prepare the *N*,α-dimethylcinnamido hermaphrodite **4.7** as shown in

Scheme 4.2.5. The crude reaction mixture was applied to anionic (DEAE) and cationic (SP) exchange resins, followed by reverse-phase HPLC, to isolate the hermaphrodite **4.7** in a yield of 43%. The hermaphrodite **4.7** was pure by elemental analysis and showed, using ESI HRMS, an $[M+H]^+$ ion at 1292.469.


Scheme 4.2.4. Synthesis of *trans*-α-methylcinnamoyl chloride **4.6**.
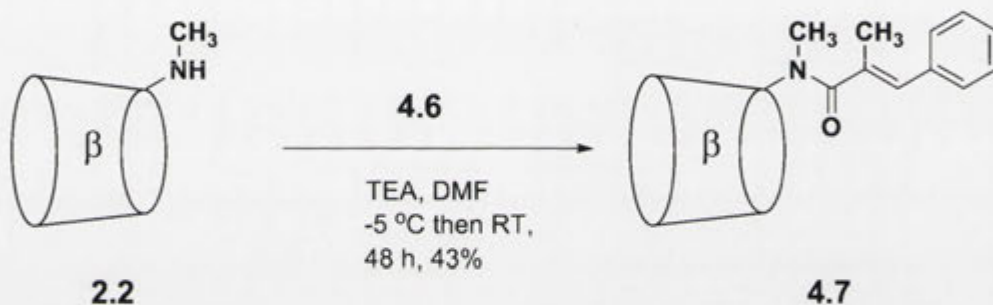
Scheme 4.2.5. Synthesis of *trans*-6^A-deoxy-6^A-(*N*,α-dimethylcinnamido)-β-CD **4.7**.

Photolysis of the *trans*-hermaphrodite **4.7** was performed in an attempt to provide access to the *cis*-isomer **4.8**, as illustrated in Scheme 4.2.6. However, treatment of the hermaphrodite **4.7** (λ_{MAX} 254 nm) with both a 254 and 300 nm light source yielded only unidentifiable bi-products. Alternatively, the *cis*-isomer of α-methylcinnamic acid **4.5** was prepared using a literature method[112] which was then to be installed onto the CD "cylinder". However, the *cis*-hermaphrodite **4.8** could not be obtained using this approach. The reasons for these outcomes are not obvious as both the *cis*-hermaphrodites **2.5** and **4.4** were successfully prepared using a photolytic method, however it is likely that either the bulk of the α-methyl substituent or steric hindrance is blocking this synthetic route.
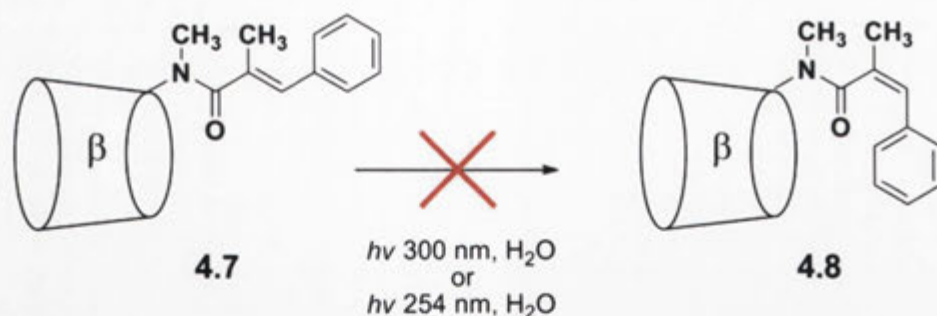
Scheme 4.2.6. Attempted synthesis of *cis*-6^A-deoxy-6^A-(*N*,α-dimethylcinnamido)-β-CD **4.8**.

## 4.3 Conformational Analysis of Cyclodextrin Based Hermaphrodites

Having prepared the hermaphrodites **4.3**, **4.4** and **4.7**, their function as machines is dependent upon their conformational behavior in d_6-DMSO, D$_2$O with 1-adamantanol and D$_2$O alone. In order to investigate this, a ^{1}H NMR strategy was employed for the purpose of distinguishing between the *Z/E*-amide isomers and determining the position of the aryl "piston" with respect to the CD "cylinder". As discussed in Chapter 2, the olefinic protons of the hermaphrodites **2.4** and **2.5** were identified as a secondary handle for quantifying the *Z/E*-amide ratio. With the hermaphrodite **4.3** and its *cis*-isomer **4.4** not having *N*-methyl substituents, the conformational analysis was to focus on their olefinic protons.

Shown in Figure 4.3.1 is a section of the ^{1}H NMR spectrum of the hermaphrodite **4.3** in d_6-DMSO. A single set of olefinic proton signals is observed at δ 6.73 and 7.42 ppm suggesting that one major species exists in solution. As already mentioned the expected population of the *E*-isomer of a secondary amide in organic solvent is 1%.[121] On this basis, without a driving force for inclusion the hermaphrodite **4.3** exists predominantly as one species which is suspected to be the *Z*-amide.
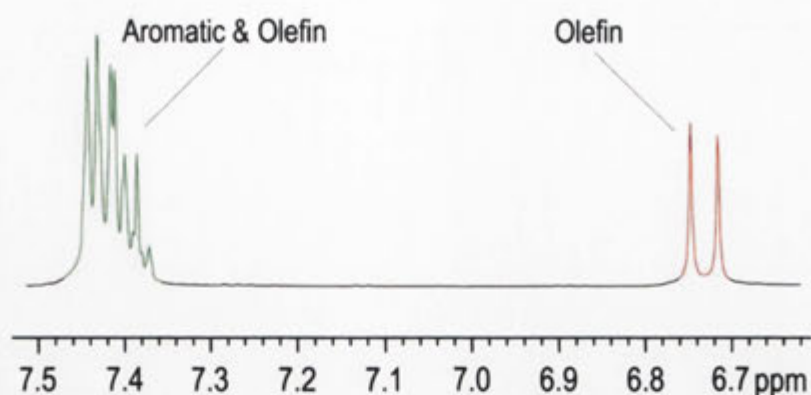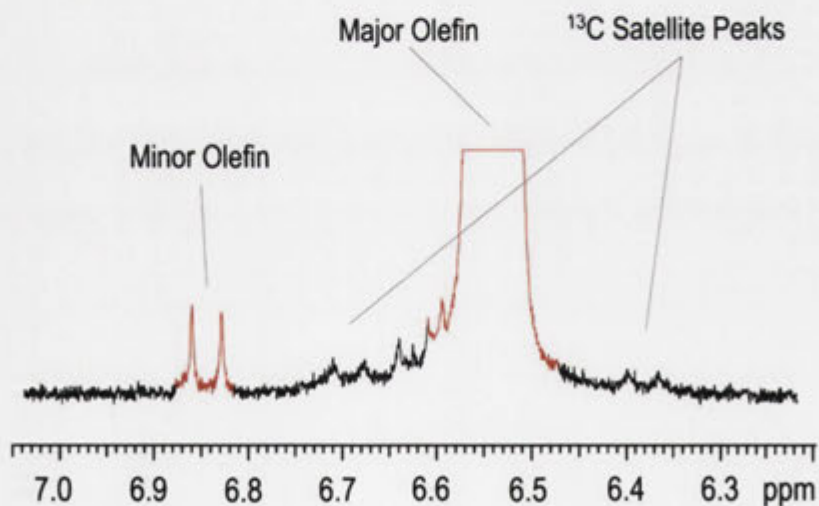
Figure 4.3.1. Section of the ^{1}H NMR spectrum (500 MHz) of the hermaphrodite **4.3** in d_6-DMSO at 25 °C.

In D_2O, the hermaphrodite **4.3** on first inspection appears to exist predominantly as one species for which the ^{1}H NMR spectrum is shown in Figure 4.3.2. In spite of this, when the olefinic region of the ^{1}H NMR spectrum is examined closely (Figure 4.3.3), a low intensity signal at δ 6.86 ppm (J = 16.0 Hz) is observed adjacent to the strong olefinic signal at δ 6.55 ppm (J = 16.5 Hz). The major signal is surrounded by ^{13}C satellite peaks (J = 160 Hz). These occur because the ^{13}C isotope has a natural abundance of 1.1% relative to [12]C. Signals of protons that are attached to ^{13}C split into two satellite peaks of 0.55% intensity that sit symmetrically astride (typically $J \approx 140$ Hz) the "parent" [12]C-^{1}H proton signal.[109] The importance of these observed ^{13}C satellite peaks is that they can be utilised in ^{1}H NMR spectra as standards and allow product ratios of up to 1000:1 to be accurately quantified.[125] On this basis, as the ratio of the minor olefinic signal to the ^{13}C satellite peaks is approximately 5:1, it follows that the ratio of minor to major species is approximately 1:40. Next, from the ROESY NMR spectrum (Figure 4.3.4) the aryl "piston" protons are observed to interact with the CD "cylinder" protons, while the olefinic protons do not. Interestingly, this is in contrast to the [*c*1] complex of the hermaphrodite **2.4** from Chapter 2 where the olefinic protons interact with the CD "cylinder". This observation is discussed in more detail in Chapter 4.5. The major isomer of the hermaphrodite **4.3** in D_2O is suspected to be the thermodynamically more stable *Z*-amide for reasons discussed in more detail below. The low abundance of the minor species makes its identity difficult to determine using the ROESY conformational analysis. However, in D_2O the hermaphrodite **4.3** exists as two species thought to be the *Z/E*-amides in a ratio of approximately 40:1.
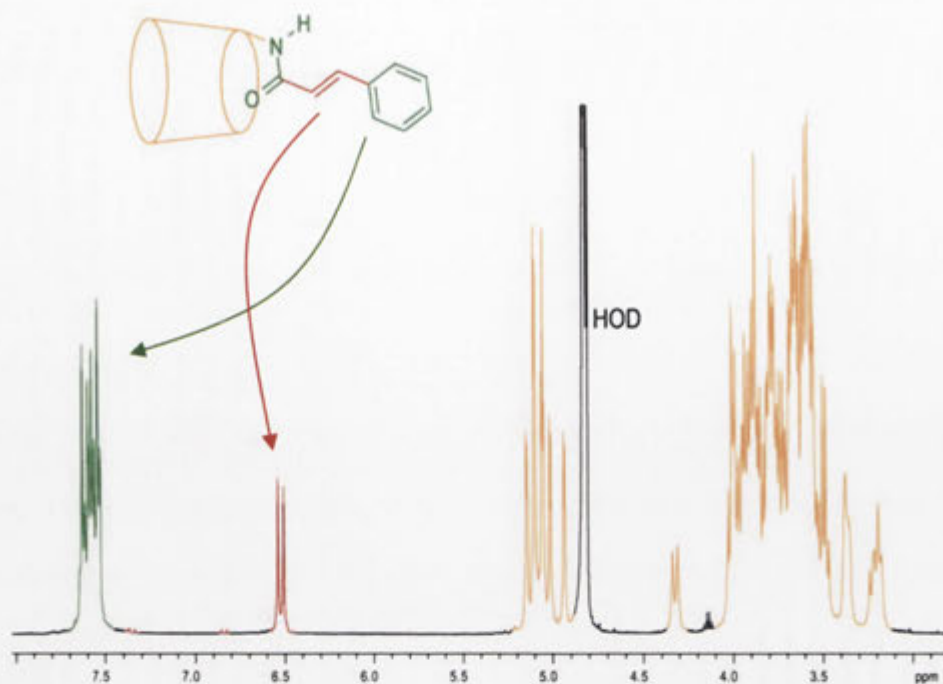
Figure 4.3.2. ^{1}H NMR spectrum (500 MHz) of the hermaphrodite **4.3** in D$_2$O at 25 °C.

Figure 4.3.3. Section of the ^{1}H NMR spectrum (500 MHz) of the hermaphrodite **4.3** in D$_2$O at 25 °C.
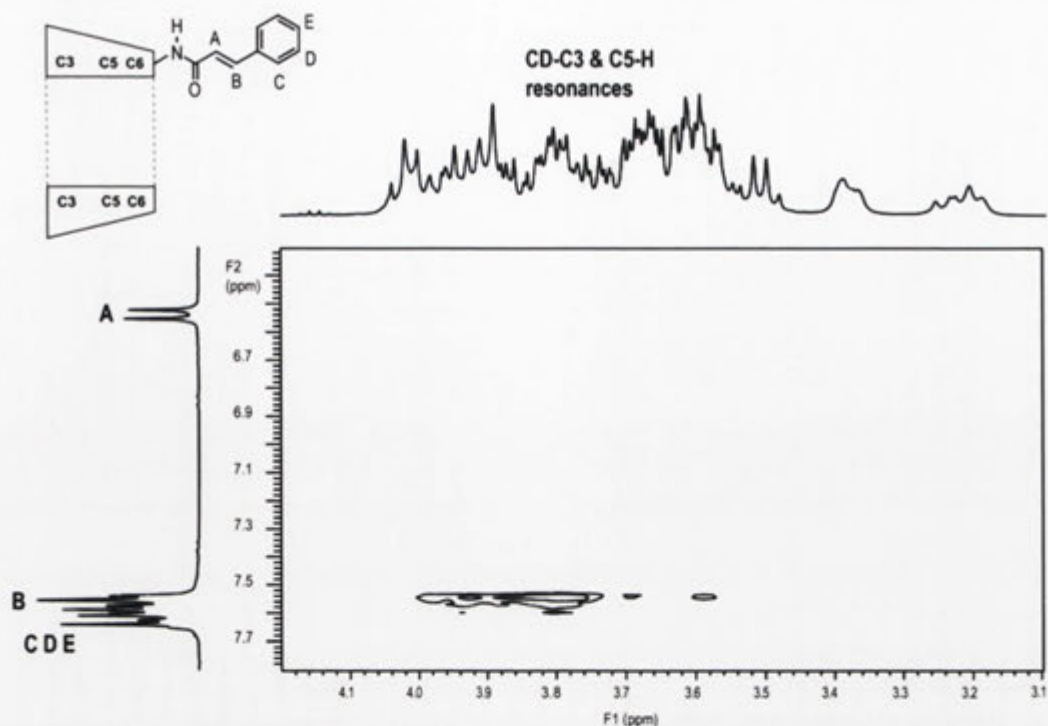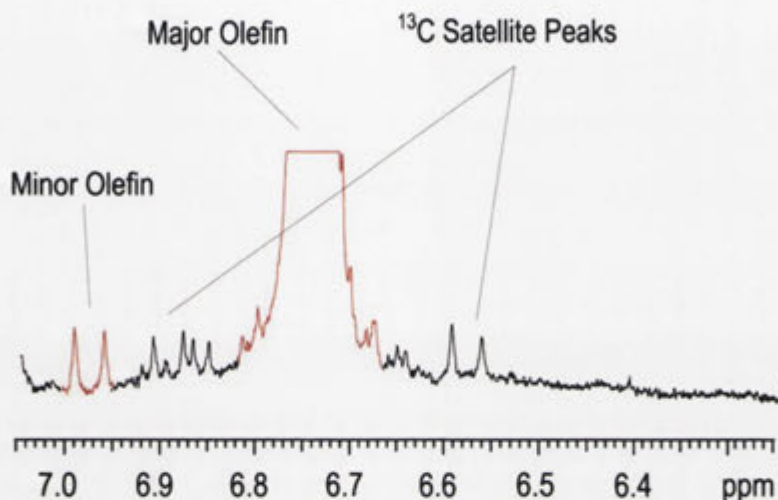
Figure 4.3.4. A section of the ROESY NMR spectrum (500 MHz) of the hermaphrodite **4.3** in D_2O (25 °C) with 0.250 ms mixing time.

Shown in Figure 4.3.5 is the ^{1}H NMR spectrum for the hermaphrodite **4.3** in D_2O with 1-adamantanol "fuel". Sitting symmetrically astride the major olefinic proton signal at δ 6.73 ppm are ^{13}C satellite peaks at δ 6.89 and δ 6.57 ppm (J = 160 Hz). Also observed is a minor olefinic signal at δ 6.97 ppm (J = 16 Hz) which corresponds to the low intensity olefinic resonance suspected to be the *E*-amide isomer observed earlier in D_2O. The minor olefinic signal and the ^{13}C satellite peaks have a ratio of approximately 1:1 and therefore correspond to species in a ratio of 1:200. The low concentration of this minor species doesn't permit conclusive analysis using ^{1}H NMR spectroscopy. However, in the presence of 1-adamantanol "fuel" and in D_2O the hermaphrodite **4.3** exists as two species with a suspected *Z/E*-amide ratio of 200:1, respectively.

To summarise the conformational behavior of the hermaphrodite **4.3**, in d_6-DMSO one major species is observed and is suspected to be the *Z*-amide isomer. In D_2O, two species are observed in a ratio of 40:1 which are most likely to be *Z*- and *E*- amides, respectively, and in D_2O in the presence of 1-adamantanol "fuel", the suspected *Z/E*-amide ratio becomes 200:1. By changing the solvent from d_6-DMSO to D_2O the population of the minor isomer increases which can logically be attributed to the formation of the [*c*1] complex as demonstrated in Chapter 2. Next, as 1-adamantanol

"fuel" is added to the hermaphrodite **4.3** in D₂O, a five-fold decrease in the quantity of the minor species towards the ratio for d_6-DMSO is observed. This is reminiscent of the shift from the [c1] complex to the [a1] competitive guest complex that corresponds to a decrease in the proportion of the E-amide isomer for the hermaphrodites **2.3** and **2.4**. Almost certainly on that basis the minor species of the hermaphrodite **4.3** in D₂O is related to the [c1] complex having the E-amide conformation.

Figure 4.3.5. Section of the ¹H NMR spectrum (500 MHz) of 1-adamantanol (3-equivalents) and the hermaphrodite **4.3** in D₂O at 25 °C.

Next, having studied the conformational behavior of the hermaphrodite **4.3** in d_6-DMSO, D₂O with 1-adamantanol and D₂O alone, its *cis*-isomer **4.4** was to be investigated. Firstly, the ¹H NMR spectrum of the hermaphrodite **4.4** in d_6-DMSO (Figure 4.3.6) shows two sets of olefinic proton signals in a ratio of approximately 100:1, with the major at δ 6.67 and 6.07 ppm and the minor at δ 6.56 and 6.17 ppm. In the organic solvent the major species is most likely to be from the more thermodynamically stable Z-amide isomer.[121] Thus, the hermaphrodite **4.4** in d_6-DMSO exists as two species with a suspected Z/E ratio of 100:1.
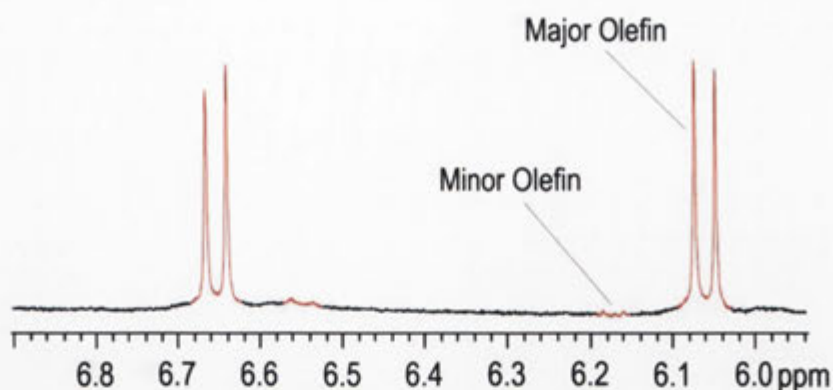
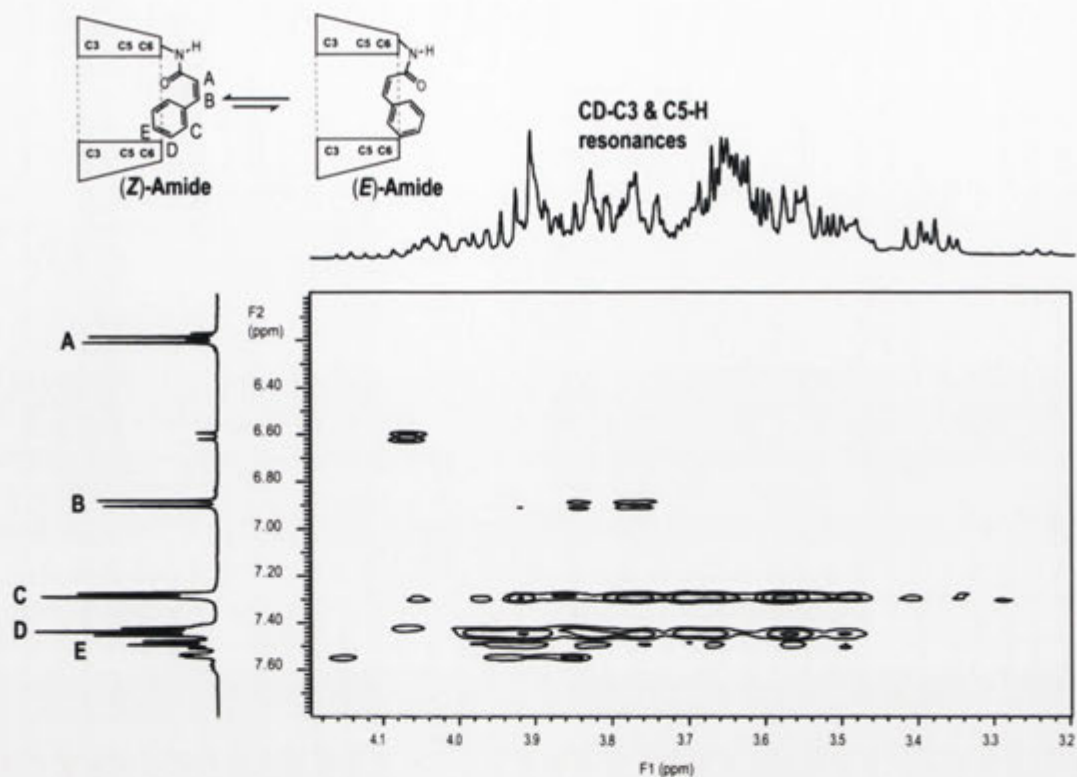**Figure 4.3.6.** Section of the ^{1}H NMR spectrum (500 MHz) of the hermaphrodite **4.4** in d_6-DMSO at 25 °C.

The ^{1}H NMR spectrum for the hermaphrodite **4.4** in D_2O alone (Figure 4.3.7) shows two sets of *cis* olefinic signals ($J = 12\text{-}13\text{Hz}$) in a ratio of 6:1. The minor olefinic set is at δ 6.62 ppm and δ 6.19 ppm and the major olefinic resonances are at δ 6.91 ppm and δ 6.20 ppm. As is discussed in more detail below the major species is thought to be the more stable *Z*-amide while the minor species is thought to be the constrained *E*-isomer. Shown from the ROESY spectrum in Figure 4.3.8, the aryl "piston" interacts with the CD "cylinder".
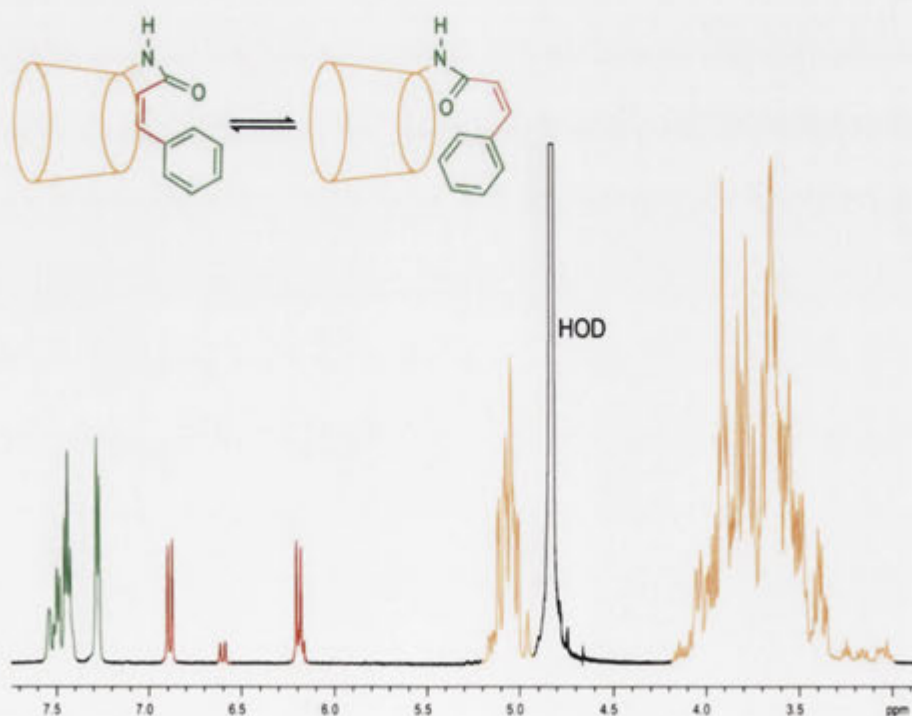
Figure 4.3.7. ^{1}H NMR spectrum (500 MHz) of the hermaphrodite **4.4** in D_2O at 25 °C.

64

Figure 4.3.8. A section of the ROESY NMR spectrum (500 MHz) of the hermaphrodite **4.4** in D_2O (25 °C) with 0.250 ms mixing time.

Shown in Figure 4.3.9 is the ^1H NMR spectrum for the hermaphrodite **4.4** in D_2O in the presence of 1-adamantanol "fuel". In this case two distinct sets of olefinic proton signals in a ratio of about 11:1 are observed with the major doublets at δ 6.94 and 6.15 ppm and the minor doublets at δ 6.81 and 6.41 ppm. The major species is likely to be the Z-amide isomer while the minor olefinic signals are from the E-amide isomer. In summary, the hermaphrodite **4.4** in D_2O and 1-adamantanol exists in a suspected Z/E-amide ratio of 11:1, respectively.

To review the conformational behavior of the hermaphrodite **4.4**, in d_6-DMSO two species are observed in a ratio of approximately 100:1 with the major conformation suspected to be the Z-amide isomer. In D_2O, two species are observed in a Z/E-amide ratio of 6:1. In D_2O with 1-adamantanol "fuel", the hermaphrodite **4.4** exists as two species in a suspected Z/E-amide ratio of 11:1. The change in the ratio of species by changing the solvent from d_6-DMSO to D_2O occurs due to the constraint by the molecular recognition process. Also, the addition of 1-adamantanol "fuel" to the hermaphrodite **4.4** in D_2O affords nearly a two-fold decrease in the concentration of the

65

minor species. On this basis and from the findings in Chapter 2, the minor species is almost certainly the *E*-amide isomer. This assignment is supported by comparison of the ^{1}H NMR spectra for the *N*-methyl hermaphrodite **2.5** and its non-*N*-methyl analogue **4.4** in D_2O which are shown in Figure 4.3.10 and in D_2O with 1-adamantanol "fuel" which are shown in Figure 4.3.11. In each case the chemical shifts of the olefinic protons of the minor and major *Z*- and *E*-amide isomers of the hermaphrodite **2.5** are almost identical to those of the major and minor *Z*- and *E*-isomers of the non-methyl analogue **4.4**.
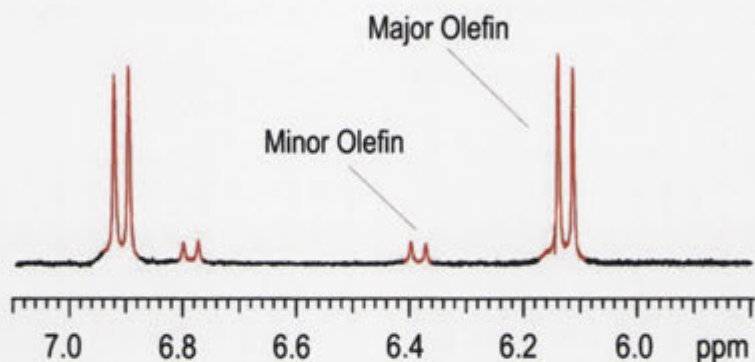
Figure 4.3.9. A section of the ^{1}H NMR spectrum (500 MHz) of 1-adamantanol (3-equivalents) and the hermaphrodite **4.4** in D_2O at 25 °C.
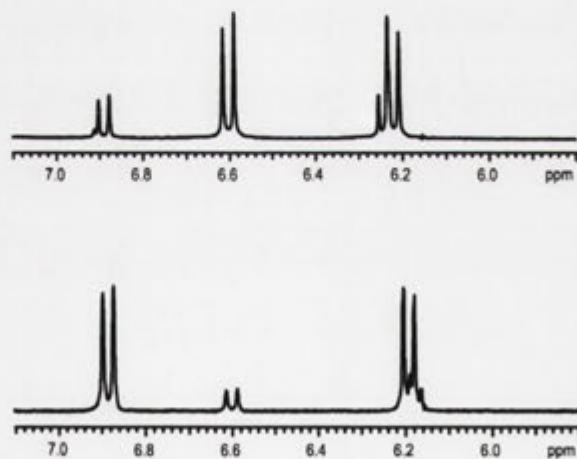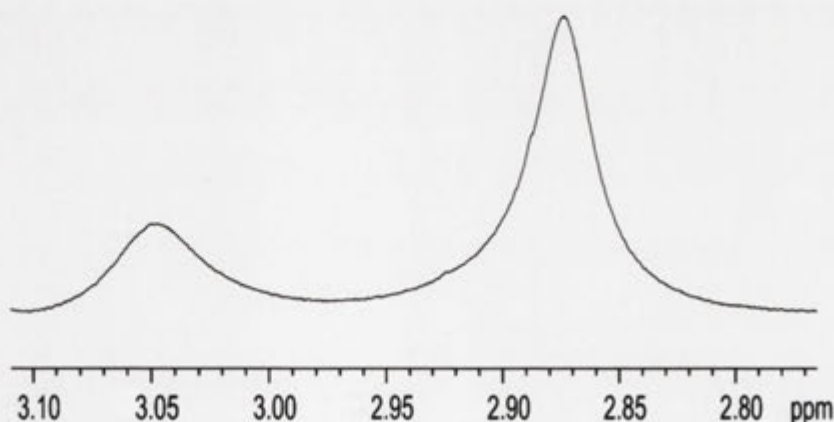

Figure 4.3.10. A section of the ^{1}H NMR spectra of the hermaphrodite **2.5** (top) and the hermaphrodite **4.4** (bottom) in D_2O at 25 °C.
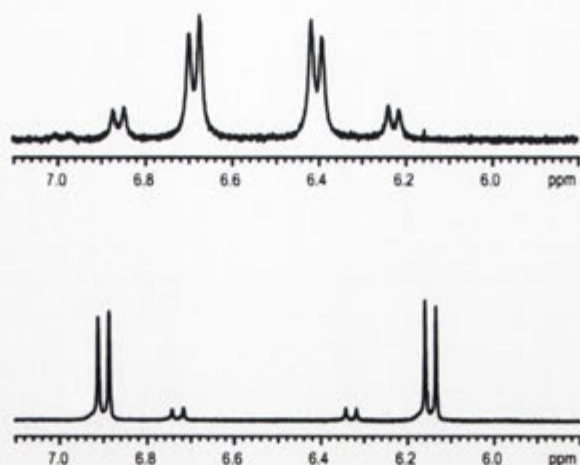
Figure 4.3.11. A section of the ^{1}H NMR spectra of the hermaphrodite **2.5** (top) and the hermaphrodite **4.4** (bottom) in D$_2$O with 1-adamantanol "fuel" at 25 °C.

Having studied the conformational behavior of the two hermaphrodites **4.3** and **4.4**, the next objective was to investigate the conformational behavior of the dimethylcinnamido hermaphrodite **4.7**. In d_6-DMSO as observed in the *N*-methyl region of the ^{1}H NMR spectrum (Figure 4.3.12), two very broad singlets are observed at δ 3.05 and 2.87 ppm in an approximate ratio of 1:2. The relative intensities of these signals indicate that there are two amide isomers of the hermaphrodite **4.7**. The broadened line shape indicates that intermediate chemical exchange occurs between these *Z/E*-amide isomers.[126] Thus, in d_6-DMSO the hermaphrodite **4.7** exists with two amide isomers in a ratio of 1:2.
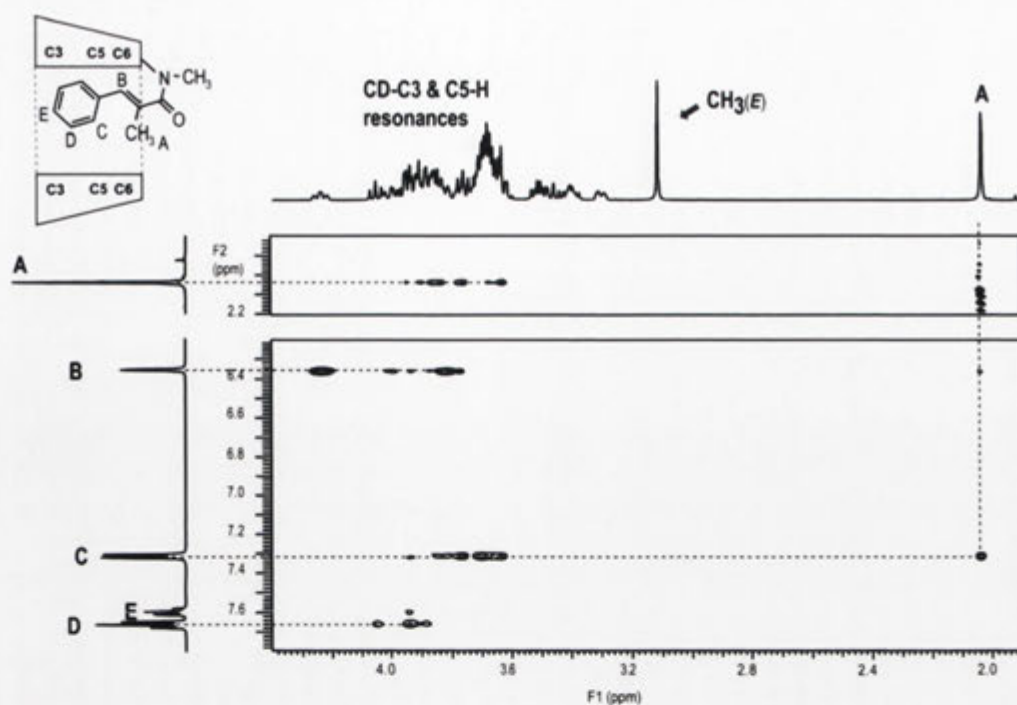

Figure 4.3.12. Section of the ^{1}H NMR spectrum (500 MHz) of the hermaphrodite **4.7** in d_6-DMSO at 25 °C.

In contrast to d_6-DMSO, in D$_2$O the hermaphrodite **4.7** appears to exist as one dominant species as shown in the ^{1}H NMR spectrum in Figure 4.3.13. In the *N*-methyl

67

region of the spectrum a high intensity proton singlet is observed at δ 3.11 ppm. From the ROESY spectrum (Figure 4.3.14) this signal (F1 axis) shows no NOE interaction with the α-methyl signal at δ 2.04 ppm (F2 axis) and is therefore assigned to the methyl group of the *E*-amide isomer. The α-methyl signal (**A**) at δ 2.04 ppm, the olefinic signal (**B**) at δ 6.35 ppm and the aromatic resonances (**C-E**) between δ 7.67-7.30 ppm (F2 axis) show cross-peaks with the CD proton signals and therefore the aryl "piston" is included within the CD "cylinder". On this basis the major conformation of the hermaphrodite **4.7** in D$_2$O is the included [*c*1] complex of the *E*-amide isomer. In spite of this, a low intensity singlet at δ 3.25 ppm that can be assigned to the *Z*-amide isomer from titrations with 1-adamantanol "fuel" (Figure 4.6.4) is identified in an *Z/E*-amide ratio of approximately 1:800 later in this Chapter.
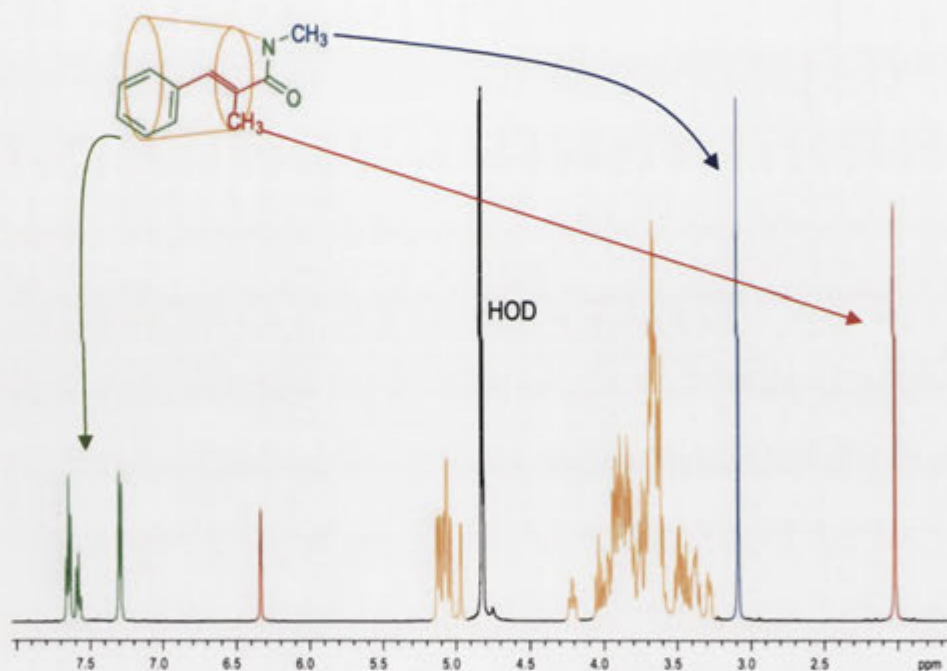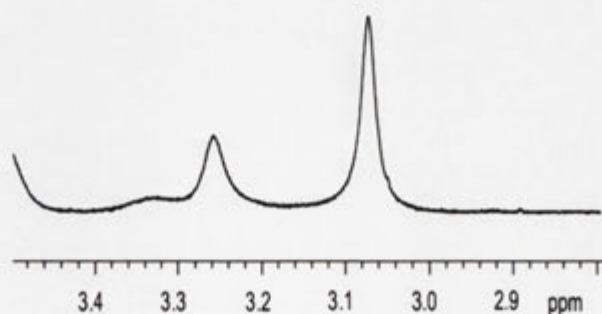

Figure 4.3.13. ^{1}H NMR spectrum (500 MHz) of the hermaphrodite **4.7** in D$_2$O at 25 °C.

Figure 4.3.14. Sections of the ROESY NMR spectrum (500 MHz) of the hermaphrodite **4.7** in D$_2$O (25 °C) with 0.250 ms mixing time.

The ^{1}H NMR spectrum of the hermaphrodite **4.7** in the presence of 1-adamantanol "fuel" in D$_2$O is shown in Figure 4.3.15. In the *N*-methyl region of the spectrum, two broad proton signals are observed at δ 3.26 and 3.07 ppm that integrate in a ratio of about 1:2.3, respectively. The broad appearance of these signals indicates that intermediate chemical exchange is occurring between the *Z/E*-amide isomers.[126] For reasons demonstrated later in the Chapter (Figure 4.6.6) the peak at δ 3.07 ppm can be assigned to the *E*-amide isomer. From this and consistent with the findings from Chapter 2, in the presence of 1-adamantanol "fuel" the hermaphrodite **4.7** in D$_2$O adopts two amide conformations with an overall *Z/E*-amide ratio of 1:2.3.

Figure 4.3.15. A section of the ^{1}H NMR spectrum (500 MHz) of 1-adamantanol (3-equivalents) and the hermaphrodite **4.7** in D$_2$O at 25 °C.

69

To summarise the conformational behavior of the hermaphrodite **4.7**, in d_6-DMSO the observed Z/E-amide ratio is 1:2. In D_2O the aryl "piston" is included and the E-amide isomer is the dominant conformation. In D_2O in the presence of 1-adamantanol "fuel", the Z/E-amide ratio is 1:2.3. By changing the solvent from d_6-DMSO to D_2O the amide ratio changes due to constraint by the molecular recognition process. By changing the conditions from D_2O to D_2O with 1-adamantanol "fuel" the competitive guest changes the Z/E-amide ratio of the hermaphrodite **4.7** so that it approaches that observed in d_6-DMSO. From these results, the conformational behaviors of the hermaphrodite **4.7** under the various conditions are consistent with the general trends observed for the hermaphrodites **2.3** and **2.4** from Chapter 2.

## 4.4 Photochemical Switching of Cyclodextrin Based Hermaphrodites

After preparing the hermaphrodites **4.3**, **4.4** and **4.7**, their conformational behaviors were investigated in d_6-DMSO, D_2O with 1-adamantanol and D_2O alone. Analogous to the hermaphrodites **2.4** and **2.5** already described in Chapter 2, the conversion from the hermaphrodite **4.3** to its *cis*-isomer **4.4** afforded a distinct change in conformational behavior, which is reminiscent of a machine-like function. Therefore the aim was to investigate the photochemical switching between the hermaphrodite **4.3** and its *cis*-isomer **4.4** in order to establish whether they comprise a reversible switch (Scheme 4.4.1). For this purpose, a combined UV/visible spectroscopic and reverse-phase HPLC strategy was employed in order to monitor the progression of the photolysis and quantify the resulting products.

Shown in Figure 4.4.1 is the UV/visible spectrum for an aqueous solution of the hermaphrodite **4.3** in H_2O (5.87 x 10^{-5} M) showing a maximum absorption (λ_{MAX}) at 278 nm. This is similar to that observed for the hermaphrodite **2.4** and for reasons described in Chapter 2 the solution of the hermaphrodite **4.3** was irradiated with light of 300 nm wavelength to obtain the *cis*-isomer **4.4**. During the course of the photochemical treatment the maximum absorbance at 278 nm decreased which corresponded to an increase in the absorption band at 254 nm. The photostationary state was reached at approximately 100 seconds. The photostationary mixture was applied to reverse-phase HPLC and monitored at the isosbestic point of 248 nm. The photostationary mixture contained the hermaphrodite **4.3** and the *cis*-isomer **4.4** in a ratio of 5:95 with the *cis*-

isomer having a λ_{MAX} of 254 nm. Next, to restore the hermaphrodite **4.3** and complete the photoisomerisation cycle, the photostationary mixture was then irradiated with 254 nm light. The photostationary state was reached at 60 seconds and the mixture contained the hermaphrodite **4.3** and the *cis*-isomer **4.4** in a ratio of 48:52. In contrast, the hermaphrodite **2.4** and its *cis*-isomer **2.5** afford photostationary states of 49:51 after exposure with 300 nm light and 92:8 for the 254 nm light. These differences could not be investigated due to time constraints, however it would be interesting to determine whether a link exists between the type of CD complexation and the efficiency of the photochemical process. This can be reasoned with the observation that the percentage of the *trans*-isomer remaining after photochemical treatment for the non-methyl analogue **4.3** is 5%, the *N*-methyl hermaphrodite **2.4** is 49% while the α-methylcinnamido hermaphrodite **4.7** is 100%, which parallels the extent of complexation observed in the ^{1}H NMR spectroscopic conformational analysis. This leads to the possibility that the hermaphrodite **4.7** is too well complexed to isomerise. Finally, the percentage of the hermaphrodite **4.3** present in the solution over three consecutive photoisomerisation cycles using 300 nm and 254 nm light is shown in Figure 4.4.2. This demonstrates that the hermaphrodite **4.3** and its *cis*-isomer **4.4** function as a reversible photochemical switch.
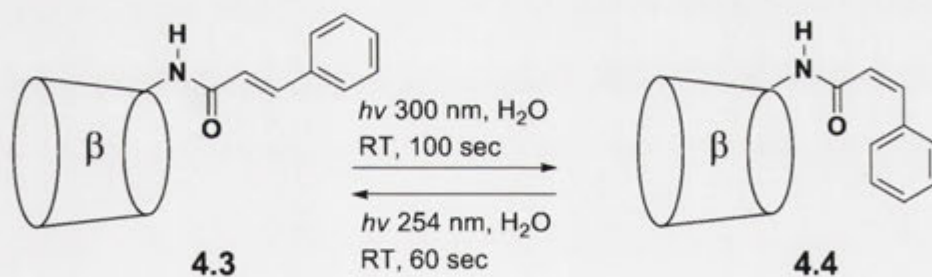
Scheme 4.4.1. Reversible photochemical isomerisation of the hermaphrodite **4.3** and its *cis*-isomer **4.4**.
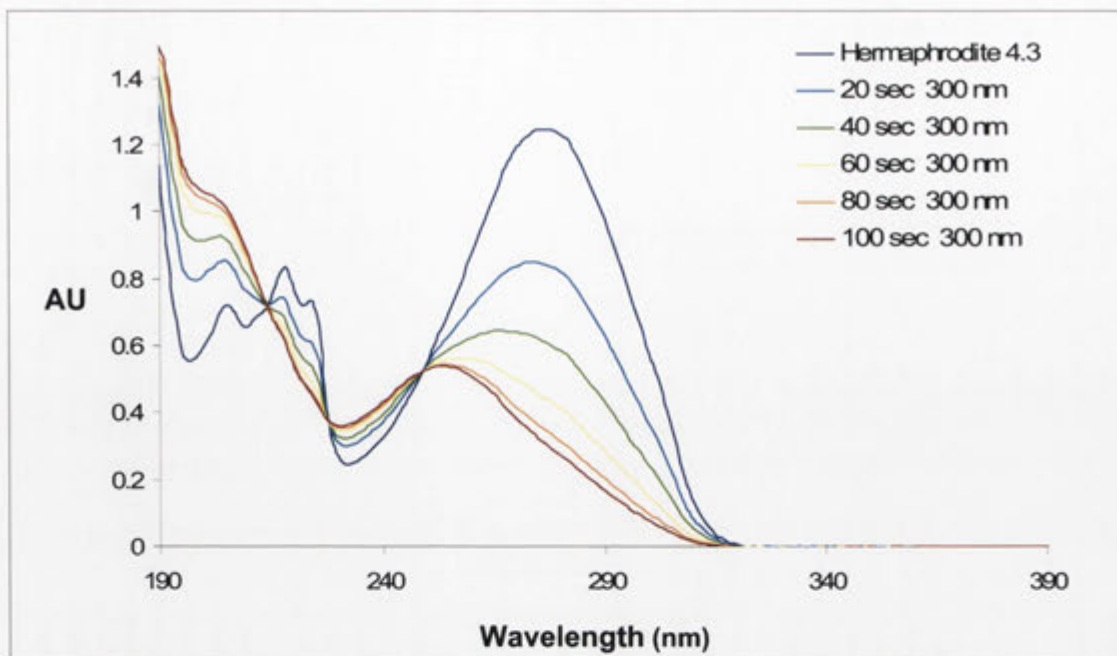
Figure 4.4.1. UV/visible spectra of the hermaphrodite **4.3** (5.87×10^{-5} M) in H_2O and after irradiation with 300 nm light.
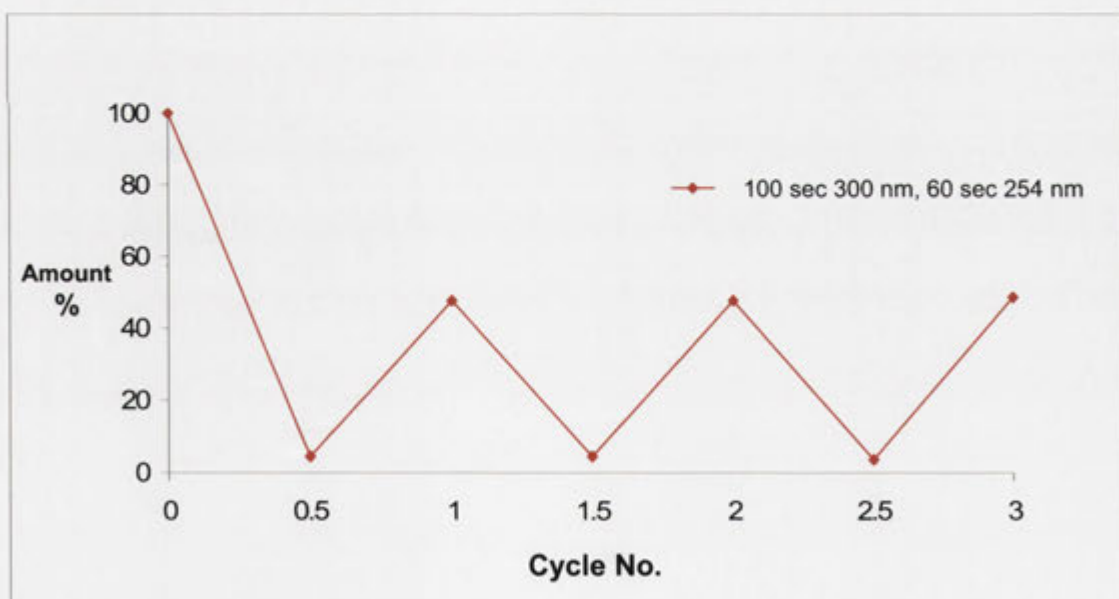
Figure 4.4.2. Amount (%) of the hermaphrodite **4.3** present after photoirradiation as determined by reverse-phase HPLC (248 nm). Each cycle consists of irradiation at 300 nm followed by 254 nm.

## 4.5 Measuring the Heats of Dilution of Complexes of Cyclodextrin Based Hermaphrodites

The purpose of synthesising the hermaphrodites **4.3**, **4.4** and **4.7** was to investigate the effects that various substituents have upon their operation and performance. As demonstrated in Chapter 2, the major conformation of the hermaphrodites **2.3** and **2.4** in aqueous solution is the [c1] complex that restricts the geometry of the amide bond to the *E*-amide isomer. From the ^{1}H NMR analysis in Chapter 4.3, the proportion of the *E*-amide isomer for the hermaphrodite **4.3** is small (2-3%). However, NOE interactions are still observed between the aryl "piston" and the CD "cylinder" for which the logical interpretation is that either the *Z*-amide can also form the [c1] complex or the complexation is an intermolecular assembly. Such concentration dependent assemblies are known for CD based hermaphrodites having rigid pendant groups however their formation is often difficult to assess using 2D NMR spectroscopy alone.[104,127] Previously, ITC has been used to establish the formation of multimeric proteins and supramolecular polymers by measuring the characteristic heat changes from their concentration dependent dissociation upon dilution.[128-130] This technique involves titrating aliquots of the self-associating compound into the ITC cell containing identical buffer and measuring the stepwise heat changes that occur from dissociation.[128] This technique was applied to the hermaphrodites **4.3**, **4.4**, **2.4** and **4.7** with the aim of measuring their heats of dilution for the purpose of identifying any concentration dependence.

Figure 4.5.1a shows ITC enthalpograms (top) and integrated peaks (bottom) for the dilution of the hermaphrodite **4.3** (5 mM) into a buffered aqueous solution. The curve shows positive enthalpic heat changes that are consistent with an endothermic process. The overall heat change decreases by 1 kcal/mol^{-1} over the course of the titration. As the concentration of the hermaphrodite **4.3** increases within the cell the difference in heat change decreases between consecutive injections, which is typical for an equilibrium shift from monomer to oligomer.[128] To establish the concentration where the intermolecular complex predominates the thermodynamic parameters for dissociation were calculated. For this a dimer dissociation least-squares regression model was used to fit the dilution curves. A dimer is the most entropically favored intermolecular complex. The intermolecular dissociation (K_D), as an average of two identical runs, was quantified as being 0.15 ± 0.02 mM which corresponds to an

intermolecular association constant (K_A) of 7000 M^{-1} ($K_A = 1/K_D$). This indicates that the intermolecular complexation occurs at lower concentrations than the ^{1}H NMR analysis from Chapter 4.3 (3.4 mM). By applying the K_D to Equation 4.5.1[129] the percentage of free monomer present ([CD]$_{MON}$) in solution can be determined for a chosen concentration of the hermaphrodite **4.3** ([CD]$_{TOT}$). Accordingly, the percentage of the hermaphrodite **4.3** monomer present during the ^{1}H NMR conformational analysis was identified to be around 15%. Hence, the hermaphrodite **4.3** exists predominantly as an intermolecular dimer of an [*a*1] CD conformation during the ^{1}H NMR spectroscopic studies, which supports the conclusions drawn from the ROESY analysis.

$$[CD]_{mon} = \frac{(-K_D + \sqrt{K_D + 8K_D[CD]_{tot}})}{4} \qquad (4.5.1)$$

In contrast, shown in Figure 4.5.1b is the ITC thermogram for the dilution of the hermaphrodite **4.4** (5 mM) into a buffered aqueous solution. In this case the endothermic heat changes for consecutive injections remain constant. This result indicates that dissociation is not occurring upon dilution and confirms that the hermaphrodite **4.4** is monomeric.
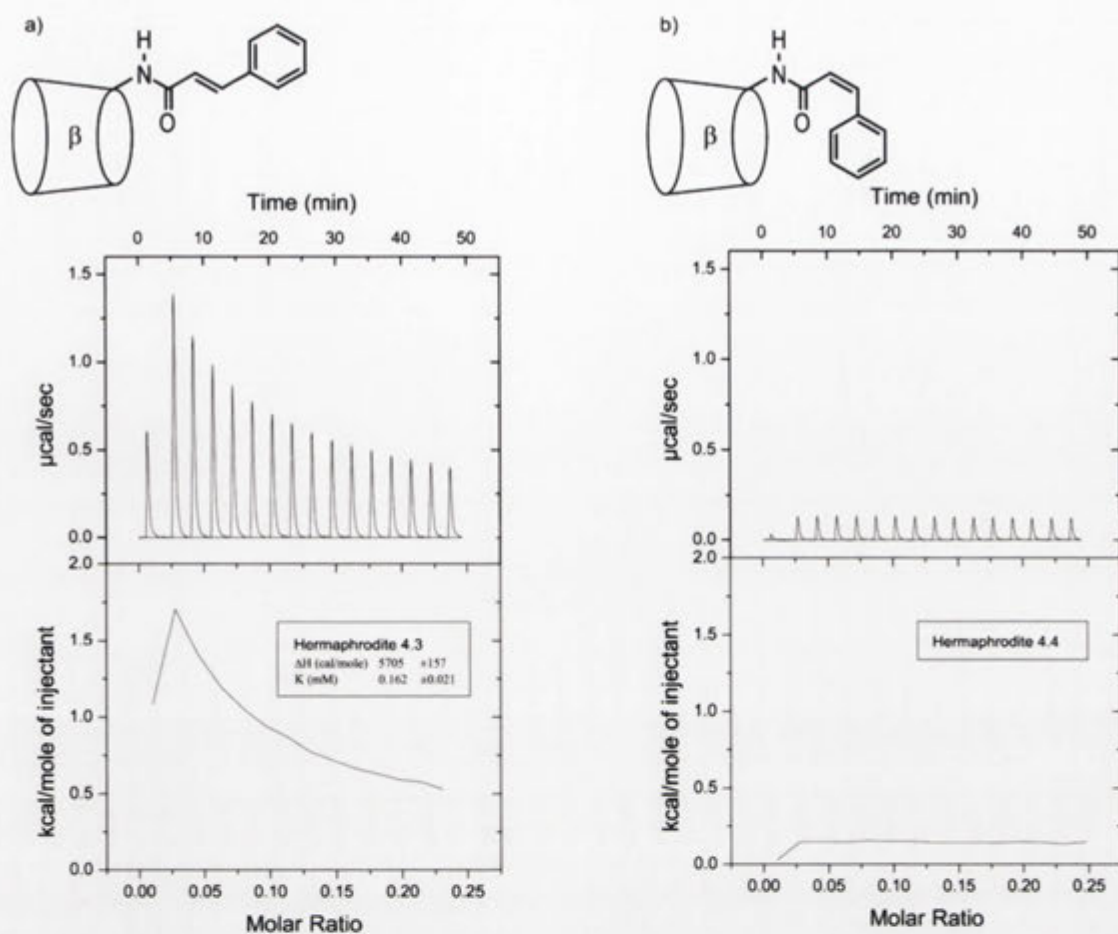
Figure 4.5.1. ITC thermograms for 15 successive injections (5 μl) of the hermaphrodite (5 mM) in 0.05 M NaH_2PO_4/Na_2HPO_4 buffer (pH 6.9) into cells containing identical buffer. a) hermaphrodite **4.3**; b) hermaphrodite **4.4**.

Knowing that the hermaphrodite **4.3** forms a dimer it was necessary to confirm that this was not occurring with the species **2.4** and **4.7** thought to form [c1] complexes. A ^1H NMR spectroscopic analysis was employed to study the concentration effects on the hermaphrodite **2.4**. The purpose of using ^1H NMR spectroscopy was to identify the formation of any intermolecular CD complex at higher concentrations than the ITC method by recording the concentration dependent changes in chemical shift.[73,131] Accordingly, Figure 4.5.2 shows the ^1H NMR spectra of the aromatic and olefinic resonances of the hermaphrodite **2.4** at various concentrations (2.5 mM - 20 mM) in D_2O. The proton signals show no observable change in chemical shift as the concentration is varied suggesting that the complexation of the hermaphrodite **2.4** is concentration independent. However, if intermolecular complexes (K_D = 0.15 mM) were dominant for the hermaphrodite **2.4** at concentrations lower than the 2.5 mM then a change in chemical shift may not be observed over this range.
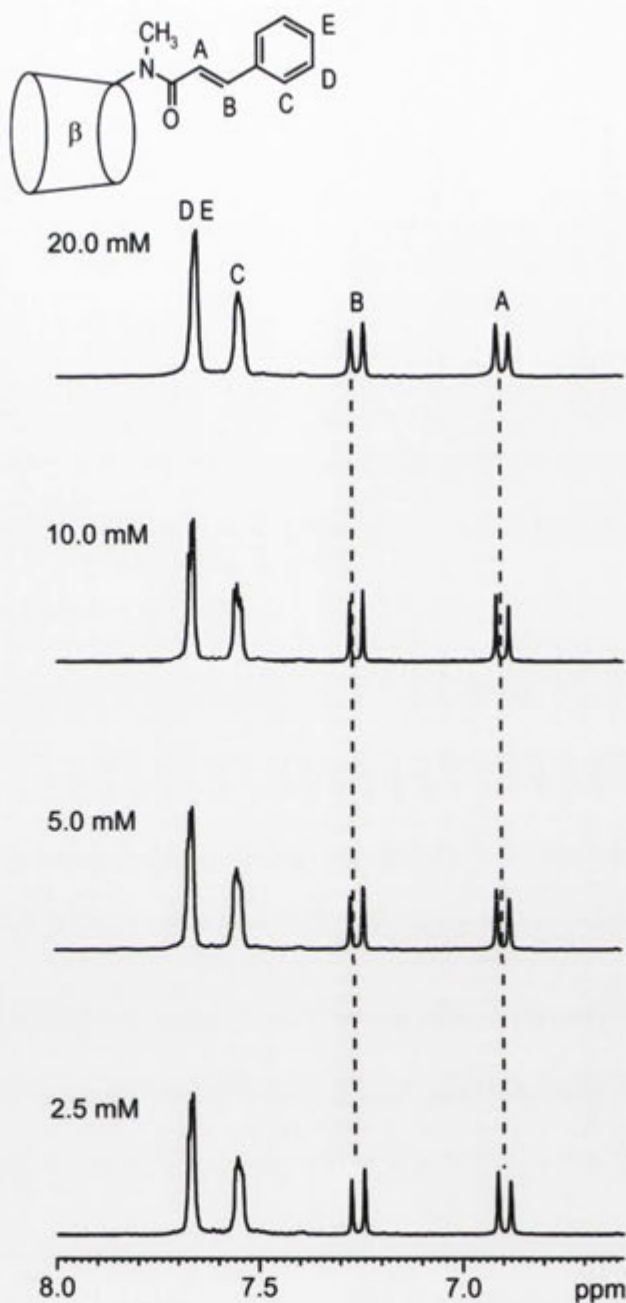
Figure 4.5.2. A section of the ^{1}H NMR spectra (500 MHz) of the hermaphrodite **2.4** in D_2O at various concentrations at 25 °C.

Next, Figure 4.5.3 shows the ITC enthalpograms and integrated peaks for the heats of dilution for the hermaphrodite **2.4** and in addition the α-methyl analogue, the hermaphrodite **4.7**. Over the chosen concentration range (18 μM – 0.3 mM) only minor overall heat changes of between 0.01 and 0.02 kcal/mol[-1] were observed for both the hermaphrodites **2.4** and **4.7** indicating that no significant equilibrium shift from monomer to oligomer occurs. These results support the conclusions from the ROESY

analysis that the hermaphrodites **2.4** and **4.7** in aqueous solutions form predominantly concentration independent [$c1$] complexes.
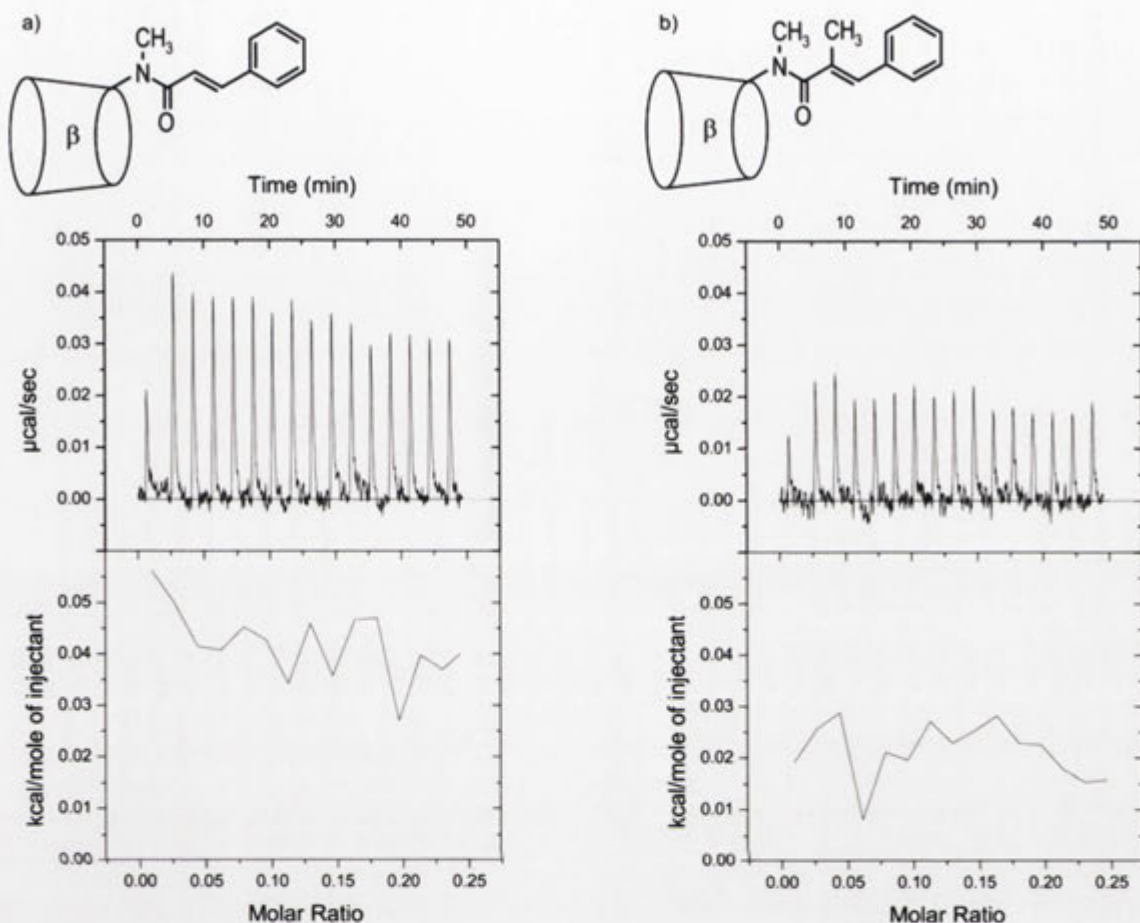
Figure 4.5.3. ITC thermograms for 15 successive injections (5 µl) of the hermaphrodite (5 mM) in 0.05 M NaH_2PO_4/Na_2HPO_4 buffer (pH 6.9) into cells containing identical buffer. a) hermaphrodite **2.4**; b) hermaphrodite **4.7**.

In summary, the heats of dilution were measured for the CD based hermaphrodites using ITC. From this, the hermaphrodite **4.3** in aqueous solution forms mainly a dimeric assembly with a K_D of 0.15 mM, whereas the hermaphrodites **2.4**, **4.7** and **4.4** in aqueous solution are monomeric and concentration independent. In combination with the ^{1}H NMR analysis this is in support of the major species for the hermaphrodite **4.3** being an [$a1$] conformation of the *Z*-amide isomer while only 2-3% is present as the [$c1$] complex of the *E*-amide isomer. The hermaphrodites **2.4** and **4.7** have the predominant species being the [$c1$] complex of the *E*-amide isomer with only a small percentage of the *Z*-amide isomer presumably in the [$a1$] conformation. As the [$a1$] conformation of the *Z*-amide is capable of forming intermolecular dimers, this

explains the difference in the concentration dependence observed between the hermaphrodite **4.3** and the hermaphrodites **2.4** and **4.7**.

## 4.6 Effect of Substituents upon the Energy Harnessed by Cyclodextrin Based Hermaphrodites

Having identified that the "piston" modifications alter the conformational behavior of the hermaphrodites **4.3**, **4.4** and **4.7**, the next step was to investigate what effects these substituents have upon the energy harnessed during their operation. The Z/E-amide ratio reflects the difference between the isomer ground state free energies (ΔG) under a set of conditions. The differences in the amide isomer ratios and ground state free energies in D_2O with and without 1-adamantanol "fuel" reflect the work output ($\delta\Delta G$) performed on the amide bond. By quantifying the $\delta\Delta G$ for the hermaphrodites **4.3**, **4.4** and **4.7** using ^1H NMR spectroscopy, the effects of the various substituents on the energies harnessed were established.

Shown in Figure 4.6.1 are the ^1H NMR spectra for the hermaphrodite **4.3** in D_2O (bottom) and in D_2O with 1-adamantanol (top). In D_2O, the hermaphrodite **4.3** affords a Z/E-amide ratio of 40:1 which represents a ΔG of -2.2 kcal mol^{-1}. In D_2O with 1-adamantanol "fuel" the Z/E-amide ratio is 200:1 resulting in a ΔG of -3.1 kcal mol^{-1}. From this, the addition of the 1-adamantanol "fuel" results in a five-fold reduction in the proportion of the E-isomer and the work harnessed in the amide bond is 0.9 kcal mol^{-1}. Compared against the N-methyl analogue **2.4** from Chapter 2, the secondary amide linkage group has decreased the work energy harnessed ($\delta\Delta G$) by the hermaphrodite **4.3** by about 1.0 kcal mol^{-1}. Although less energy is harnessed than its tertiary amide counterpart, the hermaphrodite **4.3** behaves as a molecular machine in the "ON" state.
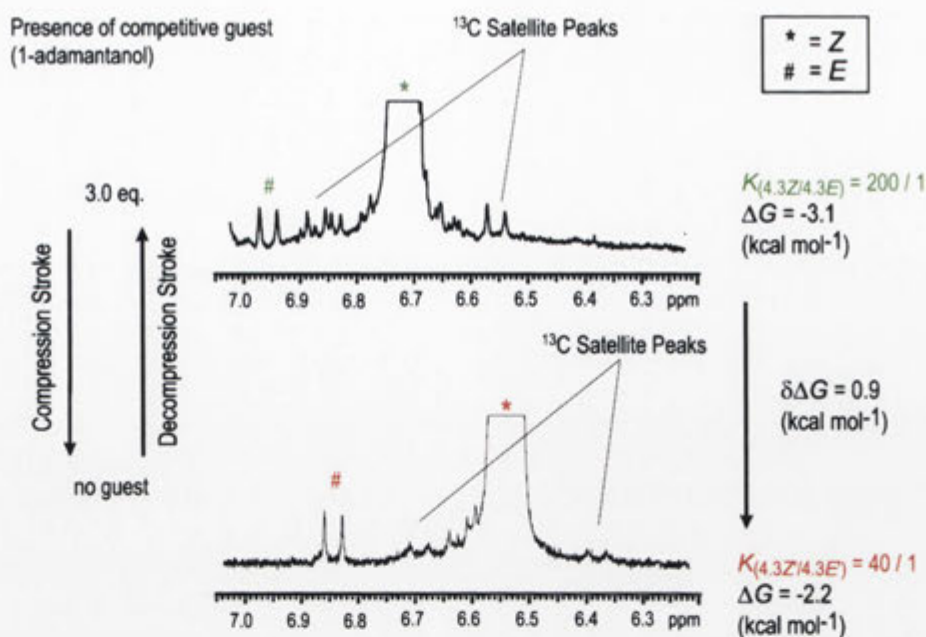
Figure 4.6.1. A section of the ^{1}H NMR spectra (500 MHz) of *trans*-6^A-deoxy-6^A-cinnamido-β-CD **4.3** in D_2O at 25 °C in the presence and absence of 1-adamantanol "fuel".

Having established that the hermaphrodite **4.3** behaves as a molecular machine the operation of its *cis*-isomer **4.4** was studied. In Figure 4.6.2 are the ^{1}H NMR spectra showing the olefinic proton signals for the hermaphrodite **4.4** with varying concentrations of 1-adamantanol "fuel". All spectra are referenced using an internal standard and have been offset for clarity. In D_2O, the *Z/E*-amide ratio is 6:1 which represents a ΔG of -1.1 kcal mol^{-1}. In D_2O with 1-adamantanol "fuel" the *Z/E*-amide ratio is 11:1 corresponding to a ΔG of -1.4 kcal mol^{-1}. During the operation the decrease in the proportion of the *E*-isomer corresponds to a work output of 0.3 kcal mol^{-1}. Relative to its *N*-methyl analogue **2.5** from Chapter 2, the hermaphrodite **4.4** performs slightly more work however this still remains small enough for the molecular machine to be considered to be in the "OFF" state. When the operation of the hermaphrodite **4.3** and its *cis*-isomer **4.4** are combined they function as a molecular machine having a photochemical "ON/OFF" switch (Scheme 4.6.1).
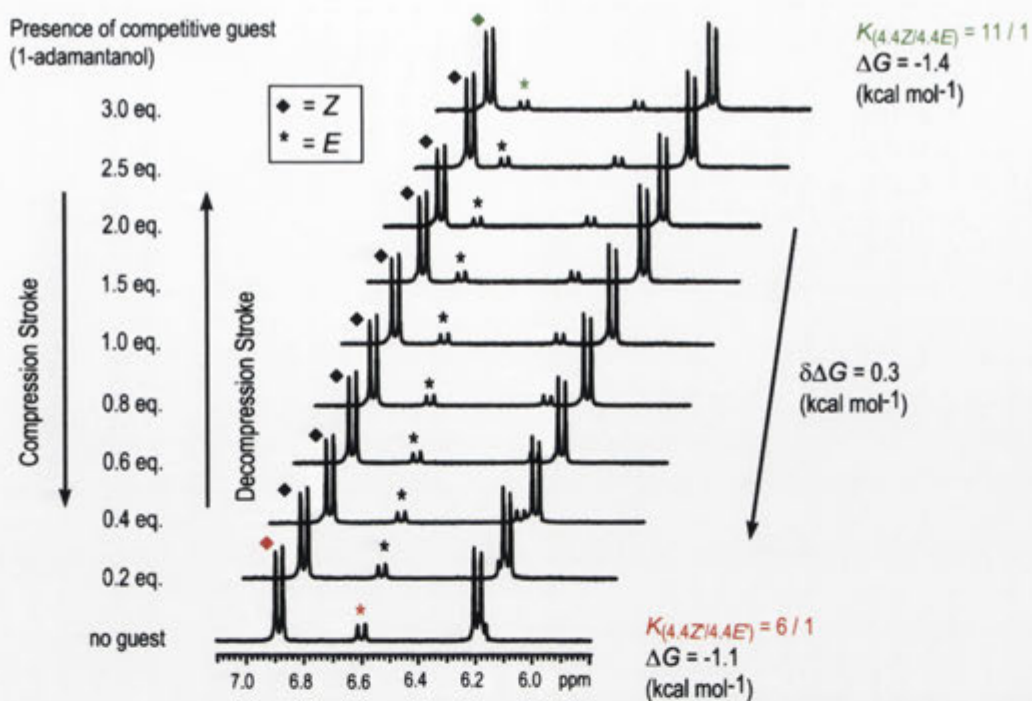
Figure 4.6.2. A section of the ^{1}H NMR spectra (500 MHz) of *cis*-6^A-deoxy-6^A-cinnamido-β-CD **4.4** in D$_2$O at 25 °C in the presence and absence of 1-adamantanol "fuel".
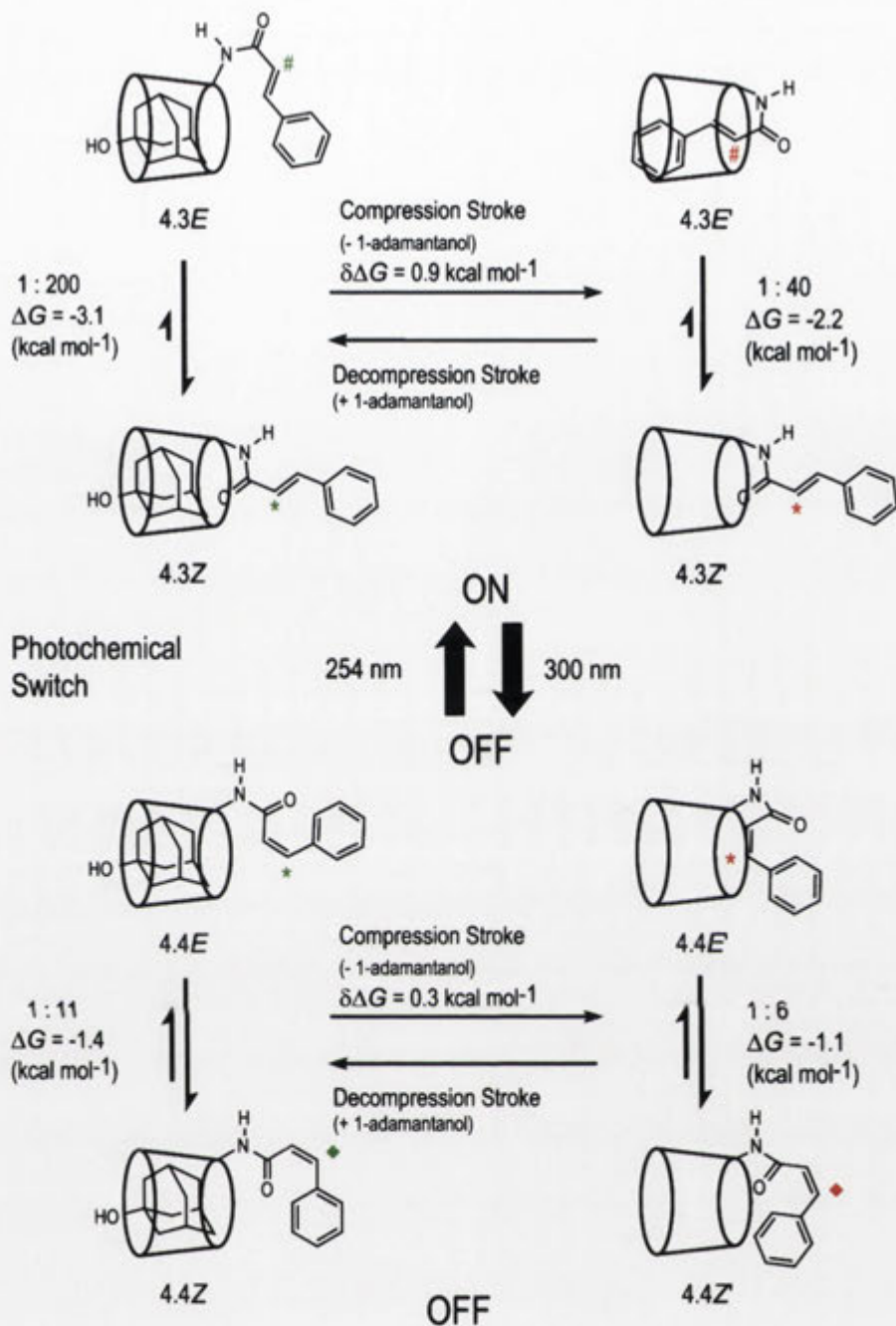
Scheme 4.6.1. Operation of *trans*-6^A-deoxy-6^A-cinnamido-β-CD **4.3** and *cis*-6^A-deoxy-6^A-cinnamido-β-CD **4.4** as a molecular pump.

Next, the operation of the *N*,α-dimethylcinnamido hermaphrodite **4.7** was investigated using 1-adamantanol "fuel". Shown in Figure 4.6.3 is the *N*-methyl region of the ^{1}H NMR spectrum for the hermaphrodite **4.7**. Sitting symmetrically astride the proton signal of the *E*-amide isomer at δ 3.11 ppm are ^{13}C satellite peaks. The ^{13}C satellite peak at δ 3.25 ppm coincides with the proton signal of the *Z*-amide isomer. This is demonstrated upon the addition of 1-adamantanol "fuel" by an increase in the

intensity of the resonance of the Z-amide isomer at δ 3.25 ppm relative to the ^{13}C satellite peak at δ 2.98 ppm (Figure 4.6.4). In D_2O alone, the difference in the integration between the ^{13}C satellite peaks at δ 3.25 and 2.98 ppm therefore reflects the proportion of the Z-amide isomer present for which the Z/E-amide ratio is 1:770. In order to validate this ratio, the ^{1}H NMR spectrum of the hermaphrodite **4.7** was recorded on a 600 MHz NMR spectrometer (Figure 4.6.5). At this frequency the ^{13}C satellite peaks have shifted and the proton signal of the Z-amide isomer is identified in the presence and absence of 1-adamantanol "fuel". Now, the resonance of the Z-isomer appears as approximately 0.25% of the ^{13}C satellite peak or 0.125% of the proton signal for the E-amide isomer at δ 3.11 ppm, thus the Z/E-amide ratio is 1:800.
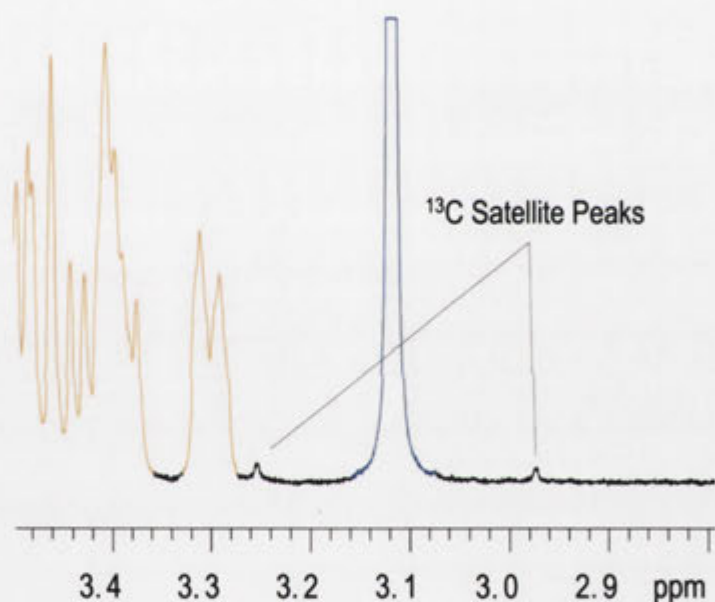
Figure 4.6.3. A section of the ^{1}H NMR spectrum (500 MHz) of the hermaphrodite **4.7** in D_2O at 25 °C.
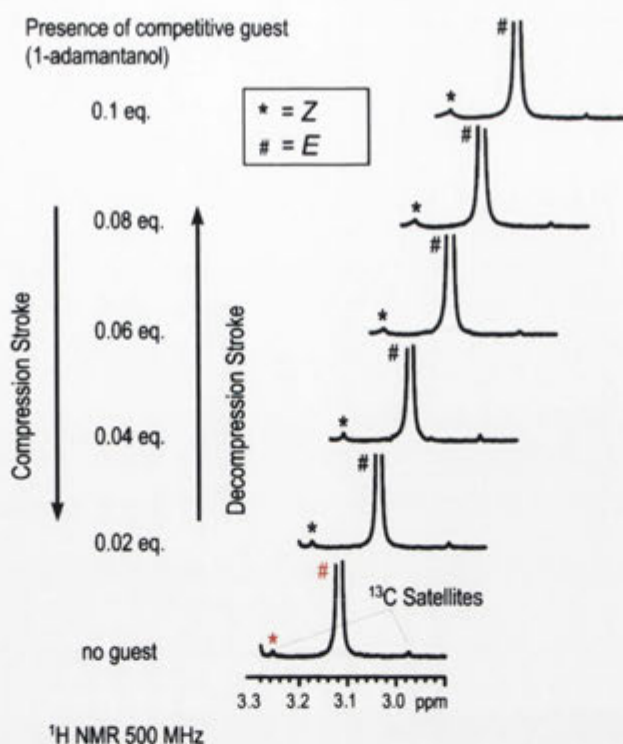
Figure 4.6.4. A section of the ^{1}H NMR spectra (500 MHz) of the hermaphrodite **4.7** in D$_2$O at 25 $^\circ$C in the presence and absence of 1-adamantanol "fuel".
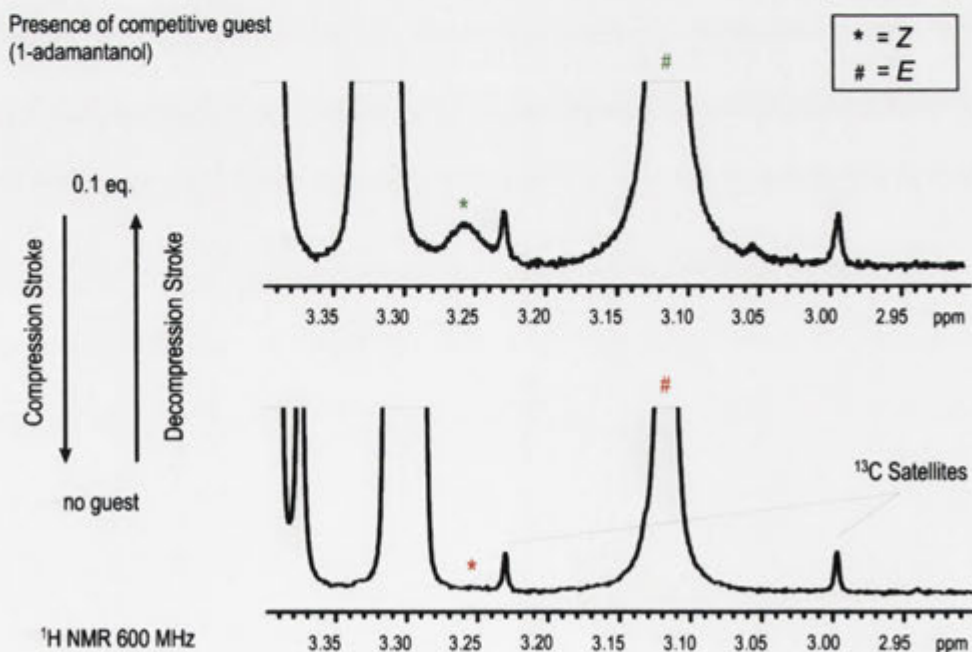
Figure 4.6.5. ^{1}H NMR spectra (600 MHz) of the hermaphrodite **4.7** in D$_2$O at 25 $^\circ$C in the presence (top) and absence (bottom) of 1-adamantanol "fuel".

It follows that in D_2O the hermaphrodite **4.7** affords a Z/E-amide ratio of approximately 1:800 which represents a ΔG of 4.2 kcal mol^{-1} (Figure 4.6.6). By titrating the hermaphrodite **4.7** with 1-adamantanol "fuel" the isomers can be traced to the endpoint where the Z/E-amide ratio is 1:2.3 which reflects a ΔG of 0.5 kcal mol^{-1}. On this basis, the work performed on the amide bond is 3.7 kcal mol^{-1} which is nearly double the energy harnessed by the most efficient of the artificial molecular machines developed in Chapter 2 which was the hermaphrodite **2.4** (2.1 kcal mol^{-1}). Shown in Scheme 4.6.2 is the operation of the hermaphrodite **4.7** as a working molecular machine.
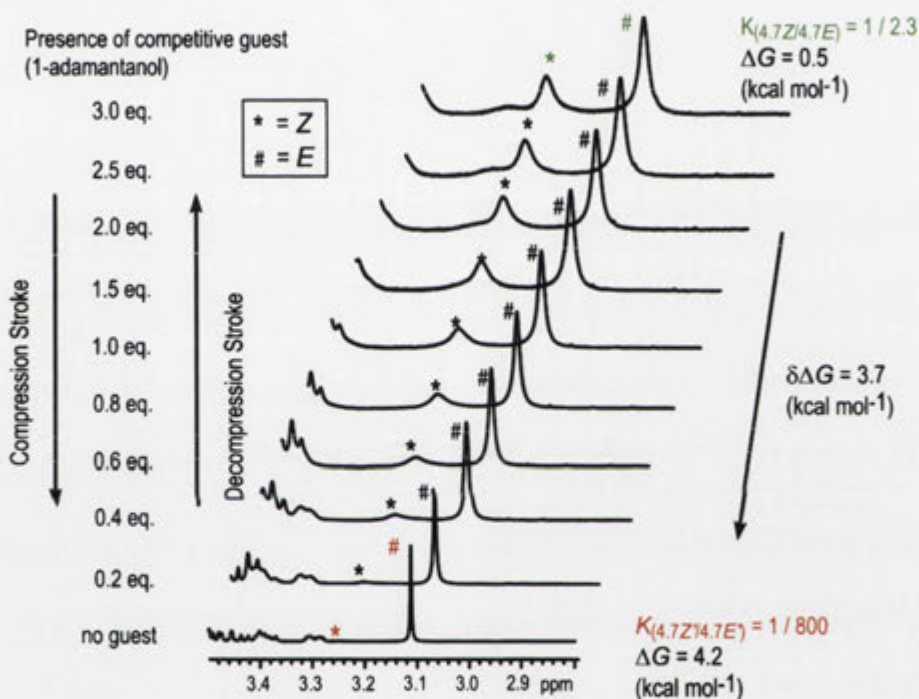
Figure 4.6.6. A section of the ^{1}H NMR spectra (500 MHz) of *trans*-6^A-deoxy-6^A-(N,α-dimethylcinnamido)-β-CD **4.7** in D_2O at 25 °C in the presence and absence of 1-adamantanol "fuel".
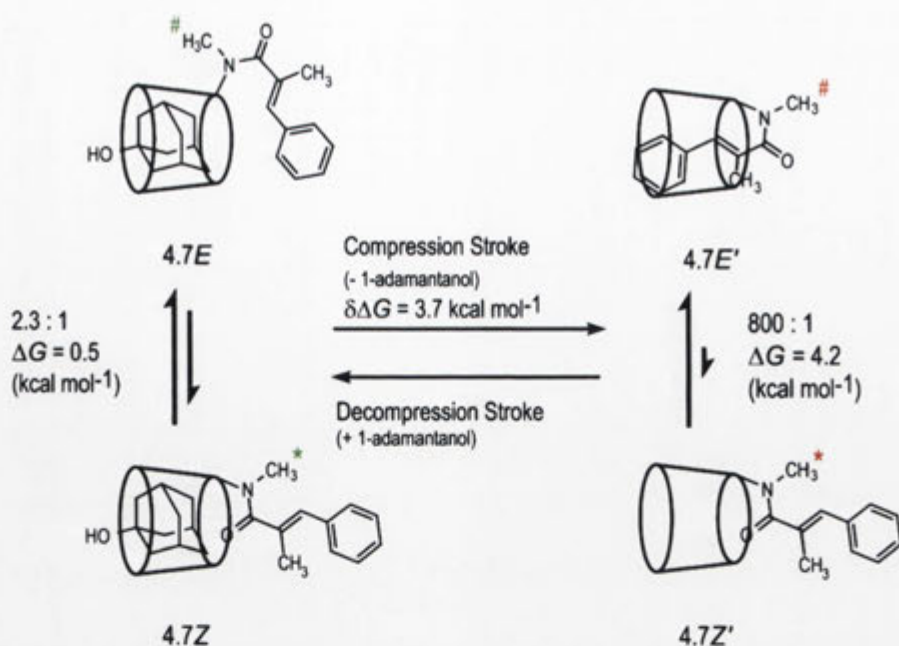
Scheme 4.6.2. Operation of *trans*-6^A-deoxy-6^A-(N,α-dimethylcinnamido)-β-CD **4.7** as a molecular pump.

To summarise these findings, the hermaphrodite **4.3** with the secondary amide bond harnesses 0.9 kcal mol^{-1} and is in the "ON" state. Its tertiary amide analogue the hermaphrodite **2.4** harnesses 2.1 kcal mol^{-1} of energy and thus the apparent effect of the secondary amide group is to decrease the work output. Next, the hermaphrodite **4.4** performs an output of 0.3 kcal mol^{-1} which is larger than the -0.2 kcal mol^{-1} observed for its *N*-methyl analogue the hermaphrodite **2.5**. Although more work is being done it remains small enough for the hermaphrodite **4.4** to be considered in the "OFF" state. As the hermaphrodite **4.3** and its *cis*-isomer **4.4** can be photochemically interconverted the harnessing of energy can therefore be switched "ON" and "OFF". Finally, the hermaphrodite **4.7** harnesses 3.7 kcal mol^{-1} of energy which is nearly double that observed for the hermaphrodite **2.4**. On this basis the effect of attaching an additional methyl group on the aryl "piston" is to increase the work output.

4.7 Isothermal Titration Calorimetry of Cyclodextrin Based Hermaphrodites

With the energy harnessed by each of the hermaphrodites **4.3**, **4.4** and **4.7** quantified, the efficiency of this output remained to be established. For this, ITC was employed to measure the thermodynamic parameters for the binding interaction between the hermaphrodites **4.3**, **4.4** and **4.7** and the "fuel". In order to obtain accurate thermodynamic data, 1-adamantanol was replaced with 1-adamantanecarboxylate "fuel" which has a relatively higher solubility. Using 1-adamantanecarboxylate "fuel" the Z/E-amide ratios for the hermaphrodites **4.3**, **4.4** and **4.7** were determined using ^{1}H NMR spectroscopy and found to afford the same $\delta\Delta G$ values as 1-adamantanol. Following the same ITC protocol discussed in detail in Chapter 3, aliquots of the 1-adamantanecarboxylate "fuel" (pH 6.9) were titrated into the ITC cell containing a known concentration of a buffered solution of the chosen hermaphrodite **4.3**, **4.4** or **4.7**. The stepwise heat changes resulting from the binding interaction were recorded as enthalpograms from which the thermodynamic parameters could be extracted using nonlinear least-squares fitting. Two independent titrations with 1-adamantanecarboxylate "fuel" were conducted for each of the hermaphrodites **4.3**, **4.4** and **4.7**, the results of which are averaged to obtain the thermodynamic parameters reported in Table 4.7.1.

CD	K_A (M^{-1})	$\delta\Delta G$ (kcal mol^{-1})[a]	ΔG (kcal mol^{-1})[b]	ΔH (kcal mol^{-1})	$T\Delta S$ (kcal mol^{-1})
β-CD	42050 ± 50	N/A	-6.3	-5.5 ± 0.0	0.8 ± 0.001
4.3	23950 ± 650	0.9	-6.0	-5.2 ± 0.1	0.8 ± 0.1
4.4	14700 ± 100	0.3	-5.7	-6.8 ± 0.2	-1.1 ± 0.2
2.4	5130 ± 30	2.1	-5.0	-6.5 ± 0.02	-1.5 ± 0.02
2.5	19500 ± 200	-0.2	-5.9	-8.3 ± 0.2	-2.4 ± 0.2
2.3	5065 ± 85	1.4	-5.1	-6.4 ± 0.03	-1.3 ± 0.02
4.7	972 ± 17	3.7	-4.0	-5.9 ± 0.05	-1.9 ± 0.06

Table 4.7.1. ITC and NMR experimental data for the binding of 1-adamantanecarboxylate "fuel" (pH 6.9) with the hermaphrodites **2.3**, **2.4**, **2.5**, **4.3**, **4.4** and **4.7**. [a]$\delta\Delta G$ values reported are amide strain energy stored from the decompression stroke of the "piston" with 1-adamantanecarboxylate as measured by ^{1}H NMR spectroscopy. [b]ΔG values calculated from $\Delta H - T\Delta S$.

The Table shows the association constant (K_A), work output ($\delta\Delta G$), free energy change (ΔG), enthalpy change (ΔH) and entropy change ($T\Delta S$) for each of the hermaphrodites **4.3**, **4.4** and **4.7**. In order to facilitate the analysis of the various substituents Table 4.7.1 also includes the thermodynamic parameters that were reported in Chapter 3 under the same conditions for the operation of the hermaphrodites **2.3**, **2.4** and **2.5**. Beginning with the hermaphrodite **4.7**, this system having the α-methylcinnamido "piston" has a K_A of 972 M^{-1} for the 1-adamantanecarboxylate "fuel". This is a greater than forty-fold decrease in affinity relative to the unhindered β-CD **1.10** control and the lowest association of all the molecular machines. This reflects that this aryl "piston" is most strongly included within the CD "cylinder" and the major species is the [c1] complex of the *E*-amide isomer as identified in the ^{1}H NMR spectroscopic and ITC conformational analyses from Chapters 4.3 and 4.5. The relative strength of the [c1] complex is also reflected in the fact that this system harnesses the largest amount of work energy ($\delta\Delta G$) in the amide bond which is 3.7 kcal mol^{-1}. This is supported by comparison with the hermaphrodites **2.3** and **2.4** that afford K_As of 5065 M^{-1} and 5130 M^{-1}, thus having a five-fold greater affinity for the "fuel" than the hermaphrodite **4.7**. On this basis, the strengths of their [c1] complexes are reduced and

for this reason the hermaphrodites **2.3** and **2.4** harness less work with $\delta\Delta G$s of 1.4 kcal mol^{-1} and 2.1 kcal mol^{-1}, respectively. Next, the hermaphrodite **4.4** with the secondary amide bond and the *cis*-cinnamido "piston" affords a K_A of 14700 M^{-1}. In this case the CD "cylinder" is less hindered by the aryl "piston" and therefore the addition of 1-adamantanecarboxylate "fuel" has little effect upon the Z/E-amide isomer ratio. As a consequence the amount of work harnessed ($\delta\Delta G$) is only 0.3 kcal mol^{-1}. Its tertiary amide analogue the hermaphrodite **2.5** has an even higher affinity for 1-adamantanecarboxylate "fuel" with a K_A of 19500 M^{-1} and accordingly harnesses less energy with a $\delta\Delta G$ of -0.2 kcal mol^{-1}. Finally, the hermaphrodite **4.3** with the secondary amide linked to the *trans*-cinnamido "piston" gave the highest affinity for the 1-adamantanecarboxylate "fuel" with a K_A of 23950 M^{-1}. The relatively higher association constant indicates that the aryl "piston" does not effectively hinder the CD "cylinder" which is consistent with the conformational analyses from Chapters 4.3 and 4.5. The major species is the [a1] conformation of the Z-amide and only a small proportion of the hermaphrodite **4.3** exists as the [c1] complex of the E-amide isomer. Although the intermolecular complex does form for the [a1] conformation it has little effect on hindering the CD annulus due to the relatively low concentration (0.40 mM) of the ITC experiment and the comparative weakness of the dimeric species. For the proportion of the [c1] complex that is present, the addition of the 1-adamantanecarboxylate "fuel" causes a five-fold reduction in the E-amide isomer and as a consequence the work output ($\delta\Delta G$) is 0.9 kcal mol^{-1}. For this reason the hermaphrodite **4.3** does not appear to follow the trend of the lower the K_A for the "fuel" the larger the $\delta\Delta G$ that is observed for the hermaphrodites **2.3**, **2.4**, **2.5**, **4.4** and **4.7**.

Following the discussion of the relationship between the K_A and the work outputs ($\delta\Delta G$), the focus shifted to the uncaptured work energy (ΔG) and the energy harnessed by the hermaphrodites **2.3**, **2.4**, **2.5**, **4.3**, **4.4** and **4.7**. Firstly, the hermaphrodite **4.7** harnesses 3.7 kcal mol^{-1} of work which is the largest of all the systems studied and is due to this "piston" increasing the strength of the [c1] complex. This has the effect of lowering the K_A for the 1-adamantanecarboxylate "fuel" and thus from the relationship of $\Delta G = -RT\ln K_A$ decreases the magnitude of ΔG. On this basis, the observed quantity of the uncaptured energy for the hermaphrodite **4.7** is the smallest of all the molecular machines with a ΔG of -4.0 kcal mol^{-1}. This is supported by the hermaphrodites **2.3** and **2.4** which afford ΔGs of -5.1 kcal mol^{-1} and -5.0 kcal mol^{-1} with $\delta\Delta G$s of 1.4 kcal mol^{-1} and 2.1 kcal mol^{-1}, respectively. These systems harness less work

energy in the amide bond ($\delta\Delta G$) than the hermaphrodite **4.7** and thus have larger values for the ΔG. For the molecular machines that are in the "OFF" state the trend continues as demonstrated by the hermaphrodite **4.4** with a ΔG of -5.7 kcal mol^{-1} and a $\delta\Delta G$ of only 0.3 kcal mol^{-1}. As this system is less effectively "OFF" its not surprising that its *N*-methyl counterpart the hermaphrodite **2.5** that is more effectively "OFF" affords a slightly larger ΔG of -5.9 kcal mol^{-1} and slightly smaller $\delta\Delta G$ of -0.2 kcal mol^{-1}. From these results a decrease in ΔG corresponds to an increase in the work output ($\delta\Delta G$). Finally, the hermaphrodite **4.3** affords a ΔG of -6.0 kcal mol^{-1} which is similar to that observed for the β-CD **1.10** control of -6.3 kcal mol^{-1}, however the binding interaction is from the major species being the [*a*1] conformation which doesn't correspond to the minor species being the [*c*1] complex that still performs a work output of 0.9 kcal mol^{-1}.

To summarise these results, the lower the molecular machine's K_A for the "fuel", the greater the proportion of the [*c*1] complex formed, the stronger the "piston" includes within the "cylinder" and the more work is done ($\delta\Delta G$) on the amide bond as demonstrated by the hermaphrodites **2.3** and **2.4**. These trends are enhanced by adding a methyl group to increase the hydrophobic surface area of the "piston" as demonstrated with the *N*,α-dimethylcinnamido hermaphrodite **4.7**. This is the most hard working molecular machine developed so far that is in the "ON" state. Alternatively, the addition of a rigid secondary amide linkage group to the hermaphrodite **4.3** leads to less of the [*c*1] complex being formed, an increase in the association for the "fuel" and a decrease in the work harnessed ($\delta\Delta G$) in the amide bond. Similarly, the higher the K_A of the "fuel" for the "cylinder", the less the "piston" hinders the cavity, and the less energy is harnessed as output ($\delta\Delta G$) as demonstrated by the hermaphrodite **4.4**. In comparison to its *N*-methyl analogue **2.5** this system is less effectively in the "OFF" state. Consistent with the findings from Chapter 3, as the K_A from binding increases the ΔG becomes more negative which is reasonable from the relationship $\Delta G = -RT\ln K_A$. Also, the decrease in the magnitude of ΔG corresponds to an increase in the work output ($\delta\Delta G$). Finally, the decompression stroke is enthalpy driven with the ΔG being dominated by ΔH contributions ($|\Delta H| \gg |T\Delta S|$). From these results, the substituents have different effects upon the thermodynamic properties of the hermaphrodites **4.3**, **4.4** and **4.7**.

After successfully measuring the thermodynamic parameters for the operation of the hermaphrodites **4.3**, **4.4** and **4.7**, the next aim was to quantify the overall performance. In order to determine the efficiency, ΔG was compared to the work energy

harnessed in the amide bond ($\delta\Delta G$), using Equation 3.2.1. However, using ΔG for determining efficiency includes the unavoidable energy cost from molecular reorganisation ($T\Delta S$) and on that basis the real energy wasted is ΔH. Therefore the efficiency was determined using the energy dissipated as heat (ΔH) with Equation 3.2.2. The energy efficiency of the work harnessed in relation to either ΔG or ΔH for the hermaphrodites, **2.5**, **4.4**, **4.3**, **2.3**, **2.4** and **4.7** at 25 °C is shown in Table 4.7.2 in increasing order of efficiency.

Nanomachine	$Eff_{\Delta G}$ (%)[a]	$Eff_{\Delta H}$ (%)[b]
2.5	-3	-2
4.4	5	4
4.3	13	15
2.3	22	18
2.4	30	24
4.7	48	39

Table 4.7.2. Efficiency of harnessing the energy of molecular recognition in the hermaphrodites **2.3**, **2.4**, **2.5**, **4.3**, **4.4** and **4.7** at 25 °C. [a]Calculated from Equation 3.2.1. [b]Calculated from Equation 3.2.2.

The hermaphrodite **4.7** has an energy efficiency of 48% ($Eff_{\Delta G}$) which decreases to 39% ($Eff_{\Delta H}$) when the favorable entropic contribution is removed from the calculation. Due to the hydrophobic aryl "piston" this molecular machine harnesses the largest amount of work energy ($\delta\Delta G$) and as a consequence performs with the highest efficiency. In support of this, the hermaphrodite **2.4** harnesses relatively less energy in the amide bond and as a result functions with lower efficiencies of 30% for $Eff_{\Delta G}$ and 24% for $Eff_{\Delta H}$. These are similar to that observed for the hermaphrodite **2.3** which performs with efficiencies of 22% for the uncaptured work energy and 18% with the heat dissipated. In contrast, the hermaphrodite **4.4** has energy efficiencies of 5% ($Eff_{\Delta G}$) and 4% ($Eff_{\Delta H}$) which are comparable to that of the hermaphrodite **2.5** which affords efficiencies of -3% ($Eff_{\Delta G}$) and -2% ($Eff_{\Delta H}$). The performance of these two systems is

measurably different from that observed for the hermaphrodites **4.7**, **2.4** and **2.3** and demonstrates that molecular machines can indeed be switched "OFF". The hermaphrodite **4.3** having the secondary amide linkage group affords energy harnessing efficiencies of 13% and 15% as calculated from the ΔG and the ΔH, respectively. In relation to the hermaphrodite **2.4** having the tertiary amide, the effect of the secondary amide group is that the hermaphrodite **4.3** is conformationally constrained in a manner which is counter productive to the performance. For this reason this system is the least efficient of the molecular machines that are in the "ON" state. In conclusion, these results demonstrate that different substituents alter the thermodynamic properties of the binding interaction for the hermaphrodites **4.3**, **4.4** and **4.7** with the 1-adamantanecarboxylate "fuel" and therefore significantly change their overall performance.

4.8 Conclusion

In this chapter several CD based hermaphrodites were developed in order to investigate the effects of various substituents upon the work output and performance of the molecular machines. It was discovered using a combined ^{1}H NMR spectroscopic and ITC strategy that modifications to the aryl "piston" can have a profound effect on the overall operation and performance of the synthetic molecular machines. This occurs due to the link that exists between the strength of the [c1] complex formed and the corresponding work that is done ($\delta\Delta G$) on the amide bond. The N,α-dimethylcinnamido hermaphrodite **4.7** formed the strongest [c1] complex, harnessed the largest amount of energy and operated with the best performance of all the molecular machines studied. Relative to the dimethyl system, the N-monomethylcinnamido hermaphrodites **2.3** and **2.4** form weaker [c1] complexes, harness slightly less energy in the amide bond and as a result operate less efficiently. Thus increasing the hydrophobic surface area of the aryl "piston" can improve performance. The non-methylcinnamido hermaphrodite **4.3** formed only 2-3% of the [c1] complex, harnessed 0.9 kcal mol^{-1} of work and operated with the lowest efficiency of all the molecular machines in the "ON" state. Although at a cost of efficiency, this shows that the [c1] complex is capable of constricting the geometry of the more rigid secondary amide bond. Finally, the *cis*-cinnamido hermaphrodites **4.4** and **2.5** harness negligible energy and demonstrate that molecular machines of this type can be switched "OFF". These results show that by modifying the

aryl "piston" it is quite reasonable that synthetic molecular machines can be developed to harness up to 6-8 kcal mol^{-1}.

CHAPTER 5

Harnessing the Energy of Intermolecular Complexation in a Nanomachine Having a Photochemical On/Off Switch

5.1 Introduction

The research described in the preceding Chapter demonstrated the effects of various substituents on the efficiency of synthetic molecular machines for harnessing work energy. The hermaphrodite **4.3** having the secondary amide group was observed to form only a small proportion of the [c1] complex while the major species was the [a1] conformation which formed intermolecular assemblies. Hermaphroditic compounds are known to form dimeric acyclic [a2] and cyclic [c2] complexes as illustrated in Figure 5.1.1.[132-134] For example, when stilbene pendant groups are installed onto the relatively narrow annulus of α-CD **1.9** the resulting hermaphrodites are sterically incapable of adopting the [c1] conformation and therefore predominantly form the [c2] complex.[75,127] The intermolecular recognition process from the formation of the [c2] complex is likely to produce strain energy upon the linkage group (Figure 5.1.2). The focus of the research described in this Chapter is therefore to harness this previously unknown quantity of strain energy from the formation of a [c2] complex.

[a1]   [a2]

[c1]   [c2]
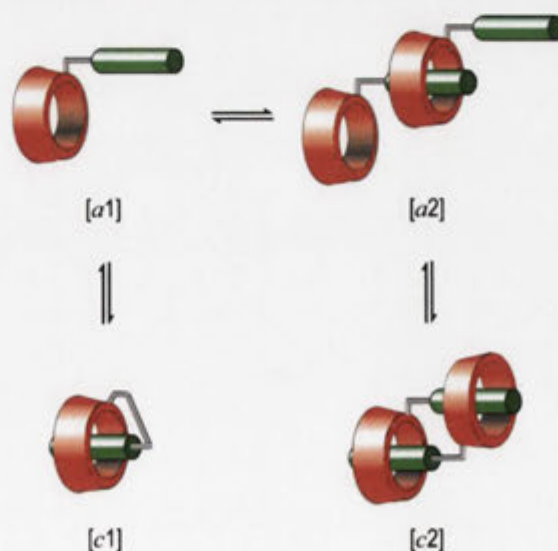
Figure 5.1.1. Schematic representation of some hermaphroditic conformations.
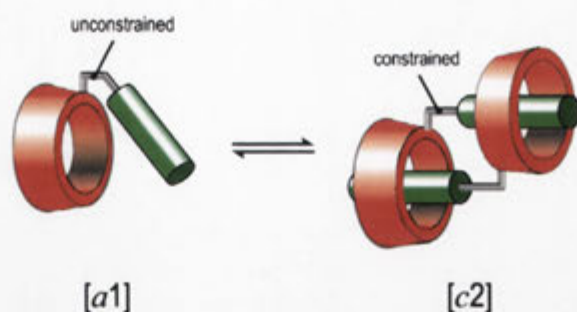
**Figure 5.1.2.** Schematic representation of the formation of a [c2] complex.

Given the aim, a new type of artificial molecular machine was designed and with its mechanical analogue is illustrated in Figure 5.1.3 and Scheme 5.2.3. For the purpose of replicating the "piston" and "cylinder" of a horizontally opposed mechanical pump, a stilbene guest was to be appended to α-CD **1.9** to produce the target hermaphrodite **5.4**. The tertiary amide "torsion bar" was chosen as a handle for reasons described in Chapter 2. The purpose was for intermolecular recognition of the stilbene "piston" by the CD "cylinder" to form the [c2] complex in aqueous solution and then by changing to organic solvent or by 1-adamantanol addition to form the [a1] conformation. Any difference in the *Z/E*-amide ratios and thus the ground state free energies between the [c2] complex and [a1] conformation reflects the work performed by the intermolecular complexation process. Measuring this change in work energy is the focus of the investigation with the aim to harness the work output of intermolecular complexation.
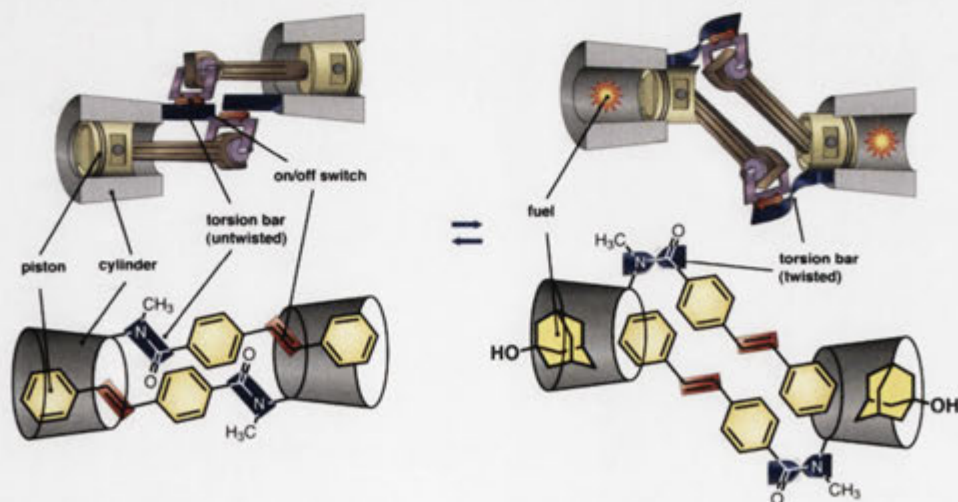
Figure 5.1.3. Schematic representation of a mechanical machine and its molecular counterpart.

5.2 Synthesis of Stilbenylamido-substituted α-Cyclodextrins

As shown in Scheme 5.2.1, the synthesis of the hermaphrodite **5.4** began with the preparation of 6^A-deoxy-6^A-methylamino-α-CD **5.2**. For this, natural α-CD **1.9** was treated with *p*-toluenesulfonyl chloride in pyridine to yield after chromatography 6^A-*O*-toluenesulfonyl-α-CD **5.1**.[83] Following the same procedure used to obtain the amino-CD **2.2**, the sulfonate **5.1** was then treated with methylamine in *N*-methyl-2-pyrrolidinone (NMP) to access, after chromatography, the amino-CD **5.2** in a yield of 86%.
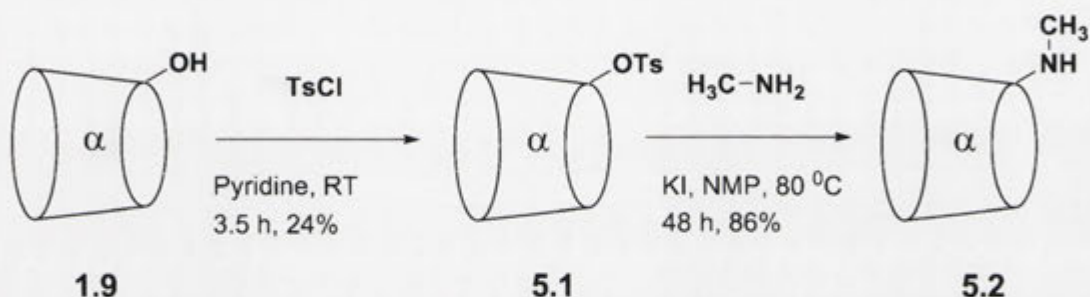
Scheme 5.2.1. Synthesis of 6^A-deoxy-6^A-methylamino-α-CD **5.2**.

With the modified CD "cylinder" on hand, the stilbene "piston" **5.3** was then prepared (Scheme 5.2.2). For this, 4-iodobenzoic acid and styrene were refluxed in the presence of palladium(II) acetate and triphenylphosphine in THF.[135] The acid **5.3** was then extracted and subsequently recrystallised from hexane and ethyl acetate in a yield of 22%. As shown in Scheme 5.2.3, the acid **5.3** was then installed onto the amino-CD **5.2** in anhydrous DMF using Castro's amide coupling reagent (BOP). The crude mixture was applied to anionic (DEAE) then cationic (SP) exchange resins, followed by reverse-phase HPLC, to isolate the hermaphrodite **5.4** in a yield of 40%. Identified from the TLC analysis were both a UV responsive aromatic group and a "positively staining" CD component.[108] The hermaphrodite **5.4** was characterised by elemental analysis and showed, using ESI HRMS, an $[M+H]^+$ ion at 1192.428.
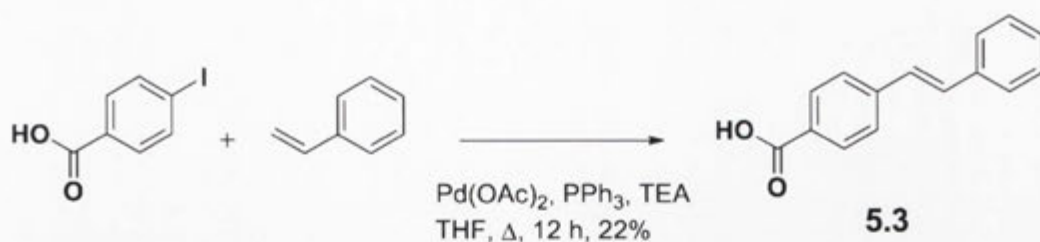
**Scheme 5.2.2.** Synthesis of *trans*-4-(2-phenylvinyl)benzoic acid **5.3**.
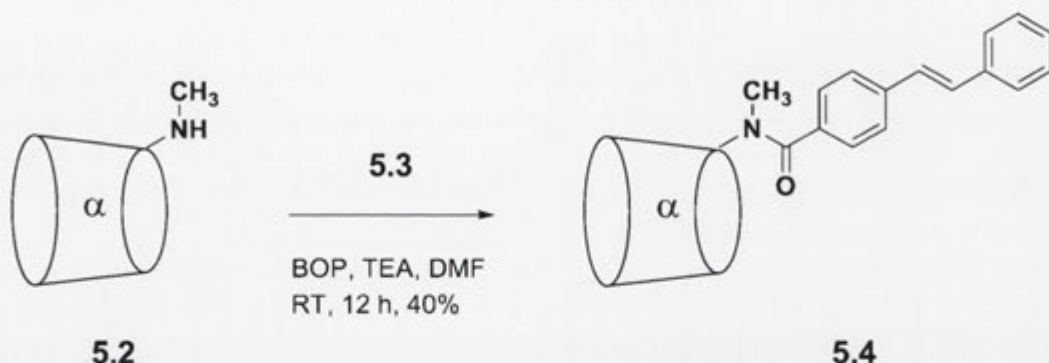
Scheme 5.2.3. Synthesis of *trans*-6^A-deoxy-6^A-(*N*-methylstilbenylamido)-α-CD **5.4**.

The advantage of the hermaphrodite **5.4** having the stilbene component was that photochemical treatment could be used to prepare its *cis*-isomer **5.5** (Scheme 5.2.4). In this case the photolysis was conducted in MeOH, which is more easily removed than water *in vacuo*, for the purpose of making the preparative method more expeditious. The solution was irradiated with 350 nm light for 2.5 minutes and chromatography of the crude mixture using reverse-phase HPLC, afforded the hermaphrodite **5.5** in 75% yield. The hermaphrodite **5.5** was characterised by elemental analysis and showed, using ESI HRMS, an [M+H]$^+$ ion at 1192.432.
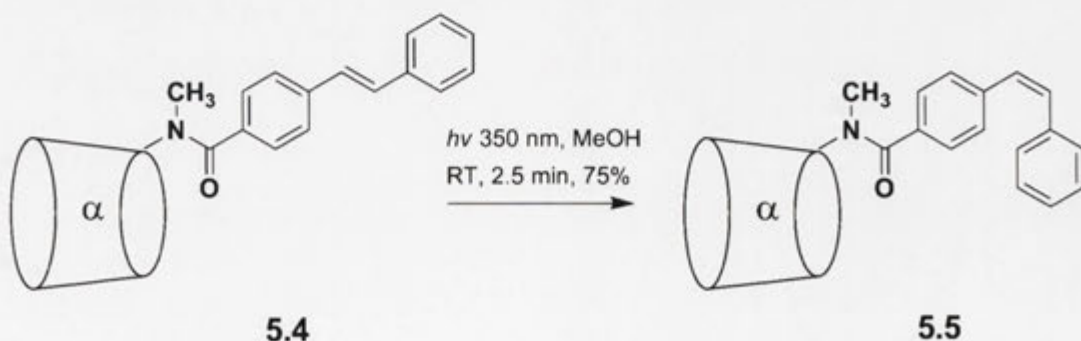
Scheme 5.2.4. Synthesis of *cis*-6^A-deoxy-6^A-(*N*-methylstilbenylamido)-α-CD **5.5**.

5.3 Conformational Analysis of Cyclodextrin Based Hermaphrodites

With the hermaphrodites **5.4** and **5.5** in hand, their operation as molecular machines as illustrated in Figure 5.1.3 is dependent upon their conformational behavior in d_6-DMSO, D_2O and in D_2O with competitive guest. In order to examine this, the hermaphrodites **5.4** and **5.5** were studied using ^1H NMR spectroscopy under the various conditions for the purpose of distinguishing between the *Z/E*-amide isomers and determining the position of the stilbene "piston" and the CD "cylinder".

Shown in Figure 5.3.1 is a section of the 1D ^1H NMR spectrum of the hermaphrodite **5.4** in d_6-DMSO. Two major proton signals are observed in the *N*-methyl region at δ 3.02 and 2.88 ppm which integrate to a ratio of about 3:1, respectively. These signals are broad presumably due to the intermediate chemical exchange occurring between the *Z/E*-amide isomers.[126] From ROESY analysis, these signals show negative exchange cross-peaks which indicate that these species are in equilibrium and the signals are assigned to the methyl groups of the amide isomers. The more intense peak at δ 3.02 ppm shows an NOE interaction with an aromatic proton signal and is assigned to be the *Z*-amide isomer. The smaller signal at δ 2.88 ppm shows no NOE with the aromatic signals and is assigned to the *E*-amide isomer. In this solvent the stilbene "piston" does not interact with the CD "cylinder" which is consistent with the fact that organic solvent does not provide driving force for inclusion.[111] On this basis, in d_6-DMSO the hermaphrodite **5.4** adopts a non-included [*a*1] conformation having two amide isomers in a *Z/E* ratio of 3:1.
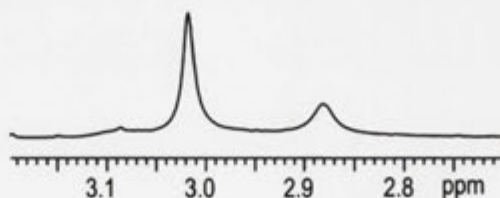
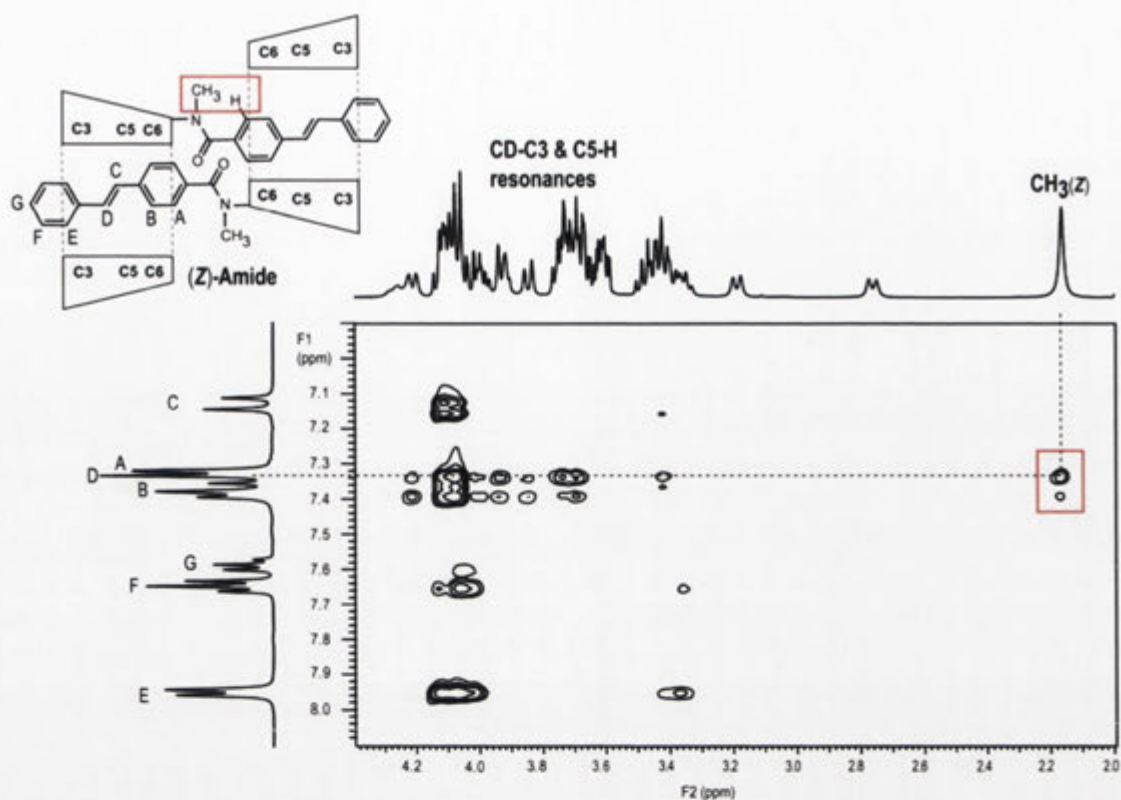
Figure 5.3.1. Section of the ^1H NMR spectrum (500 MHz) of the hermaphrodite **5.4** in d_6-DMSO at 25 °C.

As seen from the ^1H NMR spectrum shown in Figure 5.3.2, the hermaphrodite **5.4** exists in one major form in D_2O. An intense *N*-methyl proton signal is observed at δ 2.16 ppm which is more upfield than the δ ~3.0 ppm for the preceding systems studied.

This is possibly due to an aromatic stacking interaction with a neighboring aryl "piston" which is likely from the formation of an intermolecular complex. From the ROESY spectrum (Figure 5.3.3), the methyl singlet at δ 2.16 ppm (F2 axis) shows NOE interactions with the aromatic proton signals of the stilbene "piston" and is therefore assigned to the *Z*-amide isomer. The aromatic and olefinic proton signals show cross-peaks with the CD resonances so the stilbene "piston" is included within the CD "cylinder". On this basis, the major structure of the hermaphrodite **5.4** in D_2O is an included species having a dominant *Z*-amide conformation. In spite of this, a low intensity singlet at δ 3.06 ppm can be assigned to the *E*-amide isomer in a *Z/E*-amide ratio of approximately 50:1 for reasons demonstrated later in this Chapter from titrations with 1,10-decanediol "fuel" (Figure 5.3.4).
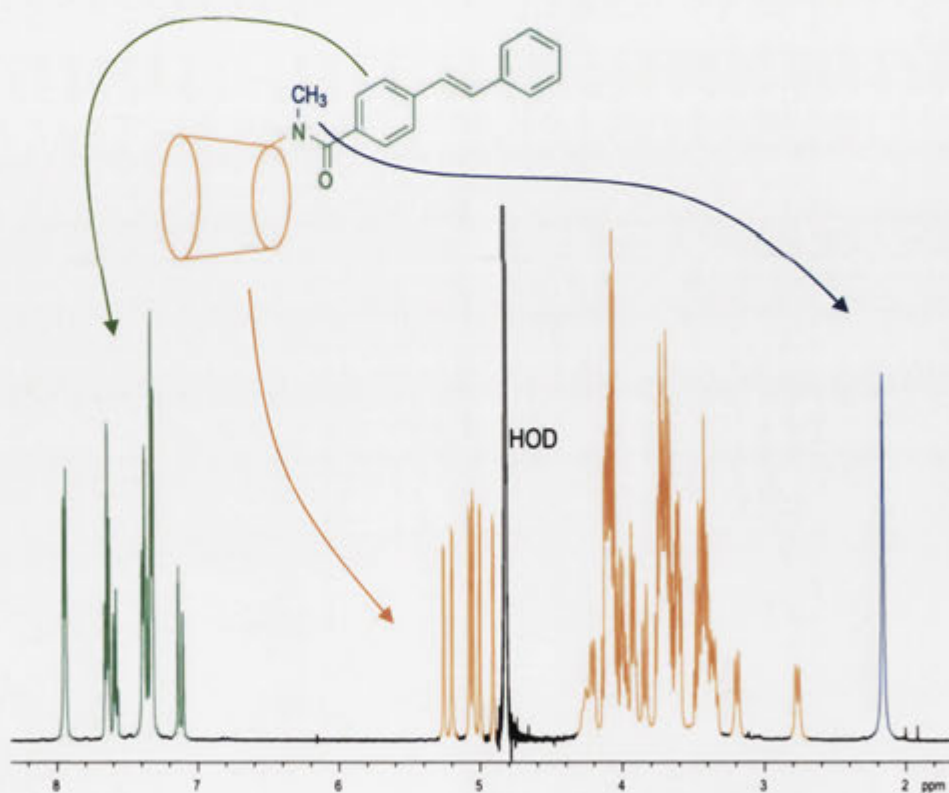
Figure 5.3.2. ^{1}H NMR spectrum (500 MHz) of the hermaphrodite **5.4** in D_2O at 25 °C.

Figure 5.3.3. Section of the ROESY NMR spectrum (500 MHz) of the hermaphrodite **5.4** in D_2O (25 °C) with 0.250 ms mixing time.

The narrow annulus of α-CD **1.9** (5.5 Å) permits only weak binding interactions for adamantane guests (1-adamantanecarboxylate, K_A = 150 M^{-1})[136] making them unsuitable as a "fuel" source. A more appropriate "fuel" is 1,10-decanediol which has an affinity of about 11000 M^{-1} for α-CD **1.9**.[137] Shown in Figure 5.3.4 is the crude ^{1}H NMR spectrum for the preliminary investigation of the hermaphrodite **5.4** in D_2O with 5 equivalents of 1,10-decanediol "fuel". In addition to the upfield Z-amide methyl signal at δ 2.16 ppm there are two proton signals at δ 3.12 and 3.06 ppm. From ROESY analysis, these signals at δ 3.12 and 3.06 ppm have negative exchange cross-peaks with the signal at δ 2.16 ppm which indicate that these species are in equilibrium. The signals at δ 3.12 and 3.06 ppm are suspected of being due to the Z- and E-amide isomers of the [*a*1] guest complex. The addition of the 1,10-decanediol "fuel" results in the precipitation of the hermaphrodite **5.4** from solution which is reasonable for the [*a*1] guest complex having an exposed stilbene "piston" which is likely to be highly insoluble. On this basis and due to time constraints it was impractical to study the
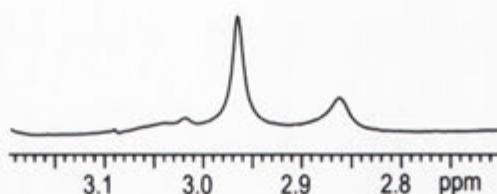
operation of the hermaphrodite **5.4** in the presence and absence of such a "fuel" source. Instead only the effect of changing the solvent was examined.
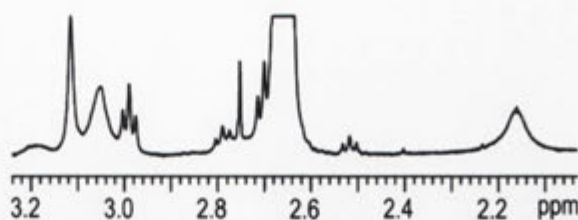
Figure 5.3.4. A section of the ^{1}H NMR spectrum (500 MHz) of the hermaphrodite **5.4** in D$_2$O (25 °C) and in the presence of 1,10-decanediol "fuel".

To review the conformational behavior of the hermaphrodite **5.4**, in d_6-DMSO the stilbene "piston" does not include and the *Z/E*-amide ratio is 3:1. In D$_2$O the stilbene "piston" does include and the Z-amide isomer is the dominate species. In d_6-DMSO the aryl "piston" does not include within the CD "cylinder" so there is no constraint upon the amide bond. However, in D$_2$O the aryl "piston" is mostly included and the formation of the complex constrains the amide bond. Presumably this is the reason for the difference observed between the *Z/E*-amide ratios in d_6-DMSO and D$_2$O.

With the conformational behavior of the hermaphrodite **5.4** investigated in d_6-DMSO and D$_2$O, the next aim was to study its *cis*-isomer **5.5**. The *N*-methyl region of the ^{1}H NMR spectrum of the hermaphrodite **5.5** in d_6-DMSO is shown in Figure 5.3.4. Observed are two broad proton signals at δ 2.96 and 2.86 ppm which integrate to a ratio of approximately 2.5:1. From the ROESY analysis the stronger proton signal shows an NOE interaction with an aromatic resonance and is assigned to the Z-amide isomer. The less intense signal at δ 2.86 ppm shows no cross-peak interactions with the aromatic signals and is assigned to the E-amide isomer. The stilbene "piston" shows no interaction with the CD "cylinder" which indicates that the dominant species is the [*a*1] conformation. It can be concluded that the hermaphrodite **5.5** forms the non-included [*a*1] conformation in d_6-DMSO with two amide isomers in a *Z/E* ratio of 2.5:1.
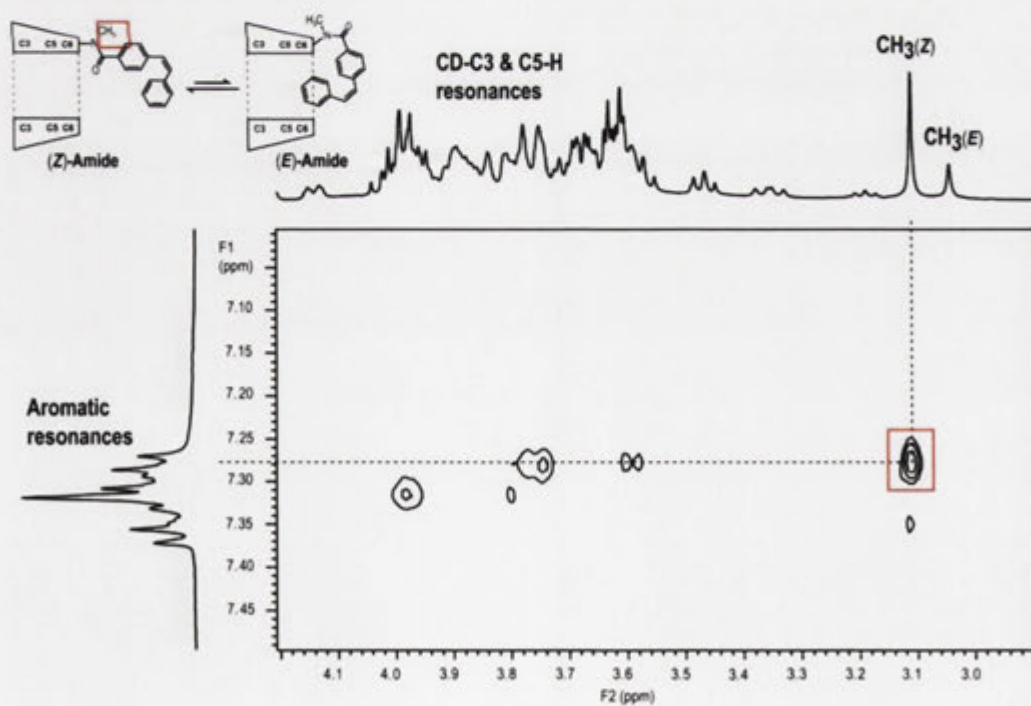
Figure 5.3.4. Section of the ^{1}H NMR spectrum (500 MHz) of the hermaphrodite **5.5** in d_6-DMSO at 25 °C.

Next, the ^{1}H NMR spectrum for the hermaphrodite **5.5** in D_2O shows that two conformations are present as shown in Figure 5.3.5. In the *N*-methyl region of the spectrum two proton signals are observed at δ 3.11 and 3.05 ppm in a ratio of about 3.1:1. Remarkably, the appearance and relative intensities of these signals are similar to that observed for this compound in d_6-DMSO. From ROESY analysis (Figure 5.3.6) the signal at δ 3.11 ppm (F2 axis) shows NOE interactions with the stilbene signals and is therefore assigned to the methyl group of the *Z*-amide isomer. The aromatic resonances show only relatively weak interactions with the CD proton signals, therefore the aryl "piston" is mostly not included within the CD "cylinder". These results indicate that the predominant structure of the hermaphrodite **5.5** in D_2O is the non-included [*a*1] complex which affords a *Z*/*E*-amide ratio of 3.1:1.

To summarise the ^{1}H NMR analysis of the hermaphrodite **5.5**, in d_6-DMSO the stilbene "piston" does not include within the CD "cylinder" and the *Z*/*E*-amide ratio is 2.5:1. In D_2O the stilbene "piston" only weakly interacts with the CD "cylinder" and the *Z*/*E*-amide ratio is 3.1:1. In d_6-DMSO the hermaphrodite **5.5** exists in the [*a*1] conformation so there is no constraint upon the amide bond. In D_2O the aryl "piston" shows only weak interactions with the CD "cylinder" so there is again little constraint upon the amide bond. For this reason there is little difference between the *Z*/*E*-amide ratios for the hermaphrodite **5.5** in d_6-DMSO and D_2O.
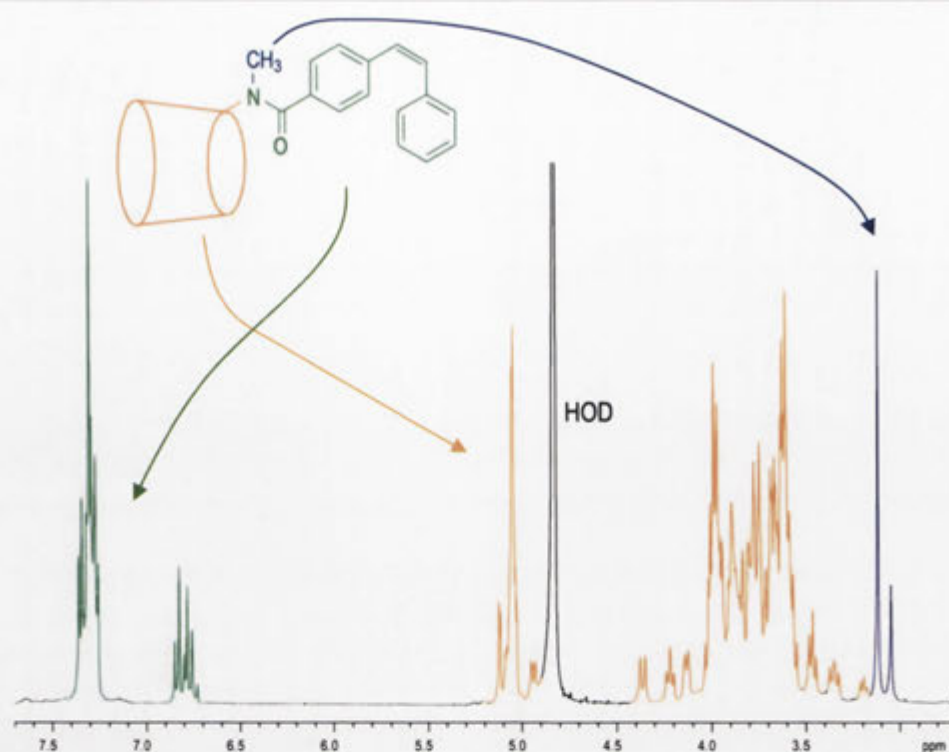
**Figure 5.3.5.** ^{1}H NMR spectrum (500 MHz) of the hermaphrodite **5.5** in D$_2$O at 25 °C.

Figure 5.3.6. Section of the ROESY NMR spectrum (500 MHz) of the hermaphrodite **5.5** in D$_2$O (25 °C) with 0.025 ms mixing time.

## 5.4 Photochemical Switching of Cyclodextrin Based Hermaphrodites

Having successfully prepared the hermaphrodites **5.4** and **5.5**, their conformational behavior was investigated in organic solvent and in D_2O. From the conversion of the hermaphrodite **5.4** to its *cis*-isomer **5.5** distinct conformational changes were observed which is characteristic of a machine-like function. For this reason, the photochemical switching between the hermaphrodites **5.4** and **5.5** was studied (Scheme 5.4.1). Analogous to that of the preceding Chapters 2 and 4, the photoirradiation process was investigated using a combined UV/visible spectroscopic and reverse-phase HPLC approach.
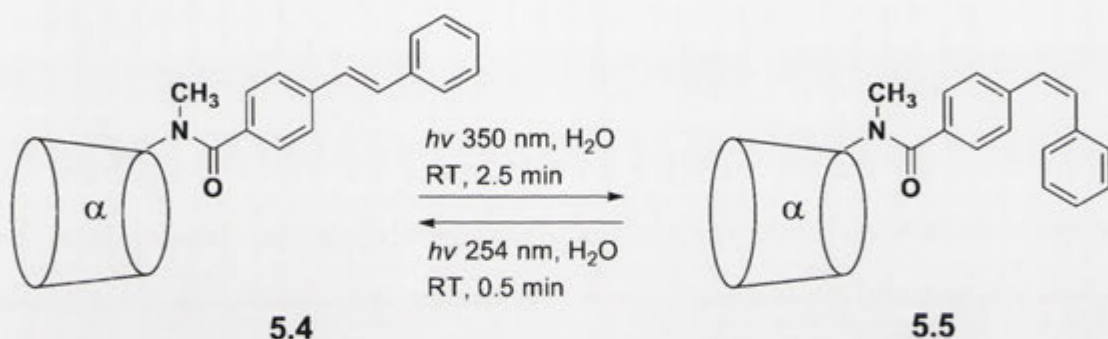
Scheme 5.4.1. Reversible photochemical isomerisation of the hermaphrodite **5.4** and its *cis*-isomer **5.5**.

Shown in Figure 5.4.1 is the UV/visible spectrum for a solution of the hermaphrodite **5.4** in H_2O (3.36 x 10^{-5} M) showing a maximum absorption (λ_{MAX}) at 316 nm. This is typical of an absorption band for a *trans*-stilbene while the expected λ_{MAX} for its *cis*-isomer is at wavelengths below 290 nm.[138] It follows that the product yield of the *cis*-isomer could be maximised by selectively irradiating the absorption band of the *trans*-isomer using a light of wavelength > 316 nm. For this reason a solution of the hermaphrodite **5.4** was irradiated with a 350 nm wavelength light to obtain the hermaphrodite **5.5**. Over the course of the exposure the maximum absorbance at 316 nm decreased which corresponded to an increase in the absorption band at wavelengths below 290 nm (Figure 5.4.1). The photostationary state was reached at approximately two minutes but irradiation was continued for half a minute longer to ensure completion. This photostationary mixture was then applied to reverse-phase

HPLC and monitored at the isosbestic point of 276 nm. Figure 5.4.2 shows the HPLC chromatogram (276 nm) of the photostationary mixture and shows the hermaphrodite **5.5** (t_R: 12.7 min) distinct from the hermaphrodite **5.4** peak (t_R: 16.4 min) in a ratio of 82:18, respectively. Next, to complete the photoisomerisation cycle and restore the hermaphrodite **5.4**, the photostationary mixture was irradiated with 254 nm light. In this case the photostationary state was reached at 0.5 minutes and afforded a ratio of 68:32 for the hermaphrodite **5.4** and the *cis*-isomer **5.5**, respectively. The relatively high percentage of the hermaphrodite **5.5** present at this photostationary state is due to the overlap in the absorption band with that of its *trans*-isomer **5.4** at 254 nm. Three consecutive photoisomerisation cycles for the hermaphrodite **5.4** with 350 nm followed by 254 nm light are shown in Figure 5.4.3. These results demonstrate that the hermaphrodite **5.4** behaves as a reversible photochemical switch.
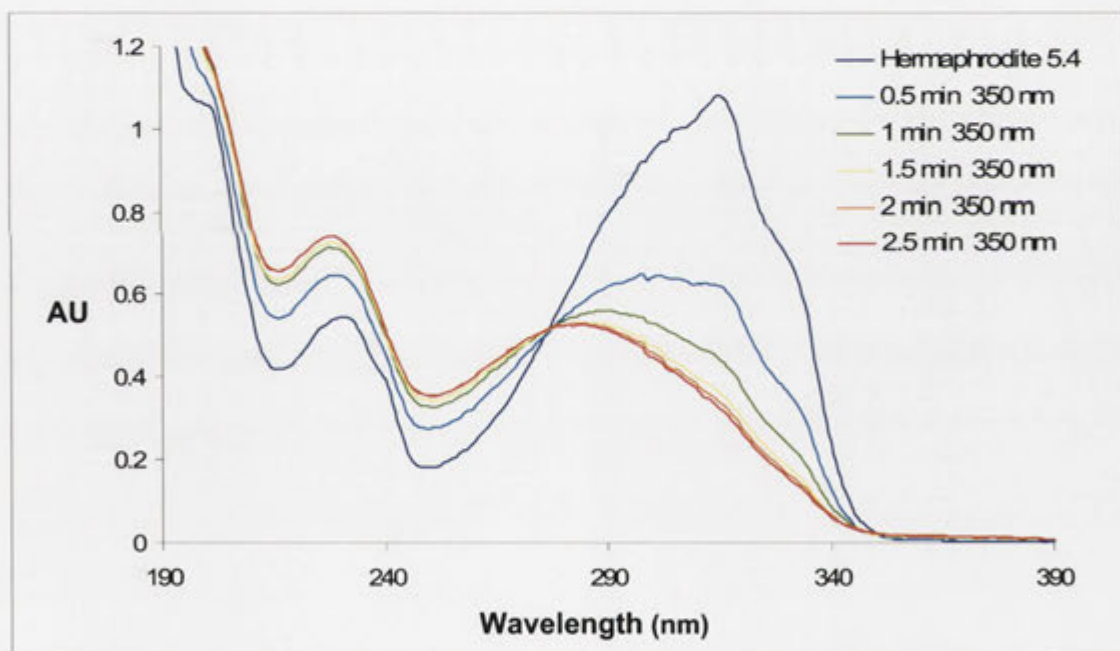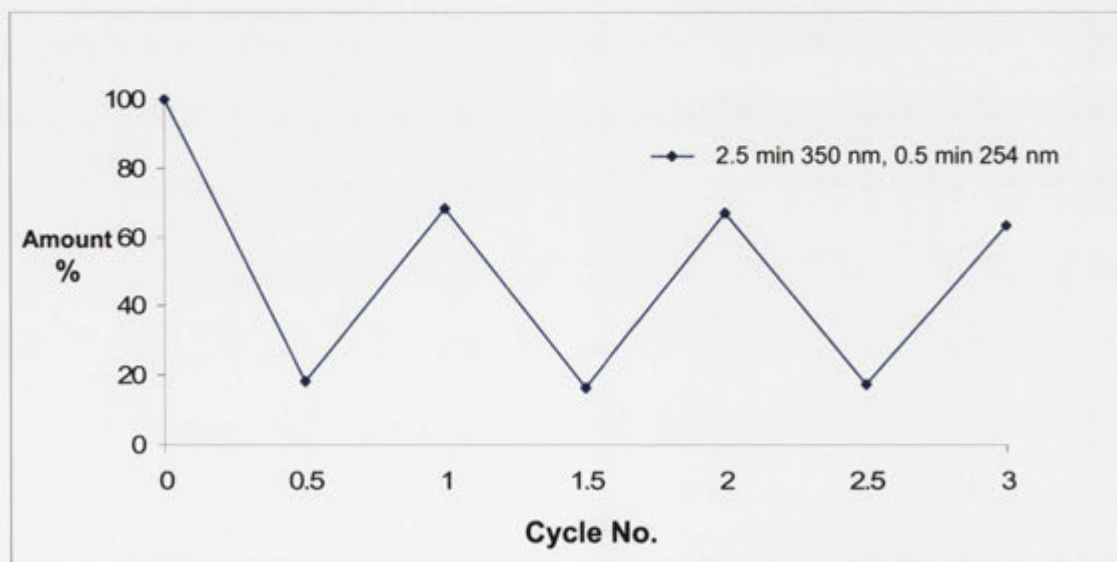

Figure 5.4.1. UV/Visible spectra of the hermaphrodite **5.4** (3.36×10^{-5} M) in H_2O and after irradiation with 350 nm light.
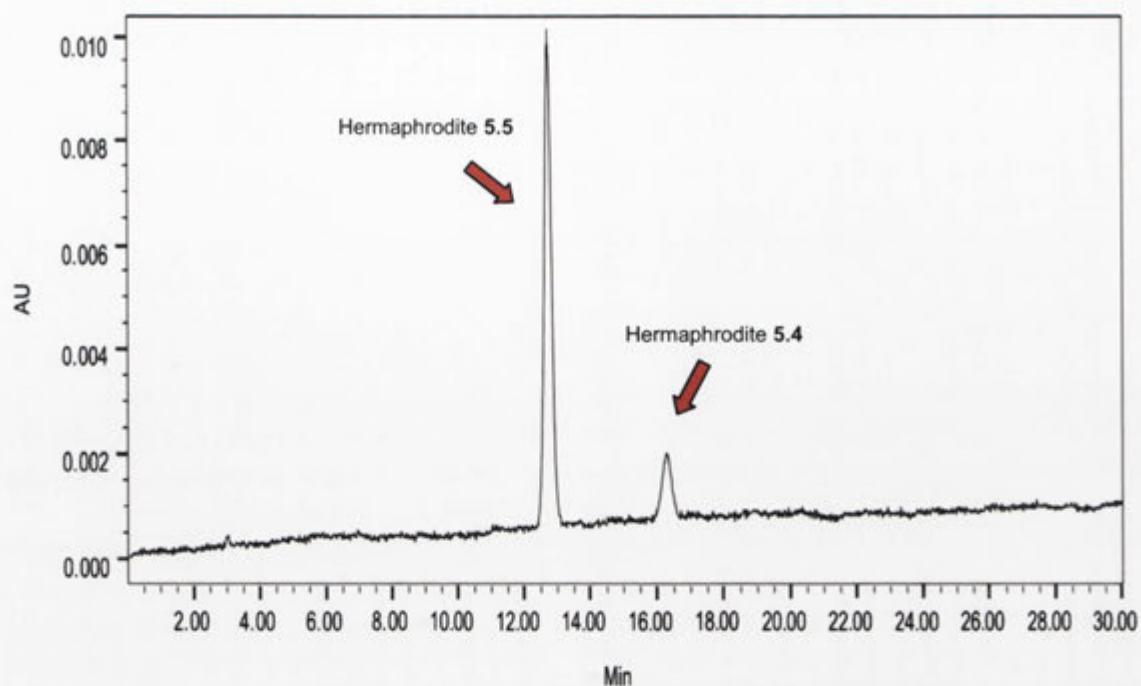
Figure 5.4.2. Reverse-phase HPLC chromatogram (276 nm) of the hermaphrodite **5.4** after photoirradiation with 350 nm light.


Figure 5.4.3. Amount (%) of the hermaphrodite **5.4** present after photoirradiation as determined by reverse-phase HPLC (276 nm). Each cycle consists of irradiation at 350 nm followed by treatment at 254 nm.

5.5 Measuring the Heats of Dilution of the Complexes of Cyclodextrin Based Hermaphrodites

The conformational behavior of the hermaphrodite **5.4** and its *cis*-isomer **5.5** were established under various conditions using ^{1}H NMR spectroscopy. Having identified conformational differences, their operation as the desired molecular machines that are illustrated in Figure 5.1.3 depends on the formation of the intermolecular [*c*2] complex. From the ^{1}H NMR analysis NOE interactions are observed between the stilbene "piston" and the CD "cylinder" for which the explanation is that either the *Z*-amide can also form the [*c*1] complex or the complexation is an intermolecular assembly. From Chapter 4, an ITC dissociation experiment was employed to measure the heats of dilution for the hermaphrodite **4.3** which was thereby identified to form concentration dependent [*c*2] complexes. The same technique was applied to measure the heats of dilution for the complexes of the hermaphrodite **5.4** and its *cis*-isomer **5.5**.

The ITC enthalpogram for the dilution of the hermaphrodite **5.4** (5 mM) into a buffered aqueous solution is shown in Figure 5.5.1a. Observed are positive enthalpic heat changes that are characteristic of an endothermic process. Over the course of the titration the overall heat change decreases by 0.5 kcal/mol^{-1} and the shape of the curve is typical of the concentration dependent equilibrium shift from monomer to oligomer.[128] The enthalpogram (Figure 5.5.1b) for the dilution of the hermaphrodite **5.5** (5 mM) also indicates that an endothermic process is occurring. In this case the relative scale of the integrated peaks is smaller and the profile of the curve is relatively flatter than that observed for its *trans*-isomer **5.4**. On this basis, the concentration dependence of the hermaphrodite **5.4** is stronger than that of the hermaphrodite **5.5**.
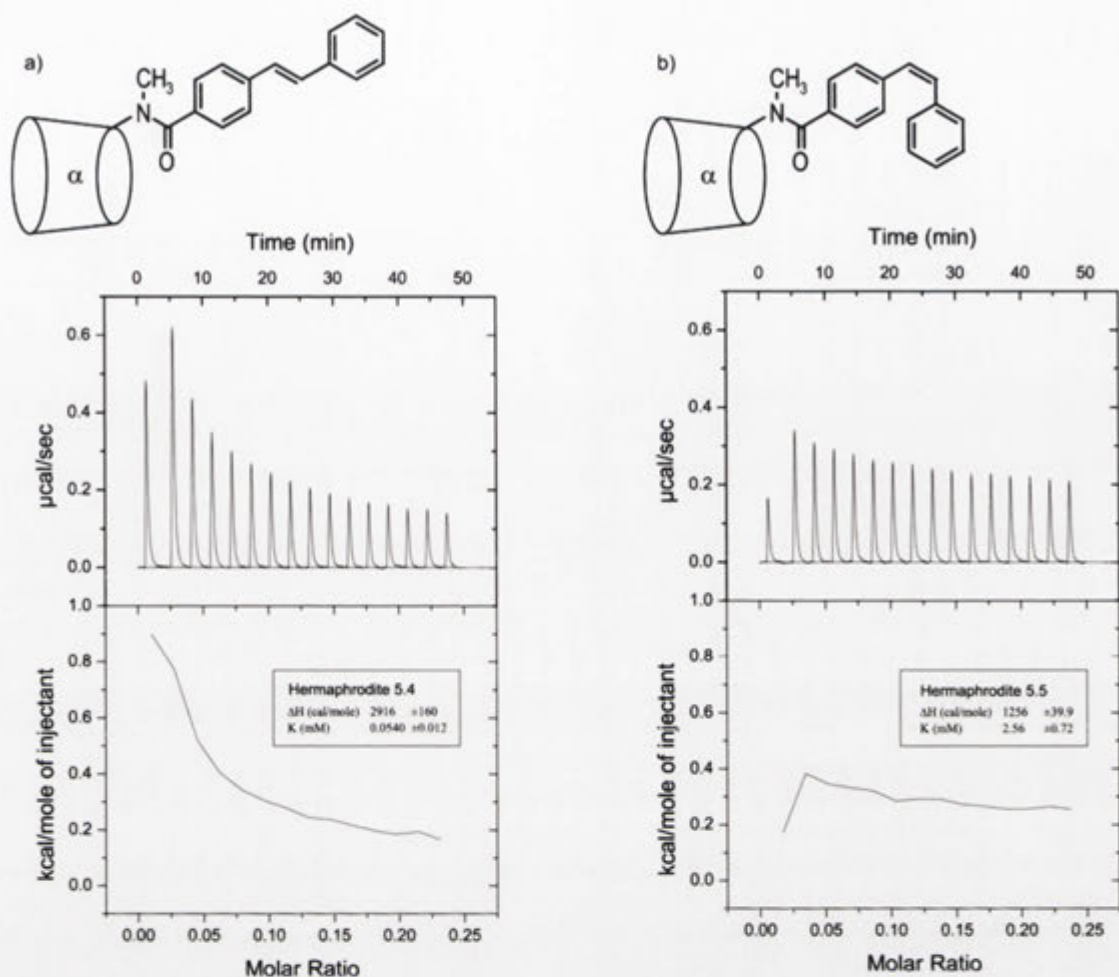
Figure 5.5.1. ITC thermograms for 15 successive injections (5 µL) of the hermaphrodite (5 mM) in 0.05 M NaH_2PO_4/Na_2HPO_4 buffer (pH 6.9) into cells containing identical buffer. a) hermaphrodite **5.4**; b) hermaphrodite **5.5**.

The heat change curves were fitted using a non-linear least squares dimer dissociation model. Of the intermolecular assemblies the dimer is the most entropically favored. From this, the complexation occurs at lower concentrations for the hermaphrodite **5.4** with a K_D of 0.06 ± 0.01 mM than for its *cis*-isomer **5.5** with a K_D of 2.7 ± 0.7 mM. These values of K_D correspond to intermolecular association constants (K_A) of 16700 M^{-1} and 370 M^{-1} ($K_A = 1/K_D$) for the hermaphrodite **5.4** and its *cis*-isomer **5.5**. From this, their photochemical interconversion affords a greater than forty-fold modulation in the strength of intermolecular complexation. From the dissociation constants (K_D), the percentage of monomer present in solution under the earlier NMR spectroscopic experimental conditions was determined, from Equation 4.5.1, to be 10% ± 1 and 47% ± 4 for the hermaphrodites **5.4** and **5.5**, respectively. On this basis, it can be

concluded that during the ^{1}H NMR spectroscopic studies the hermaphrodite **5.4** exists predominantly as an intermolecular complex while a large proportion of its *cis*-isomer **5.5** remains in the [*a*1] conformation.

In review of these analyses, the hermaphrodite **5.4** in aqueous solution forms mainly an intermolecular assembly with a K_D of 0.06 mM, whereas the hermaphrodite **5.5** exhibits weaker concentration dependence with a K_D of 2.6 mM. In combination with the ^{1}H NMR conformational analysis this is in support of the major species for the hermaphrodite **5.4** being an intermolecular complex of the Z-amide isomer. This is in contrast to the hermaphrodite **5.5** which forms an [*a*1] conformation with only a weak intermolecular association and has a larger proportion of the E-amide isomer. The difference in the strength of the intermolecular association explains the difference in the concentration dependence observed between the hermaphrodites **5.4** and **5.5**, which appears to have an effect on the Z/E-amide ratio.

## 5.6 Operation of Cyclodextrin Based Hermaphrodites by Changing the Solvent

Differences in the conformational behavior between the hermaphrodites **5.4** and **5.5** in d_6-DMSO and D_2O were observed using ^1H NMR spectroscopy. As discussed in Chapter 2, the Z/E-amide ratio reflects the difference between the isomer ground state free energies (ΔG) under a particular set of conditions. Unfortunately it was not possible to operate the hermaphrodites **5.4** and **5.5** using a "fuel" source. However, any change in the ground state free energies (ΔG) between the complex formed in aqueous solution and the [$a1$] conformation formed in organic solvent would reflect the work output ($\delta\Delta G$) performed by the intermolecular complexation process. With this in mind, the operation of the hermaphrodites **5.4** and **5.5** was investigated by quantifying the work outputs from a change in the solvent from D_2O to d_6-DMSO.

Shown in Figure 5.6.1 are the ^1H NMR spectra for the hermaphrodite **5.4** in D_2O (bottom) and in d_6-DMSO (top). In D_2O the stilbene "piston" of the hermaphrodite **5.4** includes within the CD "cylinder" and the Z/E-amide ratio is 50:1. According to the equation $\Delta G = -RT \ln K_{Z/E}$, where ΔG is the ground state free energy difference (kcal mol^{-1}), R is the universal gas constant (1.9872 cal K^{-1} mol^{-1}) and T is the temperature (298 K), this amide isomer ratio represents a ΔG of -2.6 kcal mol^{-1}. In d_6-DMSO, the stilbene "piston" does not include within the CD "cylinder" and the Z/E-amide ratio is 3:1 and the resulting ΔG is -0.7 kcal mol^{-1}. By changing the solvent from D_2O to d_6-DMSO the equilibrium shifts away from the intermolecular complex toward the [$a1$] conformation resulting in a fifteen-fold increase in the proportion of the E-amide isomer. On this basis, the change in solvent sees the work harnessed in the amide bond as -1.9 kcal mol^{-1} and therefore the hermaphrodite **5.4** behaves as a molecular machine in the "ON" state.
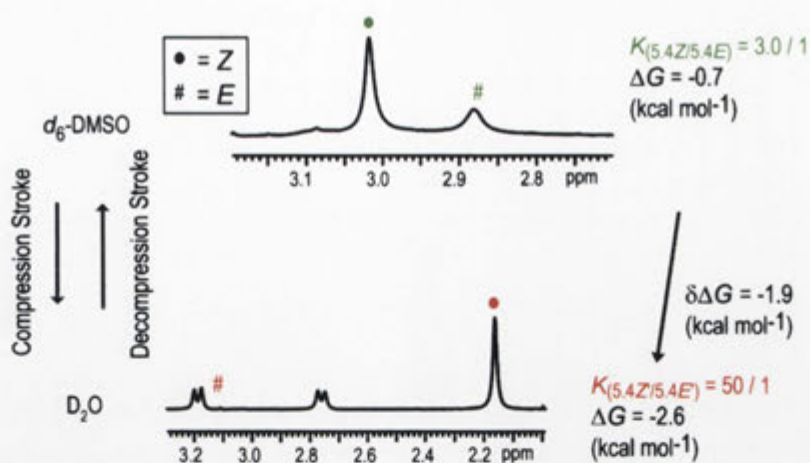
**Figure 5.6.1.** 500 MHz ^{1}H NMR spectra of the hermaphrodite **5.4** in D_2O and d_6-DMSO.

With the hermaphrodite **5.4** established to behave as a molecular machine the operation of its *cis*-isomer **5.5** was studied. In Figure 5.6.2 are the ^{1}H NMR spectra for the hermaphrodite **5.5** in D_2O (bottom) and in d_6-DMSO (top). In D_2O, the *Z/E*-amide ratio is 3.1:1 which represents a ΔG of -0.7 kcal mol^{-1}. In d_6-DMSO the *Z/E*-amide ratio is 2.5:1 resulting in a ΔG of -0.6 kcal mol^{-1}. By changing the solvent there is little effect on the amide ratio as reflected in the $\delta \Delta G$ being -0.1 kcal mol^{-1}. From this, the hermaphrodite **5.5** harnesses negligible work energy in the amide bond and this molecular machine is "OFF". When the operation of the hermaphrodite **5.4** and its *cis*-isomer **5.5** are combined they operate as a molecular machine having a photochemical "ON/OFF" switch (Scheme 5.6.1).
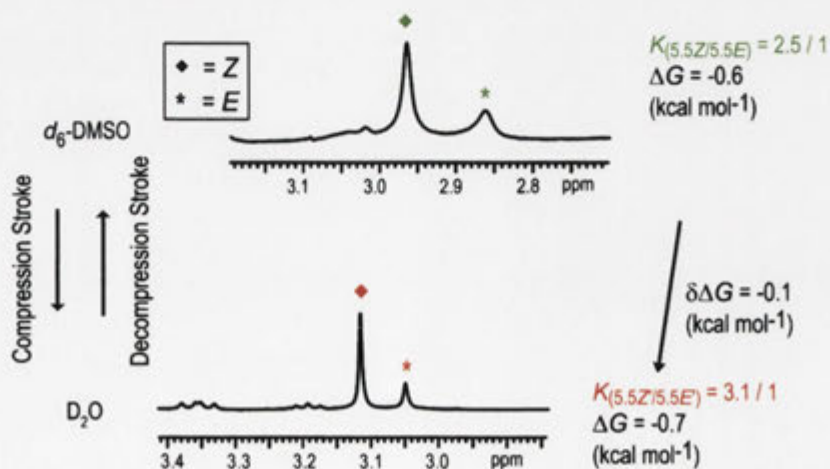
Figure 5.6.2. 500 MHz ^{1}H NMR spectra of the hermaphrodite **5.5** in D_2O and d_6-DMSO.

110
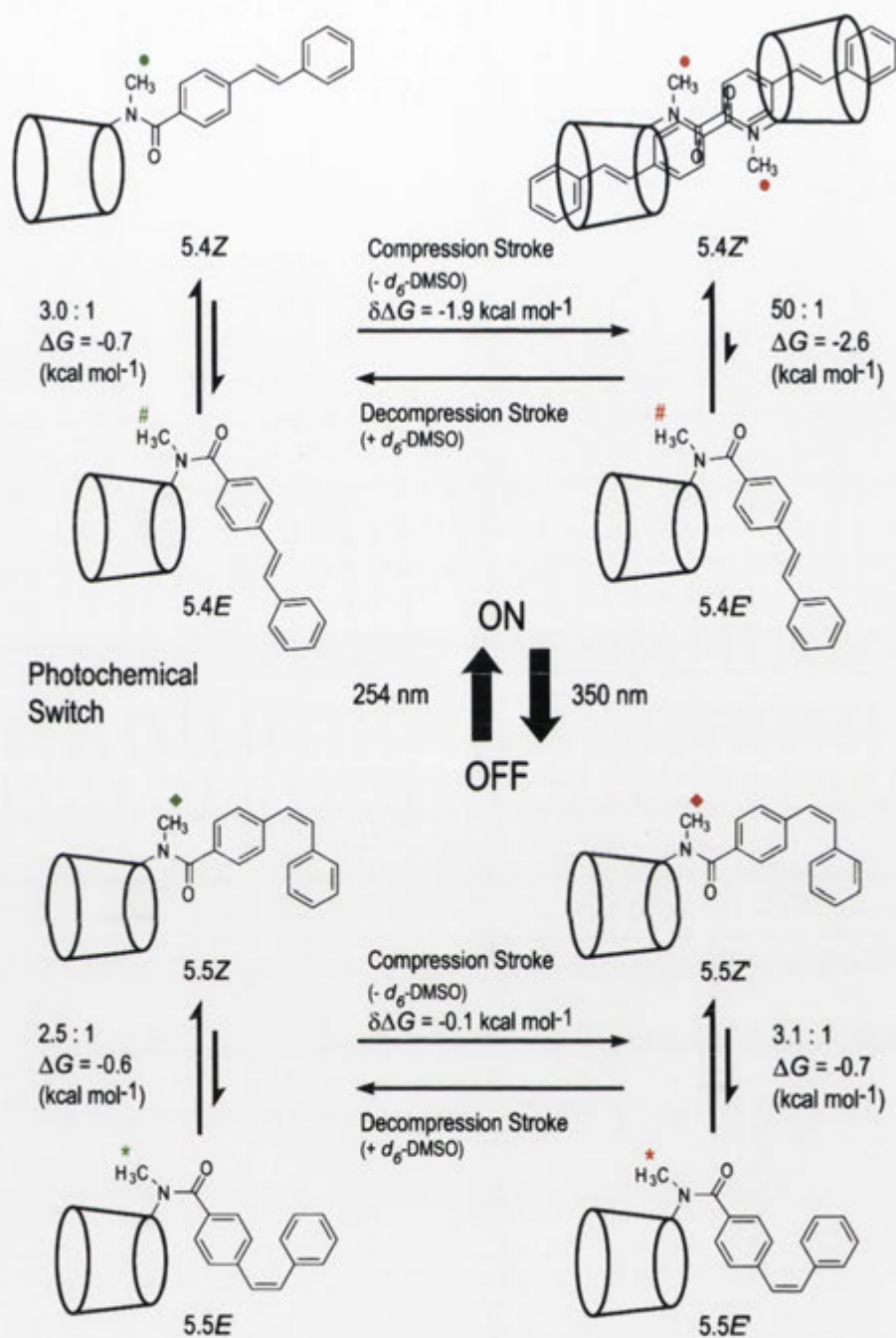
Scheme 5.6.1. Operation of *trans*-6^A-deoxy-6^A-stilbenylamido-α-CD **5.4** and *cis*-6^A-deoxy-6^A-stilbenylamido-α-CD **5.5** as a molecular pump.

5.7 Isothermal Titration Calorimetry of Cyclodextrin Based Hermaphrodites

Having measured the energies harnessed by the hermaphrodites **5.4** and **5.5** from intermolecular complexation, the next aim was to establish their energy harnessing efficiency. For this, the thermodynamic parameters for the transition between the intermolecular complex and the [*a*1] conformation were to be measured using ITC. As the operation of hermaphrodites **5.4** and **5.5** was driven by a change in solvent as detailed in Chapter 5.6, it is difficult to measure ΔG and ΔH for this process using ITC. However, the heats of dissociation experiment discussed in Chapter 5.5 provide the isotherms for the equilibrium shift from the [*a*1] conformation to the intermolecular complex in aqueous solution. Thus, from the two independent dissociation experiments for each of the hermaphrodites **5.4** and **5.5** discussed in Chapter 5.5 a non-linear least squares dimer dissociation model was used to extract the results of which were averaged to obtain the thermodynamic data presented in Table 5.7.1.

CD	K_D (mM)	K_A $(M^{-1})^a$	$\delta\Delta G$ $(kcal\ mol^{-1})^b$	ΔG $(kcal\ mol^{-1})^c$	ΔH $(kcal\ mol^{-1})$	$T\Delta S$ $(kcal\ mol^{-1})^d$
5.5	2.7 ± 0.8	370	-0.1	-3.5	-1.3	2.2
5.4	0.06 ± 0.01	16700	-1.9	-5.8	-2.8	3.0

Table 5.7.1. ITC and NMR experimental data for the intermolecular complexation of the hermaphrodites **5.4** and **5.5**. $^aK_A = 1/K_D$; $^b\delta\Delta G$ values reported are amide strain energy stored from the compression stroke of the piston as measured by ^{1}H NMR spectroscopy. $^c\Delta G = -RT\ln K_A$; $^d\Delta G = \Delta H - T\Delta S$.

The Table shows the dissociation constant (K_D), association constant (K_A), work output ($\delta\Delta G$), free energy change (ΔG), enthalpy change (ΔH) and entropy change ($T\Delta S$) for the hermaphrodites **5.4** and **5.5**. From this the hermaphrodite **5.4** having the *trans*-stilbenylamido "piston" affords the largest intermolecular association with a K_A of 16700 M^{-1}. The relatively high association constant suggests that the stilbene "piston" effectively includes within the CD "cylinder". The major species of the hermaphrodite **5.4** is an intermolecular complex of the Z-amide isomer as identified in the ^{1}H NMR

112

spectroscopic and ITC conformational analyses from Chapters 5.3 and 5.5. The relative strength of the intermolecular complex is also consistent with the fact that this system harnesses the largest amount of work energy ($\delta\Delta G$) in the amide bond which is -1.9 kcal mol^{-1}. For comparison, the hermaphrodite **5.5** with the *cis*-stilbenylamido "piston" affords a K_A of only 370 M^{-1}. In this case the "piston" only marginally interacts with the CD "cylinder" even at high concentrations when their is a driving force for inclusion.[111] As a consequence, intermolecular complexation has little effect upon the *Z/E*-amide isomer ratio and the work harnessed ($\delta\Delta G$) is a negligible -0.1 kcal mol^{-1}. From these results, the relative strength of the intermolecular complexation has a substantial effect upon the work outputs ($\delta\Delta G$) of the hermaphrodites **5.4** and **5.5**.

Having obtained the thermodynamic parameters for the operation of the hermaphrodites **5.4** and **5.5**, the overall performance can be quantified. As discussed in Chapters 3 and 4, the efficiency can be determined from ΔG, using Equation 3.2.1 or from the heat dissipated (ΔH) with Equation 3.2.2. The energy efficiency of the work output for either ΔG or ΔH for the hermaphrodites **5.4** and **5.5** at 25 °C is shown in Table 5.7.2 in increasing order of efficiency.

Nanomachine	Eff$_{\Delta G}$ (%)[a]	Eff$_{\Delta H}$ (%)[b]
5.5	3	7
5.4	25	40

Table 5.7.2. Efficiency of harnessing the energy of intermolecular complexation in the hermaphrodites **5.4** and **5.5** at 25 °C. [a]Calculated from Equation 3.2.1. [b]Calculated from Equation 3.2.2.

The hermaphrodite **5.4** affords an efficiency of 25% (Eff$_{\Delta G}$) which increases to 40% (Eff$_{\Delta H}$) when the entropic contribution is removed from the calculation. Due to the intermolecular complexation this molecular machine harnesses the largest amount of work energy ($\delta\Delta G$) and performs with the greatest efficiency. Although this energy efficiency is comparable to the hermaphrodites **2.3** and **2.4** which use the [*c*1] complex to constrict the *E*-amide, the hermaphrodite **5.4** utilises intermolecular complexation to

bias the opposite *Z*-amide isomer. In aqueous solution the hermaphrodite **5.4** is driven to form an intermolecular complex which is sterically incapable of forming the *E*-amide. The hermaphrodite **5.5** having the *cis*-stilbenylamido "piston" has energy efficiencies of 3% ($Eff_{\Delta G}$) and 7% ($Eff_{\Delta H}$) which are comparable to that of the hermaphrodites **2.5** and **4.4** from the earlier Chapters. The performance of this system is different from that observed for the hermaphrodite **5.4** and demonstrates that a molecular machine using intermolecular complexation can be switched "OFF". By photochemically switching between the hermaphrodite **5.4** and its *cis*-isomer **5.5** the energy efficiency can be modulated. On this basis, intermolecular complexation can be harnessed in a nanomachine having a photochemical "ON/OFF" switch.

5.8 Conclusion

In this chapter a new type of molecular machine was developed that harnesses the strain energy from intermolecular complexation. It was discovered using a combined ^{1}H NMR spectroscopic and ITC strategy that a *trans*-stilbenylamido "piston" installed onto the relatively narrow annulus of α-CD **1.9** leads to the formation an intermolecular complex. This complex has the effect of constraining the geometry to the *Z*-amide isomer with comparable performance of the synthetic molecular machines that form the [*c*1] complex to bias the *E*-amide isomer discussed in the preceding Chapters. It was also demonstrated that the relative stability of the intermolecular complex formed has an effect on the work that is done ($\delta \Delta G$) on the amide bond. The *trans*-stilbenylamido hermaphrodite **5.4** formed the strongest intermolecular complex and afforded the best performance. Its *cis*-stilbenylamido counterpart the hermaphrodite **5.5** harnesses negligible energy and is in the "OFF" state. Using photochemical stimulus to switch between the hermaphrodites **5.4** and **5.5** the intermolecular complexation can be modulated, the energies harnessed controlled and the molecular machine can be switched "ON" and "OFF". On this basis the energy of intermolecular complexation can be harnessed to favor the *Z*-amide isomer by an artificial molecular machine having a photochemical "ON/OFF" switch.

CHAPTER 6

Synthesis and Conformational Analysis of a Nanomachine Having a pH Dependent On/Off Switch

6.1 Introduction

Through the work discussed in the preceding Chapters it has been demonstrated that photochemically dependent synthetic molecular machines can be developed to perform quantifiable work at the molecular level with the energy efficiency of their macroscopic counterparts. Importantly, this research shows that the work output ($\delta\Delta G$) is governed by the configuration of a photosensitive aryl "piston" which can be manipulated using a photochemical stimulus. Several limitations for using photochemical control were identified which include lengthy exposure times, light promoted side reactions and incomplete conversions. Previously, the manipulation of supramolecular complexes has been demonstrated in an instantaneous, clean and efficient manner using a pH external stimulus.[139] In view of this, a pH dependent molecular machine that transitions between the [c1] and the [a1] complex (Figure 6.1.1) *via* the regulation of an acid-base equilibrium was considered likely to provide an advanced alternative to the photochemical systems.
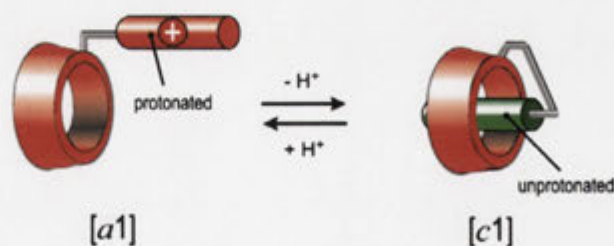
Figure 6.1.1. Schematic representation of a unimolecular hermaphrodite having a pH sensitive "piston".

Host-guest systems that utilise pH control require donor atoms such as nitrogen which can exist as amine/ammonium or pyridine/pyridinium forms.[139] The protonation and deprotonation of the donor group alters the electronic[140] and hydrophobic properties of the host-guest complex. For this reason, as demonstrated by Tato *et al.*,[141] the pH

115

control of an amino-substituted hermaphroditic CD can actuate the transition between the [c1] complex and [a1] conformation. Furthermore Liu *et al.*,[142] showed that a hermaphrodite having an indolyl pendant group that forms the [c1] complex under neutral conditions (pH 7) afforded different affinities for guest molecules than when the nitrogen donor atom was protonated under acidic conditions (pH 2). This suggests that the strength of the [c1] complex is modulated by pH which must affect the conformational constraint on the linkage group. To investigate this, a pH sensitive molecular machine was to be developed and the strain energy of molecular recognition quantified under acidic and basic conditions (Figure 6.1.2).
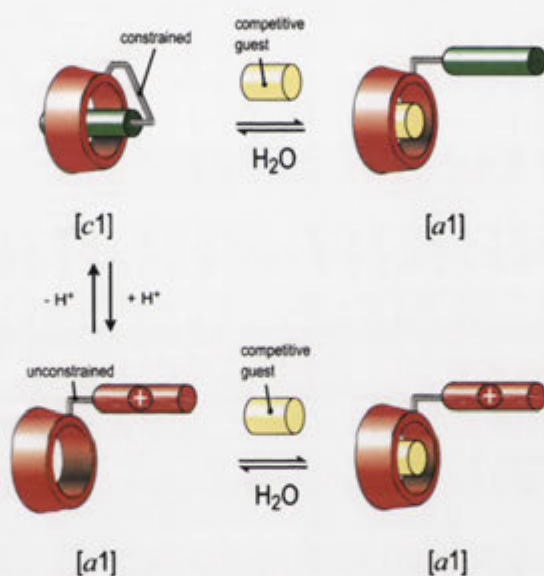
Figure 6.1.2. Schematic representation of the effect of a competitive guest on a pH sensitive hermaphrodite.

The pH dependent molecular analogue of a macroscopic mechanical pump is illustrated in Figure 6.1.3 and Scheme 6.2.2. For this an aryl "piston" with a *para*-amino phenyl group was to be installed onto β-CD **1.10** to produce the target 4-aminophenylpropionamido hermaphrodite **6.3**. Under basic conditions molecular recognition of the unprotonated aryl "piston" by the CD "cylinder" was expected to create the [c1] complex and then under acidic conditions the protonated aryl "piston" was expected to be displaced from the CD "cylinder" to form the [a1] conformation. The ratio of *Z/E*-amide isomers in both acidic and basic solutions in the absence and presence of 1-adamantanol "fuel" was to be measured and the work harnessed as output by molecular recognition quantified for each pH. From the research described in

116

Chapter 4 the properties of the "piston" significantly affect the work output. For this reason the acetamido hermaphrodite **6.6** having only a single methylene between the linkage group and the aryl substituent was also to be studied. In addition, the effect of a nitrogen donor group within the aromatic ring of the "piston" was to be examined using the pyridine analogue, the hermaphrodite **6.8**.
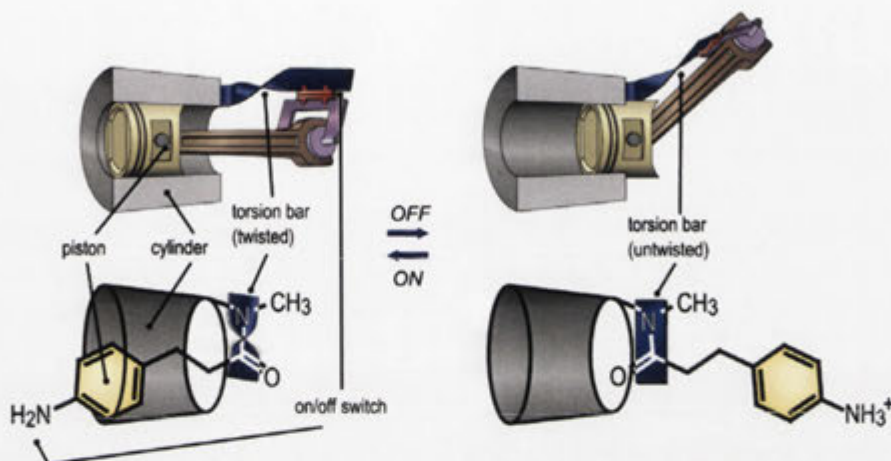

Figure 6.1.3. Schematic representation of a mechanical machine and its molecular counterpart.

6.2 Synthesis of Acetamido- and Propionamido-substituted β-Cyclodextrins

The approach to the hermaphrodite **6.3** is shown in Scheme 6.2.1, which involved the preparation of 3-(4-*tert*-butyloxycarbonylaminophenyl)propionic acid **6.1** using an established protocol.[143] The acid **6.1** was then installed onto the amino-CD **2.2** using Castro's amide coupling reagent (BOP) in DMF as shown in Scheme 6.2.2. The crude mixture was applied to anionic (DEAE) then cationic (SP) exchange resins, to isolate the hermaphrodite **6.2** in a yield of 36%. The BOC protected precursor **6.2** was then stirred in 4 M aqueous HCl before the mixture was neutralised and applied directly to Diaion (HP-20) exchange resin, to isolate after reverse-phase HPLC the hermaphrodite **6.3** in a yield of 90%. The hermaphrodite **6.3** was characterised by elemental analysis and showed, using ESI HRMS, an $[M+H]^+$ ion at 1295.482.
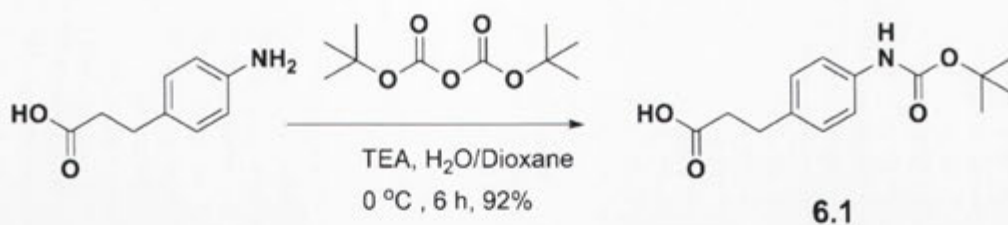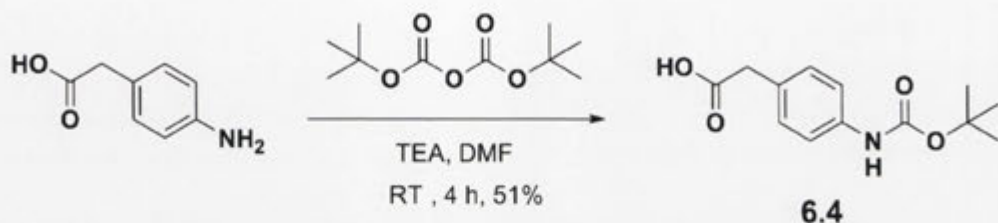
**Scheme 6.2.1.** Synthesis of 3-(4-*tert*-butyloxycarbonylaminophenyl)propionic acid **6.1**.
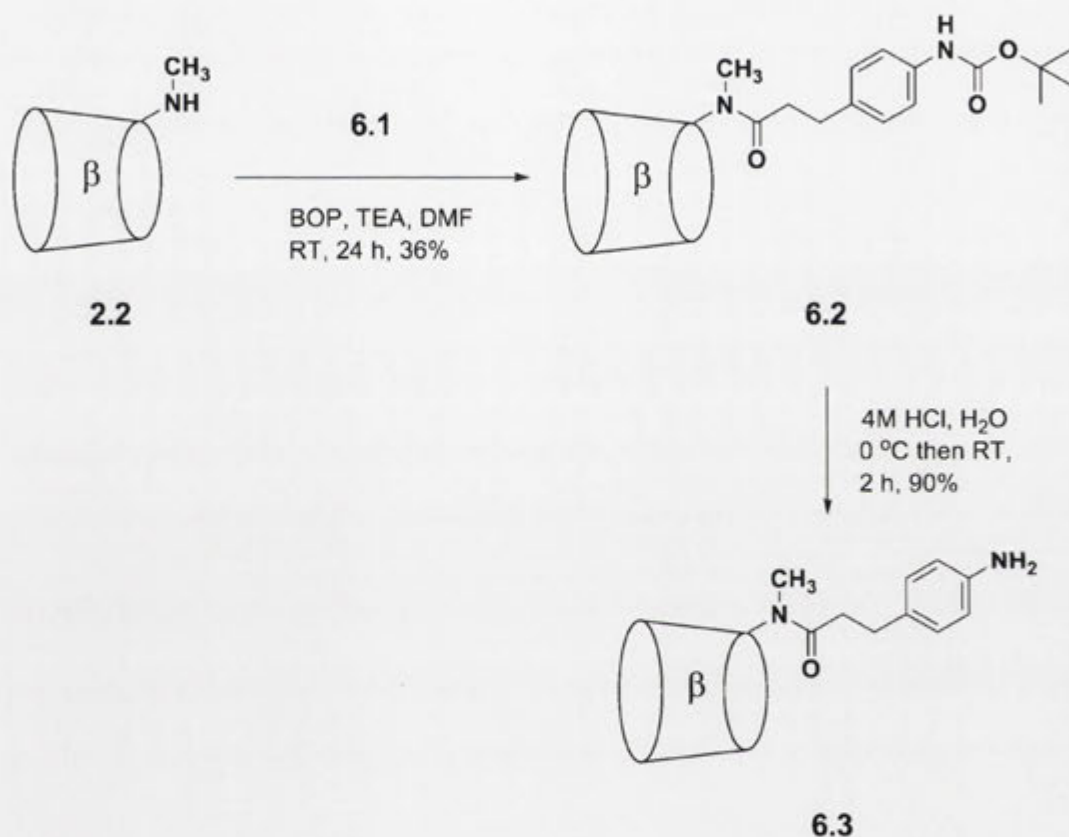
Scheme 6.2.2. Synthesis of 6^A-deoxy-6^A-(*N*-methyl-3-(4-aminophenyl)propionamido)-β-CD **6.3**.

Having successfully prepared the hermaphrodite **6.3**, the next focus was to synthesise the acetamido derivative, the hermaphrodite **6.6**. For this, 3-(4-*tert*-butyloxycarbonylaminophenyl)acetic acid **6.4** was obtained following an established protocol (Scheme 6.2.3).[144] With the amino group protected, the acid **6.4** was then coupled to the amino-CD **2.2** (Scheme 6.2.4) using the BOP reagent in DMF. The crude mixture was applied to anionic (DEAE) then cationic (SP) exchange resins, to isolate the hermaphrodite **6.5** in a yield of 52%. The BOC protected hermaphrodite **6.5** was

then treated with aqueous 4 M HCl before the solution was neutralised and applied to Diaion (HP-20) exchange resin. After concentrating the desired fraction, reverse-phase HPLC was used to isolate the hermaphrodite **6.6** as a white powder in a 65% yield. The hermaphrodite **6.6** was characterised by elemental analysis and showed using ESI HRMS, an $[M+H]^+$ ion at 1281.463.

Scheme 6.2.3. Synthesis of 3-(4-*tert*-butyloxycarbonylaminophenyl)acetic acid **6.4**.
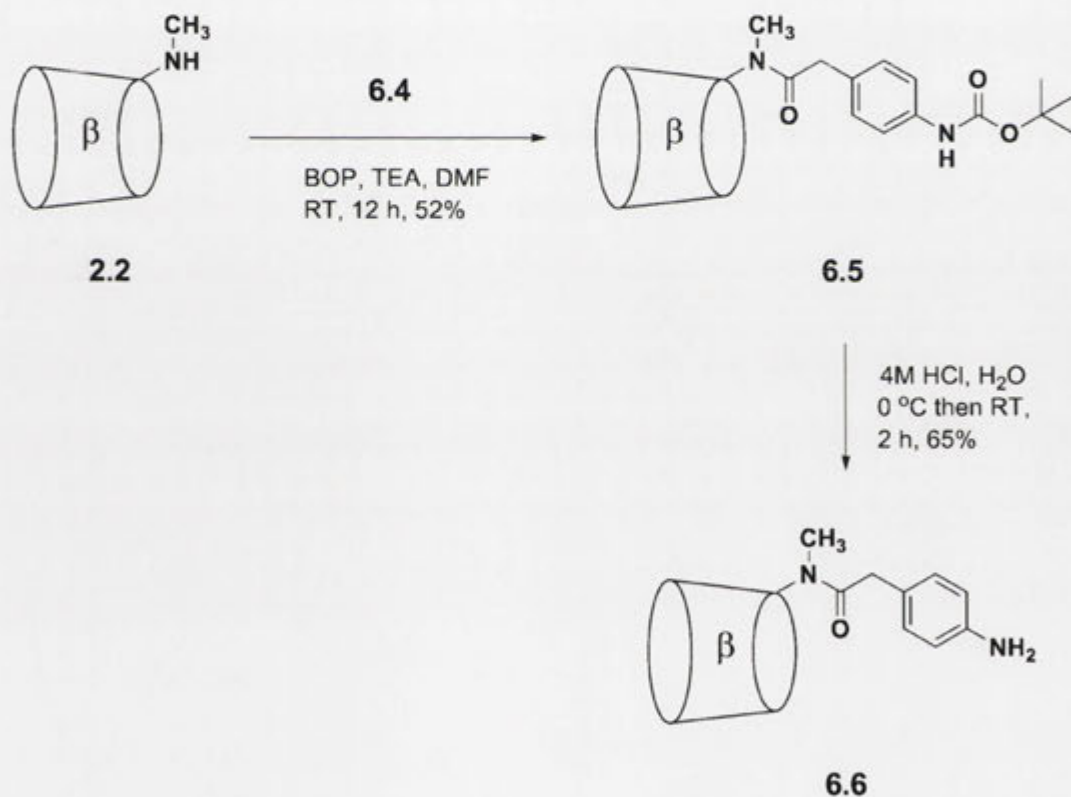
Scheme 6.2.4. Synthesis of 6^A-deoxy-6^A-(*N*-methyl-3-(4-aminophenyl)acetamido)-β-CD **6.6**.

With the hermaphrodites **6.3** and **6.6** in hand, the pyridine hermaphrodite **6.8** was prepared as shown in Scheme **6.2.5**. The commercially available 3-(3-pyridyl)propionic acid **6.7** was installed onto the amino-CD **2.2** in the presence of BOP

in DMF. The crude mixture was applied to anionic (DEAE) exchange resin followed by reverse-phase HPLC to isolate the hermaphrodite **6.8** in a yield of 74%. The hermaphrodite **6.8** was characterised by elemental analysis and showed, using ESI HRMS, an $[M+H]^+$ ion at 1281.462.
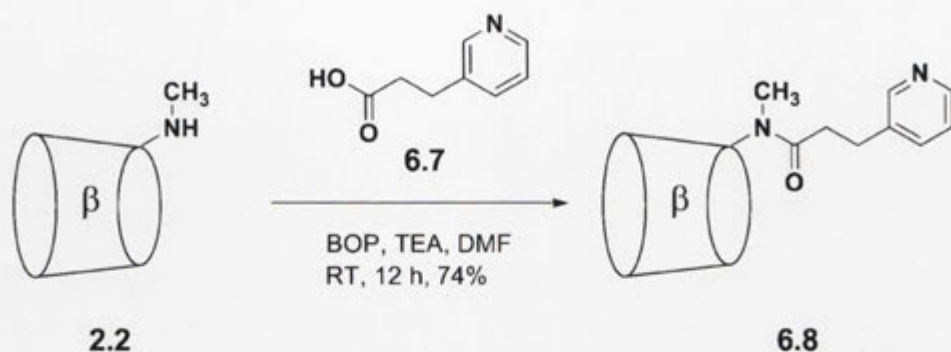
**Scheme 6.2.5.** Synthesis of 6^A-deoxy-6^A-(*N*-methyl-3-(3-pyridyl)propionamido)-β-CD **6.8**.

6.3 Conformational Analysis of Cyclodextrin Based Hermaphrodites

Having successfully prepared the hermaphrodites **6.3**, **6.6** and **6.8** their function as machines as illustrated in Figure 6.1.3 is dependent upon their conformational behavior in d_6-DMSO and in water at various pHs in the presence and absence of 1-adamantanol "fuel". For this, ^{1}H NMR analysis was employed to study each of the hermaphrodites **6.3**, **6.6** and **6.8** under the various conditions in order to identify the *Z/E*-amide isomers and the position of the aryl "piston" in relation to the CD "cylinder". As the ^{1}H NMR spectroscopic study of these systems was in deuterated solvent the correct nomenclature for the measurement of the acid-base equilibrium is pD, however as isotopic effects are unlikely to significantly alter the results pH is used to simplify the discussion. The pH for the investigation of the hermaphrodites **6.3** and **6.6** was selected for the reason that the aminophenyl functionality of the aryl "piston" resembles aniline which has a pK_a of 4.60 at 25 °C while the aryl "piston" of the hermaphrodite **6.8** was expected to parallel pyridine which has a pK_a of 5.23 at 25 °C.[145] On this basis, to observe the unprotonated and protonated states for each of the hermaphrodites **6.3**, **6.6** and **6.8** the ^{1}H NMR spectroscopic analyses were conducted at pH 9 and pH 2. Furthermore, as the pK_a of protonated planar amide bonds is ~0.9[145] and the pK_as of the hydroxy groups of a CD are >12.0[111] these functional groups are expected to have

remained unionised and have little influence upon the *Z/E*-amide equilibrium over the chosen pH range. Finally, while 1-adamantanecarboxylate "fuel" was suitable at pH 6.9, this guest was too insoluble at pH 2 and is also likely to have Coulombic interactions with the protonated hermaphrodites. For these reasons, 1-aminoadamantane "fuel" was used which has a pK_a of 10.58^{145} and thus exists predominantly in the protonated form at both pH 9 and pH 2.

The conformational behavior of the hermaphrodite **6.3** was studied in d_6-DMSO for which a section of the ^{1}H NMR spectrum is shown in Figure 6.3.1. In the *N*-methyl region two proton signals are observed at δ 2.94 and 2.77 ppm which integrate to a ratio of about 1:0.9, respectively. From 2D ROESY analysis, the signal at δ 2.94 ppm can be assigned to the *Z*-amide isomer and the aryl "piston" shows no interaction with the CD "cylinder". On this basis, without the driving force for inclusion, in the organic solvent the hermaphrodite **6.3** exists in the [*a*1] conformation with two isomers in a *Z/E*-amide ratio of 1:0.9.
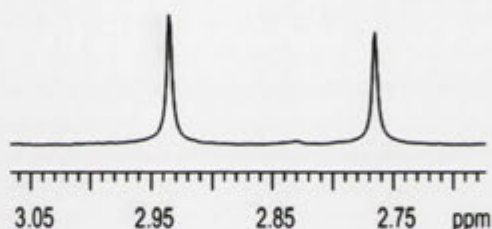
Figure 6.3.1. Section of the ^{1}H NMR spectrum (500 MHz) of the hermaphrodite **6.3** in d_6-DMSO at 25 °C.

Next, in D_2O at pH 9 the hermaphrodite **6.3** appears as two species as shown by its ^{1}H NMR spectrum in Figure 6.3.2. Similar to the propionamido hermaphrodite **2.3**, the methylene region of the spectrum is not the standard A_2B_2 resonance pattern which suggests the presence of multiple methylene conformations. In the aromatic region of the spectrum two sets of signals are observed in a ratio of about 17:1 with the major set at δ 7.04 and 6.93 ppm and the minor set at δ 7.02 and 6.82 ppm. In the *N*-methyl region of the spectrum a high intensity proton singlet is observed at δ 3.07 ppm and a low intensity singlet appears at δ 3.00 ppm that are in a ratio of about 17:1. From the ROESY spectrum (Figure 6.3.3) the resonance at δ 3.07 ppm shows no cross-peaks with the signals for the **A** methylene protons and is therefore assigned to the *E*-amide isomer. Shown in Figure 6.3.4, the aromatic proton signals show NOE interactions with the CD "cylinder" resonances and therefore the aryl "piston" is included within the CD
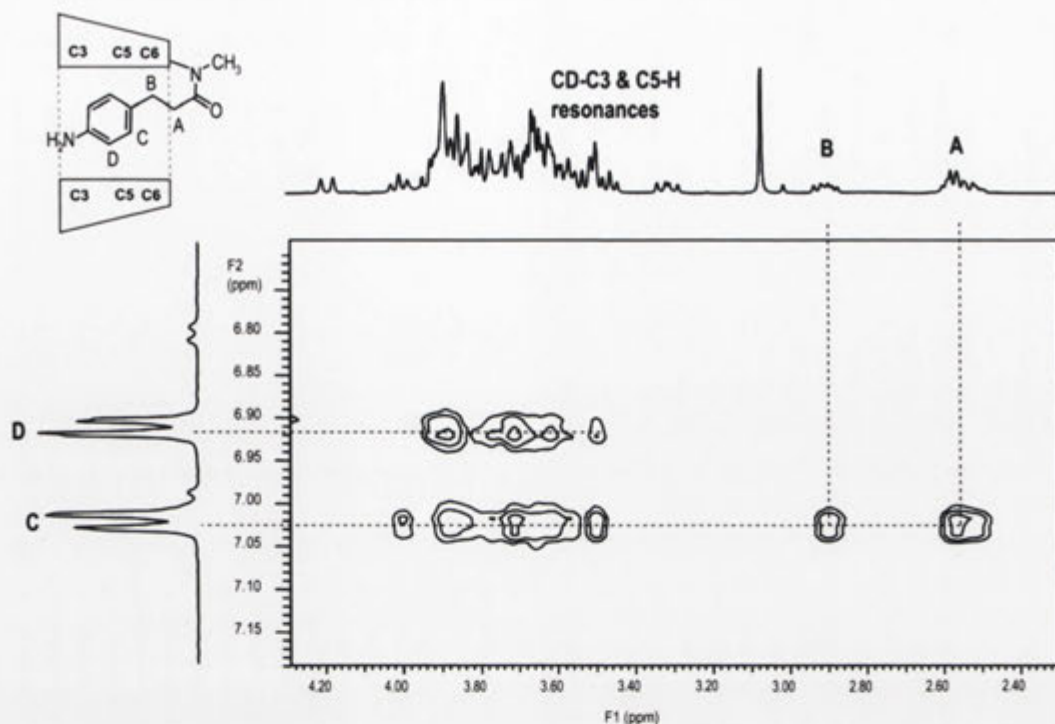
121

"cylinder". From this the dominant structure of the hermaphrodite **6.3** in D_2O at pH 9 is the included [c1] complex with a *Z/E*-amide ratio of 1:17.
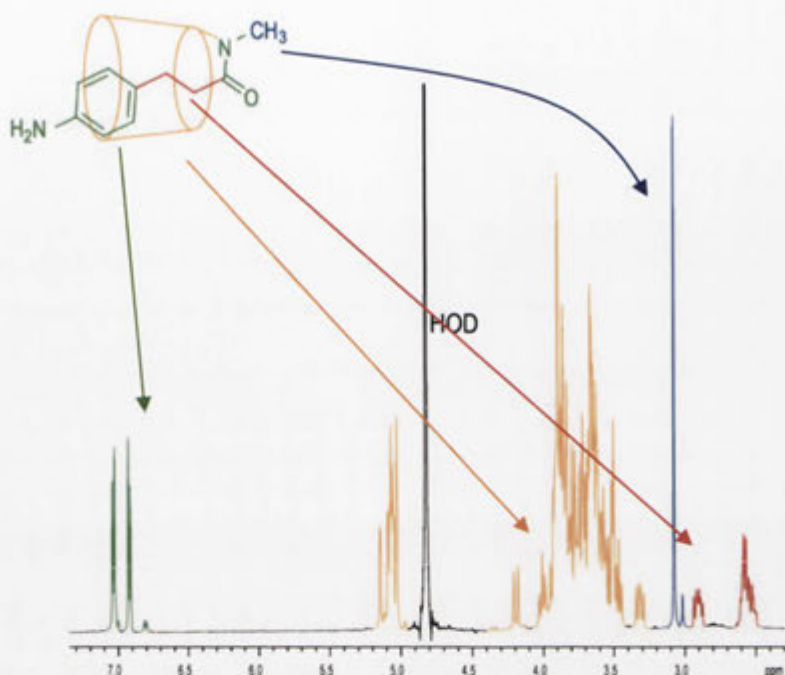
Figure 6.3.2. ^1H NMR spectrum (500 MHz) of the hermaphrodite **6.3** in D_2O (25 °C) at pH 9.
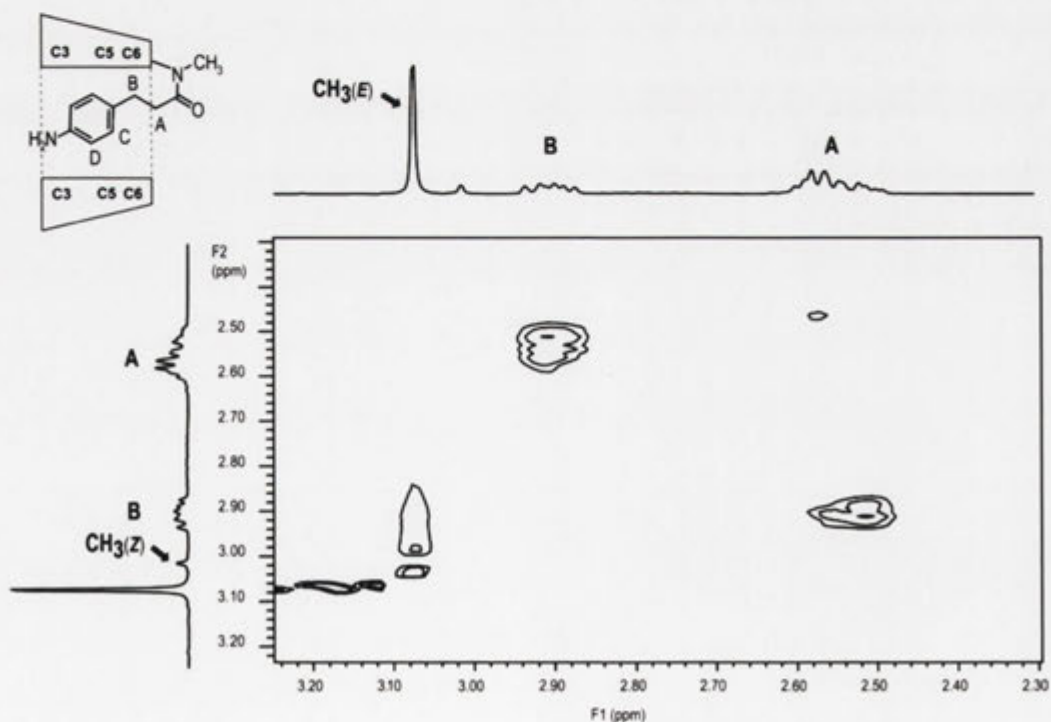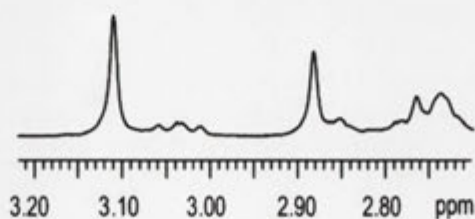

Figure 6.3.3. A section of the ROESY NMR spectrum (500 MHz) of the hermaphrodite **6.3** in D_2O (25 °C) at pH 9 with 0.250 ms mixing time.
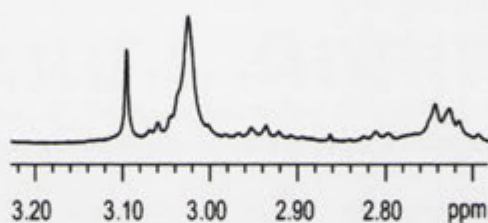
Figure 6.3.4. A section of the ROESY NMR spectrum (500 MHz) of the hermaphrodite **6.3** in D$_2$O (25 °C) at pH 9 with 0.250 ms mixing time.

A section of the ^{1}H NMR spectrum of the hermaphrodite **6.3** in D$_2$O at pH 9 in the presence of 1-aminoadamantane "fuel" is shown in Figure 6.3.5. Two *N*-methyl proton signals are observed in a ratio of about 1.4:1 at δ 3.11 and 2.88 ppm. The relative intensities are remarkably similar to those observed for the spectrum in *d$_6$*-DMSO (Figure 6.3.1). For reasons demonstrated later in Chapter 7 from titrations with 1-aminoadamantane "fuel" (Figure 7.3.1) the resonance at δ 3.11 ppm can be assigned to the *Z*-amide isomer. On this basis, the hermaphrodite **6.3** in D$_2$O at pH 9 with 1-aminoadamantane exists with a *Z/E*-amide ratio of 1.4:1.
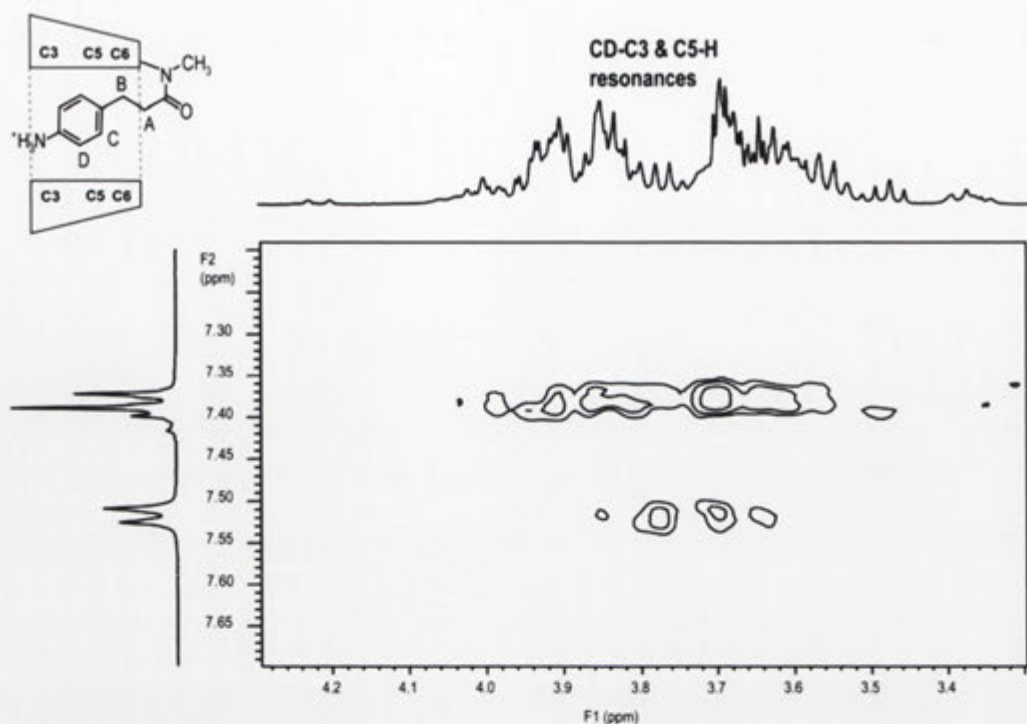

Figure 6.3.5. A section of the ^{1}H NMR spectrum (500 MHz) of the hermaphrodite **6.3** in D$_2$O (25 °C) at pH 9 and in the presence of 1-aminoadamantane "fuel".

Having studied the hermaphrodite **6.3** under basic conditions it remained for its conformation to be explored in acidic solution. From the ^{1}H NMR spectrum for the hermaphrodite **6.3** in D_2O at pH 2 (Figure 6.3.6), the methylene region shows a complex resonance pattern which suggests that multiple methylene conformations exist in equilibrium. The *N*-methyl signals are at δ 3.10 and 3.03 ppm in an approximate ratio of about 1:2. For reasons demonstrated later in the Chapter (Figure 6.5.1) the signal at δ 3.10 ppm is assigned to the *Z*-amide isomer from an acid-base titration. From the ROESY NMR spectrum shown in Figure 6.3.7, NOE cross peaks are observed between the aromatic proton signals (F2 axis) of the "piston" and the CD "cylinder" resonances (F1 axis). This suggests that the protonated ammonium form of hermaphrodite **6.3** can still exist as the self included [*c*1] complex. On this basis, the hermaphrodite **6.3** at pH 2 can still form the [*c*1] complex in an overall *Z/E*-amide ratio of about 1:2.
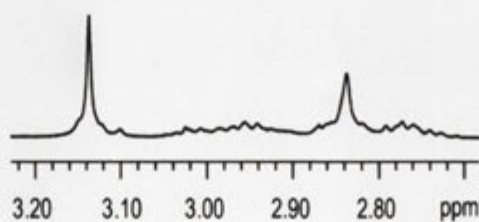

Figure 6.3.6. A section of the ^{1}H NMR spectrum (500 MHz) of the hermaphrodite **6.3** in D_2O (25 °C) at pH 2.

Figure 6.3.7. A section of the ROESY NMR spectrum (500 MHz) of the hermaphrodite **6.3** in D_2O (25 °C) at pH 2 with 0.250 ms mixing time.
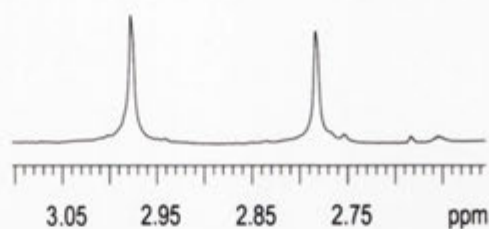
Shown in Figure 6.3.8 is a section of the ^1H NMR spectrum for the hermaphrodite **6.3** in D_2O at pH 2 with 1-aminoadamantane "fuel". Under these conditions the *N*-methyl region of the spectrum shows two proton signals at δ 3.14 and 2.84 ppm in a ratio of approximately 1.6:1. The intensity of these signals is similar to that observed for the spectrum in d_6-DMSO (Figure 6.3.1) and at pH 9 with 1-aminoadamantane (Figure 6.3.5). As shown later in this Chapter from a change in acid-base equilibrium to pH 2 (Figure 6.5.1) followed by the titration with 1-aminoadamantane "fuel" as demonstrated in Chapter 7 (Figure 7.3.2) the signal at δ 3.14 ppm is assigned to the *Z*-amide isomer. In summary, the hermaphrodite **6.3** in D_2O at pH 2 in the presence of 1-aminoadamantane "fuel" affords a *Z/E*-amide ratio of 1.6:1.

Figure 6.3.8. A section of the ^1H NMR spectrum (500 MHz) of the hermaphrodite **6.3** in D_2O (25 °C) at pH 2 and in the presence of 1-aminoadamantane "fuel".

To review the conformational behavior of the hermaphrodite **6.3**, in d_6-DMSO the aryl "piston" is not included and two major species are observed in a *Z/E*-amide ratio of 1:0.9. In D_2O at pH 9, the aryl "piston" includes within the CD "cylinder" and the *Z/E*-amide ratio is 1:17, while in the presence of 1-aminoadamantane "fuel" the *Z/E*-amide ratio becomes 1.4:1. By changing the solvent from d_6-DMSO to D_2O at pH 9 the increase in the minor isomer is due to the formation of the [*c*1] complex. By adding the 1-aminoadamantane "fuel" the *Z/E*-amide ratio changes to approach that observed for d_6-DMSO because of the transition from the [*c*1] complex to the [*a*1] guest complex. At pH 2, the "piston" of the hermaphrodite **6.3** shows interactions with the CD "cylinder" and the *Z/E*-amide ratio is 1:2, whereas in the presence of 1-aminoadamantane "fuel" the *Z/E*-amide ratio changes to 1.6:1. By changing the solvent from d_6-DMSO to D_2O at pH 2 a small increase in the minor isomer is observed as the [*c*1] complex forms. When the 1-aminoadamantane "fuel" is added at pH 2 the *Z/E*-amide ratio approaches that of d_6-DMSO, which is expected for the change from the [*c*1] complex to the [*a*1] guest complex. On the basis that at pH 2 the [*c*1] complex is still capable of forming, the *Z/E*-amide ratio of the hermaphrodite **6.3** is different from that observed in d_6-DMSO. The difference in the *Z/E*-amide isomer ratios observed between pH 9 and pH 2 suggests that the neutral and protonated forms of the amine of the aryl "piston" have an effect on the concentration of the [*c*1] complex.

Having investigated the conformational behavior of the hermaphrodite **6.3** under the various conditions, the next focus was the study of the hermaphrodite **6.6**. From the ^1H NMR spectrum of the hermaphrodite **6.6** in d_6-DMSO two proton resonances are observed at δ 2.98 and 2.78 ppm that integrate to a ratio of about 1:0.8 (Figure 6.3.9). The relative intensities of the signals for this section of the spectrum are remarkably similar to those observed in the same solvent for the hermaphrodite **6.3**. From the 2D ROESY analysis the stronger proton signal at δ 2.98 ppm can be assigned to the *Z*-amide isomer. In the d_6-DMSO solvent the aryl "piston" shows no interaction with the CD "cylinder" and the dominant species is the [*a*1] conformation. To conclude, the hermaphrodite **6.6** forms the [*a*1] conformation in d_6-DMSO with two amide isomers in a *Z/E* ratio of 1:0.8.
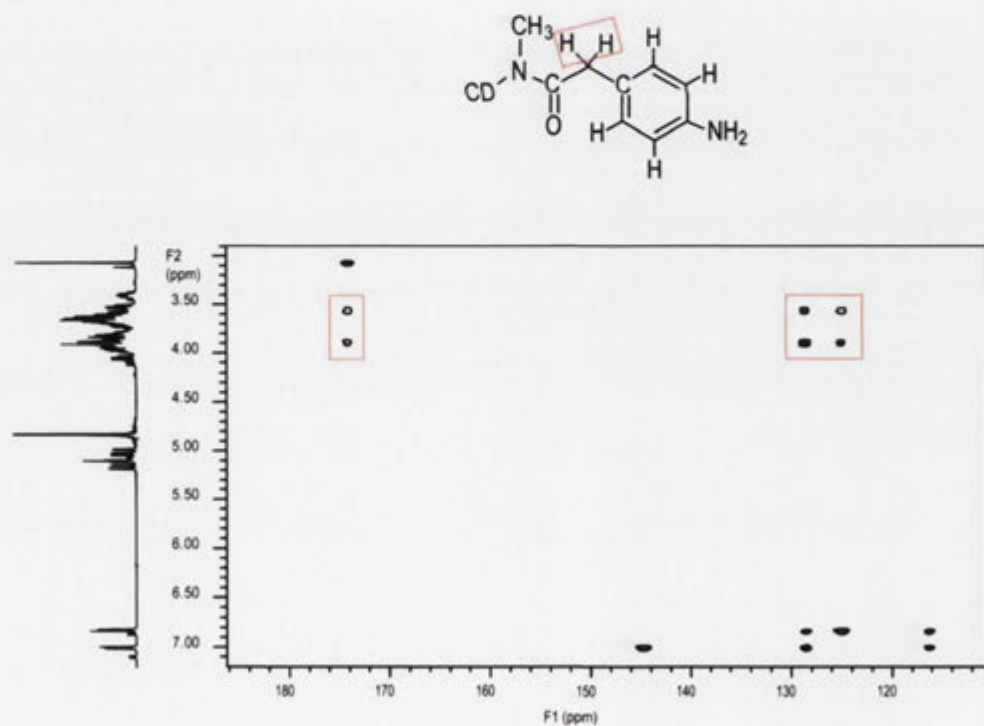
Figure 6.3.9. A section of the [^1]H NMR spectrum (500 MHz) of the hermaphrodite **6.6** in d_6-DMSO at 25 °C.

The [^1]H NMR spectrum of the hermaphrodite **6.6** in D_2O at pH 9 is shown in Figure 6.3.10. In the aromatic region of the spectrum two species are present in a ratio of about 1:7 with the less intense set of signals at δ 7.10 and 6.86 ($J = 8.0$ Hz) and the more intense set of resonances at δ 7.00 and 6.83 ppm ($J = 8.5$ Hz). In the *N*-methyl region of the spectrum two species are observed in a ratio of 1:6.7 with the minor singlet at δ 3.11 ppm and the major singlet at δ 3.07 ppm. The methylene proton signals overlap with the CD "cylinder" signals and are identified from a 2D HMBC experiment which correlates [^1]H and [^13]C peaks for atoms that are separated by multiple bonds (Figure 6.3.11). From this the methylene proton resonances appear at δ 3.88 and 3.58 ppm (F2 axis) which suggests either an AB splitting pattern or multiple conformations are present. Using a gradient heteronuclear multiple quantum coherence NMR (HMQC) spectroscopic experiment (Figure 6.3.12) the resonances at δ 3.88 and 3.58 ppm (F2 axis) correlate with the same [^13]C signal, which suggests that an AB splitting is occurring. From the ROESY analysis (Figure 6.3.13) the more intense methyl signal at δ 3.07 ppm (F1 axis) shows no NOE interaction with the either of the methylene proton signals and is therefore assigned to the methyl group of the *E*-amide isomer. From the ROESY NMR spectrum shown in Figure 6.3.14 the aryl "piston" shows NOE interactions with the CD "cylinder" thus the self included complex is being formed. In conclusion, the hermaphrodite **6.6** forms a [*c*1] conformation at pH 9 with a *Z/E*-amide isomer ratio of 1:6.7.
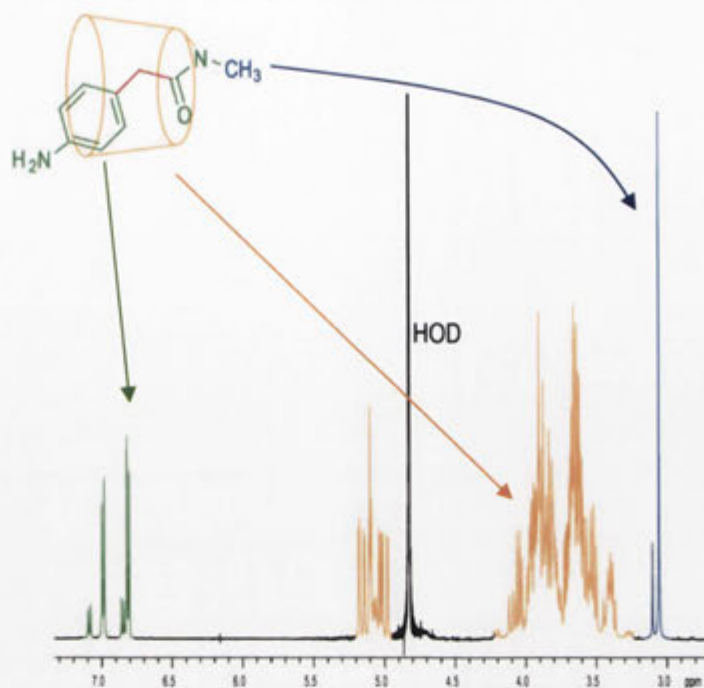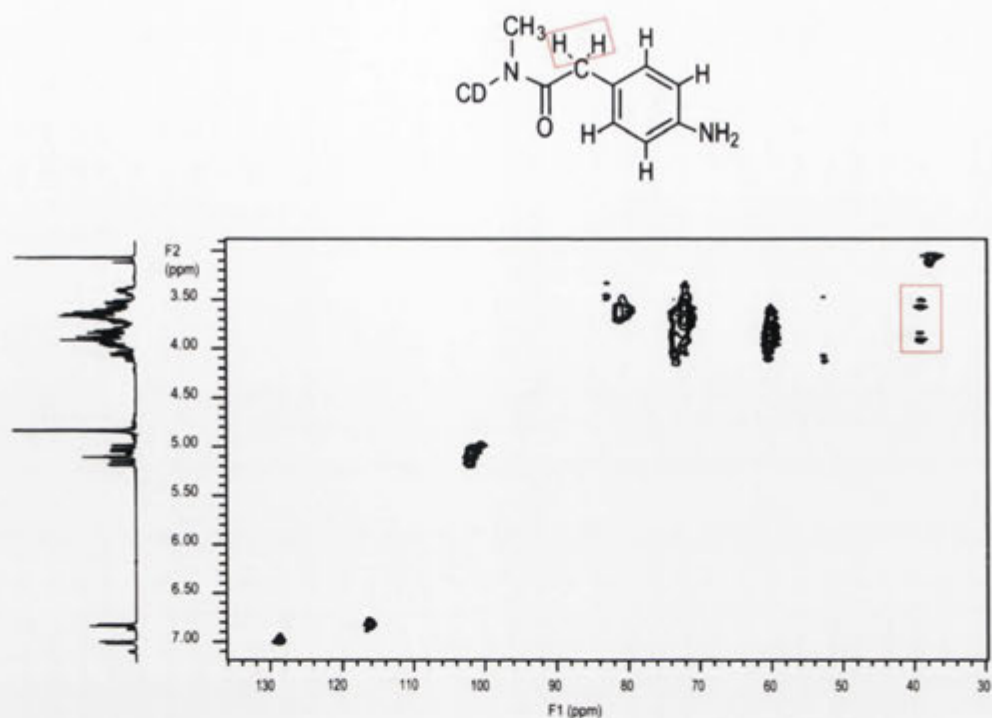
Figure 6.3.10. ^{1}H NMR spectrum (500 MHz) of the hermaphrodite **6.6** in D$_2$O (25 °C) at pH 9.
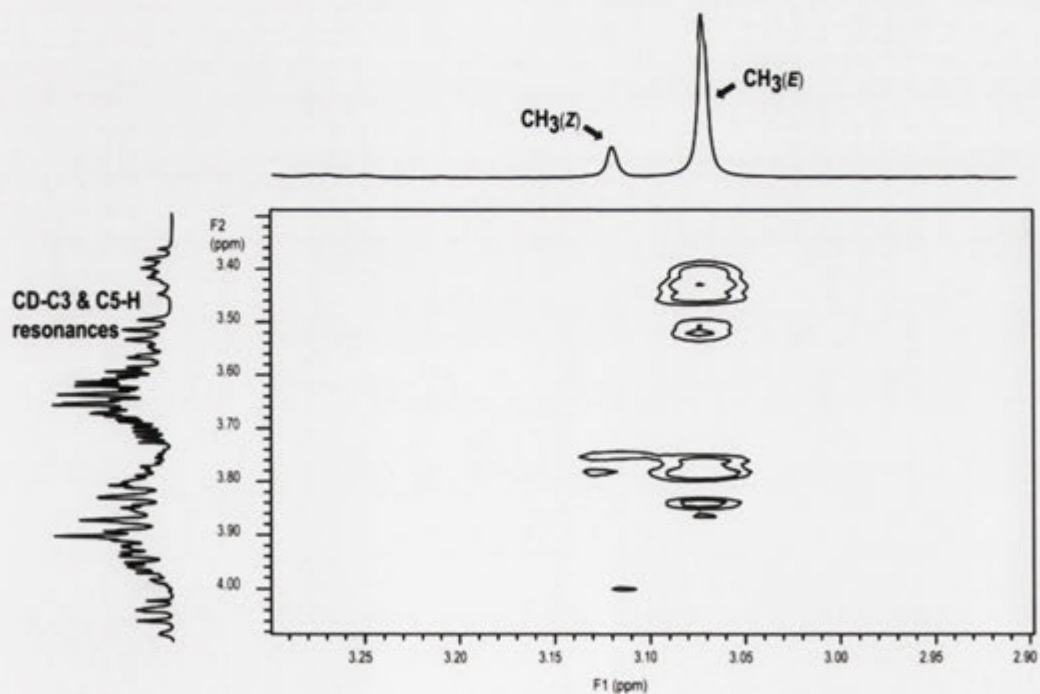

Figure 6.3.11. A section of the HMBC NMR spectrum (500 MHz) of the hermaphrodite **6.6** in D$_2$O (25 °C) at pH 9.
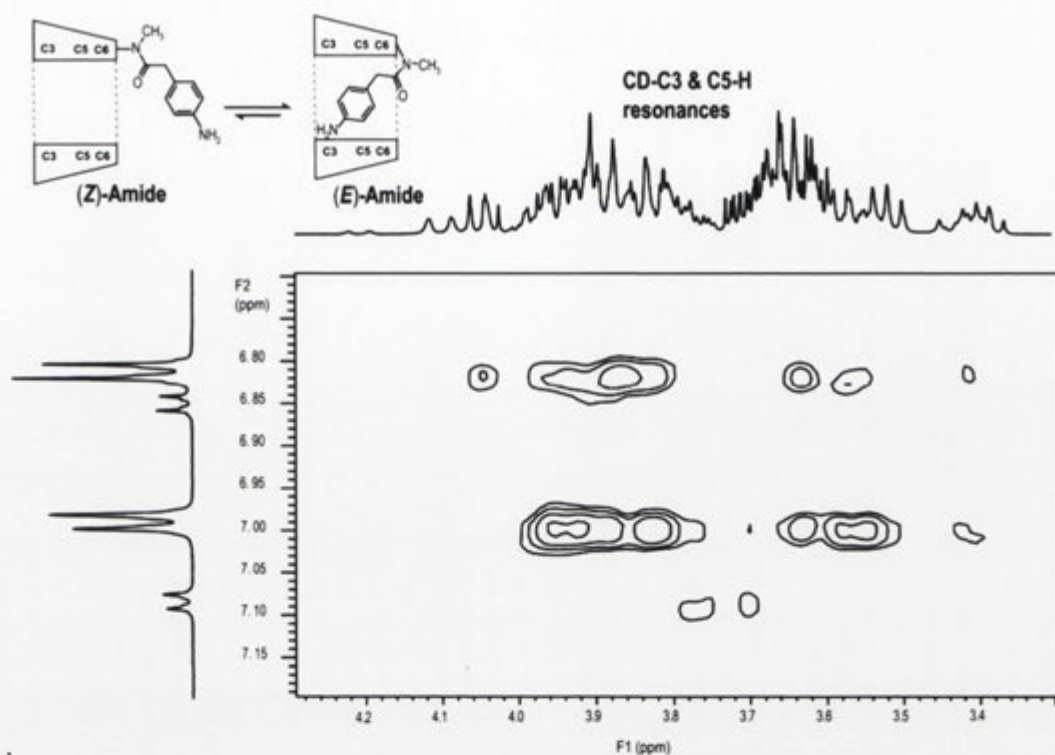
Figure 6.3.12. A section of the HMQC NMR spectrum (500 MHz) for the hermaphrodite **6.6** in D_2O (25 °C) at pH 9.

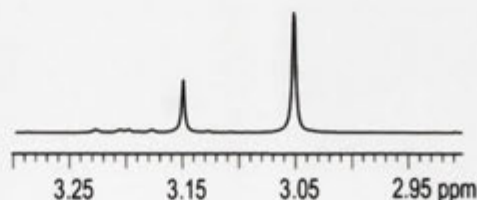
Figure 6.3.13. A section of the ROESY NMR spectrum (500 MHz) of the hermaphrodite **6.6** in D_2O (25 °C) at pH 9 with 0.250 ms mixing time.
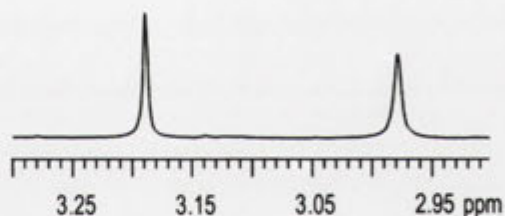
129

Figure 6.3.14. A section of the ROESY NMR spectrum (500 MHz) of the hermaphrodite **6.6** in D_2O (25 °C) at pH 9 with 0.250 ms mixing time.

Figure 6.3.15 shows a section of the *N*-methyl region of the spectrum for the hermaphrodite **6.6** in D_2O at pH 9 with 3 equivalents of 1-aminoadamantane "fuel". Two proton signals are observed at δ 3.15 and 3.06 ppm which integrate to a ratio of about 1:2.9, respectively. The less intense signal at δ 3.15 ppm is assigned to the methyl group of the Z-amide isomer from the titration with 1-aminoadamantane "fuel" described later in Chapter 7 (Figure 7.3.3). On this basis, the hermaphrodite **6.6** at pH 9 with 1-aminoadamantane "fuel" has two amide conformations in an overall *Z/E* ratio of about 1:2.9.
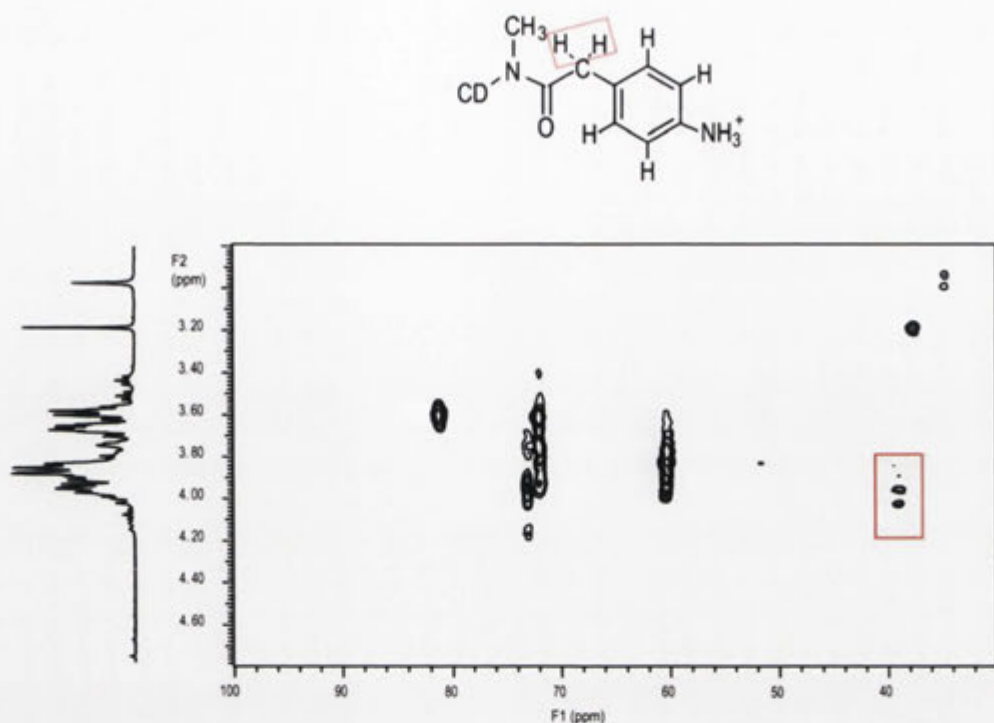

Figure 6.3.15. A section of the ¹H NMR spectrum (500 MHz) of the hermaphrodite **6.6** in D_2O (25 °C) at pH 9 and in the presence of 1-aminoadamantane "fuel".
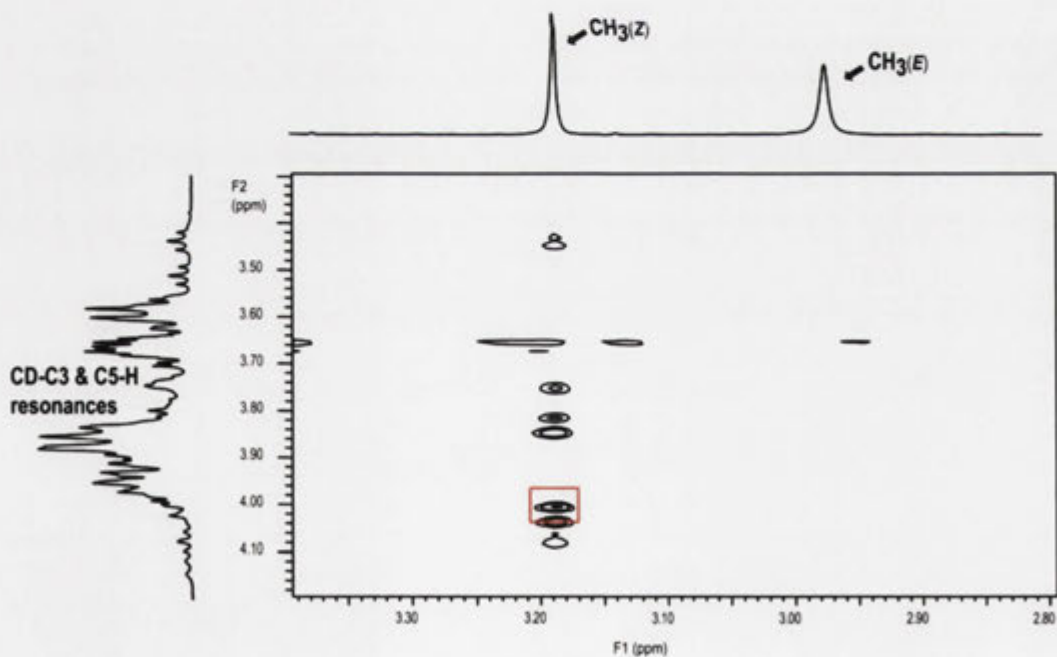
130

The ^{1}H NMR spectrum of the hermaphrodite **6.6** in D_2O at pH 2 shows two major proton signals at δ 3.19 and 2.98 ppm which integrate to a ratio of about 1:1 (Figure 6.3.16). This spectrum is quite similar to that observed for the hermaphrodite **6.6** in d_6-DMSO. From the HMQC spectrum (Figure 6.3.17) the methylene resonances are identified at δ 4.01 and 3.95 ppm. Using ROESY analysis (Figure 6.3.18) the stronger proton signal at δ 3.19 (F1 axis) is assigned to the Z-amide isomer because of the NOE interaction with the methylene proton signal at δ 4.01 ppm (F2 axis). This is supported by following the Z-amide methyl signal assigned at pH 9 from the ^{1}H NMR spectra recorded for the acid-base titration to pH 2 (Figure 6.5.3). At this pH the aryl "piston" shows through the observation of background noise very weak interactions with the CD "cylinder" which indicates that the dominant species is the [*a*1] conformation (Figure 6.3.19). Overall, the hermaphrodite **6.6** forms the non-included [*a*1] conformation in D_2O at pH 2 with two amide isomers in an Z/E ratio of 1:1.
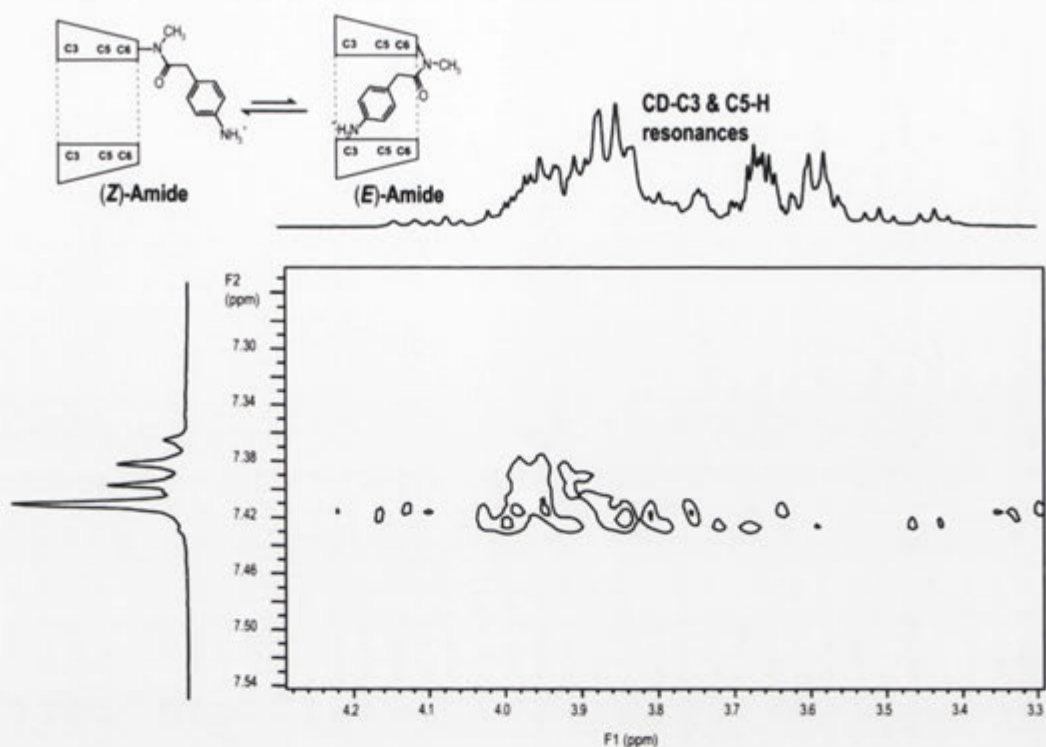

Figure 6.3.16. A section of the ^{1}H NMR spectrum (500 MHz) of the hermaphrodite **6.6** in D_2O (25 °C) at pH 2.

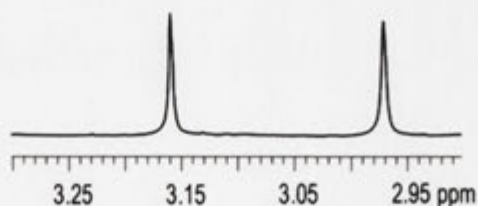**Figure 6.3.17.** HMQC NMR spectrum (500 MHz) of the hermaphrodite **6.6** in D_2O (25 °C) at pH 2.

Figure 6.3.18. A section of the ROESY NMR spectrum (500 MHz) of the hermaphrodite **6.6** in D_2O (25 °C) at pH 2 with 0.250 ms mixing time.

Figure 6.3.19. A section of the ROESY NMR spectrum (500 MHz) of the hermaphrodite **6.6** in D$_2$O (25 °C) at pH 2 with 0.250 ms mixing time.
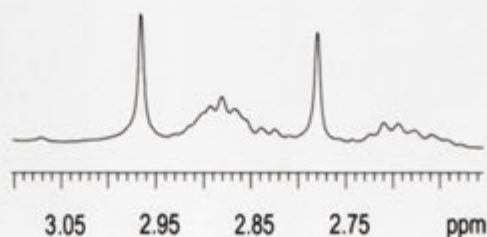
The ^{1}H NMR spectrum (Figure 6.3.20) of the hermaphrodite **6.6** in D$_2$O at pH 2 in the presence of 1-aminoadamantane "fuel" shows two major proton signals at δ 3.16 and 2.97 ppm that integrate to a ratio of approximately 1:0.8. The singlet at δ 3.16 ppm is due to the Z-amide as demonstrated in Chapter 7 from titrations with 1-aminoadamantane "fuel" (Figure 7.3.4). In summary, the hermaphrodite **6.6** in D$_2$O at pH 2 with 1-aminoadamantane "fuel" adopts a Z/E-amide ratio of 1:0.8, respectively.

Figure 6.3.20. A section of the ^{1}H NMR spectrum (500 MHz) of the hermaphrodite **6.6** in D$_2$O (25 °C) at pH 2 and in the presence of 1-aminoadamantane "fuel".

To review the conformational analysis of the hermaphrodite **6.6**, in d_6-DMSO the aryl "piston" shows no interaction with the CD "cylinder" and the *Z/E*-amide ratio is 1:0.8. In D_2O at pH 9, the aryl "piston" interacts with the CD "cylinder" and the *Z/E*-amide ratio is 1:6.7, while in the presence of 1-aminoadamantane "fuel" the *Z/E*-amide ratio becomes 1:2.9. From the change in solvent from d_6-DMSO to D_2O at pH 9 the increase in the proportion of the minor isomer is from the formation of the [*c*1] complex. From the addition of 1-aminoadamantane "fuel" at pH 9 the change in the *Z/E*-amide ratio shows that a small increase in the proportion of the [*a*1] guest complex occurs. Next, at pH 2 the aryl "piston" shows little interaction with the CD "cylinder" and the *Z/E*-amide ratio is 1:1. When 1-aminoadamantane "fuel" is added the *Z/E*-amide ratio only slightly alters to become 1:0.8. From the change in the solvent from d_6-DMSO to D_2O at pH 2 or by adding 1-aminoadamantane "fuel" at pH 2 the *Z/E*-amide ratio remains unchanged thus the [*a*1] complex predominates under each of these conditions. Due to the uncharged compound at pH 9 forming the [*c*1] complex and the protonated ammonium form predominating as the [*a*1] complex at pH 2 a difference is observed for the *Z/E*-amide isomer ratios between these conditions.

With the conformational behavior of the hermaphrodites **6.3** and **6.6** studied, the pyridine based system, the hermaphrodite **6.8** was next to be investigated. In Figure 6.3.21 is the ^{1}H NMR spectrum of the hermaphrodite **6.8** in d_6-DMSO which shows the *N*-methyl region of the spectrum. Two *N*-methyl proton signals are observed at δ 2.97 and 2.78 ppm in a ratio of approximately 1:0.9. The methylene resonances are not typical of the expected A_2B_2 pattern thus multiple conformations are likely to be present. From ROESY analysis the signal at δ 2.97 ppm can be assigned to the *Z*-amide isomer and in the organic solvent the major species is the non-included [*a*1] conformation. In summary, the hermaphrodite **6.8** in d_6-DMSO exists as the [*a*1] conformation with a *Z/E*-amide ratio of 1:0.9.
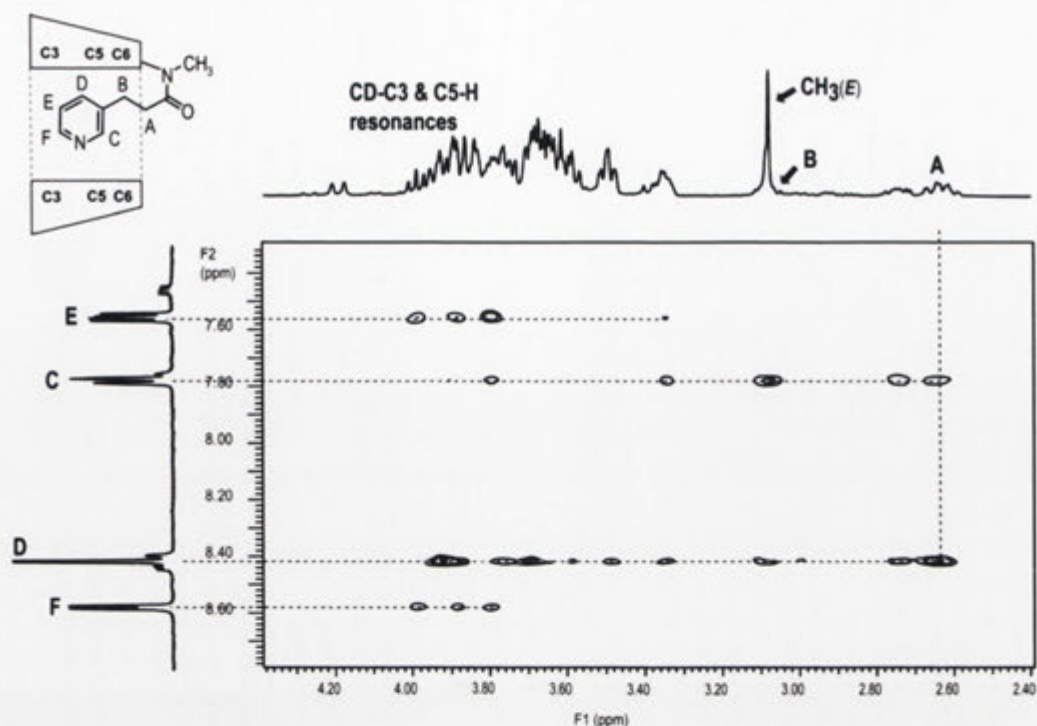

Figure 6.3.21. Section of the ^{1}H NMR spectrum (500 MHz) of the hermaphrodite **6.8** in d_6-DMSO at 25 °C.

In D_2O at pH 9 the hermaphrodite **6.8** exists as two species as shown by its ^{1}H NMR spectrum in Figure 6.3.22. The methylene region of the spectrum suggests that a mixture of methylene conformations is present. From the aromatic region of the spectrum two sets of signals are observed in a ratio of about 1:5. In the *N*-methyl region an intense proton singlet is observed at δ 3.08 ppm while the methyl signal for the minor amide isomer is at δ 3.09 ppm in a ratio of approximately 5:1 for reasons demonstrated later in the Chapter from the acid-base titration (Figure 6.5.5). The low intensity singlet at δ 3.09 ppm can be assigned to the *Z*-amide isomer by following this signal over the course of a titration with 1-aminoadamantane "fuel" shown in Chapter 7 (Figure 7.3.8) and then ROESY analysis of the endpoint shown later in this Chapter (Figure 6.3.24). In D_2O at pH 9 the ROESY spectrum (Figure 6.3.23) shows that the aryl "piston" has NOE interactions within the CD "cylinder". From this the dominant structure of the hermaphrodite **6.8** in D_2O at pH 9 is the included [*c*1] complex with a *Z*/*E*-amide ratio of 1:5.
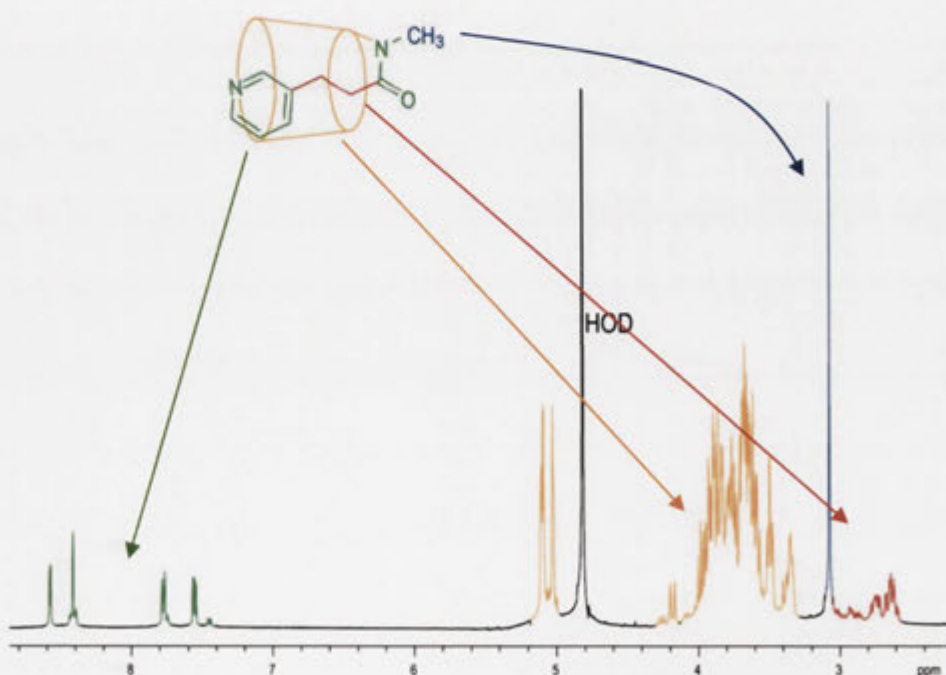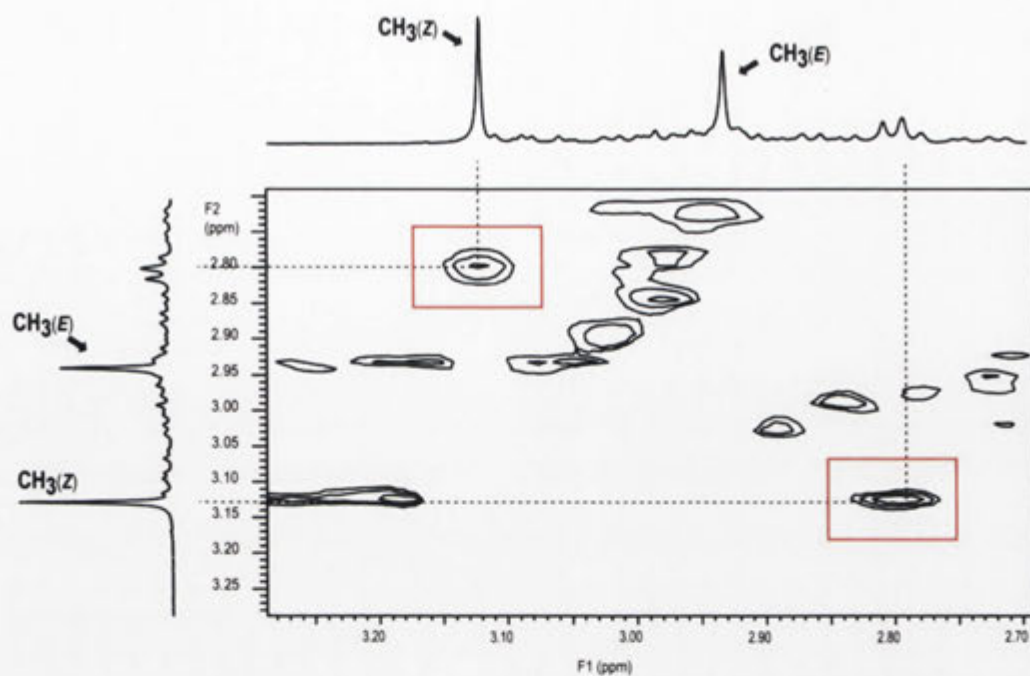

Figure 6.3.22. ^{1}H NMR spectrum (500 MHz) of the hermaphrodite **6.8** in D_2O (25 °C) at pH 9.

Figure 6.3.23. A section of the ROESY NMR spectrum (500 MHz) of the hermaphrodite **6.8** in D_2O (25 °C) at pH 9 with 0.250 ms mixing time.
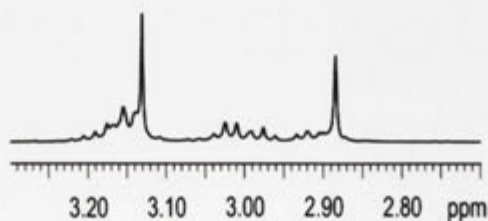
Figure 6.3.24 shows the ROESY NMR spectrum for the hermaphrodite **6.8** in D_2O at pH 9 with 3 equivalents of 1-aminoadamantane "fuel". In the *N*-methyl region of the spectrum two proton signals are observed at δ 3.12 and 2.94 ppm which integrate to a ratio of about 1:0.8, respectively. The relative intensities of these signals are remarkably similar to that observed in the d_6-DMSO spectrum. The high intensity signal at δ 3.12 ppm (F1 axis) shows an NOE interaction with the methylene proton signal at δ 2.80 ppm (F2 axis) and is therefore assigned to the methyl group of the *Z*-amide isomer. On this basis, the hermaphrodite **6.8** at pH 9 with 1-aminoadamantane "fuel" forms two conformations in an overall *Z/E*-amide ratio of about 1:0.8.

136

Figure 6.3.24. A section of the ROESY NMR spectrum (500 MHz) of 1-aminoadamantane (3-equivalents) and the hermaphrodite **6.8** in D_2O (25 °C) at pH 9 with 0.250 ms mixing time.

From the ^1H NMR spectrum for hermaphrodite **6.8** in D_2O at pH 2 (Figure 6.3.25) two proton signals are observed at δ 3.13 and 2.88 ppm in a ratio of 1:0.7. These signals have similar intensities and appearance to the *N*-methyl resonances observed in d_6-DMSO and in D_2O at pH 9 with 1-aminoadamantane "fuel". The methyl singlet at δ 3.13 ppm is assigned to the *Z*-amide isomer from the acid-base titration shown later in the Chapter (Figure 6.5.5) from a change in the pH. Using 2D ROESY analysis the aryl "piston" shows no NOE interaction with the CD "cylinder" and thus the dominant species is the [*a*1] conformation. This suggests that the protonated pyridinium form of the hermaphrodite **6.8** is predominantly in a non-included [*a*1] conformation with a *Z/E*-amide ratio of 1:0.7.

Figure 6.3.25. A section of the ^1H NMR spectrum (500 MHz) of the hermaphrodite **6.8** in D_2O (25 °C) at pH 2.

137

The ^{1}H NMR spectrum of the hermaphrodite **6.8** in the presence of 1-aminoadamantane "fuel" in D_2O at pH 2 is shown in Figure 6.3.26. In the *N*-methyl region of the spectrum, two sharp proton signals are observed at δ 3.13 and 2.86 ppm that integrate in a ratio of about 1:0.8, respectively. The appearance and relative intensities of these two resonances are reminiscent of the *N*-methyl signals observed in d_6-DMSO, D_2O at pH 9 with 1-aminoadamantane "fuel" and in D_2O at pH 2. For reasons demonstrated in Chapter 7 from the titration with 1-aminoadamantane (Figure 7.3.9) the peak at δ 3.13 ppm can be assigned to the *Z*-amide isomer. From this, in the presence of 1-aminoadamantane "fuel" the hermaphrodite **6.8** in D_2O at pH 2 adopts two amide conformations with an overall *Z/E*-amide ratio of 1:0.8.
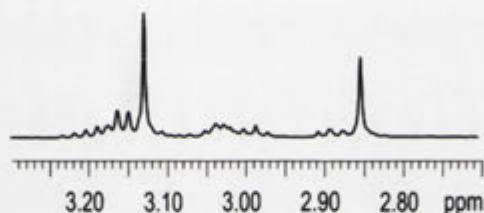
Figure 6.3.26. A section of the ^{1}H NMR spectrum (500 MHz) of the hermaphrodite **6.8** in D_2O (25 °C) at pH 2 in the presence of 1-aminoadamantane "fuel".

To summarise the findings for the conformational analysis of the hermaphrodite **6.8**, in organic solvent the aryl "piston" does not include within the CD "cylinder" and the *Z/E*-amide ratio is 1:0.9. At pH 9 in D_2O, the inclusion of the "piston" by the CD "cylinder" sees the *Z/E*-amide ratio become 1:5, which changes to 1:0.8 in the presence of 1-aminoadamantane "fuel". The difference in the *Z/E*-amide ratio from d_6-DMSO to D_2O at pH 9 is due to the increase in the proportion of the [*c*1] complex as there is a driving force for inclusion.[111] The addition of 1-aminoadamantane "fuel" at pH 9 increases the amount of the [*a*1] guest complex and the *Z/E*-amide ratio parallels the ground state that is observed for d_6-DMSO. In D_2O at pH 2 the aryl "piston" shows no interaction with the CD "cylinder" and the *Z/E*-amide ratio is 1:0.7. In the presence of 1-aminoadamantane "fuel" at pH 2 the *Z/E*-amide ratio is similar. Whether the hermaphrodite **6.8** is in d_6-DMSO, D_2O at pH 2 or in the presence of 1-aminoadamantane "fuel" at pH 2, the *Z/E*-amide ratio remains the same as the [*a*1] complex predominates under each of these conditions. By changing from the [*c*1]

complex at pH 9 to the [*a*1] complex at pH 2, the hermaphrodite **6.8** affords a pH dependent change in conformational behavior.

6.4 Measuring the Heats of Dilution of the Complexes of Cyclodextrin Based Hermaphrodites

Having studied the hermaphrodites **6.3**, **6.6** and **6.8** using ^{1}H NMR spectroscopy under various conditions, differences were observed in their conformational behavior. From this, the predominant conformation observed in D_2O at pH 9 is the [*c*1] complex of the *E*-amide isomer while a higher proportion of the [*a*1] complex of the *Z*-amide isomer is observed at pH 2. In Chapters 4 and 5, ITC was used to measure the heat changes from the dilution of the hermaphrodites for the purpose of identifying the formation of concentration dependent assemblies.[128-130] Aliquots of the self-associating compound were titrated into the ITC cell containing identical buffer and the stepwise heat changes that occur from dissociation recorded.[128] This same technique was employed for the analysis of the hermaphrodites **6.3**, **6.6** and **6.8** at both pHs to check for any concentration dependence.

Shown in Figure 6.4.1a are the ITC enthalpogram (top) and integrated peaks (bottom) for the dilution of the hermaphrodite **6.3** (5 mM) into buffered aqueous solution at pH 9. Figure 6.4.1b shows the ITC heats of dilution data for the hermaphrodite **6.3** (5 mM) titrated into buffered aqueous solution at pH 2. In both cases the isotherms show positive enthalpic peaks that are consistent with an endothermic process, while the overall heat change shows little variation over the chosen concentration range. On this basis and in support of the ^{1}H NMR spectroscopic analysis from Chapter 6.3, the hermaphrodite **6.3** exists predominantly as a concentration independent monomer and not supramolecular polymer at both pH 9 and 2.
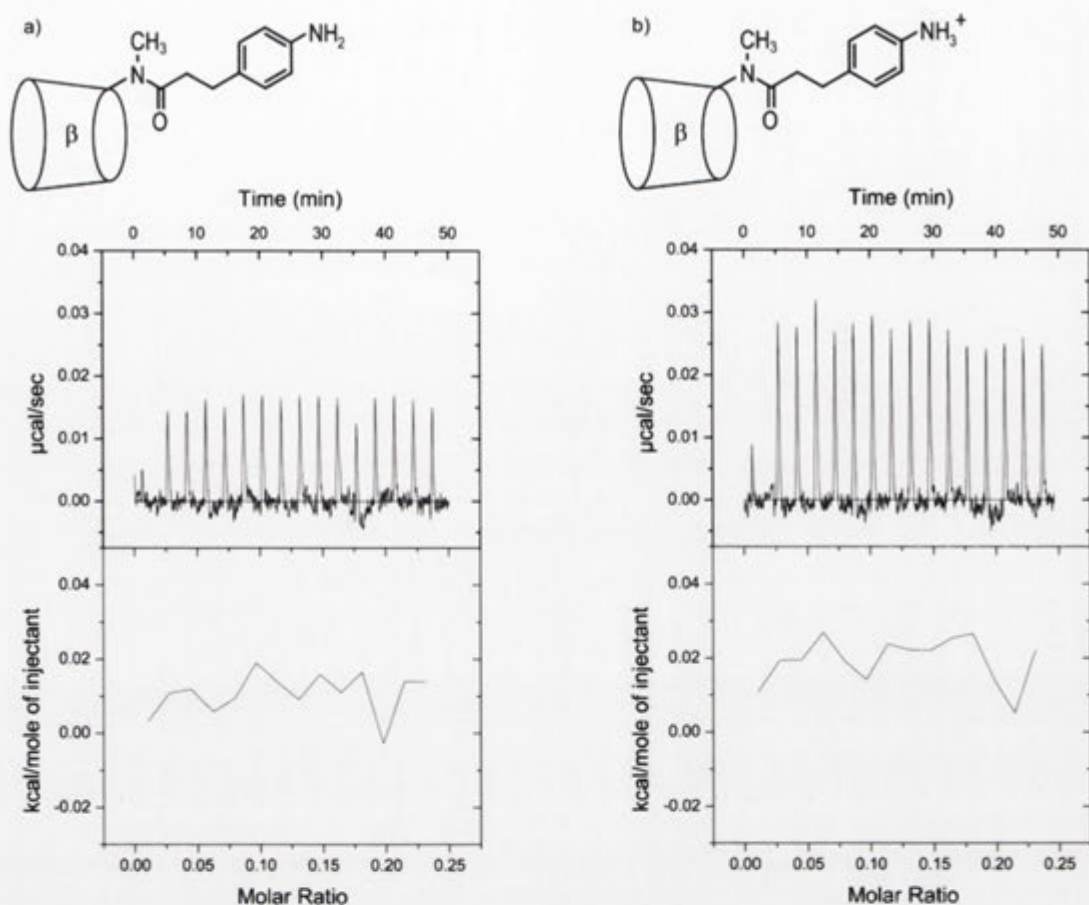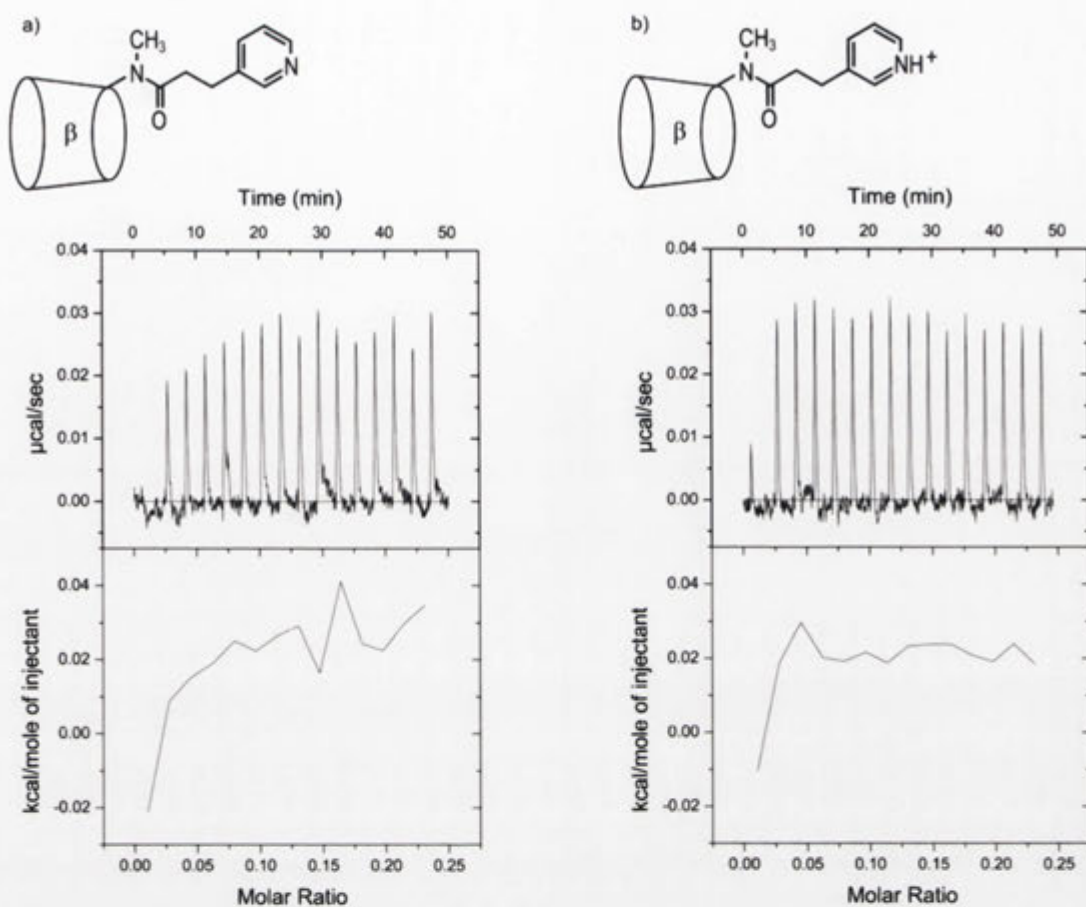
Figure 6.4.1. ITC thermograms for 15 successive injections (5 μl) of the hermaphrodite **6.3** (5 mM) in a) 0.05 M $Na_2B_4O_7 \cdot 10H_2O$ buffer (pH 9); b) 0.05 M NaH_2PO_4 buffer (pH 2.0) into cells containing identical buffer.

Next, the heats of dilution were measured for the hermaphrodite **6.6**. Figure 6.4.2a shows the enthalpogram (top) and integrated peaks (bottom) for the dilution of the hermaphrodite **6.6** at pH 9 while in Figure 6.4.2b is the isotherm for the heat of dilution experiment at pH 2. Although the magnitude of the heat changes for the hermaphrodite **6.6** is greater at pH 9 than at pH 2, in both instances there is little concentration dependence. This supports the ^{1}H NMR spectroscopic analysis from Chapter 6.3, and shows the hermaphrodite **6.6** remains as a monomer at pH 9 and at pH 2.
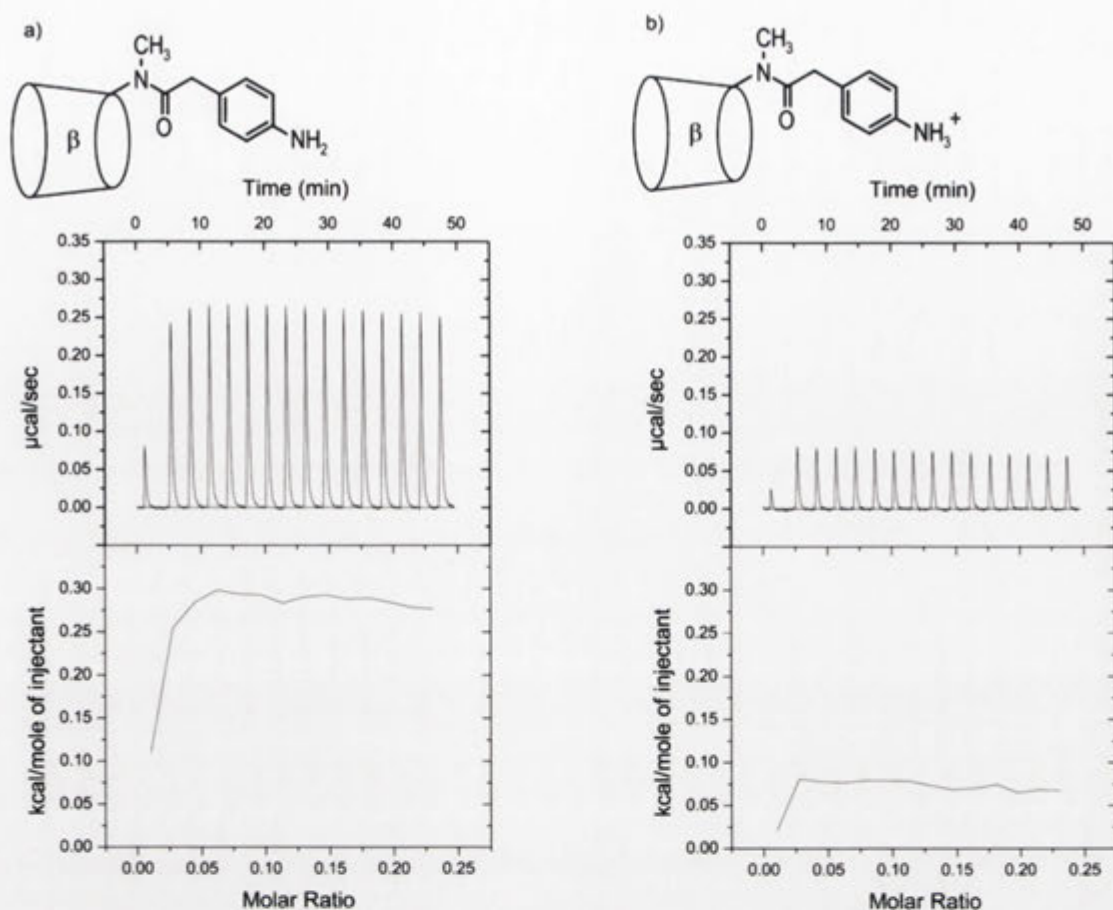
Figure 6.4.2. ITC thermograms for 15 successive injections (5 μl) of the hermaphrodite **6.6** (5 mM) in a) 0.05 M $Na_2B_4O_7 \cdot 10H_2O$ buffer (pH 9); b) 0.05 M NaH_2PO_4 buffer (pH 2.0) into cells containing identical buffer.

Finally, shown in Figure 6.4.3a and Figure 6.4.3b are the heats of dilution isotherms for the hermaphrodite **6.8** into aqueous buffer at pH 9 and pH 2, respectively. These curves show negligible variation over the course of the titration characteristic of a concentration independent species. From this the hermaphrodite **6.8** appears to exist predominantly as a monomeric species at both pH 9 and 2 which confirms the ^{1}H NMR spectroscopic results from Chapter 6.3.

141

Figure 6.4.3. ITC thermograms for 15 successive injections (5 μl) of the hermaphrodite **6.8** (5 mM) in a) 0.05 M $Na_2B_4O_7 \cdot 10H_2O$ buffer (pH 9); b) 0.05 M NaH_2PO_4 buffer (pH 2.0) into cells containing identical buffer.

In summary of the heat of dilution results and in combination with the ^{1}H NMR spectroscopy, the hermaphrodites **6.3**, **6.6** and **6.8** show little concentration dependence over the chosen concentration range. On this basis, these systems remain predominantly as [c1] complexes of the *E*-amide isomer at pH 9 and have increased proportions of the [a1] conformations of the *Z*-amide at pH 2.

6.5 pH Effect on Cyclodextrin Based Hermaphrodites

From the ^{1}H NMR spectroscopic analysis of the hermaphrodites **6.3**, **6.6** and **6.8** in D$_2$O, the change between pH 9 and pH 2 resulted in distinct changes in conformational behavior which are reminiscent of a machine-like function. For this reason the pH induced changing between the protonated and deprotonated forms of the hermaphrodites **6.3**, **6.6** and **6.8** was studied further using ^{1}H NMR spectroscopy. To investigate this each hermaphrodite was dissolved in unbuffered D$_2$O before an aliquot of dilute DCl in D$_2$O was added and the pH and ^{1}H NMR spectrum were recorded. Consecutive spectra were obtained over a range of $\pm$ 2 pH units from the expected pK_a of the nitrogen donor group of the chosen hermaphrodite. The purpose was to study the transition between the deprotonated and protonated forms by monitoring the *Z/E*-amide isomers with the changing pH.

Shown in Figure 6.5.1 are the ^{1}H NMR spectra showing the *N*-methyl region for the hermaphrodite **6.3** in D$_2$O at various pHs. An internal standard has been used to reference all spectra which have been offset for clarity. At pH 6.90, the hermaphrodite **6.3** exists in the amino form and affords a *Z/E*-amide ratio of 1:17 which represents a ΔG of 1.7 kcal mol^{-1}. As the pH decreases the quantity of the *E*-amide species also decreases which corresponds to an increase in the *Z*-amide species. At pH 2.40, the hermaphrodite **6.3** exists in the ammonium form and the *Z/E*-amide ratio is 1:2 resulting in a ΔG of 0.4 kcal mol^{-1}. As the hermaphrodite **6.3** shows a pH dependent conformational change the changing pH induces a difference in the *Z/E*-amide isomer ratios and accordingly in the ground state free energies (ΔG) which results in 1.3 kcal mol^{-1} of work being harnessed.
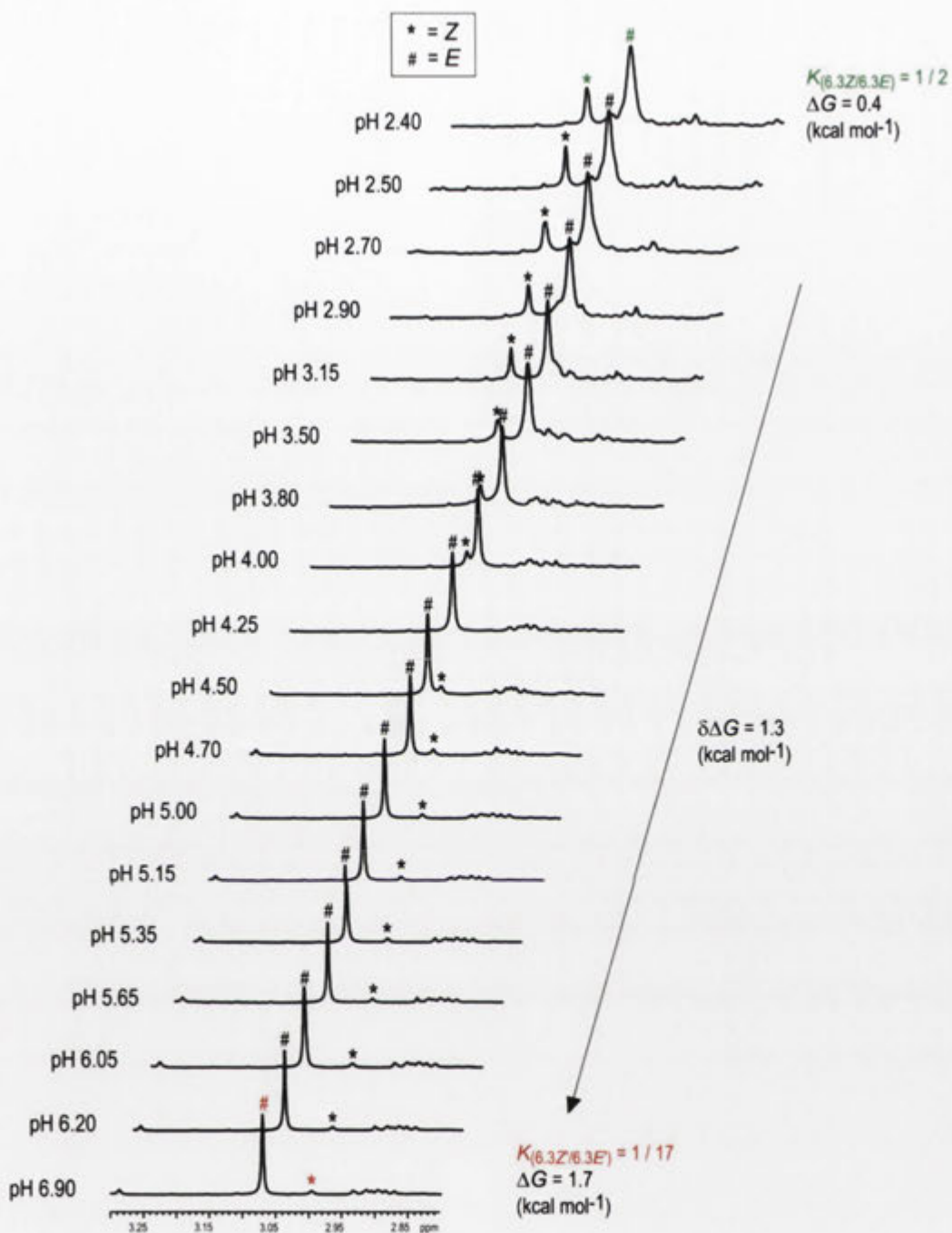
Figure 6.5.1. A section of the ^{1}H NMR spectra of the hermaphrodite **6.3** in D$_2$O at various pHs.

With the decreasing pH a change in the *Z/E*-amide ratio is observed which is characteristic of the transition from the [*c*1] complex toward the [*a*1] conformation. With this in mind, as the acid-base equilibrium for the nitrogen donor group of the aryl "piston" is a fast exchange process,[146] and the equilibrium between the [*c*1] complex and the [*a*1] conformation is a slow exchange process, then the change in chemical shift

($\Delta\delta$ ppm) of the amide resonances with pH allows the pK_a of the system to be measured using Equation 6.5.1.[141] Shown in Figure 6.5.2 is the chemical shift for the methyl signal of the *Z*-amide isomer plotted against pH. From this, the hermaphrodite **6.3** was determined to have a pK_a of 4.4 ± 0.1 and therefore exists in the amine form at pH 9 and in the protonated ammonium ion form at pH 2. From these findings, as a consequence of a pH induced conformational change the hermaphrodite **6.3** harnesses 1.3 kcal mol^{-1} of work in the amide bond.

$$pH = pK_a + \log \frac{\delta - \delta_{RNH_3^+}}{\delta_{RNH_2} - \delta} \qquad (6.5.1)$$
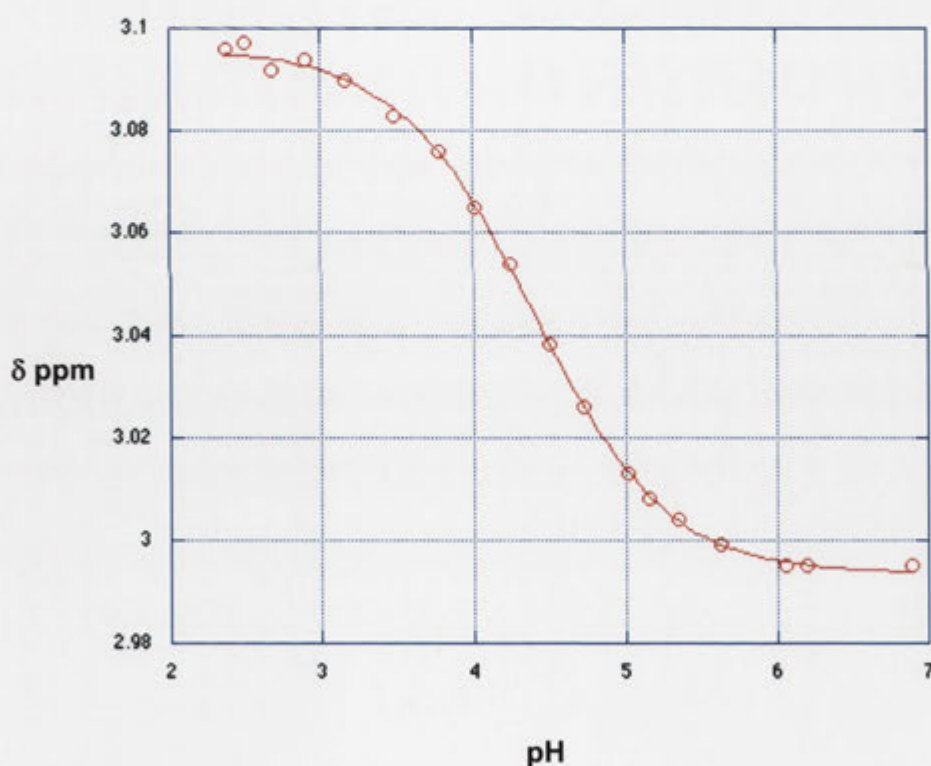
Figure 6.5.2. Plot of the ^{1}H chemical shift for the $CH_3(Z)$ of the hermaphrodite **6.3** with pH. Correlation curve generated from Equation 6.5.1 with p$K_a = 4.4 \pm 0.1$, δ RNH$_3^+$ = 3.10, and δ RNH$_2$ = 3.00.

Having established the pH changes and pK_a of the hermaphrodite **6.3**, the next system to be studied was the hermaphrodite **6.6**. In Figure 6.5.3 are the ^{1}H NMR spectra

of the *N*-methyl proton resonances for the hermaphrodite **6.6** in D_2O at various pHs. At pH 6.30, the aryl "piston" includes within the CD "cylinder" and the *Z/E*-amide ratio is 1:6.7 which represents a ΔG of 1.1 kcal mol^{-1}. At pH 2.00, the [*a*1] conformation predominates and the *Z/E*-amide ratio is 1:1 resulting in a ΔG of 0 kcal mol^{-1}. By changing between the neutral and the protonated states of the hermaphrodite **6.6** a conformational change occurs which as a consequence alters the *Z/E*-amide ratio and harnesses 1.1 kcal mol^{-1} of energy as work output.
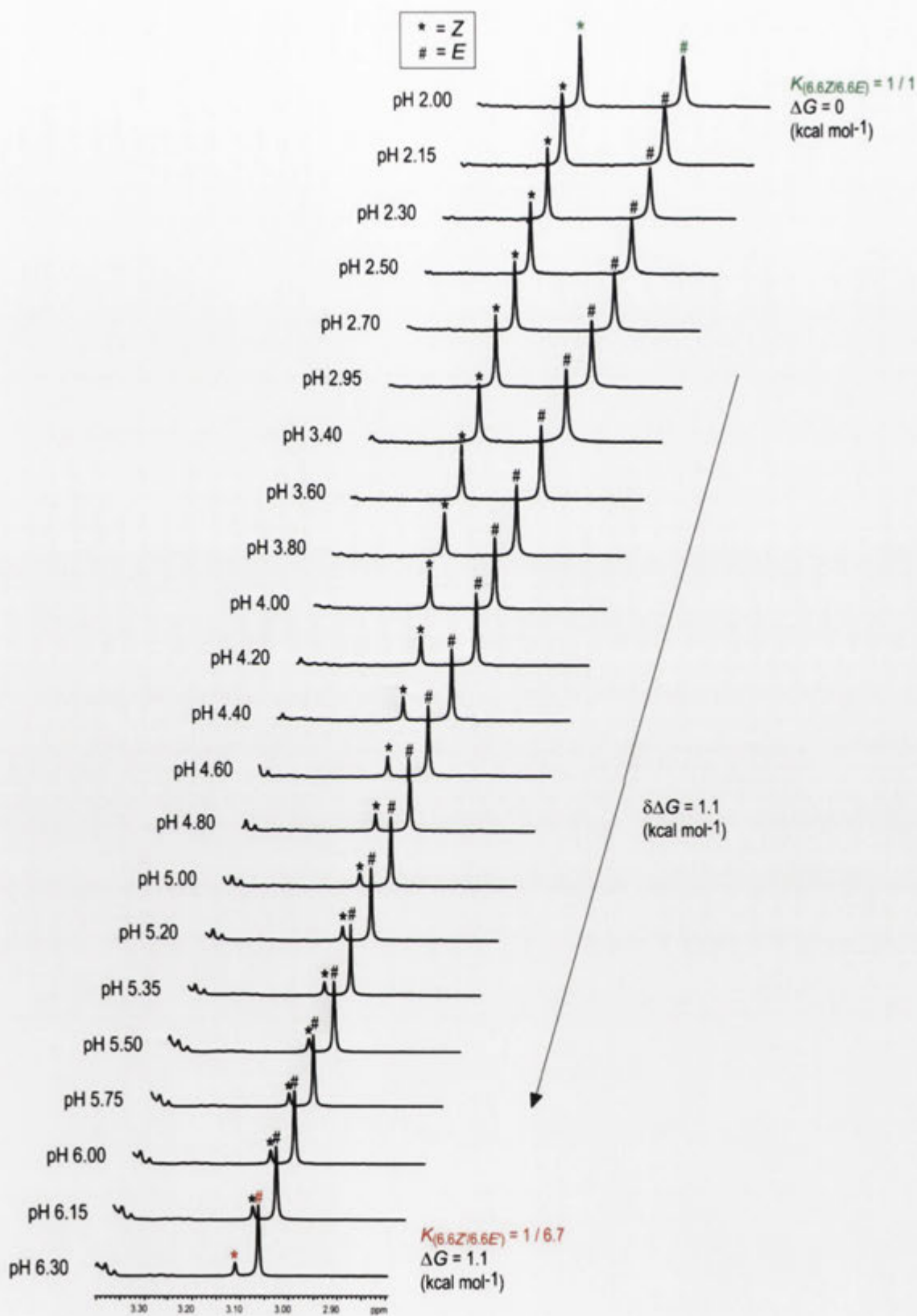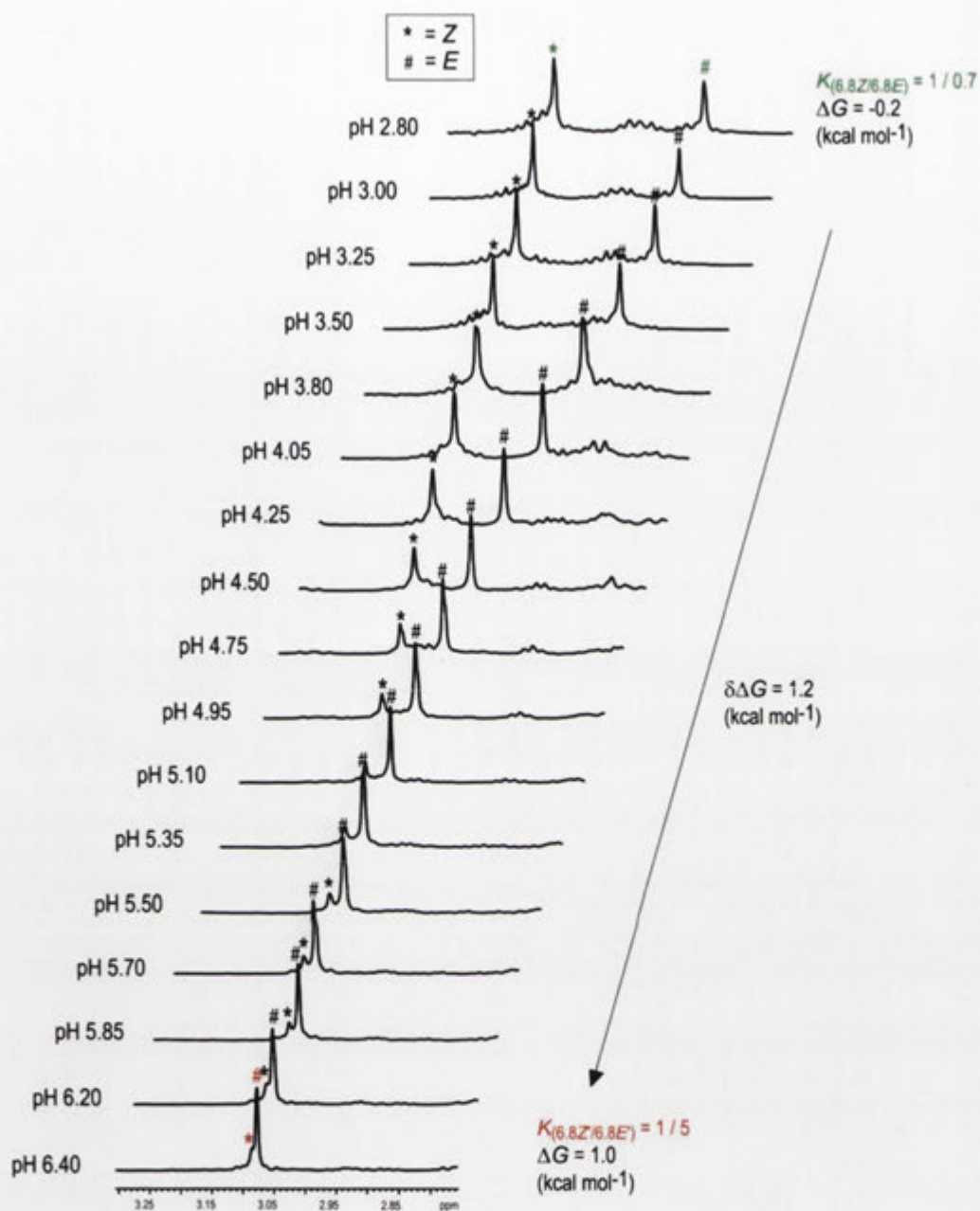
Figure 6.5.3. A section of the ^{1}H NMR spectra of the hermaphrodite **6.6** in D_2O at various pHs.

Shown in Figure 6.5.4 is the plot of the chemical shift of the *Z*-amide methyl proton signal for the hermaphrodite **6.6** against the pH. Using Equation 6.5.1[141] the pK_a of the hermaphrodite **6.6** is determined as 4.2 ± 0.1. Thus, the hermaphrodite **6.6** has a pK_a of 4.2 and harnesses 1.1 kcal mol^{-1} of energy in the amide bond from the pH induced conformational change.
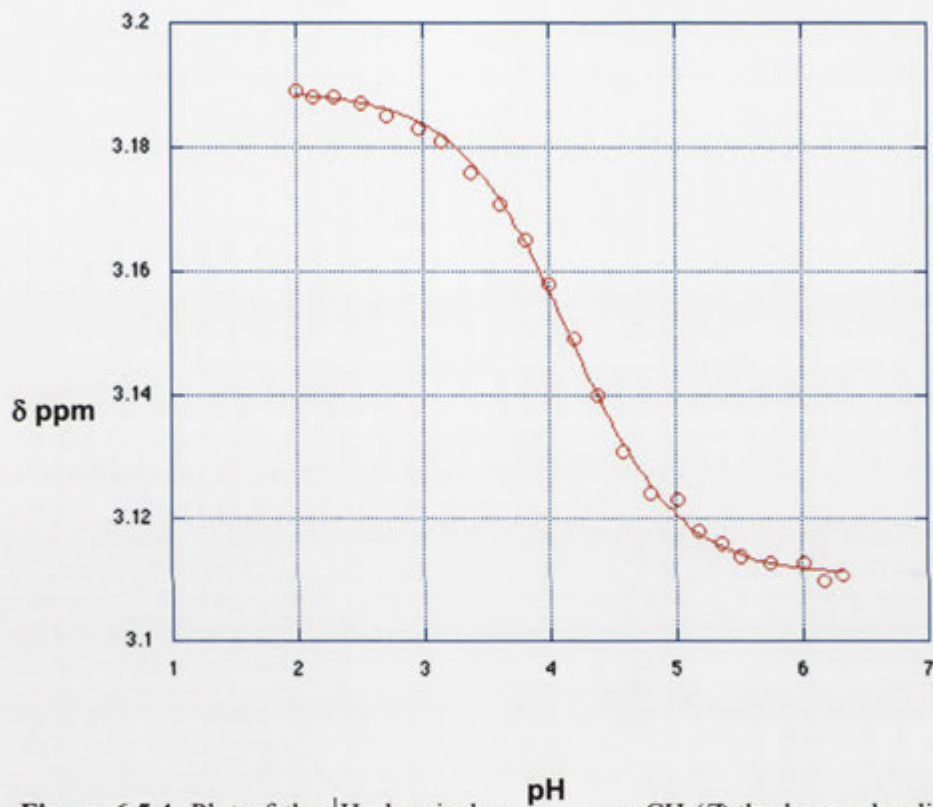
Figure 6.5.4. Plot of the ^1H chemical s **pH** e $CH_3(Z)$ the hermaphrodite **6.6** with pH. Correlation curve generated from Equation 6.5.1 with $pK_a = 4.2 \pm 0.1$, $\delta RNH_3^+ = 3.19$, and $\delta RNH_2 = 3.11$.

Finally, the ^1H NMR spectra for the pH titration of the hermaphrodite **6.8** are shown in Figure 6.5.5. At pH 6.40, the [*c*1] complex is dominant and the *Z/E*-amide ratio is 1:5 which corresponds to a ΔG of 1.0 kcal mol^{-1}. At pH 2.80, the aryl "piston" does not include within the CD "cylinder" and the *Z/E*-amide ratio is 1:0.7 and ΔG -0.2 kcal mol^{-1}. By changing the pH the transition between the [*c*1] complex and the [*a*1] conformation sees the *Z/E*-amide ratio change and the energy harnessed in the amide bond as 1.2 kcal mol^{-1}.

Figure 6.5.5. A section of the ^{1}H NMR spectra of the hermaphrodite **6.8** in D$_2$O at various pHs.

Next, the pK_a for the hermaphrodite **6.8** was determined by plotting the chemical shift of the Z-amide methyl proton signal against pH (Figure 6.5.6). Using Equation 6.5.1[141] the pK_a was measured as 4.8 ± 0.1 and therefore the hermaphrodite **6.8** exists in the pyridine form at pH 9 and the pyridinium ion form at pH 2. From this, the hermaphrodite **6.8** alters conformations by changing the pH around its pK_a of 4.8 and as a consequence of the conformational change captures 1.2 kcal mol^{-1} of energy.
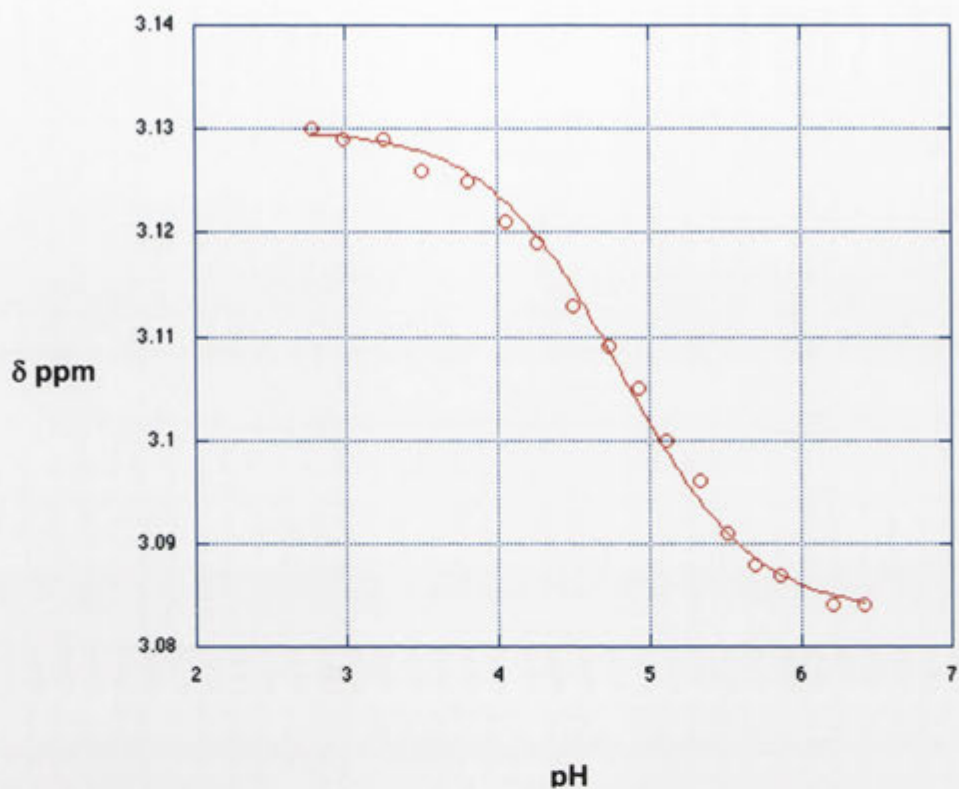
Figure 6.5.6. Plot of the ^{1}H chemical shift for the $CH_3(Z)$ of the hermaphrodite **6.8** with pH. Correlation curve generated from Equation 6.5.1 with $pK_a = 4.8 \pm 0.1$, $\delta RNH_3^+ = 3.13$, and $\delta RNH_2 = 3.08$.

6.6 Conclusion

In this chapter several pH dependent switches were prepared and their conformational behaviors investigated in d_6-DMSO and at various pHs in the presence and absence of 1-aminoadamantane "fuel". From ^{1}H NMR spectroscopic and ITC dissociation studies the hermaphrodites **6.3**, **6.6** and **6.8** were determined to form monomeric conformations at pH 9 and pH 2. The hermaphrodites **6.3**, **6.6** and **6.8** are sensitive to a pH stimulus and switch between protonated and deprotonated states with pK_as of 4.4, 4.2, 4.8, respectively. The link between the acid-base equilibrium of the aryl "pistons" nitrogen donor group and the transition between [c1] complex and [a1] conformation allows the Z/E-amide isomer ratios to be significantly controlled.

CHAPTER 7

Operation and Efficiency of Harnessing the Energy of Molecular Recognition in a Nanomachine Having a pH Dependent On/Off Switch

7.1 Introduction

The research described in Chapter 6 discussed the synthesis and conformational analysis of the pH dependent hermaphrodites **6.3**, **6.6** and **6.8** which were developed for the purpose of harnessing the energy of molecular recognition as a quantifiable work output. In Chapters 2 to 4 the operation and the performance of the hermaphrodites **2.3**, **2.4**, **2.5**, **4.3**, **4.4** and **4.7** for harnessing energy in the amide bond were assessed using ^{1}H NMR spectroscopy and ITC. From this investigation it was discovered that the work output ($\delta\Delta G$) is dependent on the ΔH, ΔS, ΔG and K_A of the binding interaction between the "fuel" and the hermaphrodite. It seemed likely that the operation of the pH dependent hermaphrodites **6.3**, **6.6** and **6.8** would be governed by the binding interaction with 1-aminoadamantane "fuel" (Figure 7.1.1). To investigate the operation and performance of the hermaphrodites **6.3**, **6.6** and **6.8**, the following research was carried out to obtain both the work outputs and thermodynamic parameters for their operation at various pHs using ^{1}H NMR spectroscopy and ITC.
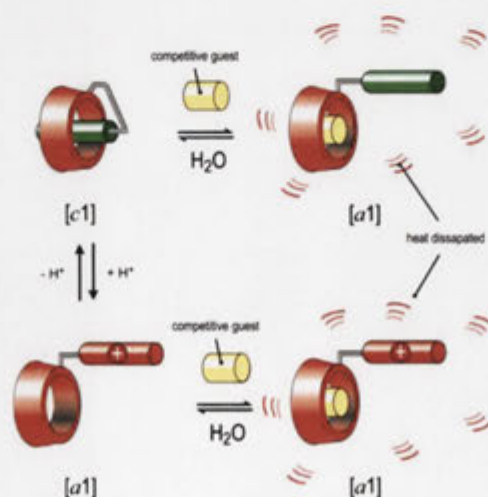
Figure 7.1.1. Schematic representation of the heat transfer effect of a competitive guest and a pH dependent hermaphrodite in acidic and basic conditions.

By comparing the work output ($\delta\Delta G$) at both pH 9 and pH 2, as quantified using ^{1}H NMR spectroscopy, to the uncaptured work energy (ΔG) and the heat dissipated (ΔH) at the same pH, as determined using ITC, the efficiency of harnessing the energy of molecular recognition using 1-aminoadamantane "fuel" was to be established.

7.2 Operation of Cyclodextrin Based Hermaphrodites by Changing the Solvent

From the ^{1}H NMR spectroscopic analysis of the hermaphrodites **6.3**, **6.6** and **6.8** detailed in Chapter 6.3, distinct conformational differences were observed between d_6-DMSO and D_2O at pH 9. As already discussed, the ratio of Z/E-amide isomers for a particular set of conditions represents the difference between the ground state free energies (ΔG). On this basis, the differences in the Z/E-amide isomer ratios between the [$c1$] complex formed at pH 9 in D_2O and the [$a1$] complex formed in d_6-DMSO would reflect the work output performed by molecular recognition. With this in mind the ground state free energies (ΔG) for the hermaphrodites **6.3**, **6.6** and **6.8** were determined in D_2O at pH 9 and in d_6-DMSO in order to quantify their work outputs ($\delta\Delta G$) harnessed from a change in the solvent.

For the hermaphrodite **6.3** in D_2O at pH 9, the aryl "piston" is included within the CD "cylinder" and the Z/E-amide ratio is about 1:17 as shown in Figure 7.2.1. This reflects a ΔG of 1.7 kcal mol^{-1}. In d_6-DMSO, the aryl "piston" is not included within the CD "cylinder" and the Z/E-amide ratio is 1:0.9 resulting in a ΔG of -0.1 kcal mol^{-1}. By changing the solvent the work performed on the amide bond by the molecular recognition process is 1.8 kcal mol^{-1}.
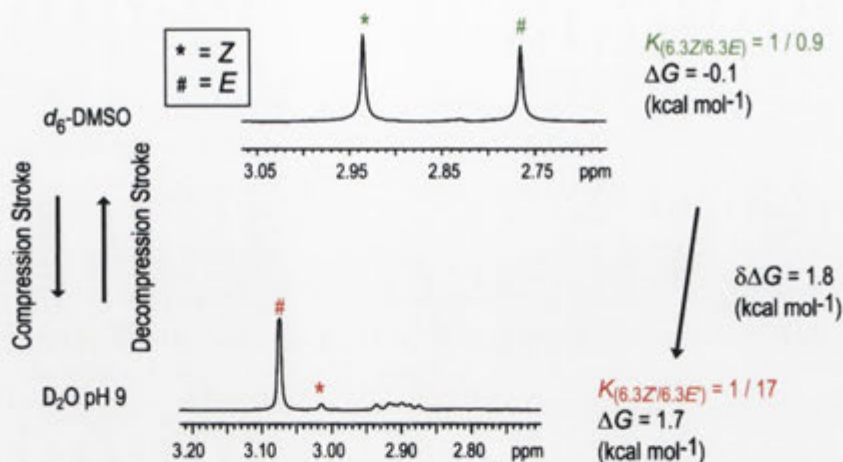
Figure 7.2.1. 500 MHz ^{1}H NMR spectra of the hermaphrodite **6.3** in D_2O at pH 9 (bottom) and d_6-DMSO (top).

Next, the hermaphrodite **6.6** in D_2O at pH 9 affords an Z/E-amide ratio of 1:6.7 (Figure 7.2.2) which represents a ΔG of 1.1 kcal mol^{-1}. In contrast, in d_6-DMSO the Z/E-amide ratio is 1:0.8, which affords a ΔG of -0.1 kcal mol^{-1}. From this change in the polarity of the solvent the hermaphrodite **6.6** performs 1.1 kcal mol^{-1} of work upon the amide bond.
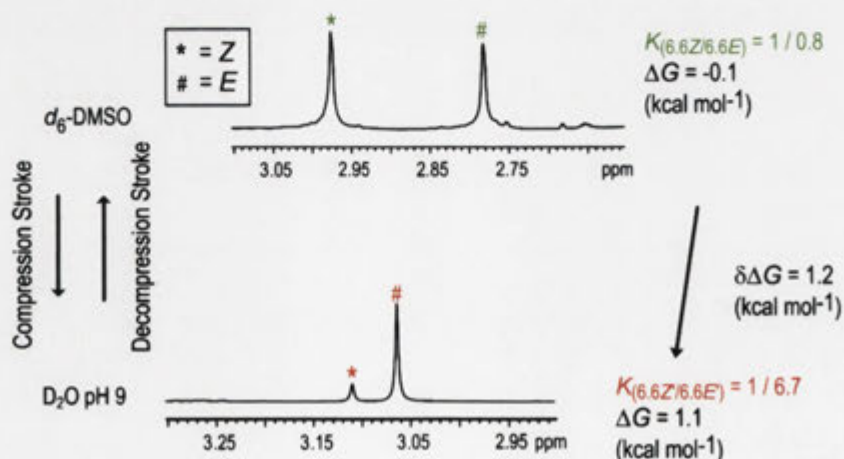
Figure 7.2.2. 500 MHz ^{1}H NMR spectra of the hermaphrodite **6.6** in D_2O at pH 9 (bottom) and d_6-DMSO (top).

Finally, the hermaphrodite **6.8** in D_2O at pH 9 affords a *Z/E*-amide ratio of 1:5 representing a ground state free energy difference (ΔG) of 1.0 kcal mol^{-1}. Alternatively, in d_6-DMSO, the *Z/E*-amide ratio becomes 1:0.9 and the free energy difference (ΔG) is -0.1 kcal mol^{-1}. In this case the work performed on the amide bond by the change in the solvent is 1.1 kcal mol^{-1} (Figure 7.2.3).
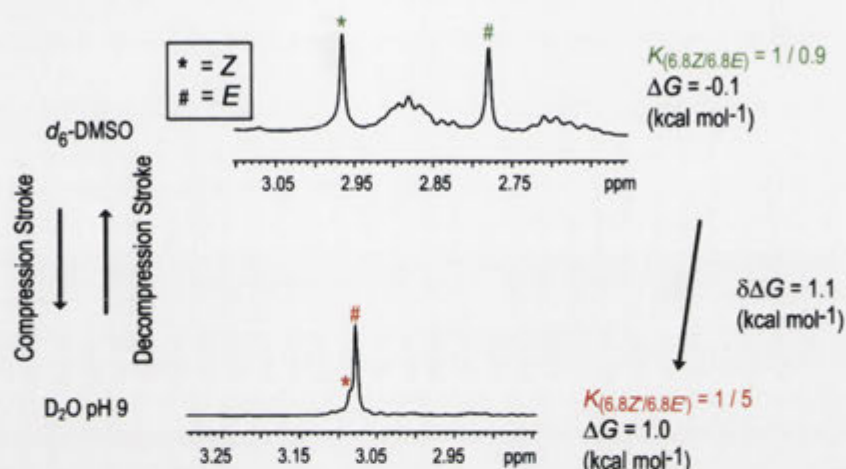

Figure 7.2.3. 500 MHz ^{1}H NMR spectra of the hermaphrodite **6.8** in D_2O at pH 9 (bottom) and d_6-DMSO (top).

7.3 Operation of pH Sensitive Cyclodextrin Based Hermaphrodites by Competitive Guest

With the operation of the hermaphrodites **6.3**, **6.6** and **6.8** investigated for a change in the solvent, it remained to be studied the effect of a competitive guest on their energies of molecular recognition. The differences in the amide isomer ratios and ground state free energies between the [*c*1] complex formed in D_2O and [*a*1] competitive guest complex formed on the addition of 1-aminoadamantane "fuel" reflects the work output ($\delta\Delta G$) performed on the amide bond. Due to the machine-like function identified in Chapter 6.3 by the conformational differences by changing between pH 9 and pH 2, the work outputs of the hermaphrodites **6.3**, **6.6** and **6.8** for the "fuel" were also measured in D_2O at different pH. Using ^{1}H NMR spectroscopy to quantify the $\delta\Delta G$ for the hermaphrodites **6.3**, **6.6** and **6.8** from the addition of 1-

aminoadamantane "fuel", the energies harnessed by the pH sensitive molecular machines using molecular recognition were established.

Shown in Figure 7.3.1 are the ^{1}H NMR spectra for the hermaphrodite **6.3** in D$_2$O at pH 9 recorded at increasing concentrations of 1-aminoadamantane "fuel". All spectra are referenced with an internal standard and have been offset for clarity. In D$_2$O alone, the hermaphrodite **6.3** affords a *Z/E*-amide ratio of 1:17 which represents a ΔG of 1.7 kcal mol^{-1}. The nonprotonated aryl "piston" is included within the CD "cylinder" and the major species is the [*c*1] complex of the *E*-amide isomer as discussed in Chapters 6.3 and 6.4. In the presence of 3 equivalents of 1-aminoadamantane "fuel" the *Z/E*-amide ratio is 1.4:1 resulting in a ΔG of -0.2 kcal mol^{-1}. Thus, the addition of the 1-aminoadamantane "fuel" displaces the aryl "piston" from the CD "cylinder" and the apparent work harnessed in the amide bond is 1.9 kcal mol^{-1}. The hermaphrodite **6.3** in D$_2$O at pH 9 behaves as a molecular machine in the "ON" state.
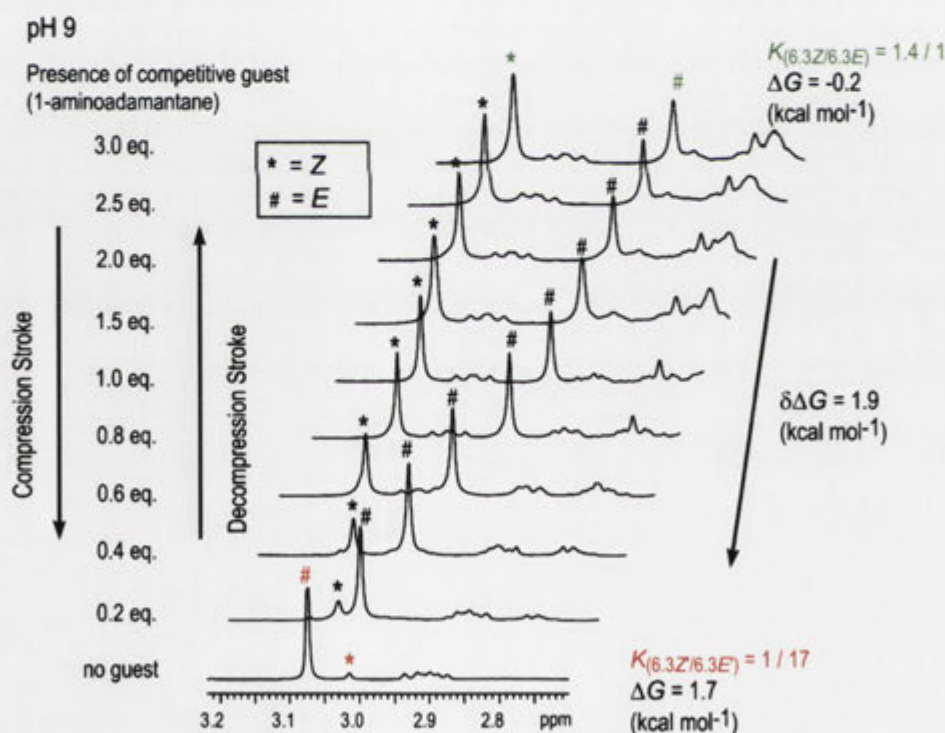
Figure 7.3.1. A section of the ^{1}H NMR spectra (500 MHz) of 6^A-deoxy-6^A-(*N*-methyl-3-(4-aminophenyl)propionamido)-β-CD **6.3** in D$_2$O at pH 9 (0.05 M Na$_2$B$_4$O$_7$·10H$_2$O buffer) in the presence and absence of 1-aminoadamantane "fuel".
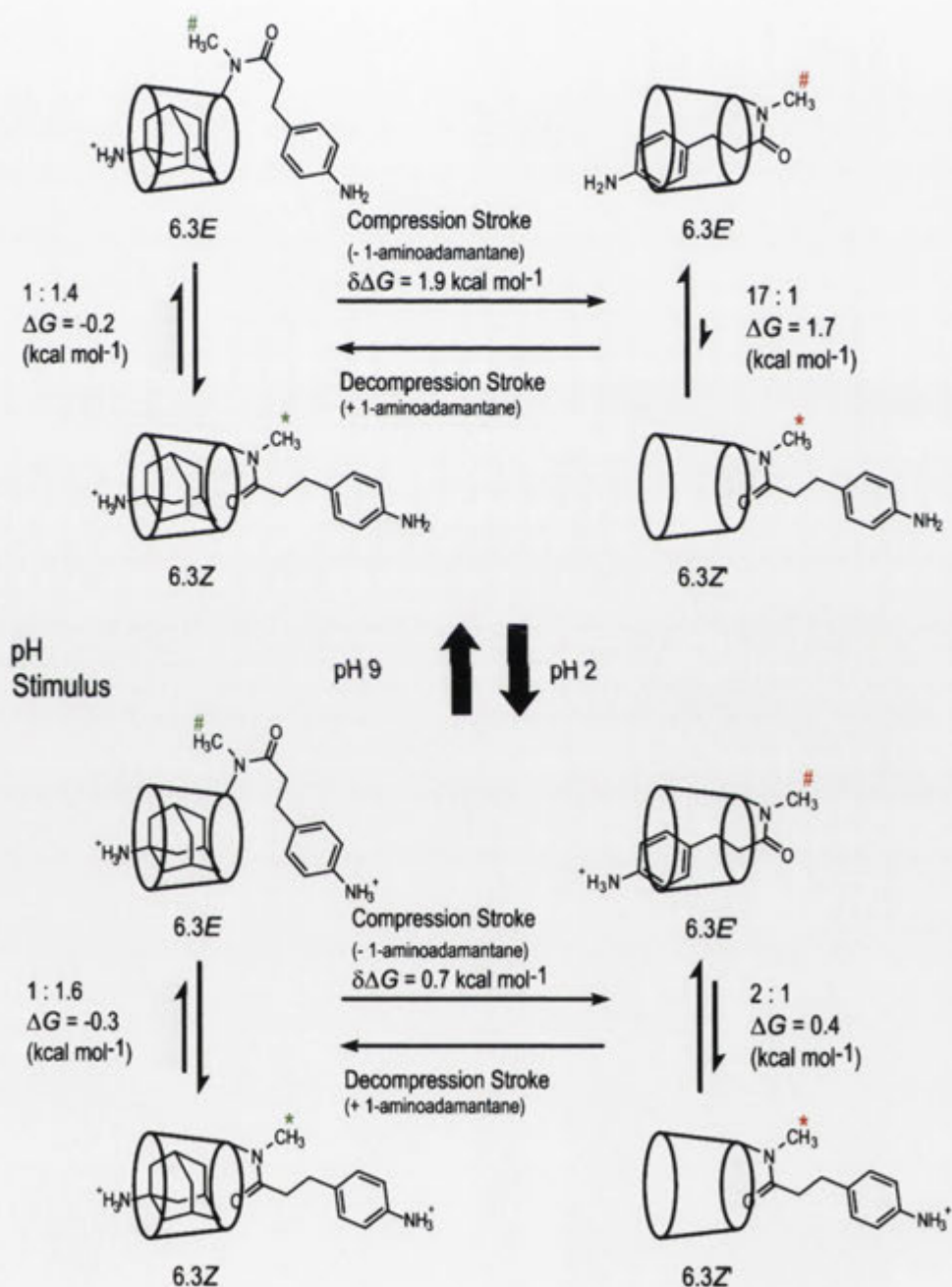
Next, the operation of the hermaphrodite **6.3** was investigated with 1-aminoadamantane "fuel" in D_2O at pH 2 (Figure 7.3.2). In the absence of the "fuel" the hermaphrodite **6.3** affords a *Z/E*-amide ratio of approximately 1:2 which represents a ΔG of 0.4 kcal mol^{-1}. By titrating the hermaphrodite **6.3** with 1-aminoadamantane "fuel" the isomers can be traced to the endpoint where the *Z/E*-amide ratio is 1.6:1 and ΔG is -0.3 kcal mol^{-1}. For the reason that the "fuel" induces the transition from [*c*1] complex to the [*a*1] guest complex, the system still performs 0.7 kcal mol^{-1} of work on the amide bond. On this basis, the hermaphrodite **6.3** is only partially turned "OFF" at pH 2. From Chapter 6.3, this system at pH 2 still forms the [*c*1] complex of the *E*-amide isomer which suggests that the protonated part of the aryl "piston" extends far enough through the annulus not to effectively interact with the CD "cylinder".
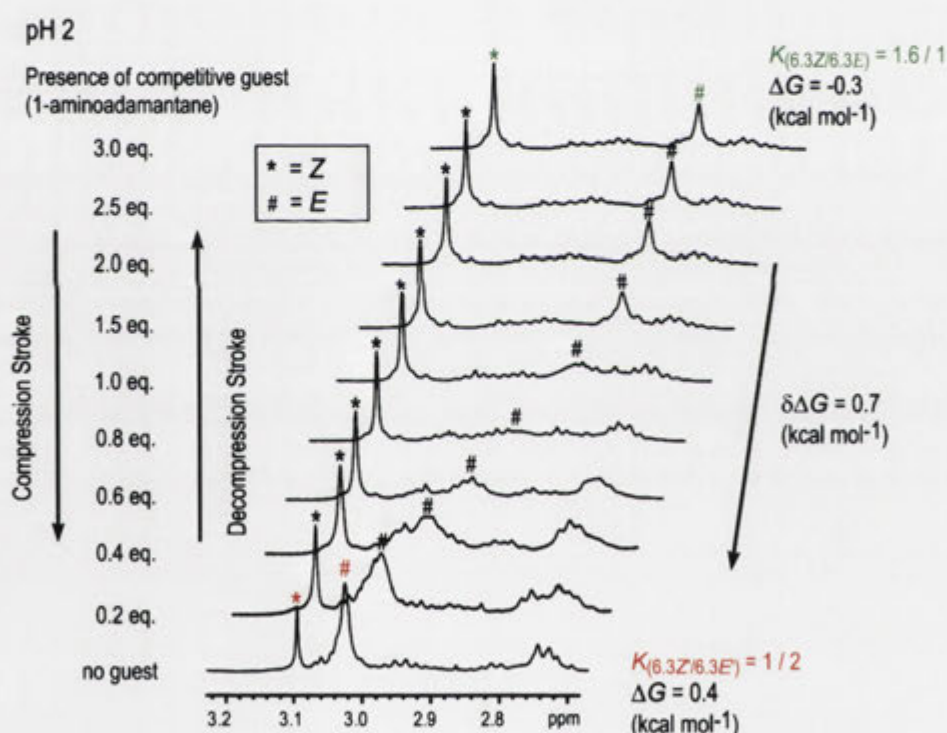
Figure 7.3.2. A section of the ^{1}H NMR spectra (500 MHz) of 6^A-deoxy-6^A-(*N*-methyl-3-(4-aminophenyl)propionamido)-β-CD **6.3** in D_2O at pH 2 (0.05 M NaH$_2$PO$_4$ buffer) in the presence and absence of 1-aminoadamantane "fuel".

In summary, Scheme 7.3.1 illustrates the operation of the hermaphrodite **6.3** in D_2O as a molecular pump with 1-aminoadamantane "fuel" at pHs 9 and 2. At pH 9 the aryl "piston" is included within the CD "cylinder" and the addition of the "fuel" leads to a decompression stroke with 1.9 kcal mol^{-1} of work energy harnessed. At pH 2 the

protonated form of the aryl "piston" is unable to completely destabilise the [c1] complex and thus the system still harnesses 0.7 kcal mol^{-1} of work in the amide bond. On this basis, the hermaphrodite **6.3** operates as a molecular machine that is "ON" at pH 9 and is only partially turned "OFF" at pH 2.

Scheme 7.3.1. Operation of 6^A-deoxy-6^A-(*N*-methyl-3-(4-aminophenyl)propionamido)-β-CD **6.3** as a molecular pump at pH 9 (top) and pH 2 (bottom).

Next, the operation of the hermaphrodite **6.6** was studied using 1-aminoadamantane "fuel". Figure 7.3.3 shows the ^{1}H NMR spectra for the hermaphrodite **6.6** at pH 9 in D_2O alone (bottom) and in the presence of 3 equivalents of 1-aminoadamantane (top). In D_2O alone, the hermaphrodite **6.6** affords a *Z/E*-amide ratio of about 1:6.7 which reflects a ΔG of 1.1 kcal mol^{-1}. The unprotonated "piston" interacts with the CD "cylinder" with the predominant species being the [*c*1] complex having the *E*-amide isomer. Unexpectedly, when 3 equivalents of the "fuel" are added only a small change in the *Z/E*-amide ratio is observed to approximately 1:2.9 which reflects a ΔG of 0.6 kcal mol^{-1}. Relative to its propionamido counterpart the hermaphrodite **6.3**, the shorter aryl "piston" of the hermaphrodite **6.6** is unable to be effectively displaced by this "fuel". The result is that the work energy harnessed in the amide bond by molecular recognition is only 0.5 kcal mol^{-1} and the hermaphrodite **6.6** only partially operates as a working molecular machine at pH 9 with 1-aminoadamantane "fuel".
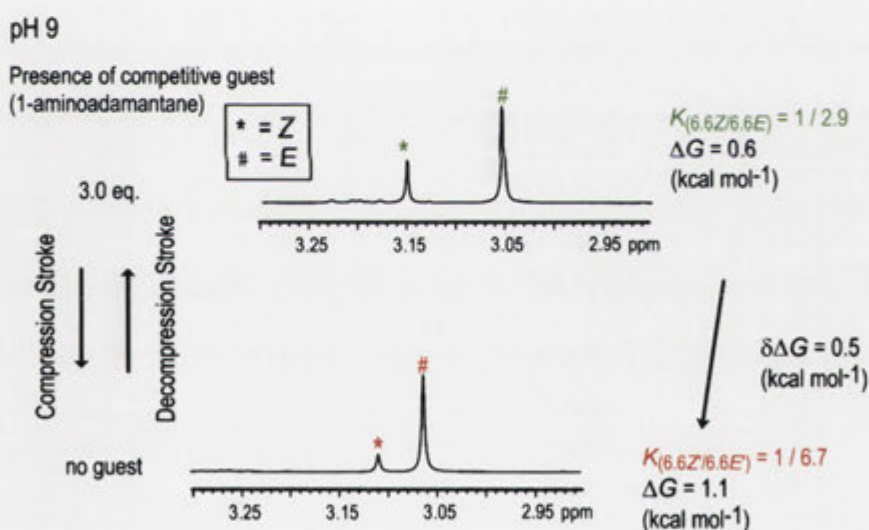
Figure 7.3.3. A section of the ^{1}H NMR spectra (500 MHz) of 6^A-deoxy-6^A-(*N*-methyl-3-(4-aminophenyl)acetamido)-β-CD **6.6** in D_2O at pH 9 (0.05 M $Na_2B_4O_7 \cdot 10H_2O$ buffer) in the presence and absence of 1-aminoadamantane "fuel".

Interestingly, from the ^{1}H NMR spectra of the hermaphrodite **6.6** at pH 2 the appearance of the *N*-methyl signals in the absence (bottom) and presence (top) of 1-aminoadamantane "fuel" (Figure 7.3.4) are remarkably similar to each other and to that observed in d_6-DMSO (Figure 6.3.9). In the absence of the "fuel" the hermaphrodite **6.6**

affords a *Z/E*-amide ratio of about 1:1 which reflects a ΔG of 0 kcal mol^{-1}. From Chapter 6.3 at this pH the aryl "piston" only weakly interacts with the CD "cylinder" and the predominant species is the [*a*1] conformation. Therefore the addition of 3 equivalents of 1-aminoadamantane "fuel" has little effect on the *Z/E*-amide ratio which is 1:0.8 while the ΔG is -0.1 kcal mol^{-1}. For the reason that the [*a*1] conformation predominates at this pH the hermaphrodite **6.6** harnesses only -0.1 kcal mol^{-1} of work energy and is accordingly in the "OFF" state. The difference observed in the work outputs between the hermaphrodites **6.3** and **6.6** at pH 2 is due to former still being able to adopt the [*c*1] complex while the latter does not. This difference suggests that the charged group alone is not the driving force for the formation of the [*a*1] conformation but that the position of the nitrogen donor group is important.
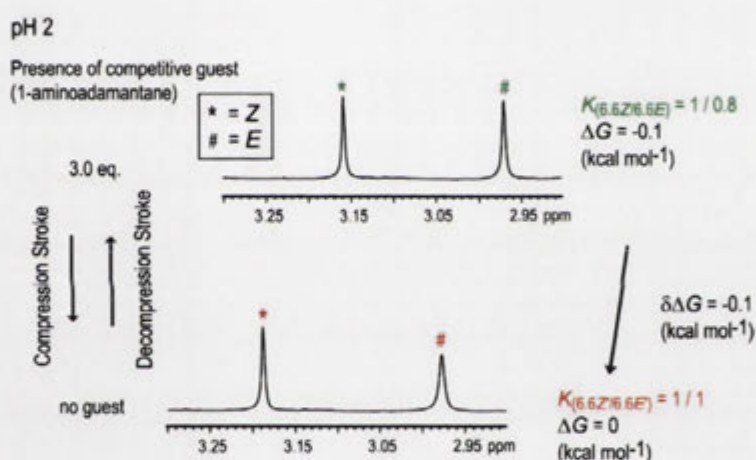
Figure 7.3.4. A section of the ^{1}H NMR spectra (500 MHz) of 6^A-deoxy-6^A-(*N*-methyl-3-(4-aminophenyl)acetamido)-β-CD **6.6** in D$_2$O at pH 2 (0.05 M NaH$_2$PO$_4$ buffer) in the presence and absence of 1-aminoadamantane "fuel".

From the ^{1}H NMR spectroscopic analysis the apparent work ($\delta\Delta G$) harnessed by the hermaphrodite **6.6** with 1-aminoadamantane "fuel" at pH 9 is only 0.5 kcal mol^{-1}. As this system is forming the [*c*1] complex of the *E*-amide isomer the logical interpretation for the small work output is that either 1-aminoadamantane is too weak (β-CD **1.10**, 8912 M^{-1})[147] to displace the aryl "piston" from the CD "cylinder" or that the "fuel" is binding the cavity however the relatively shorter "piston" isn't being displaced effectively enough from the primary face to change the *Z/E*-amide ratio. In order to investigate this, 6-(*p*-toluidino)-2-naphthalenesulfonic acid (TNS) was

employed as an alternative "fuel" due to its relatively longer structure than adamantane based guests and moderate affinity for β–CD **1.10** (3030 M^{-1}).[148] Now, as shown in Figure 7.3.5 the operation of the hermaphrodite **6.6** was investigated in D$_2$O at pH 9 with the TNS "fuel". Firstly, a significant upfield shift of the *N*-methyl signals was observed from the addition of 0.2 equivalents of the "fuel" which is possibly due to an aromatic stacking interaction with the TNS "fuel". In order to trace the methyl resonances additional ^{1}H NMR spectra were recorded using smaller aliquots (0.02 eq.) of TNS which are shown in Figure 7.3.6. It now follows, that the hermaphrodite **6.6** at pH 9 in the absence of the TNS "fuel" affords a *Z/E*-amide ratio of 1:6.7 which reflects a Δ*G* of 1.1 kcal mol^{-1}. Interestingly, in the presence of the larger "fuel" the *Z/E*-amide ratio is 1.2:1 and the Δ*G* is -0.1 kcal mol^{-1}. From this, the apparent work (δΔ*G*) harnessed in the amide bond is now 1.2 kcal mol^{-1} and the hermaphrodite **6.6** at pH 9 operates as a molecular machine in the "ON" state. From the fact that the TNS has a weaker association for β-CD **1.10** than 1-aminoadamantane, it is likely the relatively longer "fuel" is effectively displacing the aryl "piston" far enough from the primary face of the CD "cylinder" to alter the *Z/E*-amide ratio.
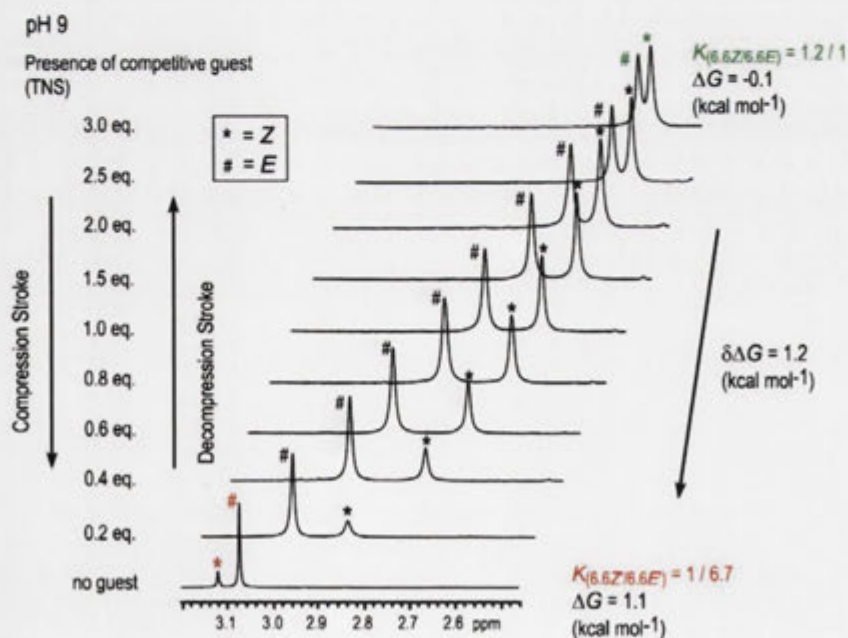
Figure 7.3.5. A section of the ^{1}H NMR spectra (500 MHz) of 6^A-deoxy-6^A-(*N*-methyl-3-(4-aminophenyl)acetamido)-β-CD **6.6** in D$_2$O at pH 9 (0.05 M Na$_2$B$_4$O$_7$·10H$_2$O buffer) in the presence and absence of 6-(*p*-toluidino)-2-naphthalenesulfonic acid "fuel".
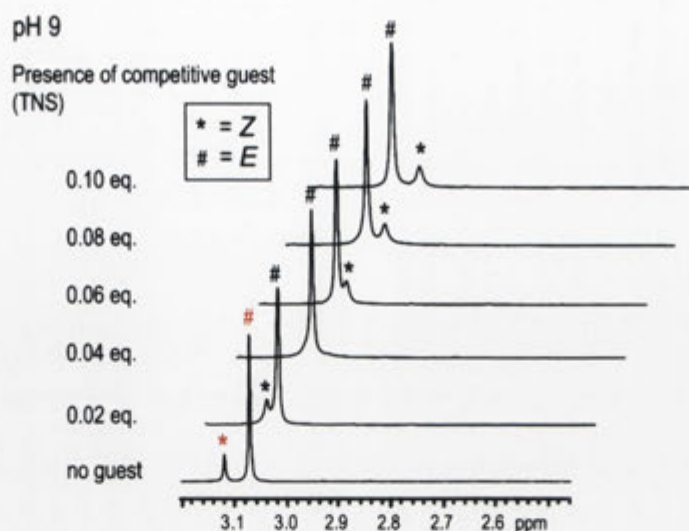
Figure 7.3.6. A section of the ^{1}H NMR spectra (500 MHz) of 6[A]-deoxy-6[A]-(*N*-methyl-3-(4-aminophenyl)acetamido)-β-CD **6.6** in D_2O at pH 9 (0.05 M $Na_2B_4O_7 \cdot 10H_2O$ buffer) in the presence and absence of between 0 and 0.1 eq. of 6-(*p*-toluidino)-2-naphthalenesulfonic acid "fuel".

Next, as shown in Figure 7.3.7, the operation of the hermaphrodite **6.6** was investigated in D_2O at pH 2. In the absence of the TNS "fuel" the *Z/E*-amide ratio is about 1:1 which reflects a ΔG of 0 kcal mol^{-1}. The ^{1}H NMR spectrum at the endpoint with the TNS "fuel" sees only a small difference between the *Z*- and *E*-amide isomers which are in a ratio of 1:0.8. This is reasonable as the hermaphrodite **6.6** adopts the [*a*1] conformation at pH 2. Thus, the work ($\delta \Delta G$) harnessed in the amide bond at pH 2 is a marginal -0.1 kcal mol^{-1} and the molecular machine is in the "OFF" state.
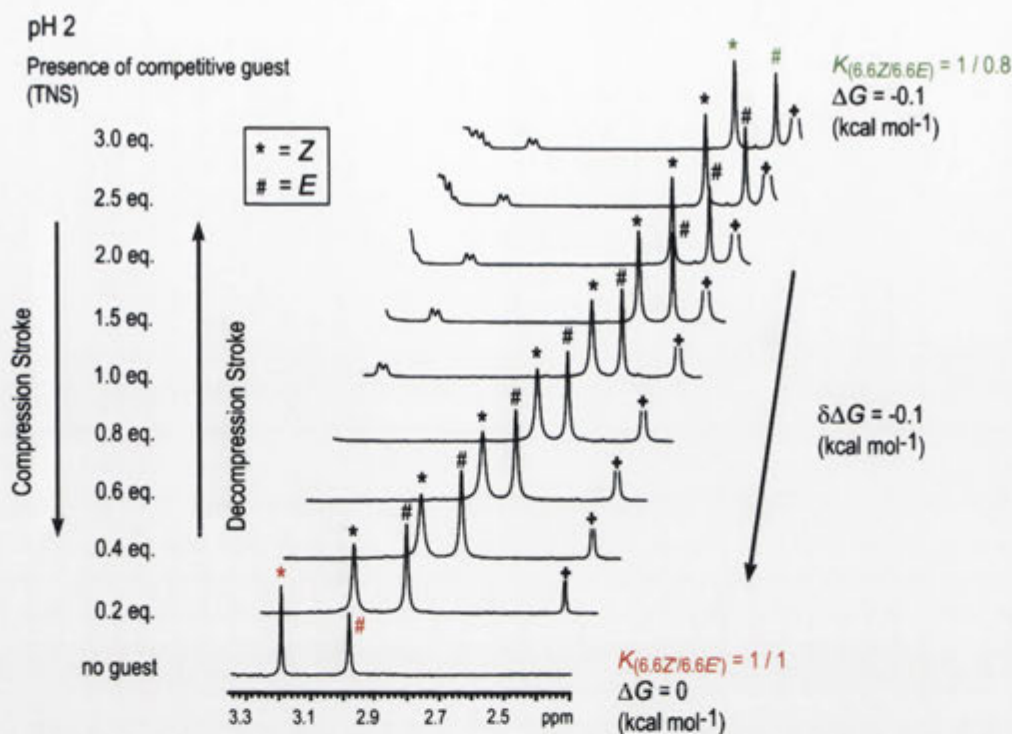
Figure 7.3.7. A section of the ^{1}H NMR spectra (500 MHz) of 6^A-deoxy-6^A-(*N*-methyl-3-(4-aminophenyl)acetamido)-β-CD **6.6** in D_2O at pH 2.0 (0.05 M NaH_2PO_4 buffer) in the presence and absence of 6-(*p*-toluidino)-2-naphthalenesulfonic acid "fuel". (+) CH_3 signal of TNS "fuel" deleted for clarity.

Scheme 7.3.2 summarises the operation of the hermaphrodite **6.6** with TNS "fuel". At pH 9 as the aryl "piston" includes within the CD "cylinder", the addition of the TNS "fuel" affords a work output of 1.2 kcal mol^{-1} thus the molecular machine is in the "ON" state. For the reason that the hermaphrodite **6.6** has a shorter "piston" a greater amount of work energy could be extracted at pH 9 using a larger "fuel" source than 1-aminoadamantane. At pH 2 the aryl "piston" has little interaction with the CD "cylinder" and the work output using TNS "fuel" is a negligible -0.1 kcal mol^{-1} so the molecular machine is "OFF". On this basis, the hermaphrodite **6.6** operates as a molecular machine harnessing the energy of molecular recognition having a pH dependent "ON/OFF" switch.

162
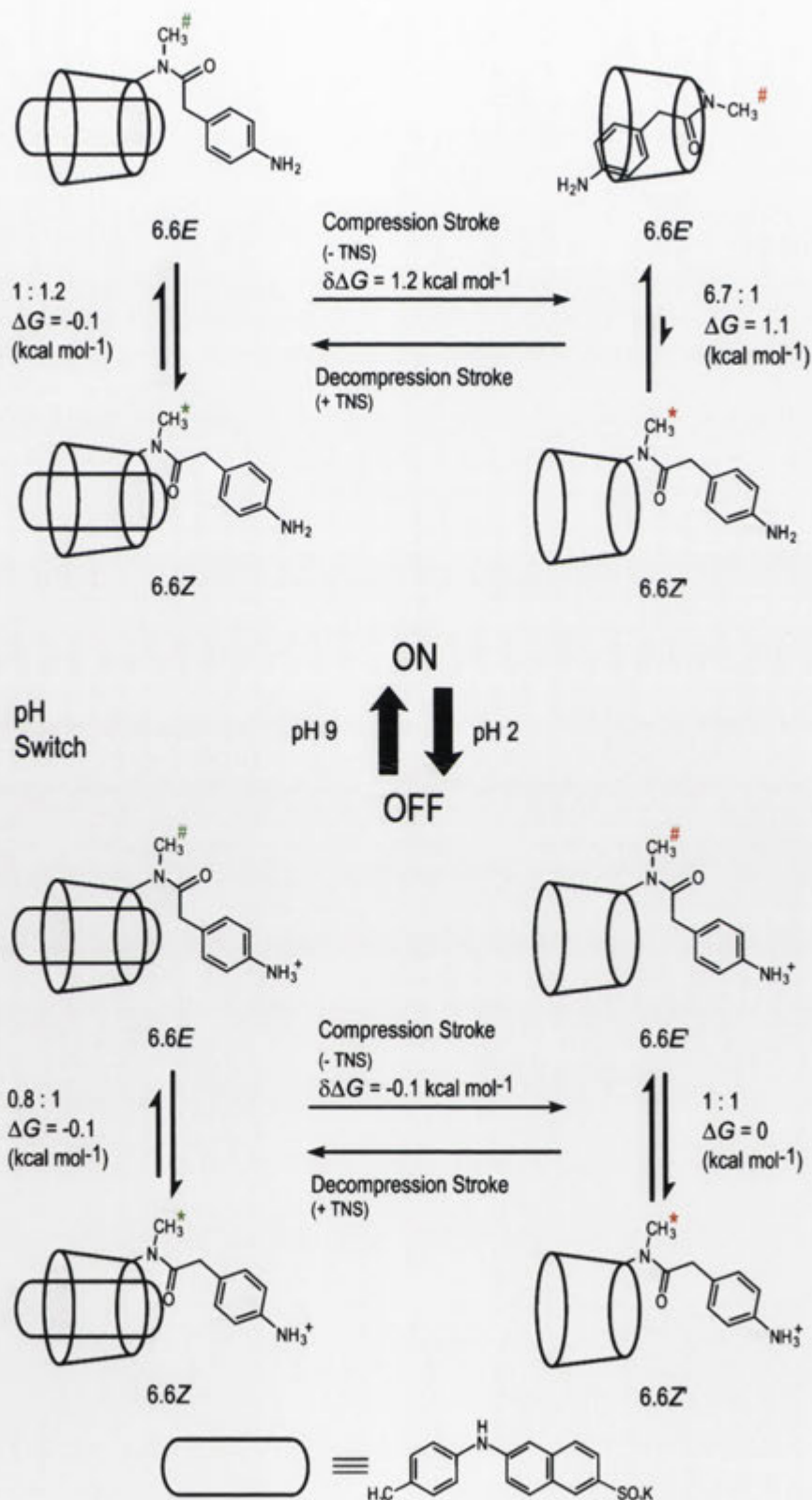
Scheme 7.3.2. Operation of 6^A-deoxy-6^A-(*N*-methyl-3-(4-aminophenyl)acetamido)-β-CD **6.6** as a molecular pump having a pH dependent "ON/OFF" switch.

Having demonstrated that the hermaphrodite **6.6** behaves as a pH dependent molecular machine, the hermaphrodite **6.8** was studied. The operation of the hermaphrodite **6.8** was investigated in D_2O at pH 9 with 1-aminoadamantane "fuel" using ^{1}H NMR spectroscopy for which the spectra are shown in Figure 7.3.8. From this, the *Z/E*-amide isomer ratio in the absence of the "fuel" is 1:5 representing a ΔG of 1 kcal mol^{-1}. At this pH the hermaphrodite **6.8** is forming the [*c*1] complex of the *E*-amide isomer which from the *Z/E*-amide ratio is of comparable strength to its acetamido counterpart **6.6**. When the 1-aminoadamantane "fuel" is added the *Z/E*-amide ratio becomes 1:0.8 and the ΔG is -0.1 kcal mol^{-1}. On this basis, the energy harnessed as work ($\delta\Delta G$) from the displacement of the aryl "piston" by the "fuel" is 1.1 kcal mol^{-1} and the hermaphrodite **6.8** is in the "ON" state at pH 9. Remarkably, the relative intensities and pattern of the *N*-methyl signals for the spectrum with 3 equivalents of 1-aminoadamantane "fuel" (Figure 7.3.8) are similar to that observed from the change in solvent (Figure 7.2.3). Thus, by adding the competitive guest at pH 9 or by changing the polarity of the solvent the hermaphrodite **6.8** harnesses around 1.1 kcal mol^{-1} of work energy.
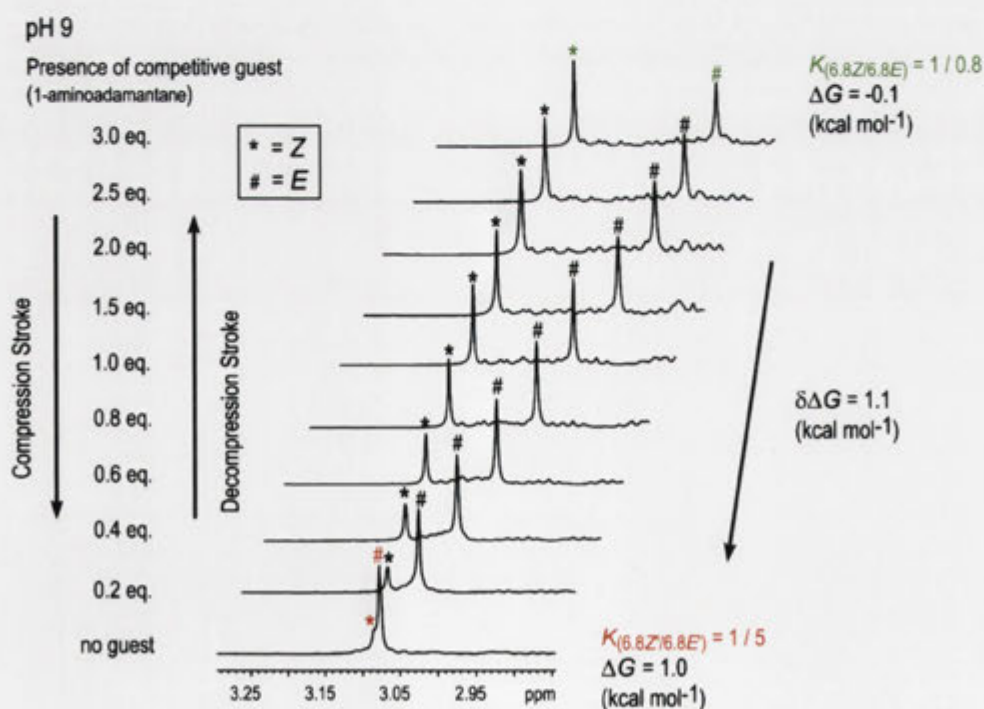
Figure 7.3.8. A section of the ^{1}H NMR spectra (500 MHz) of 6^A-deoxy-6^A-(*N*-methyl-3-(3-pyridyl)propionamido)-β-CD **6.8** in D_2O at pH 9.0 (0.05 M $Na_2B_4O_7 \cdot 10H_2O$ buffer) in the presence and absence of 1-aminoadamantane "fuel".

Next, the operation of the hermaphrodite **6.8** with 1-aminoadamantane "fuel" was investigated in D_2O at pH 2 for which the ^{1}H NMR spectra are shown in Figure 7.3.9. Without the "fuel" the *Z/E*-amide ratio is approximately 1:0.7 and the ΔG is -0.2 kcal mol^{-1}. In contrast to its aminophenyl counterpart the hermaphrodite **6.3**, at this pH the protonated aryl "piston" shows no interaction with the CD "cylinder" and the [*a*1] conformation has little bias on the *Z/E*-amide ratio. For this reason the ^{1}H NMR spectra show little variation with the addition of the 1-aminoadamantane "fuel" and the *Z/E*-amide ratio is 1:0.8 representing -0.1 kcal mol^{-1}. From this, at pH 2 the hermaphrodite **6.8** harnesses a negligible work energy ($\delta\Delta G$) of -0.1 kcal mol^{-1} and the molecular machine is in the "OFF" state.

Figure 7.3.9. A section of the ^{1}H NMR spectra (500 MHz) of 6^A-deoxy-6^A-(*N*-methyl-3-(3-pyridyl)propionamido)-β-CD **6.8** in D_2O at pH 2.0 (0.05 M NaH_2PO_4 buffer) in the presence and absence of 1-aminoadamantane "fuel".

Shown in Scheme 7.3.3 is the operation of the hermaphrodite with 1-aminoadamantane "fuel". As the aryl "piston" includes within the CD "cylinder" at pH 9, the titration with the "fuel" leads to a change in the amide isomer ratio, a work output of 1.1 kcal mol^{-1} and accordingly the molecular machine is "ON". At pH 2 the aryl "piston" has no interaction with the CD "cylinder" and the work output from the

addition of the 1-aminoadamantane "fuel" affords a negligible -0.1 kcal mol^{-1} of work so the molecular machine is "OFF". For this reason, the hermaphrodite **6.8** behaves as a molecular machine harnessing the energy of molecular recognition having a pH dependent "ON/OFF" switch.

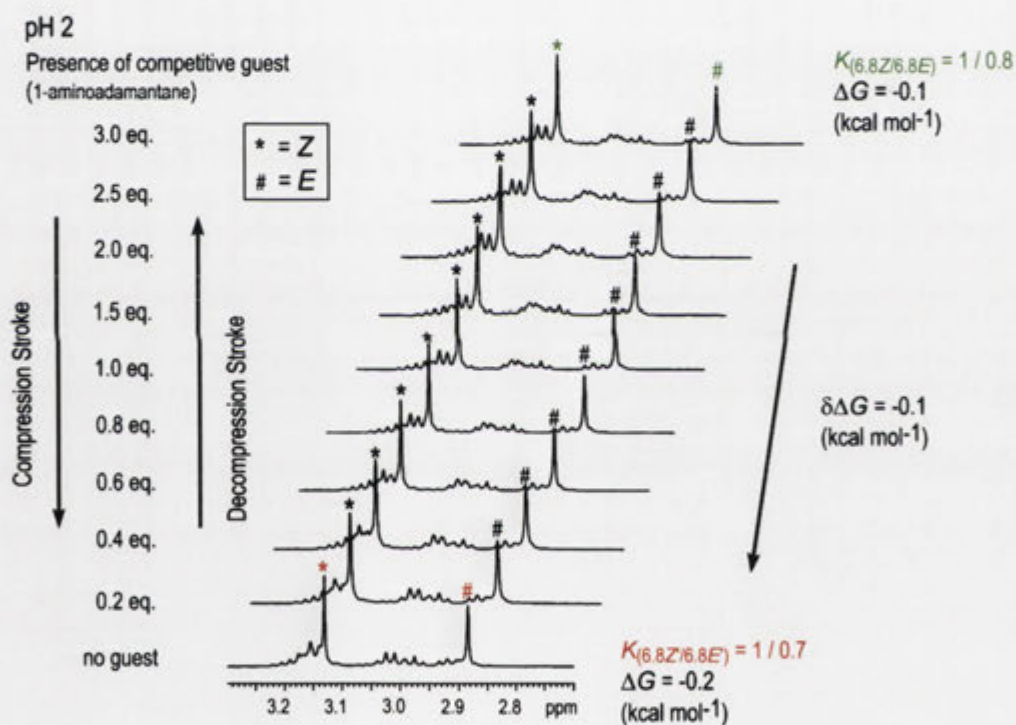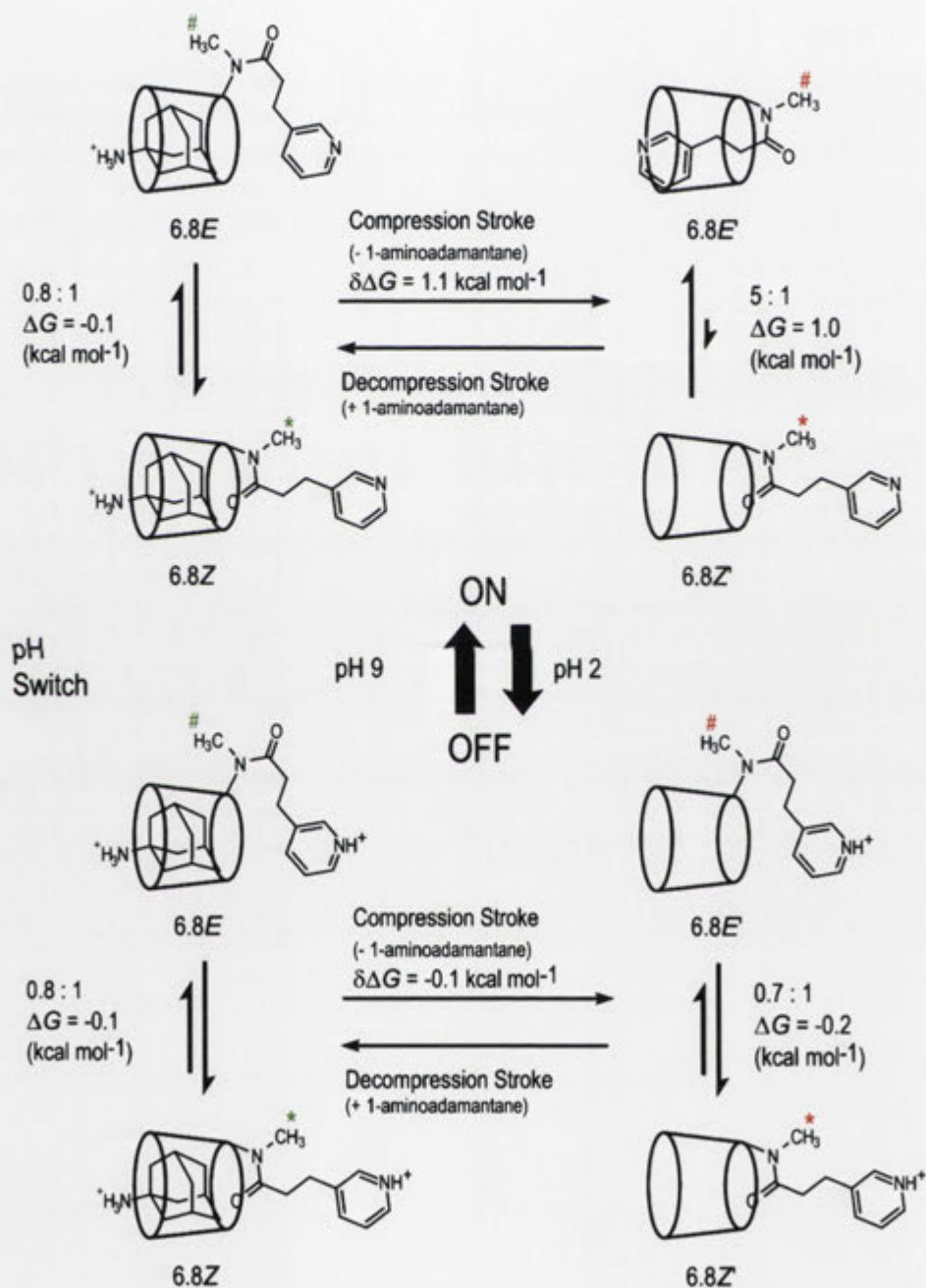
**Scheme 7.3.3.** Operation of 6^A-deoxy-6^A-(N-methyl-3-(3-pyridyl)propionamido)-β-CD **6.8** as a molecular pump having a pH dependent "ON/OFF" switch.

7.4 Isothermal Titration Calorimetry of Cyclodextrin Based Hermaphrodites

Having quantified the work outputs ($\delta\Delta G$) for each of the hermaphrodites **6.3**, **6.6** and **6.8** in acidic and basic conditions with 1-aminoadamantane "fuel" the performance of their operation was next to be established at both pHs. For this, ITC was employed to measure the thermodynamic parameters for the binding interaction between each of the hermaphrodites **6.3**, **6.6** and **6.8** and the "fuel". The main purpose for using 1-aminoadamantane "fuel" apart from its suitability for the ^{1}H NMR conformational analysis, was that at pH 9 and pH 2 this guest has the appropriate solubility at the concentrations required to obtain accurate ITC data. This is due to 1-aminoadamantane having a pKa of 10.58[145] so the nitrogen donor group exists in the cationic form under both conditions. As mentioned earlier the ITC and ^{1}H NMR spectroscopic experiments are conducted in H_2O and D_2O, respectively, however the isotopic difference is considered too small to substantially alter K_A and the overall efficiency result.[114,115] Thus, the data for the operation of the hermaphrodites **6.3**, **6.6** and **6.8** as determined with ^{1}H NMR spectroscopy can be directly compared to the ITC thermodynamic parameters.

In order to obtain the thermodynamic data aliquots of the 1-aminoadamantane "fuel" were titrated into the ITC cell at the desired pH which contained a known concentration of the chosen hermaphrodite in identical buffer. To illustrate this, the stepwise heat changes (top) and integrated peaks (bottom) for the binding interaction between the 1-aminoadamantane "fuel" and the hermaphrodite **6.8** at pHs 9 and 2 are shown in Figures 7.4.1a and b, respectively. The negative heat changes indicate that an exothermic process is occurring, while the curves have inflection points at molar ratios of about 1.0 which suggests a 1:1 complex is formed between the 1-aminoadamantane "fuel" and the hermaphrodite **6.8**. To ensure accurate and reliable data were being generated the concentrations of the individual components of the titration experiment were optimised to obtain curves having suitable c values as discussed in Chapter 3.2. From the isotherms nonlinear least-squares fitting was used to provide the thermodynamic parameters.
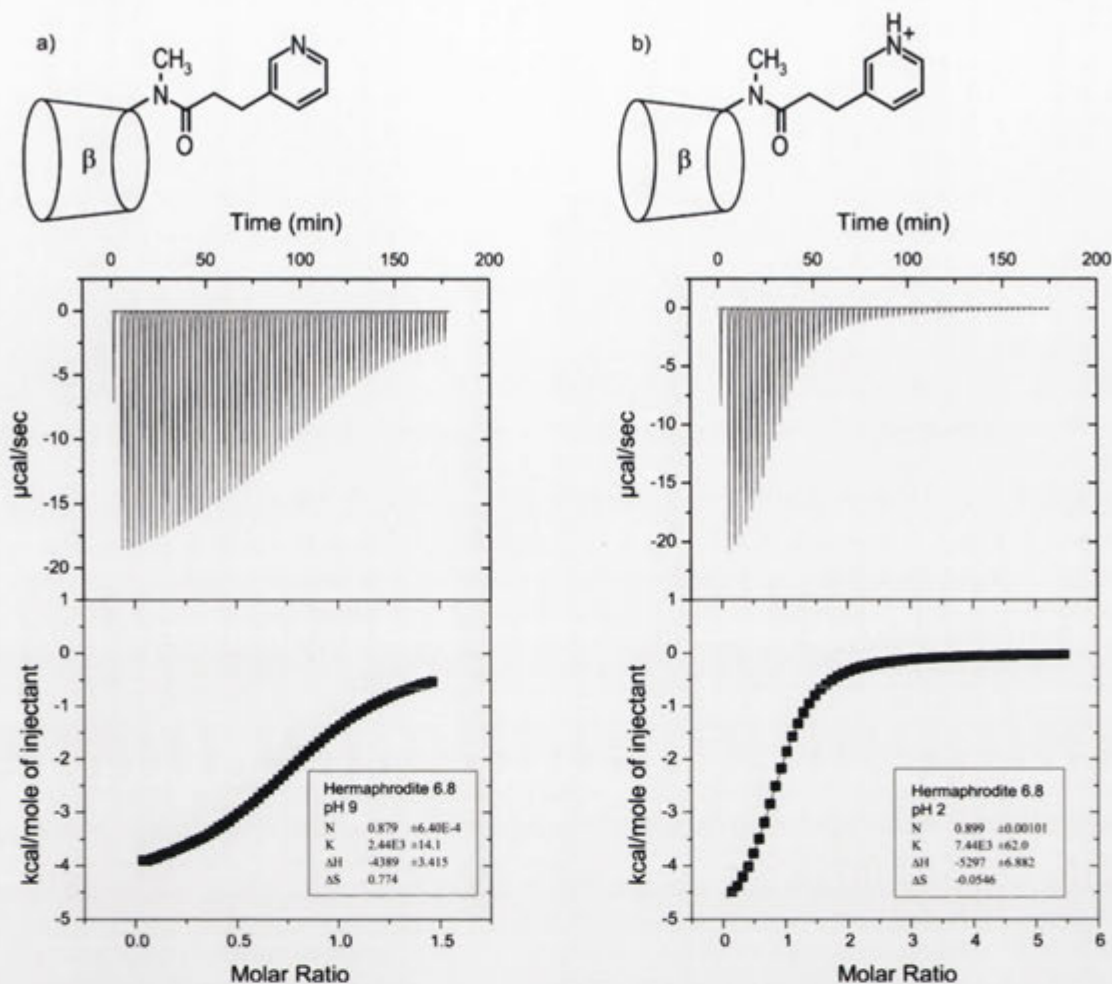
Figure 7.4.1. ITC thermograms for 60 successive injections (5 μl) of 1-aminoadamantane (26 mM) into cells containing the hermaphrodite **6.8** in identical buffer (a) pH 9, 0.05 M $Na_2B_4O_7 \cdot 10H_2O$ buffer or (b) pH 2, 0.05 M NaH_2PO_4 buffer.

For each of the hermaphrodites **6.3**, **6.6** and **6.8**, two runs with 1-aminoadamantane "fuel" were conducted at separate pHs the results of which were averaged to obtain the thermodynamic parameters reported in Table 7.4.1. The Table shows the association constant (K_A), work output ($\delta\Delta G$), free energy change (ΔG), enthalpy change (ΔH) and entropy change ($T\Delta S$) for each of the CDs. As a guide to the reliability of the thermodynamic data the results for β-CD **1.10** and 1-aminoadamantane were compared against reported values (UV/visible spectroscopy).[147]

CD	pH	K_A (M^{-1})	$\delta\Delta G$ (kcal mol^{-1})[a]	ΔG (kcal mol^{-1})[b]	ΔH (kcal mol^{-1})	$T\Delta S$ (kcal mol^{-1})
β-CD	9	8195 ± 40	N/A	-5.3	-4.0 ± 0.00	1.3 ± 0.01
	2	6915 ± 115	N/A	-5.3	-5.3 ± 0.01	0.0 ± 0.07
β-CD[c]	2.5	8912 ± 1000	N/A	-5.4	-5.9 ± 0.45	-0.5 ± 0.57
6.3	9	861 ± 35	1.9	-4.0	-4.0 ± 0.01	0.0 ± 0.01
	2	2735 ± 25	0.7	-4.7	-6.5 ± 0.01	-1.8 ± 0.01
6.6	9	5980 ± 65	0.5	-5.1	-5.1 ± 0.01	0.0 ± 0.00
	2	7470 ± 55	-0.1	-5.3	-5.5 ± 0.01	-0.2 ± 0.01
6.8	9	2415 ± 15	1.1	-4.6	-4.4 ± 0.00	0.2 ± 0.00
	2	7430 ± 65	-0.1	-5.3	-5.3 ± 0.01	0.0 ± 0.01

Table 7.4.1. ITC and NMR experimental data for the binding of 1-aminoadamantane "fuel" with the hermaphrodites **6.3**, **6.6** and **6.8** at pH 9 and pH 2. [a]ΔG values reported are amide strain energy stored from the decompression stroke of the "piston" with 1-aminoadamantane as measured by ^{1}H NMR spectroscopy. [b]ΔG values calculated from ΔH-$T\Delta S$. [c]Data from Gelb and Schwartz, 1989.[147]

Beginning with the control experiments, at pH 9 β-CD **1.10** has an association for the "fuel" of 8195 M^{-1} while at pH 2 the K_A is 6915 M^{-1}. This shows that the effect on the binding interaction from the difference between the pH and buffers is only weak. Of the molecular machines, the hermaphrodite **6.3** affords a K_A of 861 M^{-1} for the 1-aminoadamantane "fuel" at pH 9. This is a greater than nine and a half-fold decrease in affinity relative to β-CD **1.10** and is the lowest K_A of all the molecular machines studied at this pH. The "fuel" is being impeded by the unprotonated aryl "piston" which is strongly including within the CD "cylinder" to form the [c1] complex of the E-amide isomer. The relative strength of the [c1] complex also ensures that the hermaphrodite **6.3** at pH 9 harnesses the greatest amount of work energy ($\delta\Delta G$) which is 1.9 kcal mol^{-1}.

In the acidic conditions (pH 2) the hermaphrodite **6.3** affords a K_A of 2735 M^{-1} for the "fuel" which is considerably lower than β-CD **1.10** control and supports the notion that the protonated form of the aryl "piston" is still forming the [c1] complex with reasonable strength. As a consequence this molecular machine at pH 2 performs a small amount of work (0.7 kcal mol^{-1}). Next, the hermaphrodite **6.6** having the acetonamido "piston" forms a relatively weaker [c1] complex at pH 9 as identified from the K_A of 5980 M^{-1} for the "fuel". The result is that only 0.5 kcal mol^{-1} of work is being harnessed (δΔG) in the amide bond by this system in the basic conditions. From the fact that adamantane based compounds prefer to bind from the secondary face[149] of the annulus of β-CD **1.10** it is likely that the aryl "piston" of the hermaphrodite **6.6** is too short to be effectively displaced to increase the proportion of the *Z*-amide isomer. This is supported by the findings from Chapter 7.3 in that a greater amount of work energy (1.2 kcal mol^{-1}) is extracted at pH 9 using a longer "fuel" source than 1-aminoadamantane. Interestingly at pH 2, the hermaphrodite **6.6** affords a K_A of 7470 M^{-1} for the 1-aminoadamantane "fuel" which is comparable to β-CD **1.10** (6915 M^{-1}) under the same conditions. On this basis and from the ^{1}H NMR conformational analysis in Chapter 6.3, the [a1] conformation is dominant for the ammonium form of the hermaphrodite **6.6** and accordingly the "fuel" has unrestricted access to the CD "cylinder". In support of this, the addition of the "fuel" sees negligible work harnessed in the amide bond with a δΔG of -0.1 kcal mol^{-1}. Finally, the hermaphrodite **6.8** having the pyridyl "piston" shows a K_A of 2415 M^{-1} for the 1-aminoadamantane "fuel" at pH 9. As identified in Chapters 6.3 and 6.4 at this pH the pyridyl "piston" is included within the CD "cylinder" with the [c1] complex of the *E*-amide isomer the dominant conformation. For this reason the addition of the "fuel" sees the transition from the [c1] complex to the [a1] competitive guest complex which results in a δΔG of 1.1 kcal mol^{-1}. Alternatively, at pH 2 the hermaphrodite **6.8** has a K_A of 7430 M^{-1} for the "fuel" that is nearly identical to that of the hermaphrodite **6.6** (7470 M^{-1}) and comparable to β-CD **1.10** (6915 M^{-1}) under the same conditions. This is in support of the ^{1}H NMR conformational analysis in Chapter 6.3 in that the hermaphrodite **6.8** adopts the [a1] conformation in the protonated pyrydinium form. As the "piston" is incapable of restricting access to the CD "cylinder" the 1-aminoadamantane "fuel" has negligible effect on the *Z/E*-amide ratio and thus a δΔG of -0.1 kcal mol^{-1}is observed.

Having discussed the link between the strength of the [*c*1] complex and the work outputs ($\delta\Delta G$), the focus shifts to the uncaptured work energies (ΔG) and the energies harnessed by the hermaphrodites **6.3**, **6.6** and **6.8**. Firstly, the hermaphrodite **6.3** at pH 9 harnesses 1.9 kcal mol^{-1} of work in the amide bond which is the largest of all the pH sensitive systems studied. As a consequence of the decreased K_A for the 1-aminoadamantane "fuel" the magnitude of ΔG also decreases due to the relationship of $\Delta G = -RT\ln K_A$. For this reason the amount of uncaptured energy for the hermaphrodite **6.3** at pH 9 is the smallest in magnitude of all the molecular machines with a ΔG of -4.0 kcal mol^{-1}. In acidic conditions (pH 2) the hermaphrodite **6.3** affords a ΔG of -4.7 kcal mol^{-1} and a $\delta\Delta G$ of 0.7 kcal mol^{-1}. At this pH the system harnesses a small amount of work energy in the amide bond ($\delta\Delta G$) and thus ΔG is less negative than β-CD **1.10** (-5.3 kcal mol^{-1}). For the hermaphrodite **6.6** at pH 9 a $\delta\Delta G$ of 0.5 kcal mol^{-1} is obtained and ΔG is slightly more positive at -5.1 kcal mol^{-1} when compared to that observed for β-CD **1.10** (-5.3 kcal mol^{-1}) at the same pH. When the hermaphrodite **6.6** is at pH 2 a ΔG of -5.3 kcal mol^{-1} is observed which is identical to that for β-CD **1.10**. As little work energy ($\delta\Delta G$) is being harnessed (-0.1 kcal mol^{-1}) then the thermodynamic quantity of ΔG mirrors that observed for β-CD **1.10**. For the hermaphrodite **6.8** at pH 9 the energy harnessed is 1.1 kcal mol^{-1} which is accompanied by a ΔG that is -4.6 kcal mol^{-1}. This result follows the trend that the more work harnessed the larger the decrease in the magnitude of ΔG relative to β-CD **1.10** for 1-aminoadamantane "fuel". At pH 2 the work output for the hermaphrodite **6.8** is only -0.1 kcal mol^{-1} and thus affords a ΔG that has similar to both the hermaphrodite **6.6** and β-CD **1.10** at the same pH. Finally, the binding interaction between 1-aminoadamantane "fuel" and each of the hermaphrodites **6.3**, **6.6** and **6.8** with was enthalpically driven with ΔG dominated by the ΔH contributions ($|\Delta H| \gg |T\Delta S|$).

To review the findings for the hermaphrodites **6.3**, **6.6** and **6.8**, when the aryl "piston" is in the uncharged form, the lower the K_A of the 1-aminoadamantane "fuel" for the CD "cylinder", the stronger the [*c*1] complex and the more energy harnessed ($\delta\Delta G$). At pH 9 these molecular machines are in the "ON" state. At pH 2, when the aryl "piston" is in the charged form, the higher the K_A of the 1-aminoadamantane "fuel" for the CD "cylinder", the less the "piston" hinders the cavity and the less energy that is harnessed as output ($\delta\Delta G$). For the reason that the aryl "piston" of the hermaphrodite

6.3 still includes within the CD "cylinder", this machine is only partially switched "OFF" at pH 2. On the other hand, the thermodynamic parameters of the hermaphrodites **6.6** and **6.8** show that these molecular machines can indeed be switched "OFF" at pH 2. Of the molecular machines, the decrease in ΔG corresponds to an increase in the work output ($\delta\Delta G$) which is consistent with the findings from Chapters 3 and 4, showing that the greater the work output the less unharnessed work energy measured.

Having quantified the thermodynamic parameters for the binding interaction of the hermaphrodites **6.3**, **6.6** and **6.8** for 1-aminoadamantane "fuel", the aim was then to determine the energy harnessing efficiency. For this, the uncaptured work energy (ΔG) was compared to the work output ($\delta\Delta G$), using Equation 3.2.1. As this includes the unavoidable energy cost that is incurred from molecular reorganisation ($T\Delta S$), the performance was also assessed from the energy dissipated as heat (ΔH) with Equation 3.2.2. Shown in Table 7.4.2 is the energy harnessing efficiency for the hermaphrodites **6.3**, **6.6** and **6.8** in relation to either ΔG or ΔH for 1-aminoadamantane "fuel" at 25 °C.

Nanomachine	pH	$\text{Eff}_{\Delta G}$ (%)[a]	$\text{Eff}_{\Delta H}$ (%)[b]
6.3	9	32	32
	2	13	10
6.6	9	9	9
	2	-2	-2
6.8	9	19	20
	2	-2	-2

Table 7.4.2. Efficiency of harnessing the energy of molecular recognition in the hermaphrodites **6.3**, **6.6** and **6.8** at 25 °C. [a]Calculated from Equation 3.2.1. [b]Calculated from Equation 3.2.2.

The energy efficiency of the hermaphrodite **6.3** at pH 9 remains at 32% for both Eff$_{\Delta G}$ and Eff$_{\Delta H}$. This is due to the binding interaction being enthalpically driven without any entropic contribution. This molecular machine harnesses the largest amount of work energy ($\delta \Delta G$) and performs with the highest efficiency of the pH sensitive machines studied. Under acidic conditions (pH 2), the energy efficiency of the hermaphrodite **6.3** is lower at 13% (Eff$_{\Delta G}$) and 10% (Eff$_{\Delta H}$). Although the efficiency has decreased and considerably less energy is harnessed in the amide bond, this system demonstrates that more than just a charged aryl "piston" is required to realise the "OFF" state. Next, the hermaphrodite **6.6** affords energy efficiencies of 9% for both Eff$_{\Delta G}$ and Eff$_{\Delta H}$ at pH 9. The weaker performance of this system in the "ON" state is due to the shortened aryl "piston" not being displaced effectively from the primary face of the CD by 1-aminoadamantane "fuel" as demonstrated through the use of the longer TNS guest in Chapter 7.3. The hermaphrodite **6.6** at pH 2 shows energy harnessing efficiencies of - 2% for both the uncaptured work energy and the heat dissipated, respectively. The binding interaction between this system and 1-aminoadamantane "fuel" at this pH is similar to that of β-CD **1.10** and it is reasonable that this molecular machine is switched "OFF". Next, the hermaphrodite **6.8** having the pyridyl "piston" affords energy harnessing efficiencies at pH 9 of 19% and 20% as calculated from ΔG and ΔH. Under these conditions this pH sensitive molecular machine is able to perform with the comparable energy harnessing efficiency to that of a macroscopic motor.[113] This performance is distinct from that observed at pH 2, where the protonated form of the hermaphrodite **6.8** affords energy harnessing efficiencies of -2% for both Eff$_{\Delta G}$ and Eff$_{\Delta H}$. On this basis this system at pH 2 can be switched "OFF". From these results it appears that in order to effectively destabilise the [c1] complex and achieve the "OFF" state the nitrogen donor group must be positioned relatively closer to the CD "cylinder" which comes with the cost of lowering the performance in the "ON" state. In spite of this, a molecular machine having a pH dependent "ON/OFF" switch can be developed to perform a work output at the atomic level with comparable energy efficiency to that of a macroscopic machine.[113]

7.5 Conclusion

The thermodynamic parameters for the operation of the hermaphrodites **6.3**, **6.6** and **6.8** with 1-aminoadamantane "fuel" was investigated at both pH 9 and pH 2. From this research the strength of the [c1] complex could be modulated by acid-base regulation of the nitrogen donor group on the aryl "piston", which in turn altered the association of the "fuel" for the CD "cylinder" for the enthalpically driven binding interaction. Consistent with the findings from Chapters 3 and 4 the strength of the [c1] complex has an influence on the corresponding work that is done ($\delta\Delta G$) on the amide bond. Of the pH sensitive systems, the propionamido hermaphrodite **6.3** formed the strongest [c1] complex at pH 9, harnessed the largest amount of energy and operated with the best efficiency (~30%). At pH 2, the operation of the hermaphrodite **6.3** (~13%) is demonstrably different from that observed for both the hermaphrodites **6.6** and **6.8** (~2%) under the same conditions. This shows that a destabilising interaction between the charged nitrogen donor group and the CD "cylinder" is required for the molecular machines to be switched "OFF". Importantly, it can be concluded that pH dependent artificial molecular machines can be developed to perform work outputs at the molecular level with the efficiency of their macroscopic counterparts. For these reasons harnessing the energy of molecular recognition with artificial molecular machines having pH dependent "ON/OFF" switches provides an alternative to the photochemical systems.

CHAPTER 8

Conclusions and Future Directions

This work describes the synthesis and operation of several CD based molecular machines that generate strain energy from the formation of a [*c*1] complex which can be harnessed to do mechanical work and restrict the geometry of an amide bond. In Chapter 2, the *trans*-cinnamide **2.4** in D_2O forms the [*c*1] complex upon the removal of the "fuel" 1-adamantanol, and the *Z/E*-amide ratio changes from 1:2.6 to 1:100. In contrast, its *cis*-isomer **2.5** is in the "OFF" state as the aryl "piston" has little interaction with the CD "cylinder". Irradiation at 300 nm converts the *trans*-cinnamide **2.4** to its *cis*-isomer **2.5**, while the reverse process occurs at 254 nm, thus this molecular machine has a photochemical "ON/OFF" switch. In Chapter 3, the amount of work that can potentially be harnessed by the molecular machines using the "fuel" was quantified to be about 6-8 kcal mol^{-1}, of which the hermaphrodites **2.4** and **2.5** have efficiencies of 30% and -3% in the "ON" and "OFF" states, respectively. Chapter 4 details the impact of different substituents on the performance of the molecular machines, as highlighted by the secondary amide cinnamido hermaphrodite **4.3** harnessing only 0.9 kcal mol^{-1} (Eff$_{\Delta G}$: 13%) and the *N*,α-dimethylcinnamido hermaphrodite **4.7** harnessing 3.7 kcal mol^{-1} (Eff$_{\Delta G}$: 48%). Prepared in Chapter 5 is the *trans*-stilbenylamido hermaphrodite **5.4** that forms an intermolecular complex that can constrain the geometry to the *Z*-amide isomer to harness 1.9 kcal mol^{-1} with an efficiency of 25%. The photochemical isomerisation between the hermaphrodite **5.4** and its *cis*-stilbenylamido counterpart **5.5** allows the molecular machine to be switched "ON" and "OFF". Finally, the research in Chapters 6 and 7 demonstrates the preparation, operation and performance of pH dependent molecular machines that overcome some of the switching limitations that were identified in their photochemical counterparts from Chapters 2-5.

The research covered in this thesis demonstrates that not only can molecular machines perform quantifiable work output at the molecular level, they also operate with the efficiency of their macroscopic counterparts. This demonstration that work output can be harnessed and quantified in such molecular devices takes us one step closer to their practical application.

From the findings of this thesis, 2-4 kcal mol^{-1} of work can be performed on an amide "torsion bar" that is built into a molecular machine. It is likely to be more advantageous if this harnessed energy can be transferred into another molecule. This is reminiscent of how enzymes use the binding energy of a substrate to distort the geometry of that substrate towards the more reactive conformer. This has the potential to be exploited to develop the CD based artificial enzyme that is shown in Figure 8.1. For the purpose of replicating the hydrophobic pocket of an enzymes active site, two CDs are tethered together to produce the target dimer. The intended purpose is for molecular recognition of the non-rigid substrate by the CDs active site to stabilise the geometry of the reactive conformer. Maximum binding interactions are not realised until the preferred geometry is obtained, thus the artificial enzyme does work on the substrate. Synthetic treatment of the bound substrate can be exploited to generate regio- and stereo-controlled products, and thus capture the work energy that is done on the substrate. Provided that the CD based artificial enzyme is not consumed in the reaction and that the product has weaker association for the binding pocket than the bound form of the substrate, the system is also likely to be catalytic.
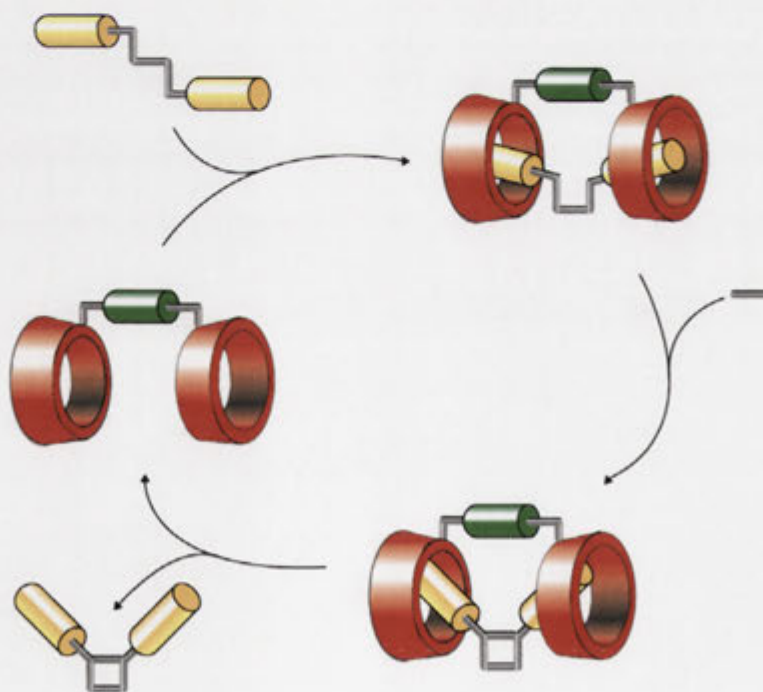
Figure 8.1. Schematic representation of the catalytic cycle of a CD based artificial enzyme.

As the molecular machines developed within this thesis operate in aqueous solution, it is possible to look towards biological processes for inspiration for future directions. For example, peptides can form alpha helical tertiary structures that are stabilised by non-covalent hydrogen bonds. Considering that the hydrogen bond strength in such conformers in water is between 0.5-2.0 kcal mol^{-1},[150,151] and around 2.0-4.0 kcal mol^{-1} of work can be harnessed by the synthetic molecular devices developed in this thesis, then it is possible that a CD based molecular machine can be developed to unfold the conformation of a peptide. Illustrated in Figure 8.2 is the schematic representation of a stimuli responsive artificial molecular pump that could be designed for the purpose of unfolding an alpha helix. In the "OFF" state, the CD preferentially complexes a photochemically sensitive binding station and the machine adopts a conformation that stabilises the formation of the alpha helix. In the "ON" state, when the molecule has been exposed to UV light, the CD is displaced from the photochemically sensitive binding station and the work output of the shuttling is harnessed to disrupt the hydrogen bonds and the alpha helix can be unfolded.
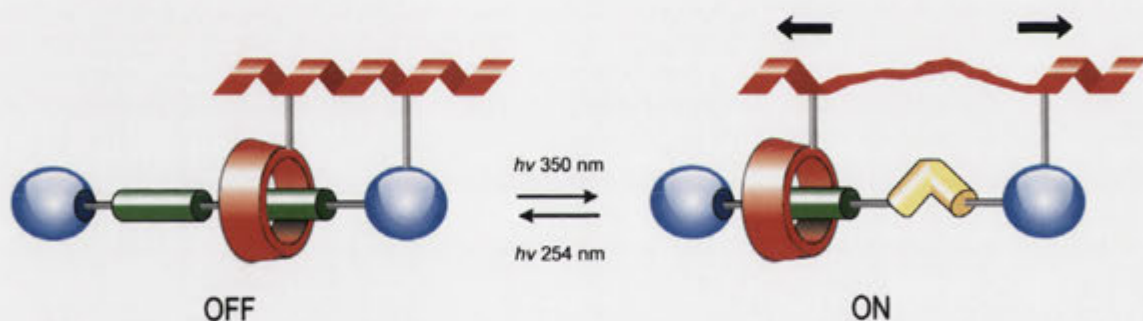
Figure 8.2. Schematic representation of a CD based molecular pump that regulates the tertiary structure of a peptide.

The switching function of the molecular machines developed within this thesis allowed the access to the CD "cylinder" for a particular guest to be regulated in response to photochemical and chemical stimuli. The transition between the [c1] complex and the [a1] conformation with hv or pH is reminiscent of the opening and closing of the gate on a channel which is illustrated in Figure 8.3. This concept extends the research of Gin *et al.*,[152] who inserted a β-CD having one face substituted with hydrophobic oligoether chains into a phospholipid bilayer, and demonstrated that the
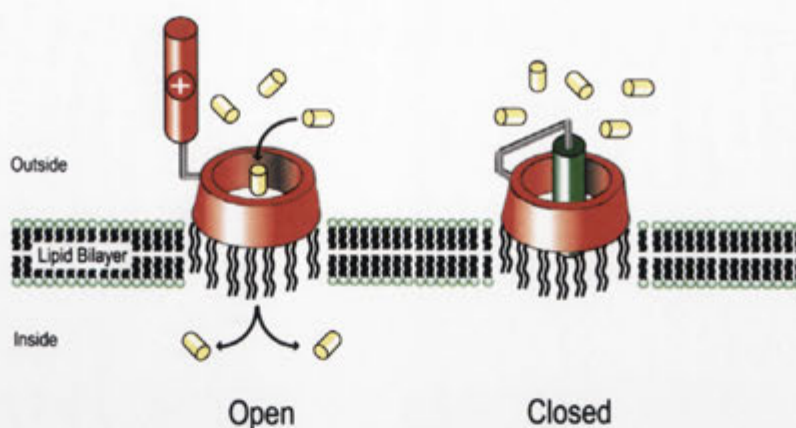
Figure 8.3. Schematic representation of the stimuli responsive gated channel.

molecule functions as a non-gated channel for the selective permeation of anions. By per-functionalising the secondary face of the hermaphrodites **4.3**, **4.4**, **6.6** and **6.8** using established protocols,[153] these stimuli responsive systems could also be inserted into lipid bilayers. When the aryl "gate" includes within the CD "channel" the pore is "closed" to anion flux, while excluding the aryl "gate" from the CD "channel" "opens" the pore to allow the anions to freely permeate across the lipid bilayer. In a more biologically based system, Bayley and coworkers[154] demonstrated that β-CD **1.10** could be covalently attached into the lumen of α-hemolysin protein pore to allow selective ion conductance. Using Bayley's technique it is likely that the hermaphrodites **4.3**, **4.4**, **6.6** and **6.8** could also be directly incorporated into α-hemolysin, thus allowing a stimuli responsive gating mechanism to be incorporated into a protein channel that allows the selective flux of ions.

CHAPTER 9

Experimental

9.1 General Experimental

NMR spectra were recorded using a Varian Mercury 300 spectrometer operating at 300 MHz (^{1}H) or 75 MHz (^{13}C), a Varian Inova 500 spectrometer working at 500 MHz (^{1}H) or 125 MHz (^{13}C), or a Bruker Avance 600 spectrometer functioning at 600 MHz (^{1}H). d_6-Dimethyl sulfoxide (d_6-DMSO) with an isotopic purity of 99.9%, deuterium oxide (D_2O) with an isotopic purity of 99.75% and chloroform ($CDCl_3$) with an isotopic purity of 99.8% were purchased from Cambridge Isotope Laboratories Inc., MA. Isothermal microcalorimetry experiments were performed on a MicroCal VP-ITC® microcalorimeter and the data processed with MicroCal® Origin software. Electrospray ionisation (ESI) low-resolution mass spectra (LRMS) were recorded on a Micromass VG Quattro II triple quadruple mass spectrometer. Electron impact LRMS were recorded on a Micromass VG Autospec M mass spectrometer. ESI high-resolution mass spectra (HRMS) were recorded with a Bruker Apex 4.7T FTICR-MS mass spectrometer. Elemental analyses were performed by The Australian National University Microanalytical service. UV/visible spectra were recorded using a Shimadzu UV-2101PC UV-Vis scanning spectrophotometer. Thin-layer chromatography (TLC) was performed on aluminium backed Kieselgel 60 F_{254} coated plates (Merck Chemical Co.). Developed plates were visualised using ultraviolet light (254 nm lamp) and/or by dipping the plates into a solution of 0.1% napthelene-1,3-diol in 200:157:43 v/v/v $EtOH$-H_2O-H_2SO_4 followed by heating with a heat-gun. High-performance liquid chromatography (HPLC) was carried out using a Waters 717plus Autosampler with a Waters 2996 photodiode array detector. HPLC grade solvents were purchased from LabScan Asia, Bangkok, Thailand and filtered through Waters PVDF filters (0.45 μm). Deionised H_2O was treated (> 18.2 MΩ cm^{-1}) using an ELGA Labwater® PURELAB classic UV reagent system. Photochemical experiments were conducted using a Luzchem LZC-ORG photolysis reactor (Luzchem Research Inc., Ottawa, Canada). pH experiments were conducted using a Orion PerpHect LogR meter Model 320 with Orion PerpHect ROSS combination pH micro electrode. Melting points were determined on a

Kofler hot stage melting point apparatus under a Reichert microscope. β-CD (99.1%) was purchased from Nihon Shokuhin Kako Co., Japan, and recrystallised from H_2O then dried *in vacuo* over P_2O_5 before use. 1-Aminoadamantane (>99%), 1-adamantanecarboxylic acid (>99%), 1-adamantanol (>99%), 4-aminophenylacetic acid (>99%), 3-(4-aminophenyl)-propionic acid (97%), *trans*-cinnamoyl chloride (>98%), deuterium chloride solution in D_2O (99 Atom % D), *N,N*-dimethylformamide anhydrous (DMF), 1,4-dioxane (>99%), hydrocinnamoyl chloride (>98%), 4-iodobenzoic acid (98%), methylamine (2 M in THF), *N*-methyl-2-pyrrolidinone anhydrous (NMP), oxalyl chloride (>98%), palladium(II) acetate (98%), 3-pyridinepropionic acid (98%), sodium azide (99.5%), sodium dihydrogen phosphate anhydrous (NaH_2PO_4), sodium phosphate dibasic (Na_2HPO_4), *p*-toluenesulfonyl chloride (>99%), 6-(*p*-toluidino)-2-naphthalenesulfonic acid (85%), triphenylphosphine (PPh$_3$; 99%) were purchased from Sigm-Aldrich Co. α-Methyl cinnamic acid was purchased from Chemicals Procurement Laboratories. Ammonia solution (28%), hydrochloric acid solution (36%), sodium hydroxide (NaOH) pellets, pyridine, and triethylamine (TEA) were purchased from Ajax Finechem Ltd. Benzotriazole-1-yloxy-tris(dimethylamino)phosphonium hexafluorophosphate (BOP) and di-*tert*-butyl dicarbonate (BOC) were purchased from Auspep Ltd. Diaion HP-20, Toyopearl DEAE-650M anion-exchange and SP-650M cation-exchange resins were all purchased through Supelco, PA.

Resin Preparation

Diaion HP-20 Column: The resin (50 g) was wetted with MeOH (150 mL), and the MeOH then decanted off. Further wetting of the resin was with a gradient solvent system from 0% - 100% MeOH-H_2O in 25% increments (*ca.* 4 × 150 mL).

DEAE-650M Column: The diethylaminoethyl (DEAE) resin (50 g) was rinsed with EtOH (100 mL) and H_2O (100 mL) before NaOH 0.5 M (200 mL) was eluted through the column. The column was then rinsed with H_2O until neutral pH (*ca.* 200 mL).

SP-650M Column: The strong cationic exchange (SP) resin (50 g) was rinsed with EtOH (100 mL) and H_2O (100 mL) before HCl 0.5 M (200 mL) was eluted through the column. The column was then rinsed with H_2O until neutral pH (*ca.* 200 mL).

9.2 Experimental for Chapter 3

^{1}H NMR Titrations for the Hermaphrodites 2.3, 2.4 and 2.5 with 1-adamantanecarboxylate "fuel"

Buffer. Phosphate buffer (0.05 M) was prepared by combining Na_2HPO_4 (24 mM) and NaH_2PO_4 (26 mM) in D_2O and adjusted to pH 6.9 with NaOD.

Titration. The hermaphrodites **2.3**, **2.4** and **2.5** (3 mg, 2.3 µmol) were dissolved in D_2O (700 µL) of phosphate buffer (0.05 M, pH 6.9) at 25 °C. ^{1}H NMR spectra were recorded before and after the addition of an aliquot (300 µL, 3 equivalents) of a solution of 1-adamantanecarboxylic acid (4.2 mg, 23 µmol) in buffered D_2O (1 mL). All spectra were referenced using a TSP internal standard. Integration of amide peaks afforded the ratio of isomers at the start and end points of the titration with 1-adamantanecarboxylate "fuel". The same protocol was followed for the variable temperature ^{1}H NMR titrations of the hermaphrodite **2.4** at 10 °C, 25 °C, 40 °C and 55 °C.

### Isothermal Titration Calorimetry for the Hermaphrodites 2.3, 2.4 and 2.5 with 1-adamantanecarboxylate "fuel"

Buffer. Phosphate buffer (0.05 M) was prepared by combining Na_2HPO_4 (24 mM) and NaH_2PO_4 (26 mM) in H_2O and adjusted to pH 6.9 with NaOH.

Microcalorimetry. Isothermal titration calorimetry experiments were conducted at 25 °C with each titration consisting of 60 successive injections (1 × 3 µL, 59 × 5 µL) of a degassed solution of 1-adamantanecarboxylic acid (6.5-13.28 mM) in 0.05 M phosphate buffer (pH 6.9). The titrant was injected into a thermostated reaction cell containing a known volume (1.44 mL) of the CD (0.398-1.84 mM) in identical degassed buffer. Injection duration was 16.6 s every 180 s and the solutions were stirred at 450 rpm. Independent heat of dilution experiments were conducted and used to correct the complexation experiments. Variable temperature microcalorimetry involved running the titrations at 10 °C, 25 °C, 40 °C and 55 °C. MicroCal® Origin software was used to determine the equilibrium constants (K_A), change in enthalpies (ΔH), and change in

entropies (ΔS). The difference in Gibbs free energies (ΔG) were calculated from these experimentally determined values. Experiments were duplicated (Appendix 1.1-1.6) and the system checked against literature data for β–CD:1-adamantanecarboxylic acid.[122,155]

9.3 Experimental for Chapter 4

6^A-Azido-6^A-deoxy-β-CD (4.1)
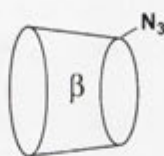
4.1

6^A-O-*p*-Toluenesulfonyl-β-CD **2.1** (12 g, 9.32 mmol) and sodium azide (12 g, 0.18 mol) were dissolved in H_2O (300 mL), and the mixture heated at 80 °C for 3 h before cooling to room temperature. The solution was concentrated *in vacuo* with the resulting solution (50 mL) added to vigorously stirred acetone (500 mL). The precipitate was separated and washed with acetone (3 × 50 mL) and diethyl ether (2 × 50 mL). The precipitate was resuspended in H_2O and lyophilised to give the title product **4.1** (9.9 g, 92%) as a white powder with physical and spectral properties that are consistent with literature values.[106]

TLC R_f: 0.35, *n*-BuOH/EtOH/H_2O, 5:4:3.

^{1}H NMR (300 MHz, d_6-DMSO) δ: 5.78-3.23 (m, 69H) ppm.

LRMS (ESI, +ve): *m/z* 1182 [M+Na]$^+$.

6^A-Amino-6^A-deoxy-β-CD (4.2)
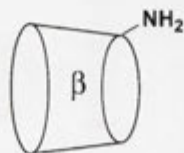
4.2

6^A-Azido-6^A-deoxy-β-CD **4.1** (9.5 g, 8.18 mmol) and PPh$_3$ (3.95 g, 0.015 mol) were dissolved in DMF (112 mL). An ammonia solution (28%, 26 mL) was added and the

reaction mixture stirred at room temperature for 24 h. The resulting solution (50 mL) was added to vigorously stirred acetone (500 mL) and the precipitate separated and washed with diethyl ether (50 mL) and acetone (100 mL). The crude material was resuspended in H_2O (250 mL) and applied to a Bio-Rex 70 cation exchange resin (H^+ form), which was then eluted with ammonia (500 mL, 0.1 mol L^{-3}). The eluant was concentrated *in vacuo* and lyophilised to yield the title compound **4.2** (3.2 g, 35%) as a white powder with physical and spectral properties that are consistent with literature values.[83]

TLC R_f: 0.45, *i*-PrOH/EtOH/H_2O/AcOH, 5:4:3:2.

^{1}H NMR (300 MHz, D_2O) δ: 4.95 (m, 7H), 3.87-3.72 (m, 26H), 3.54-3.42 (m, 13H), 3.35 (t, 1H, $J = 9.6$ Hz), 3.05 (d, 1H, $J = 14.0$ Hz), 2.75 (dd, 1H, $J = 7.0$ Hz, $J = 14.0$ Hz) ppm.

LRMS (ESI, +ve): *m/z* 1134 $[M+H]^+$.

HPLC t_R 4.3 min. [Column: YMC ODS-AQ, 250 × 20 mm; MeCN/H_2O (10:90), flow rate: 10 mL min^{-1}].

trans-6^A-Deoxy-6^A-cinnamido-β-CD (4.3)
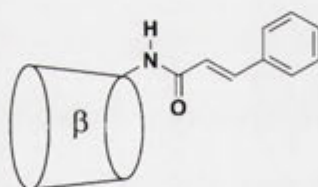
4.3

6^A-Amino-6^A-deoxy-β-CD **4.2** (1 g, 0.88 mmol) and TEA (159 μL) were dissolved in anhydrous DMF (25 mL), and the solution cooled to −5 °C. *trans*-Cinnamoyl chloride (190 mg, 1.15 mmol) was added and the reaction mixture warmed to room temperature before stirring for 3 h. H_2O (1 mL) was added and the resulting solution added dropwise to vigorously stirred acetone (500 mL). The precipitate was separated and washed with acetone (3 × 50 mL) and diethyl ether (2 × 50 mL), before it was applied to Toyoperl DEAE-650M anion exchange resin, and then Toyoperl SP-650M cation-exchange resin. The eluant was concentrated *in vacuo* and the residue resuspended in MeCN/H_2O (15:85) before being applied to preparative HPLC. The desired HPLC fractions were

concentrated *in vacuo* and lyophilised to give the title compound **4.3** (315 mg, 28%) as a white powder.

m.p. 285-290 °C dec.

TLC R_f: 0.52, *n*-BuOH/EtOH/H$_2$O, 5:4:3.

^{1}H NMR (500 MHz, D$_2$O) δ: 7.63-7.54 (m, 6H, Ar, CH), 6.55 (d, 1H, J = 16.5 Hz, CH), 5.14-4.95 (m, 7H), 4.33-3.20 (m, 42H) ppm. In addition a low intensity doublet was observed at δ 6.86 (d, J = 16.0 Hz, CH) for the olefinic signal of the *E*-amide isomer.

^{13}C NMR (125 MHz, d_6-DMSO) δ: 165.2, 138.8, 135.0, 129.4, 128.9, 127.5, 122.1, 102.2, 102.0, 83.7, 81.6, 73.0, 72.4, 72.0, 67.7, 60.0 ppm.

LRMS (ESI, +ve): *m/z* 1264 [M+H]$^+$; **HRMS** (ESI, +ve): Found *m/z* 1264.436. Calculated *m/z* for C$_{51}$H$_{78}$NO$_{35}$ [M+H]$^+$ is 1264.435.

Elemental analysis Found C, 44.75; H, 6.55; N, 0.98%. C$_{55}$H$_{77}$NO$_{35}$·6H$_2$O requires C, 44.64%; H, 6.54%; N, 1.02%.

λ_{MAX}: 277 nm; ε: 44640 M^{-1} cm^{-1} (H$_2$O).

HPLC t_R 13 min. [Column: Alltech Altima C18, 250 × 10 mm; MeCN/H$_2$O (15:85), flow rate: 3 mL min^{-1}].

cis-6^A-Deoxy-6^A-cinnamido-β-CD (4.4)

4.4
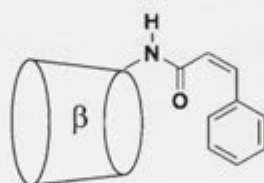
trans-6^A-Deoxy-6^A-cinnamido-β-CD **4.3** (50 mg, 0.04 mmol) was dissolved in H$_2$O (20 mL), in a quartz round-bottom flask, and the solution was irradiated at 300 nm for 2 h, then it was concentrated to dryness. The crude residue was resuspended in MeCN/H$_2$O (15:85) and applied to semi-preparative HPLC. The desired HPLC fractions were concentrated *in vacuo* and lyophilised to give the title compound **4.4** (18 mg, 35%) as a white powder.

m.p. 285-290 °C dec.

TLC R_f: 0.42, *n*-BuOH/EtOH/H$_2$O, 5:4:3.

¹H NMR (500 MHz, D$_2$O) δ: 7.54-7.42 (m, 3H, Ar), 7.28 (d, 2H, J = 7.5 Hz, Ar), 6.91 (d, 1H, J = 12.0 Hz, CH), 6.20 (d, 1H, J = 12.0 Hz, CH), 5.16–5.01 (m, 7H), 4.16-3.02 (m, 42H) ppm. In addition low intensity doublets were observed at δ 6.62 (d, J = 13.0 Hz, CH) and at δ 6.19 (d, J = 13.0 Hz, CH) for the olefinic signals, respectively, of the *E*-amide isomer.

¹³C NMR (125 MHz, d_6-DMSO)δ: 166.2, 136.1, 135.3, 129.6, 128.2, 127.9, 124.3, 102.3, 102.0, 83.8, 81.7, 81.4, 73.1, 72.4, 72.1, 69.6, 59.8 ppm.

LRMS (ESI, +ve): m/z 1286 [M+Na]$^+$; **HRMS** (ESI, +ve): Found m/z 1264.439. Calculated m/z for C$_{51}$H$_{78}$NO$_{35}$ [M+H]$^+$ is 1264.435.

Elemental analysis Found C, 44.21; H, 6.36; N, 0.93%. C$_{55}$H$_{77}$NO$_{35}$·7H$_2$O requires C 44.06; H, 6.60; N, 1.01%.

λ_{MAX}: 251 nm; ε: 20641 M^{-1} cm^{-1} (H$_2$O).

HPLC t_R 5.8 min. [Column: Alltech Altima C18, 250 × 10 mm; MeCN/H$_2$O (15:85), flow rate: 3 mL min^{-1}].
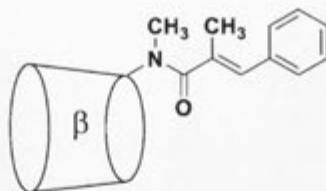
trans-α-Methylcinnamoyl chloride (4.6)

4.6
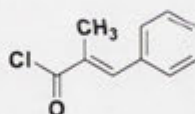
trans-α-Methylcinnamic acid **4.5** (200 mg, 1.23 mmol) in 10 mL of DCM, oxalyl chloride 2M in DCM (470 mg, 3.69 mmol) and a catalytic amount of DMF (2 drops of a solution of 3 drops of DMF in 1 mL of DCM) was stirred at 0 °C. After 10 min, the reaction mixture was allowed to warm to room temperature and stirred for 3 h. The solvent was removed *in vacuo* and the solid resuspended in DCM (2 mL) before again concentrating *in vacuo* to yield the title compound **4.6** (197 mg, 89 %) as a light yellow powder with physical and spectral properties that are consistent with literature values.[156]

m.p. 47-50 °C.

¹H NMR (300 MHz, CDCl$_3$) δ: 8.05 (s, 1H, CH), 7.46-7.40 (m, 5H, Ar), 2.20 (s, 3H, CH$_3$) ppm.

¹³C NMR (75 MHz, CDCl$_3$) δ: 170.6, 147.9, 135.0, 132.9, 130.5, 130.2, 129.1, 15.6 ppm.

LRMS (EI): m/z 180 [M$^+$].

***trans*-6^A-Deoxy-6^A-(*N*,α-dimethylcinnamido)-β-CD (4.7)**

4.7

6^A-Deoxy-6^A-methylamino-β-CD **2.2** (300 mg, 0.261 mmol) and TEA (50 µL) were dissolved in anhydrous DMF (4 mL) at −5 °C. *trans*-α-Methylcinnamoyl chloride **4.6** (56 mg, 0.313 mmol) in DMF (0.5 mL) was added and the reaction mixture gradually warmed to room temperature. The mixture was stirred for 48 h with an additional portion of the chloride **4.6** (56 mg, 0.313 mmol) and TEA (25 µL) added after 30 h. The reaction was quenched with H_2O (1 mL) and the resulting solution added dropwise to vigorously stirred acetone (150 mL). The precipitate was separated and washed with acetone (3 × 50 mL) and diethyl ether (2 × 50 mL), before it was applied to Toyoperl DEAE-650M anion exchange resin, and then Toyoperl SP-650M cation-exchange resin. The eluant was concentrated *in vacuo* and the residue resuspended in MeCN/H_2O (10:90) before being applied to semi-preparative HPLC. The desired HPLC fractions were concentrated *in vacuo* and lyophilised to give the title compound **4.7** (144 mg, 43 %) as a white powder.

m.p. 282-287 °C dec.

TLC R_f: 0.37, *n*-BuOH/EtOH/H_2O, 5:4:3.

¹H NMR (500 MHz, D_2O) δ: 7.67-7.30 (m, 5H, Ar), 6.35 (s, 1H, CH), 5.15-4.98 (m, 7H), 4.26-3.29 (m, 42H), 3.11 (s, 3H, CH_3), 2.04 (s, 3H, CH_3) ppm.

¹³C NMR (125 MHz, D_2O) δ: 179.0, 137.5, 135.8, 132.8, 132.2, 131.5, 130.8, 103.4, 77.0, 75.8, 74.9, 73.8, 62.2, 39.9, 17.8 ppm.

LRMS (ESI, +ve): *m/z* 1293 [M+H]⁺; **HRMS** (ESI, +ve): Found *m/z* 1292.469. Calculated *m/z* for $C_{52}H_{82}NO_{35}$ [M+H]⁺ is 1292.467.

Elemental analysis Found C, 46.28; H, 6.44; N, 1.13%. $C_{53}H_{81}NO_{35} \cdot 5H_2O$ requires C, 44.05%; H, 6.64%; N, 1.01%.

λ_{MAX}: 254 nm; ε: 20653 $M^{-1}cm^{-1}$ (H_2O).

HPLC t_R 8.6 min. [Column: Prevail C18, 250 × 10 mm; MeCN/H$_2$O (10:90), flow rate: 3 mL min^{-1}].

Photochemical Isomerisation of the Hermaphrodites 4.3 and 4.4

Solution. The hermaphrodite **4.3** (1.5 mg, 1.19 µmol) was made up to a concentration of 5.87 × 10^{-5} M in H$_2$O (20 mL).

Irradiation. The solution of the hermaphrodite **4.3** was analysed by injecting 20 µL onto an analytical reverse-phase HPLC column. An aliquot (1 mL) of the same solution was sealed in a quartz cuvette and studied using UV/visible spectrometry. The cuvette containing the solution was then placed in a photolysis reactor and irradiated with ten 300 nm UV-B lamps for 100 sec. The cuvette was then placed in the UV/visible spectrometer and the irradiated solution analysed. An aliquot (20 µL) of this solution was then injected onto the analytical reverse-phase HPLC column. The cuvette containing the solution was then placed back in the photolysis reactor and irradiated with ten 254 nm UV-C lamps for 60 sec. The solution was then analysed with UV/visible spectroscopy and analytical reverse-phase HPLC.

HPLC. [Column: YMC ODS-AQ, 250 × 4.6 mm; MeCN/H$_2$O (15/85), flow rate: 1 mL min^{-1}].

Dissociation Titrations for the Hermaphrodites 4.3, 4.4, 2.4 and 4.7

Buffer. Phosphate buffer (0.05 M) was prepared by combining Na$_2$HPO$_4$ (24 mM) and NaH$_2$PO$_4$ (26 mM) in H$_2$O and adjusted to pH 6.9 with NaOH.

Microcalorimetry. Isothermal titration calorimetry experiments were conducted at 25 °C with each titration consisting of 16 successive injections (1 × 3 µL, 15 × 5 µL) of a degassed solution of the CD (5 mM) in 0.05 M phosphate buffer (pH 6.9). The titrant was injected into a thermostated reaction cell containing a known volume (1.44 mL) of identical degassed buffer. Injection duration was 16.6 s every 180 s and the solutions were stirred at 450 rpm. Independent buffer heat of dilution experiments were

conducted and used to correct the complexation experiments. MicroCal® Origin software was used to determine the dissociation constant (K_D) and change in enthalpy (ΔH) for intermolecular species. Experiments were duplicated (Appendix 1.11-1.12).

^{1}H NMR Titrations for the Hermaphrodites 4.3, 4.4 and 4.7 with 1-adamantanol "fuel"

Titration. The hermaphrodites **4.3**, **4.4** and **4.7** (3 mg, 2.3 µmol) were dissolved in D_2O (700 µL) at 25 °C. ^{1}H NMR spectra were recorded for the sequential addition of aliquots (5 × 20 µL, 5 × 0.46 µmol, to 1 equiv., and then 4 × 50 µL, 4 × 1.15 µmol, to 3 equiv.) of a solution of 1-adamantanol (3.5 mg, 23 µmol) in D_2O (1 mL). All spectra were referenced using a TSP internal standard. Integration of olefinic and methyl signals afforded the ratio of isomers at the start and end points of the titration with 1-adamantanol "fuel".

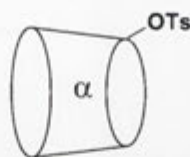## ^{1}H NMR Titrations for the Hermaphrodites 4.3, 4.4 and 4.7 with 1-adamantanecarboxylate "fuel"

Buffer and Titration. See Section 9.2.

Isothermal Titration Calorimetry for the Hermaphrodites 4.3, 4.4 and 4.7 with 1-adamantanecarboxylate "fuel"

Buffer and Microcalorimetry. See Section 9.2.

## 9.4 Experimental for Chapter 5

6^A^-*O*-Toluenesulfonyl-α-CD (5.1)

5.1

Dried α-CD **1.9** (8 g, 8.22 ×10^{-3} mol) was dissolved in pyridine (800 mL) and the solution cooled to 0 - 5 °C in an ice-water bath. Small portions of *p*-toluenesulfonyl chloride (8 g, 42.1 × 10^{-3} mol) were added to the chilled solution and the yellow mixture allowed to room temperature. The reaction was monitored by TLC (*n*-BuOH/EtOH/H$_2$O, 5:4:3) until equal quantities of the di- and mono-tosylates were observed (3.5 h). The reaction was quenched with H$_2$O (50 mL) and the solution concentrated (*ca.* 100 mL) before a final portion of H$_2$O was added (50 mL). The concentrate was added dropwise to vigorously stirred ice-cold acetone (3.5 L) and the fine precipitate left to settle over night. The precipitate was isolated by filtration and resuspended in H$_2$O (300 mL), which was applied to a Diaion HP-20 column (340 × 25 mm). The column was flushed with H$_2$O (2 L) to remove unreacted α-CD **1.9** and then treated with a gradient solvent system from 10% - 30% MeOH-H$_2$O in 10% increments (3 × 2 L). The fractions containing the desired compound were combined and concentrated *in vacuo*. The concentrate was lyophilised to yield the title compound **5.1** (2.2 g, 24%) as a white powder with physical and spectral properties that are consistent with literature values.[157]

m.p. 159-161 °C dec.

TLC R_f: 0.53, *n*-BuOH/EtOH/H$_2$O, 5:4:3.

^{1}H NMR (300 MHz, D$_2$O) *δ*: 7.63 (d, 2H, *J* = 8.4 Hz, Ar), 7.33 (d, 2H, *J* = 8.4 Hz, Ar), 4.82-3.23 (m, 42H), 2.25 (s, 3H, CH$_3$) ppm.

LRMS (ESI, +ve): *m/z* 1149 [M+Na]$^+$.

6^A-Deoxy-6^A-methylamino-α-CD (5.2)
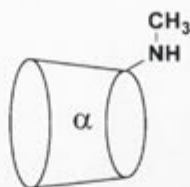
5.2

In a Schlenk tube under argon, 6^A-O-*p*-toluenesulfonyl-α-CD **5.1** (2.0 g, 1.77 mmol) and a catalytic amount of KI (40 mg, 0.26 mmol) were combined in anhydrous NMP (5 mL). Methylamine in THF (2M, 5.6 mL, 11.6 mmol) was then added and the reaction heated at 80 °C for 48 h. The reaction mixture was added to vigorously stirred acetone (200 mL) to form a precipitate, which was sonicated (20 min) and centrifuged (10 min, 5000 rpm) to yield a white solid. The crude material was resuspended in H$_2$O (50 mL) before being applied to Toyoperl SP-650M cation-exchange resin. The eluant was concentrated *in vacuo* and lyophilised to give the title product **5.2** (1.51 g, 86 %) as an off-white powder.

TLC R_f. 0.28, *i*-PrOH/EtOH/H$_2$O/AcOH, 5:4:3:2.

^{1}H NMR (500 MHz, d_6-DMSO) δ. 5.57-5.45 (m, 12H), 4.83-4.80 (m, 6H), 4.55-4.40 (m, 5H), 3.80-3.30 (m, 35H), 2.93-2.68 (m, 2H), 2.30 (s, 3H, CH$_3$) ppm.

LRMS (ESI, +ve): *m/z* 986 [M+H]$^+$; **HRMS** (ESI, +ve): Found *m/z* 986.360. Calculated *m/z* for C$_{37}$H$_{64}$NO$_{29}$ [M+H]$^+$ is 986.357.

trans-4-(2-Phenylvinyl)benzoic acid (5.3)
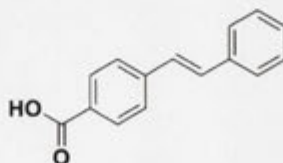
5.3

Following the method of Nishimura *et al.*,[135] 4-iodobenzoic acid (4.0g, 16 mmol) and styrene (1.8 mL, 14.9 mmol) were combined in dry THF (20 mL) with TEA (20 mL). To the solution palladium(II) acetate (75 mg, 0.33 mmol) and PPh$_3$ (94 mg, 0.35 mmol)
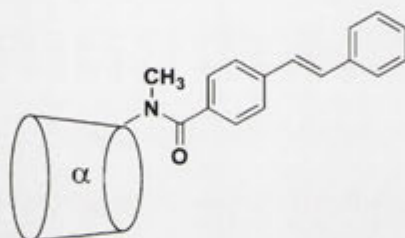
were added and the mixture was refluxed for 12 h. The solvent was removed *in vacuo* and the solid taken up in EtOAc (150 mL) and washed with H_2O (3 × 50 mL). The organic layer was concentrated *in vacuo* and the crude solid recrystallised from EtOAc and hexane to afford the title compound **5.3** (550 mg, 22%) as a light brown powder with physical and spectral properties that are consistent with literature values.[135]

TLC R_f: 0.3, EtOAc/Hexane, 1:1.

¹H NMR (500 MHz, d_6-DMSO) δ: 12.9 (br s, 1H, COOH), 7.95 (d, 2H, J = 7.0 Hz, Ar), 7.74 (d, 2H, J = 7.0 Hz, Ar), 7.66 (d, 2H, J = 7.0 Hz, Ar), 7.44-7.32 (m, 5H, CH, Ar) ppm.

LRMS (ESI, -ve): *m/z* 222.9 [M-H]⁻.

trans-6^A^-Deoxy-6^A^-(*N*-methylstilbenylamido)-α-CD (5.4)

5.4

6^A^-Deoxy-6^A^-methylamino-α-CD **5.2** (0.25 g, 0.25 mmol), *trans*-4-(2-phenylvinyl)benzoic acid **5.3** (73 mg, 0.33 mmol) and BOP (146 mg, 0.33 mmol) were combined in anhydrous DMF (2 mL). TEA (0.11 mL, 0.75 mmol) was added and the reaction mixture was stirred for 12 h. The resulting mixture was added dropwise to rapidly stirring acetone (100 mL) and the precipitate was separated by centrifugation and washed with acetone (3 × 50 mL) and then diethyl ether (3 × 50 mL). The solid was resuspended in H_2O (50 mL) and applied to Toyoperl DEAE-650M anion exchange resin, and then Toyoperl SP-650M cation-exchange resin. The eluant was concentrated *in vacuo* and the residue resuspended in MeCN/H_2O (25:75) before being applied to preparative HPLC. The desired HPLC fractions were concentrated *in vacuo* and lyophilised to give the title compound **5.4** (120 mg, 40%) as a white powder.

m.p. 275-278 °C dec.

TLC R_f: 0.55, *n*-BuOH/EtOH/H_2O, 5:4:3.

^{1}H NMR (500 MHz, D$_2$O) δ: 7.95 (d, 2H, Ar), 7.66-7.63 (m, 2H, Ar), 7.60-7.57 (m, 1H, Ar), 7.39-7.32 (m, 5H, Ar, CH), 7.14 (d, 1H, J = 16.5 Hz, CH), 5.26 (d, 1H, J = 2.5 Hz, CH), 5.20 (d, 1H, J = 2.5 Hz, CH), 5.08 (d, 1H, J = 3.0 Hz, CH), 5.05 (d, 1H, J = 3.0 Hz, CH), 5.00 (d, 1H, J = 3.0 Hz, CH), 4.91 (d, 1H, J = 3.0 Hz, CH), 4.26-3.33 (m, 34H), 3.20 (m, 1H, CH), 2.78 (m, 1H, CH), 2.16 (s, 3H, CH$_3$) ppm.

^{13}C NMR (125 MHz, D$_2$O) δ: 176.2, 139.8, 138.6, 138.0, 133.9, 132.7, 131.5, 130.3, 129.4, 129.3, 129.2, 105.2, 105.0, 104.8, 104.7, 86.9, 84.9, 84.2, 84.0, 83.7, 76.6, 76.3, 76.0, 75.8, 75.6, 75.1, 74.5 ppm.
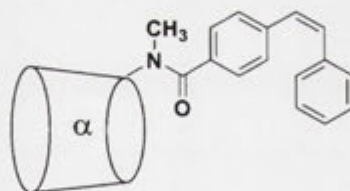
LRMS (ESI, +ve): *m/z* 1214.8 [M+Na]$^+$; **HRMS** (ESI, +ve): Found *m/z* 1192.428. Calculated *m/z* for C$_{52}$H$_{74}$NO$_{30}$ [M+H]$^+$ is 1192.430.

Elemental analysis Found C, 46.28; H, 6.50; N, 1.00%. C$_{52}$H$_{73}$NO$_{30}$·9H$_2$O requires C, 46.12%; H, 6.77%; N, 1.03%.

λ_{MAX}: 316 nm; ε: 31900 M^{-1} cm^{-1} (H$_2$O).

HPLC t_R 22.95 min. [Column: YMC ODS-AQ, 250 × 20 mm; MeCN/H$_2$O (25:75), flow rate: 10 mL min^{-1}].

cis-6^A-Deoxy-6^A-(*N*-methylstilbenylamido)-α-CD (5.5)

5.5

trans-6^A-Deoxy-6^A-(*N*-methylstilbenylamido)-α-CD **5.4** (50 mg, 0.04 mmol) was dissolved in MeOH (300 mL) and the mixture irradiated for 2.5 min at 350 nm (10 UV-A lamps) in a photolysis reactor. After irradiation the solution was concentrated *in vacuo* and the residue resuspended in MeCN/H$_2$O (25:75) before being applied to preparative HPLC. The desired HPLC fractions were concentrated *in vacuo* and lyophilised to give the hermaphrodite **5.5** (32 mg, 75 %) as a white powder.

m.p. 280-285 °C dec.

TLC R_f: 0.55, *n*-BuOH/EtOH/H$_2$O, 5:4:3.

¹H NMR (500 MHz, D_2O) δ: 7.37-7.27 (m, 9H, Ar), 6.84-6.72 (m, 2H, CH), 5.13-4.92 (m, 6H), 4.38-3.21 (m, 36H), 3.11 (s, 3H, CH_3). In addition a low intensity singlet was observed at δ 3.05 ppm for the methyl signal of the *E*-amide isomer.

¹³C NMR (75 MHz, D_2O) δ: 176.0, 142.3, 139.8, 136.3, 134.6, 132.3, 131.8, 131.7, 131.3, 130.4, 129.7, 104.3-104.0, 86.8, 84.1, 83.8, 83.4, 76.1, 74.9, 74.6, 73.1, 63.1, 52.8, 42.7, 37.1 ppm.

LRMS (ESI, +ve): m/z 1214.4 [M+Na]⁺; **HRMS** (ESI, +ve): Found m/z 1192.432. Calculated m/z for $C_{52}H_{74}NO_{30}$ [M+H]⁺ is 1192.430.

Elemental analysis Found C, 47.24; H, 6.44; N, 1.20%. $C_{52}H_{73}NO_{30}\cdot 7H_2O$ requires C, 47.38%; H, 6.65%; N, 1.06%.

λ_{MAX}: 286 nm; ε: 15100 M^{-1} cm^{-1} (H_2O).

HPLC t_R 18.25 min. [Column: YMC ODS-AQ, 250 × 20 mm; MeCN/H_2O (25:75), flow rate: 10 mL min^{-1}].

Photochemical Isomerisation of the Hermaphrodites 5.4 and 5.5

Solution. The hermaphrodite **5.4** (1.0 mg, 0.84 µmol) was made up to a concentration of 3.36×10^{-5} M in H_2O (25 mL).

Irradiation. From the solution of the hermaphrodite **5.4** an aliquot (20 µL) was injected onto an analytical reverse-phase HPLC column while a separate aliquot (1 mL) of the same solution was sealed in a quartz cuvette and analysed using UV/visible spectrometry. This cuvette was then placed in a photolysis reactor and irradiated with ten 350 nm UV-A lamps for 2.5 min. The cuvette was then placed in the UV/visible spectrometer and the irradiated solution analysed. An aliquot (20 µL) of this solution was then injected onto the analytical reverse-phase HPLC column. The cuvette containing the solution was then placed back in the photolysis reactor and irradiated with ten 254 nm UV-C lamps for 0.5 min. After which the solution was again analysed with UV/visible spectroscopy and analytical reverse-phase HPLC.
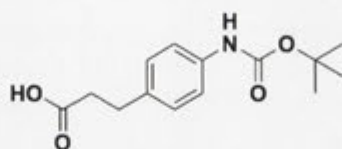
HPLC. [Column: YMC ODS-AQ, 250 × 4.6 mm; MeCN/H_2O (25/75), flow rate: 1 mL min^{-1}].

Dissociation Titrations for the Hermaphrodites 5.4 and 5.5

Buffer and Microcalorimetry. See Section 9.3. Experiments were duplicated (Appendix 1.13).

9.5 Experimental for Chapter 6

3-(4-tert-Butyloxycarbonylaminophenyl)propionic acid (6.1)


6.1

Following the method of Lu *et al.*,[143] di-*tert*-butyl-dicarbonate (2 g, 9.2 mmol) in aqueous dioxane (1:1, 3.5 mL) was added dropwise to a solution of 3-(4-aminophenyl)propionic acid (1.0 g, 6.1 mmol) in aqueous dioxane (1:1, 3.5 mL) and TEA (1.3 mL , 9.2 mmol) at 0 °C. The mixture was stirred at 0 °C for 6 h before H_2O (30 mL) and EtOAc (40 mL) were added and the organic layer discarded. The aqueous layer was acidified with citric acid (6 N) and extracted three times with EtOAc (3 × 50 mL). The separated organic layer was dried over $MgSO_4$ and concentrated *in vacuo* to afford the title product **6.1** (1.78 g, 92%) as a pale yellow powder.

m.p. 190-193 °C.

^{1}H NMR (500 MHz, d_6-DMSO) δ: 12.1 (bs, 1H, COOH), 9.25 (s, 1H, NH), 7.36 (d, 2H, J = 8.5 Hz, Ar), 7.11 (d, 2H, J = 8.5 Hz, Ar), 2.75 (t, 2H, J = 7.5 Hz, CH_2), 2.49 (t, 2H, J = 7.5 Hz, CH_2), 1.48 (s, 9H, *t*-Bu).

^{13}C NMR (125 MHz, d_6-DMSO)δ: 174.5, 153.5, 138.2, 135.1, 129.0, 118.8, 79.5, 36.1, 30.9, 28.8 ppm.

LRMS (ESI, +ve): *m/z* 288 [M+Na]$^+$; **HRMS** (ESI, +ve): Found *m/z* 288.121. Calculated *m/z* for $C_{14}H_{19}NO_4Na$ [M+Na]$^+$ is 288.121.

6^A-Deoxy-6^A-(*N*-methyl-3-(4-aminophenyl)propionamido)-β-CD (6.3)
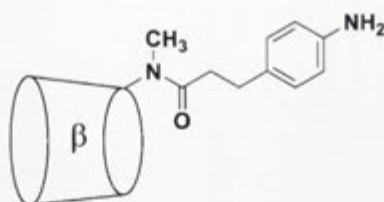
6.3

6^A-Deoxy-6^A-methylamino-β-CD **2.2** (0.3 g, 0.26 mmol), 3-(4-*tert*-butyloxycarbonylaminophenyl)propionic acid **6.1** (0.09 g, 0.34 mmol) and BOP (0.15 g, 0.34 mmol) were combined in anhydrous DMF (2 mL). TEA (0.11 mL, 0.75 mmol) was added and the reaction mixture was stirred for 24 h. The resulting mixture was added dropwise to rapidly stirring acetone (100 mL) and the precipitate was separated and washed with diethyl ether (2 × 50 mL). The solid was resuspended in H_2O (60 mL) and applied to Toyoperl DEAE-650M anion exchange resin, and then Toyoperl SP-650M cation-exchange resin. The eluant was concentrated and lyophilised to give the BOC protected precursor **6.2** (130 mg, 36%) as a white powder. The BOC protected precursor **6.2** (130 mg, 0.09 mmol) was dissolved in 4 M HCl (25 mL) at 0 °C then allowed to room temperature and stirred for 2 h. The mixture was then neutralised with 4 M NaOH and applied directly to a Diaion HP-20 column (250 × 15 mm). The eluant was concentrated *in vacuo* and the residue resuspended in MeCN/H_2O (15:85) before being applied to preparative HPLC. The desired HPLC fractions were concentrated *in vacuo* and lyophilised to give the title compound **6.3** (108 mg, 90%) as a white powder.

m.p. 280-283 °C dec.

TLC R_f: 0.3, *n*-BuOH/EtOH/H_2O, 5:4:3.

^{1}H NMR (500 MHz, D_2O) δ: 7.04 (d, 2H, J = 8.5 Hz, Ar), 6.93 (d, 2H, J = 8.5 Hz, Ar), 5.15-5.03 (m, 7H), 4.21 (d, 1H), 4.03-3.29 (m, 41H), 3.07 (s, 3H, CH_3), 2.90 (m, 1H, CH_2), 2.58 (m, 3H, CH_2) ppm. In addition low intensity doublets at δ 7.02 (d, J = 8.0 Hz, Ar) and δ 6.82 (d, J = 8.0 Hz, Ar), and a low intensity singlet were observed at δ 3.00 ppm for the aromatic and methyl signals, respectively, of the *Z*-amide isomer.

^{13}C NMR (75 MHz, D_2O) δ: 178.1, 147.7, 134.0, 131.0, 119.5, 105.0, 104.6, 104.5, 103.3, 85.8, 84.0, 83.9, 83.6, 82.4, 76.8, 76.0, 74.8, 74.3, 62.9, 62.1, 54.8, 40.2, 37.7, 34.4 ppm.

LRMS (ESI, +ve): *m/z* 1318 [M+Na]$^+$; **HRMS** (ESI, +ve): Found *m/z* 1295.482. Calculated *m/z* for $C_{52}H_{83}N_2O_{35}$ [M+H]$^+$ is 1295.478.

Elemental analysis Found C, 44.30; H, 6.61; N, 1.98%. $C_{52}H_{82}N_2O_{35}\cdot 6H_2O$ requires C, 44.51%; H, 6.75%; N, 2.00%.

HPLC t_R 6.8 min. [Column: Alltech Prevail C18, 250 × 10 mm; MeCN/H_2O (15/85), flow rate: 3 mL min^{-1}].

3-(4-*tert*-Butyloxycarbonylaminophenyl)acetic acid (6.4)


6.4
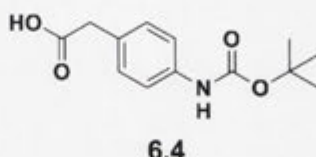
4-Aminophenylacetic acid (1g, 6.6 mmol) and TEA (0.96 mL, 6.6 mmol) were combined in DMF (10 mL) before di-*tert*-butyl-dicarbonate (2.04g, 7.28 mmol) was added. After 4 h, H_2O (30 mL) and EtOAc (40 mL) were added and the organic layer discarded. The aqueous layer was acidified with citric acid (6 N) and extracted three times with EtOAc (3 × 100 mL). The extracts were combined and washed with H_2O (250 mL) and dried over anhydrous $MgSO_4$. The solvent was removed *in vacuo* to give the title compound **6.4** (0.85 g, 51 %) as a pale yellow powder with physical and spectral properties that are consistent with literature values.[144]

m.p. 138-143 ^{o}C.

^{1}H NMR (300 MHz, d_6-DMSO) δ: 12.26 (bs, 1H, COOH), 9.33 (s, 1H, NH), 7.37 (d, 2H, *J* = 8.4 Hz, Ar), 7.11 (d, 2H, *J* = 8.4 Hz, Ar), 3.48 (s, 2H, CH_2), 1.48 (s, 9H, *t*-Bu).

LRMS (EI): m/z 251.1 [M$^{+\cdot}$].

6^A-Deoxy-6^A-(*N*-methyl-3-(4-aminophenyl)acetonamido)-β-CD (6.6)

6.6
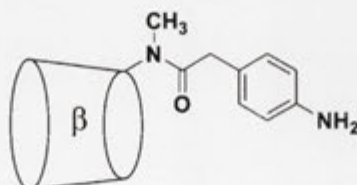
6^A-Deoxy-6^A-methylamino-β-CD **2.2** (0.25 g, 0.22 mmol), 3-(4-*tert*-butyloxycarbonylaminophenyl)acetic acid **6.4** (85 mg, 0.34 mmol) and BOP (0.15 g,

0.34 mmol) were combined in anhydrous DMF (2 mL). TEA (0.11 mL, 0.75 mmol) was added and the reaction mixture was stirred for 12 h. The resulting mixture was added dropwise to rapidly stirring acetone (100 mL) and the precipitate was separated and washed with diethyl ether (2 × 50 mL). The solid was resuspended in H_2O (60 mL) and applied to Toyoperl DEAE-650M anion exchange resin, and then Toyoperl SP-650M cation-exchange resin. The eluant was concentrated and lyophilised to give the BOC protected precursor **6.5** (156 mg, 52%) as a white powder. The BOC precursor **6.5** (130 mg, 0.09 mmol) was dissolved in 4 M HCl (25 mL) at 0 °C then allowed to room temperature and stirred for 2 h. The mixture was then neutralised with 4 M NaOH and applied directly to a Diaion HP-20 column (250 × 15 mm). The eluant was concentrated *in vacuo* and the residue resuspended in MeCN/H_2O (25:75) before being applied to preparative HPLC. The desired HPLC fractions were concentrated *in vacuo* and lyophilsed to give the title compound **6.6** (78 mg, 65%) as a white powder.

m.p. 295-297 °C dec.

TLC R_f: 0.33, *n*-BuOH/EtOH/H_2O, 5:4:3.

¹H NMR (500 MHz, D_2O) δ: 7.00 (d, 2H, J = 8.0 Hz, Ar), 6.83 (d, 2H, J = 8.0 Hz, Ar), 5.18-4.98 (m, 7H), 4.12-3.37 (m, 44H), 3.07 (s, 3H, CH_3) ppm. In addition low intensity doublets at δ 7.10 (d, J = 8.0 Hz, Ar) and δ 6.86 (d, J = 8.0 Hz, Ar), and a low intensity singlet were observed at δ 3.11 ppm for the aromatic and methyl signals, respectively, of the *Z*-amide isomer.

¹³C NMR (75 MHz, d_6-DMSO) δ: 171.9, 171.0, 146.8, 129.6, 129.4, 123.15, 122.5, 113.8, 102.1, 84.6, 84.1, 82.0, 81.6, 73.0, 72.5, 72.4, 72.0, 69.3, 68.5, 59.9, 59.3, 38.2, 36.5, 33.5 ppm.

LRMS (ESI, +ve): m/z 1304 [M+Na]⁺; **HRMS** (ESI, +ve): Found m/z 1281.463. Calculated m/z for $C_{51}H_{80}N_2O_{35}$ [M+H]⁺ is 1281.462.

Elemental analysis Found C, 44.17; H, 6.54; N, 2.14%. $C_{51}H_{80}N_2O_{35} \cdot 6H_2O$ requires C, 44.09%; H, 6.67%; N, 2.02%.

HPLC t_R 6.2 min. [Column: Grace Prevail Carbohydrate ES 9u, 300 × 20 mm; MeCN/H_2O (25/75), flow rate: 10 mL min⁻¹].

6^A-Deoxy-6^A-(*N*-methyl-3-(3-pyridyl)propionamido)-β-CD (6.8)
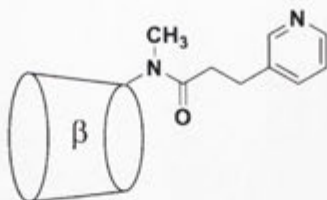
6.8

6^A-Deoxy-6^A-methylamino-β-CD **2.2** (0.2 g, 0.17 mmol), 3-(3-pyridyl)propionic acid **6.7** (44 mg, 0.29 mmol) and BOP (0.1 g, 0.29 mmol) were combined in anhydrous DMF (1.5 mL). TEA (72 μL, 0.52 mmol) was added and the reaction mixture was stirred for 12 h. The resulting mixture was added dropwise to rapidly stirring acetone (100 mL) and the precipitate was separated and washed with diethyl ether (2 × 50 mL). The solid was resuspended in H_2O (60 mL) and applied to Toyoperl DEAE-650M anion exchange resin. The eluant was concentrated *in vacuo* and the residue resuspended in MeCN/H_2O (15:85) before being applied to preparative HPLC. The desired HPLC fractions were concentrated and lyophilised to give the compound **6.8** (165 mg, 74%) as a white powder. **m.p.** 270-275 °C dec.

TLC R_f: 0.2, *n*-BuOH/EtOH/H_2O, 5:4:3.

¹H NMR (500 MHz, D_2O) δ: 8.58 (d, 1H, *J* = 5.0 Hz, Ar), 8.42 (s, 1H, Ar), 7.77 (d, 1H, *J* = 8.0 Hz, Ar), 7.56 (m, 1H, Ar), 5.11-5.00 (m, 7H), 4.20 (m, 1H), 4.00-3.33 (m, 41H), 3.08 (s, 3H, CH_3), 3.08-2.59 (m, 4H, CH_2). In addition a low intensity signal at δ 7.46 (m, Ar) and a low intensity singlet were observed at δ 3.09 ppm for the aromatic and methyl signals of the *Z*-amide isomer.

¹³C NMR (75 MHz, D_2O) δ: 177.1, 150.8, 150.2, 139.6, 139.3, 127.2, 105.1, 104.9, 104.7, 104.4, 103.7, 85.7, 83.8, 82.8, 76.4, 76.0, 74.9, 62.9, 62.1, 54.7, 40.0, 37.2, 32.4 ppm.

LRMS (ESI, +ve): m/z 1281.7 $[M+H]^+$; HRMS (ESI, +ve): Found m/z 1281.462. Calculated m/z for $C_{51}H_{81}N_2O_{35}$ $[M+H]^+$ is 1281.462.

Elemental analysis Found C, 43.46; H, 6.65; N, 1.85%. $C_{51}H_{80}N_2O_{35}$·$7H_2O$ requires C, 43.53%; H, 6.73%; N, 1.99%.

HPLC t_R 6.1 min. [Column: Alltech Prevail C18, 250 × 10 mm; MeCN/H_2O (15/85), flow rate: 3 mL min^{-1}].

Dissociation Titrations for the Hermaphrodites 6.3, 6.6 and 6.8

Buffer. NaH_2PO_4 (0.05 M) in H_2O and adjusted to pH 2.0 with HCl. $Na_2B_4O_7 \cdot 10H_2O$ buffer (0.05 M) was prepared in H_2O and adjusted to pH 9.0 with NaOH.

Microcalorimetry. Isothermal titration calorimetry experiments were conducted at 25 °C with each titration consisting of 16 successive injections (1 × 3 µL, 15 × 5 µL) of a degassed solution of the CD (5 mM) in either 0.05 M borate buffer (pH 9.0) or 0.05 M phosphate buffer (pH 2.0). The titrant was injected into a thermostated reaction cell containing a known volume (1.44 mL) of identical degassed buffer. Injection duration was 16.6 s every 180 s and the solutions were stirred at 450 rpm. Independent buffer heat of dilution experiments were conducted and used to correct the complexation experiments. Experiments were duplicated (Appendix 1.14-1.16).

Measuring the pK_a of the Hermaphrodites 6.3, 6.6 and 6.8 using ^{1}H NMR Spectroscopy

Titration. The chosen CD (9 mg, 7 µmol) was dissolved in 1.6 mL of unbuffered D_2O. To this, an aliquot (2-20 µL) of a solution of deuterium chloride in D_2O (6 µL in 1 mL) was added before the pH was measured and then a 1D ^{1}H NMR spectrum recorded. All spectra were referenced using a TSP internal standard. The titration was continued until no change in δ ppm of the amide methyl peaks was observed. Integration of amide peaks afforded the ratio of isomers at the start and end points of the pKa titration.

9.6 Experimental for Chapter 7

^{1}H NMR Titrations for the Hermaphrodites 6.3, 6.6 and 6.8 with 1-aminoadamantane "fuel" and TNS

Buffer. NaH_2PO_4 (0.05 M) in D_2O and adjusted to pH 2.0 with DCl. $Na_2B_4O_7 \cdot 10H_2O$ buffer (0.05 M) was prepared in D_2O and adjusted to pH 9.0 with NaOD.

Titration. The hermaphrodites **6.3**, **6.6** and **6.8** (3 mg, 2.3 μmol) were dissolved in D_2O (700 μL) with either phosphate buffer (0.05 M, pH 2.0) or borate buffer (0.05 M, pH 9.0) at 25 °C. ^1H NMR spectra were recorded after the sequential addition of aliquots (5 × 20 uL, 5 × 0.46 umol, to 1 equiv., and then 4 × 50 uL, 4 × 1.15 μmol, to 3 equiv.) of a solution of 1-aminoadamantane (4.4 mg, 23 μmol) in identical buffered D_2O (1 mL). Identical protocol was followed for the hermaphrodite **6.6** and TNS (8.2 mg, 23 μmol). All spectra were referenced using a TSP internal standard. Integration of amide methyl signals afforded the ratio of isomers at the start and end points of the titration with 1-aminoadamantane "fuel".

Isothermal Titration Calorimetry for the Hermaphrodites 6.3, 6.6 and 6.8 with 1-aminoadamantane "fuel"

Buffer. NaH_2PO_4 (0.05 M) in H_2O and adjusted to pH 2.0 with HCl. $Na_2B_4O_7 \cdot 10H_2O$ buffer (0.05 M) was prepared in H_2O and adjusted to pH 9.0 with NaOH.

Microcalorimetry. Isothermal titration calorimetry experiments were conducted at 25 °C with each titration consisting of 60 successive injections (1 × 3 μL, 59 × 5 μL) of a degassed solution of 1-aminoadamantane (26 mM) in either 0.05 M borate buffer (pH 9.0) or 0.05 M phosphate buffer (pH 2.0). The titrant was injected into a thermostated reaction cell containing a known volume (1.44 mL) of the CD (0.92-4.00 mM) in identical degassed buffer. Injection duration was 16.6 s every 180 s and the solutions were stirred at 450 rpm. Independent heat of dilution experiments were conducted and used to correct the complexation experiments. Experiments were duplicated (Appendix 1.7-1.10) and the system checked against literature data for β–CD:1-aminoadamantane.[147]

References

(1)   Lehn, J.-M. *Science* **2002**, *295*, 2400-2403.

(2)   Lehn, J.-M. *Angew. Chem. Int. Ed.* **1988**, *27*, 89-112.

(3)   Cram, D. J. *Angew. Chem. Int. Ed.* **1988**, *27*, 1009-1020.

(4)   Pedersen, C. J. *Angew. Chem. Int. Ed.* **1988**, *27*, 1021-1027.

(5)   Reinhoudt, D. N.; Crego-Calama, M. *Science* **2002**, *295*, 2403-2407.

(6)   Balzani, V.; Credi, A.; Raymo, F. M.; Stoddart, J. F. *Angew. Chem. Int. Ed.* **2000**, *39*, 3348-3391.

(7)   Easton, C. J.; Lincoln, S. F.; Barr, L.; Onagi, H. *Chem. Eur. J.* **2004**, *10*, 3120-3128.

(8)   Balzani, V.; Credi, A.; Ferrer, B.; Silvi, S.; Venturi, M. *Top. Curr. Chem.*; Springer-Verlag Berlin Heidelberg, 2005; Vol. 262.

(9)   Schulz, M. *Nature* **1999**, *399*, 729-730.

(10)   Feynman, R. P. *Saturday Rev.* **1960**, 43, 45.

(11)   Feynman, R. P. *Eng. Sci.* **1960**, *23*, 22-36.

(12)   Kay, E. R.; Leigh, D. A. *Pure Appl. Chem.* **2008**, *80*, 17-29.

(13)   Shinkai, S.; Nakaji, T.; Nishida, Y.; Ogawa, T.; Manabe, O. *J. Am. Chem. Soc.* **1980**, *102*, 5860-5865.

(14)   Shinkai, S.; Nakaji, T.; Ogawa, T.; Shigematsu, K.; Manabe, O. *J. Am. Chem. Soc.* **1981**, *103*, 111-115.

(15)   Balzani, V. *Pure Appl. Chem.* **2008**, *80*, 1631-1650.

(16)   Anelli, P. L.; Spencer, N.; Stoddart, J. F. *J. Am. Chem. Soc.* **1991**, *113*, 5131-5133.

(17)   Altieri, A.; Bottari, G.; Dehez, F.; Leigh, D. A.; Wong, J. K. Y.; Zerbetto, F. *Angew. Chem. Int. Ed.* **2003**, *42*, 2296-2300.

(18)   Serreli, V.; Lee, C.-F.; Kay, E. R.; Leigh, D. A. *Nature* **2007**, *445*, 523-527.

(19)   Balzani, V.; Clemente-León, M.; Credi, A.; Ferrer, B.; Venturi, M.; Flood, A. H.; Stoddart, J. F. *Proc. Natl. Acad. Sci. USA* **2006**, *103*, 1178.

(20)   Jiménez, M. C.; Dietrich-Buchecker, C.; Sauvage, J.-P. *Angew. Chem. Int. Ed.* **2000**, *39*, 3284-3287.

(21)   Dawson, R. E.; Lincoln, S. F.; Easton, C. J. *Chem. Commun.* **2008**, 3980-3982.

(22) Jishan, W.; Ken Cham-Fai, L.; Diego, B.; Ja-Young, H.; Stuart , J. C.; Lei, F.; Stoddart, J. F. *Angew. Chem. Int. Ed.* **2008**, *47*, 7470-7474.

(23) Ashton, P. R.; Ballardini, R.; Balzani, V.; Boyd, S. E.; Credi, A.; Gandolfi, M. T.; Gómez-López, M.; Iqbal, S.; Philp, D.; Preece, J. A.; Prodi, L.; Ricketts, H. G.; Stoddart, J. F.; Tolley, M. S.; Venturi, M.; White, A. J. P.; Williams, D. J. *Chem. Eur. J.* **1997**, *3*, 152-170.

(24) Liu, Y.; Flood, A. H.; Stoddart, J. F. *J. Am. Chem. Soc.* **2004**, *126*, 9150-9151.

(25) *Molecular Switches*; Feringa, B. L., Ed.; WILEY-VCH: Weinheim, 2001.

(26) "Molecular Machines Special Issue" (Stoddart, J. F., Guest Ed.) *Acc. Chem. Res.* **2001**, *34*, 409-522.

(27) Kinbara, K.; Aida, T. *Chem. Rev.* **2005**, *105*, 1377-1400.

(28) Browne, W. R.; Feringa, B. L. *Nature Nanotech.* **2006**, *1*, 25-35.

(29) Kay, E. R.; Leigh, D. A.; Zerbrotto, F. *Angew. Chem. Int. Ed.* **2007**, *46*, 72-191.

(30) Balzani, V.; Credi, A.; Venturi, M. *Chem. Soc. Rev.* **2009**, *38*, 1542-1550.

(31) Silvi, S.; Venturi, M.; Credi, A. *J. Mater. Chem.* **2009**, *19*, 2279-2294.

(32) Villiers, A. *Compt. Rend.* **1891**, *112*, 536.

(33) Szejtli, J. *Chem. Rev.* **1998**, *98*, 1743-1754.

(34) Schardinger, F. *Unters. Nahr. u. Genussm.* **1903**, *6*, 865.

(35) Schardinger, F. *Zentralbl. Bakteriol. Parasitenk. Abt. 2* **1911**, *29*, 188.

(36) Freudenberg, K.; Meyer-Delius, M. *Ber. Dtsch. Chem. Ges.* **1938**, *71*, 1596.

(37) Szejtli, J. *Cyclodextrin Technology*; Kluwer: Dordrecht, 1988.

(38) Hingerty, B.; Saenger, W. *J. Am. Chem. Soc.* **1976**, *98*, 3357-3365.

(39) Casu, B.; Reggiani, M.; Gallo, G.; Vigevani, A. *Tetrahedron* **1966**, *22*, 3061-3083.

(40) Wolfram, S. *Angew. Chem. Int. Ed.* **1980**, *19*, 344-362.

(41) D'Souza, V. T.; Lipkowitz, K. B. *Chem. Rev.* **1998**, *98*, 1741-1742.

(42) Davis, M. E.; Brewster, M. E. *Nature Rev. Drug Discov.* **2004**, *3*, 1023-1035.

(43) *Cyclodextrins and Their Complexes*; Dodziuk, H., Ed.; Wiley-VCH: Weinheim, 2006.

(44) Connors, K. A. *Chem. Rev.* **1997**, *97*, 1325-1358.

(45) Liu, L.; Guo, Q.-X. *J. Incl. Phenom. Macrocycl. Chem.* **2002**, *42*, 1-14.

(46) Rekharsky, M. V.; Inoue, Y. *Chem. Rev.* **1998**, *98*, 1875-1917.

(47) Hallen, D.; Schon, A.; Shehatta, I.; Wadso, I. *J. Chem. Soc., Faraday Trans.* **1992**, *88*, 2859-2863.

(48) Hamai, S. *Bull. Chem. Soc. Jpn.* **1992**, *65*, 2323-2327.

(49) Kano, K.; Yoshiyasu, K.; Yasuoka, H.; Hata, S.; Hashimoto, S. *J. Chem. Soc., Perkin Trans. 2* **1992**, 1265-1269.

(50) Amato, M. E.; Djedaini-Pilard, F.; Perly, B.; Scarlata, G. *J. Chem. Soc., Perkin Trans. 2* **1992**, 2065-2069.

(51) Kinoshita, T.; Iinuma, F.; Tsuji, A. *Chem. Pharm. Bull.* **1974**, *22*, 2413-2420.

(52) Croft, A. K.; Easton, C. J.; Lincoln, S. F.; May, B. L.; Papageorgiou, J. *Aust. J. Chem.* **1997**, *50*, 857-860.

(53) Bouchemal, K. *Drug Discov. Today* **2008**, *13*, 960-972.

(54) Wiseman, T.; Williston, S.; Brandts, J.; Lin, L. *Anal. Biochem.* **1989**, *179*, 131-137.

(55) Bjelic, S.; Jelesarov, I. *J. Mol. Recognit.* **2008**, *21*, 289-312.

(56) Holdgate, G. A.; Ward, W. H. J. *Drug Discov. Today* **2005**, *10*, 1543-1550.

(57) Anderson, S.; Anderson, H. L.; Sanders, J. K. M. *Acc. Chem. Res.* **1993**, *26*, 469-475.

(58) Nepogodiev, S. A.; Stoddart, J. F. *Chem. Rev.* **1998**, *98*, 1959-1976.

(59) Ogino, H. *J. Am. Chem. Soc.* **1981**, *103*, 1303-1304.

(60) Murakami, H.; Kawabuchi, A.; Kotoo, K.; Kunitake, M.; Nakashima, N. *J. Am. Chem. Soc.* **1997**, *119*, 7605-7606.

(61) Murakami, H.; Kawabuchi, A.; Matsumoto, R.; Ido, T.; Nakashima, N. *J. Am. Chem. Soc.* **2005**, *127*, 15891-15899.

(62) Stanier, C. A.; Alderman, S. J.; Claridge, T. D. W.; Anderson, H. L. *Angew. Chem. Int. Ed.* **2002**, *41*, 1769-1772.

(63) Wang, Q.-C.; Qu, D.-H.; Ren, J.; Chen, C.; Tian, H. *Angew. Chem. Int. Ed.* **2004**, *43*, 2661-2665.

(64) Zhao, Y.-L.; Dichtel, W. R.; Trabolsi, A.; Saha, S.; Aprahamian, I.; Stoddart, J. F. *J. Am. Chem. Soc.* **2008**, *130*, 11294-11296.

(65) Khan, A. R.; Forgo, P.; Stine, K. J.; D'Souza, V. T. *Chem. Rev.* **1998**, *98*, 1977-1996.

(66)   Tian, S.; Zhu, H.; Forgo, P.; D'Souza, V. T. *J. Org. Chem.* **2000**, *65*, 2624-2630.

(67)   Engeldinger, E.; Armspach, D.; Matt, D. *Chem. Rev.* **2003**, *103*, 4147-4174.

(68)   Ueno, A.; Moriwaki, F.; Osa, T.; Hamada, F.; Murai, K. *J. Am. Chem. Soc.* **1988**, *110*, 4323-4328.

(69)   Tong, L.-H.; Hou, Z.-J.; Inoue, Y.; Tai, A. *J. Chem. Soc., Perkin Trans. 2* **1992**, 1253-1257.

(70)   Bugler, J.; Sommerdijk, N. A. J. M.; Visser, A. J. W. G.; van Hoek, A.; Nolte, R. J. M.; Engbersen, J. F. J.; Reinhoudt, D. N. *J. Am. Chem. Soc.* **1999**, *121*, 28-33.

(71)   McAlpine, S. R.; Garcia-Garibay, M. A. *J. Am. Chem. Soc.* **1998**, *120*, 4269-4275.

(72)   Mirzoian, A.; Kaifer, A. E. *Chem. Commun.* **1999**, 1603-1604.

(73)   Fujimoto, T.; Sakata, Y.; Kaneda, T. *Chem. Commun.* **2000**, 2143-2144.

(74)   Hoshino, T.; Miyauchi, M.; Kawaguchi, Y.; Yamaguchi, H.; Harada, A. *J. Am. Chem. Soc.* **2000**, *122*, 9876-9877.

(75)   Fujimoto, T.; Nakamura, A.; Inoue, Y.; Sakata, Y.; Kaneda, T. *Tetrahedron Lett.* **2001**, *42*, 7987-7989.

(76)   Onagi, H.; Easton, C. J.; Lincoln, S. F. *Org. Lett.* **2001**, *3*, 1041-1044.

(77)   Liu, Y.; Fan, Z.; Zhang, H.-Y.; Diao, C.-H. *Org. Lett.* **2003**, *5*, 251-254.

(78)   Miyauchi, M.; Takashima, Y.; Yamaguchi, H.; Harada, A. *J. Am. Chem. Soc.* **2005**, *127*, 2984-2989.

(79)   Zhang, J. Honours Thesis, The Australian National University, 2008.

(80)   Ueno, A.; Tomita, Y.; Osa, T. *J. Chem. Soc., Chem. Commun.* **1983**, 976-977.

(81)   Ueno, A.; Minato, S.; Suzuki, I.; Fukushima, M.; Ohkubo, M.; Osa, T.; Hamada, F.; Murai, K. *Chem. Lett.* **1990**, *19*, 605-608.

(82)   Ueno, A.; Kuwabara, T.; Nakamura, A.; Toda, F. *Nature* **1992**, *356*, 136-137.

(83)   Hamasaki, K.; Ikeda, H.; Nakamura, A.; Ueno, A.; Toda, F.; Suzuki, I.; Osa, T. *J. Am. Chem. Soc.* **1993**, *115*, 5035-5040.

(84)   Wang, Y.; Ikeda, T.; Ikeda, H.; Ueno, A.; Toda, F. *Bull. Chem. Soc. Jpn.* **1994**, *67*, 1598-1607.

(85)   McAlpine, S. R.; Garcia-Garibay, M. A. *J. Am. Chem. Soc.* **1996**, *118*, 2750-2751.

(86)   Inoue, Y.; Wada, T.; Sugahara, N.; Yamamoto, K.; Kimura, K.; Tong, L.-H.; Gao, X.-M.; Hou, Z.-J.; Liu, Y. *J. Org. Chem.* **2000**, *65*, 8041-8050.

(87)   Fukuhara, G.; Fujimoto, T.; Kaneda, T. *Chem. Lett.* **2003**, *32*, 536-537.

(88)   Park, J. W.; Lee, S. Y.; Song, H. J.; Park, K. K. *J. Org. Chem.* **2005**, *70*, 9505-9513.

(89)   Inoue, Y.; Miyauchi, M.; Nakajima, H.; Takashima, Y.; Yamaguchi, H.; Harada, A. *J. Am. Chem. Soc.* **2006**, *128*, 8994-8995.

(90)   Inoue, Y.; Kuad, P.; Okumura, Y.; Takashima, Y.; Yamaguchi, H.; Harada, A. *J. Am. Chem. Soc.* **2007**, *129*, 6396-6397.

(91)   Ke, C.; Yang, C.; Mori, T.; Wada, T.; Liu, Y.; Inoue, Y. *Angew. Chem. Int. Ed.* **2009**, *48*, 6675-6677.

(92)   Kawanami, Y.; Pace, T. C. S.; Mizoguchi, J.-i.; Yanagi, T.; Nishijima, M.; Mori, T.; Wada, T.; Bohne, C.; Inoue, Y. *J. Org. Chem.* **2009**, *74*, 7908-7921.

(93)   Harada, A. *Acc. Chem. Res.* **2001**, *34*, 456-464.

(94)   Pauling, L. *The Nature of the Chemical Bond*; Cornell University Press: N. Y., 1948.

(95)   Gardner, R. R.; McKay, S. L.; Gellman, S. H. *Org. Lett.* **2000**, *2*, 2335-2338.

(96)   Thomas, K. M.; Naduthambi, D.; Zondlo, N. J. *J. Am. Chem. Soc.* **2006**, *128*, 2216-2217.

(97)   Jiménez, M. C.; Dietrich-Buchecker, C.; Sauvage, J.-P.; De Cian, A. *Angew. Chem. Int. Ed.* **2000**, *39*, 1295-1298.

(98)   Ashton, P. R.; Baxter, I.; Cantrill, S. J.; Fyfe, M. C. T.; Glink, P. T.; Stoddart, J. F.; White, A. J. P.; Williams, D. J. *Angew. Chem. Int. Ed.* **1998**, *37*, 1294-1297.

(99)   Ashton, P. R.; Parsons, I. W.; Raymo, F. M.; Stoddart, J. F.; White, A. J. P.; Williams, D. J. *Angew. Chem. Int. Ed.* **1998**, *37*, 1913-1916.

(100) Corradini, R.; Dossena, A.; Marchelli, R.; Panagia, A.; Sartor, G.; Saviano, M.; Lombardi, A.; Pavone, V. *Chem. Eur. J.* **1996**, *2*, 373-381.

(101) Corradini, R.; Dossena, A.; Galaverna, G.; Marchelli, R.; Panagia, A.; Sartor, G. *J. Org. Chem.* **1997**, *62*, 6283-6289.

(102) Takahashi, K.; Imotani, K.; Kitsuta, M. *Polym. J.* **2001**, *33*, 242-247.

(103) Yamada, T.; Fukuhara, G.; Kaneda, T. *Chem. Lett.* **2003**, *32*, 534-535.

(104) Miyauchi, M.; Harada, A. *J. Am. Chem. Soc.* **2004**, *126*, 11418-11419.

(105) Coulston, R. J.; Onagi, H.; Lincoln, S. F.; Easton, C. J. *J. Am. Chem. Soc.* **2006**, *128*, 14750-14751.

(106) Brown, S. E.; Coates, J. H.; Coghlan, D. R.; Easton, C. J.; Vaneyk, S. J.; Janowski, W.; Lepore, A.; Lincoln, S. F.; Luo, Y.; May, B. L.; Schiesser, D. S.; Wang, P.; Williams, M. L. *Aust. J. Chem.* **1993**, *46*, 953-958.

(107) Byun, H. S.; Zhong, N.; Bittman, R. *Org. Synth.* **2000**, *77*, 220-224.

(108) Yamamura, H.; Iida, D.; Araki, S.; Kobayashi, K.; Katakai, R.; Kano, K.; Kawai, M. *J. Chem. Soc., Perkin Trans. 1* **1999**, 3111-3115.

(109) Silverstein, R. M.; Webster, F. X.; Kiemle, D. *J. Spectrometric identification of organic compounds*; 7th ed.; John Wiley & Sons: Danvers, 2005.

(110) Schneider, H.-J.; Hacket, F.; Rudiger, V.; Ikeda, H. *Chem. Rev.* **1998**, *98*, 1755-1785.

(111) Easton, C. J.; Lincoln, S. F. *Modified Cylodextrins: Scaffolds and Templates for Supramolecular Chemistry*; Imperial College Press: London, 1999.

(112) Lewis, F. D.; Oxman, J. D.; Gibson, L. L.; Hampsch, H. L.; Quillen, S. L. *J. Am. Chem. Soc.* **1986**, *108*, 3005-3015.

(113) Demirdoven, N.; Deutch, J. *Science* **2004**, *305*, 974-976.

(114) Inoue, Y.; Yamamoto, K.; Wada, T.; Everitt, S.; Gao, X.-M.; Hou, Z.-J.; Tong, L.-H.; Jiang, S.-K.; Wu, H.-M. *J. Chem. Soc., Perkin Trans. 2* **1998**, *8*, 1807-1816.

(115) Rekharsky, M. V.; Inoue, Y. *J. Am. Chem. Soc.* **2002**, *124*, 12361-12371.

(116) Turnbull, W. B.; Daranas, A. H. *J. Am. Chem. Soc.* **2003**, *125*, 14859-14866.

(117) Cromwell, W. C.; Bystrom, K.; Eftink, M. R. *J. Phys. Chem.* **1985**, *89*, 326-332.

(118) Zhang, B.; Breslow, R. *J. Am. Chem. Soc.* **1993**, *115*, 9353-9354.

(119) Houk, K. N.; Leach, A. G.; Kim, S. P.; Zhang, X. *Angew. Chem. Int. Ed.* **2003**, *42*, 4872-4897.

(120) Harrison, J. C.; Eftink, M. R. *Biopolymers* **1982**, *21*, 1153-1166.

(121) Micheau, J.-C.; Zhao, J. *J. Phys. Org. Chem.* **2007**, *20*, 810-820.

(122) Rekharsky, M.; Inoue, Y. *J. Am. Chem. Soc.* **2000**, *122*, 4418-4435.

(123) Gololobov, Y. G.; Zhmurova, I. N.; Kasukhin, L. F. *Tetrahedron* **1981**, *37*, 437-472.

(124) Vaultier, M.; Knouzi, N.; Carrié, R. *Tetrahedron Lett.* **1983**, *24*, 763-764.

(125) Claridge, T. D. W.; Davies, S. G.; Polywka, M. E. C.; Roberts, P. M.; Russell, A. J.; Savory, E. D.; Smith, A. D. *Org. Lett.* **2008**, *10*, 5433-5436.

(126) Bain, A. D. *Prog. Nucl. Magn. Reson. Spectrosc.* **2003**, *43*, 63-103.

(127) Yamauchi, K.; Takashima, Y.; Hashidzume, A.; Yamaguchi, H.; Harada, A. *J. Am. Chem. Soc.* **2008**, *130*, 5024-5025.

(128) Arnaud, A.; Bouteiller, L. *Langmuir* **2004**, *20*, 6858-6863.

(129) Czypionka, A.; Ruiz de los Panos, O.; Mateu, M. G.; Barrera, F. N.; Hurtado-Gomez, E.; Gomez, J.; Vidal, M.; Neira, J. L. *Biochemistry* **2007**, *46*, 12764-12776.

(130) Burrows, S. D.; Doyle, M. L.; Murphy, K. P.; Franklin, S. G.; White, J. R.; Brooks, I.; McNulty, D. E.; Scott, M. O.; Knutson, J. R. *Biochemistry* **1994**, *33*, 12741-12745.

(131) Harada, A.; Kawaguchi, Y.; Hoshino, T. *J. Incl. Phenom. Macrocycl. Chem.* **2001**, *41*, 115-121.

(132) Park, J. W.; Choi, N. H.; Kim, J. H. *J. Phys. Chem.* **1996**, *100*, 769-774.

(133) Fujimoto, T.; Uejima, Y.; Imaki, H.; Kawarabayashi, N.; Jung, J. H.; Sakata, Y.; Kaneda, T. *Chem. Lett.* **2000**, *29*, 564-565.

(134) Fujimoto, T.; Sakata, Y.; Kaneda, T. *Chem. Lett.* **2000**, *29*, 764-765.

(135) Nishimura, D.; Oshikiri, T.; Takashima, Y.; Hashidzume, A.; Yamaguchi, H.; Harada, A. *J. Org. Chem.* **2008**, *73*, 2496-2502.

(136) Eftink, M. R.; Andy, M. L.; Bystrom, K.; Perlmutter, H. D.; Kristol, D. S. *J. Am. Chem. Soc.* **1989**, *111*, 6765-6772.

(137) Bastos, M.; Briggner, L. E.; Shehatta, I.; Wadso, I. *J. Chem. Thermodynamics* **1990**, *22*, 1181-1190.

(138) Waldeck, D. H. *Chem. Rev.* **1991**, *91*, 415-436.

(139) Leung, K. C.-F.; Chak, C.-P.; Lo, C.-M.; Wong, W.-Y.; Xuan, S.; Cheng, C. H. K. *Chem. Asian J.* **2009**, *4*, 364-381.

(140) Yamasaki, R.; Tanatani, A.; Azumaya, I.; Saito, S.; Yamaguchi, K.; Kagechika, H. *Org. Lett.* **2003**, *5*, 1265-1267.

(141) Alcalde, M. A.; Gancedo, C.; Jover, A.; Carrazana, J.; Soto, V. H.; Meijide, F.; Tato, J. V. *J. Phys. Chem. B* **2006**, *110*, 13399-13404.

(142) Liu, Y.; You, C.-C.; He, S.; Chen, G.-S.; Zhao, Y.-L. *J. Chem. Soc., Perkin Trans. 2* **2002**, 463-469.

(143) Lu, Q.; Wang, D.-S.; Chen, C.-S.; Hu, Y.-D.; Chen, C.-S. *J. Med. Chem.* **2005**, *48*, 5530-5535.

(144) Gibbs, R. A.; Benkovic, P. A.; Janda, K. D.; Lerner, R. A.; Benkovic, S. J. *J. Am. Chem. Soc.* **1992**, *114*, 3528-3534.

(145) Perrin, D. D. *Dissociation Constants of Organic Bases in Aqueous Solution: Supplement 1972*; Butterworth: London, 1972.

(146) Grunwald, E.; Loewenstein, A.; Meiboom, S. *J. Chem. Phys.* **1957**, *27*, 641-642.

(147) Gelb, R. I.; Schwartz, L. M. *J. Incl. Phenom. Macrocycl. Chem.* **1989**, *7*, 537-543.

(148) Pham, D.-T.; Clements, P.; Easton, C. J.; Papageorgiou, J.; May, B. L.; Lincoln, S. F. *New J. Chem.* **2008**, *32*, 712-718.

(149) Carrazana, J.; Jover, A.; Meijide, F.; Soto, V. H.; Tato, J. V. *J. Phys. Chem. B* **2005**, *109*, 9719-9726.

(150) Fersht, A. R.; Shi, J.-P.; Knill-Jones, J.; Lowe, D. M.; Wilkinson, A. J.; Blow, D. M.; Brick, P.; Carter, P.; Waye, M. M. Y.; Winter, G. *Nature* **1985**, *314*, 235-238.

(151) Sheu, S.-Y.; Yang, D.-Y.; Selzle, H. L.; Schlag, E. W. *Proc. Natl Acad. Sci. USA* **2003**, *100*, 12683-12687.

(152) Madhavan, M.; Robert, E. C.; Gin, M. S. *Angew. Chem. Int. Ed.* **2005**, *44*, 7584-7587.

(153) Díaz-Moscoso, A.; Le Gourriérec, L.; Gómez-García, M.; Benito, J. M.; Balbuena, P.; Ortega-Caballero, F.; Guilloteau, N.; Di Giorgio, C.; Vierling, P.; Defaye, J.; Ortiz Melletm, C.; García Fernández, J. M. *Chem. Eur. J.* **2009**, Article online in advance of print.

(154) Wu, H.-C.; Astier, Y.; Maglia, G.; Mikhailova, E.; Bayley, H. *J. Am. Chem. Soc.* **2007**, *129*, 16142-16148.

(155) Godinez, L. A.; Schwartz, L.; Criss, C. M.; Kaifer, A. E. *J. Phys. Chem. B* **1997**, *101*, 3376-3380.

(156) Rupe, H. *Liebigs Ann. Chem.* **1909**, *369*, 311.

(157) Melton, L. D.; Slessor, K. N. *Carbohyd. Res.* **1971**, *18*, 29-37.

Appendix
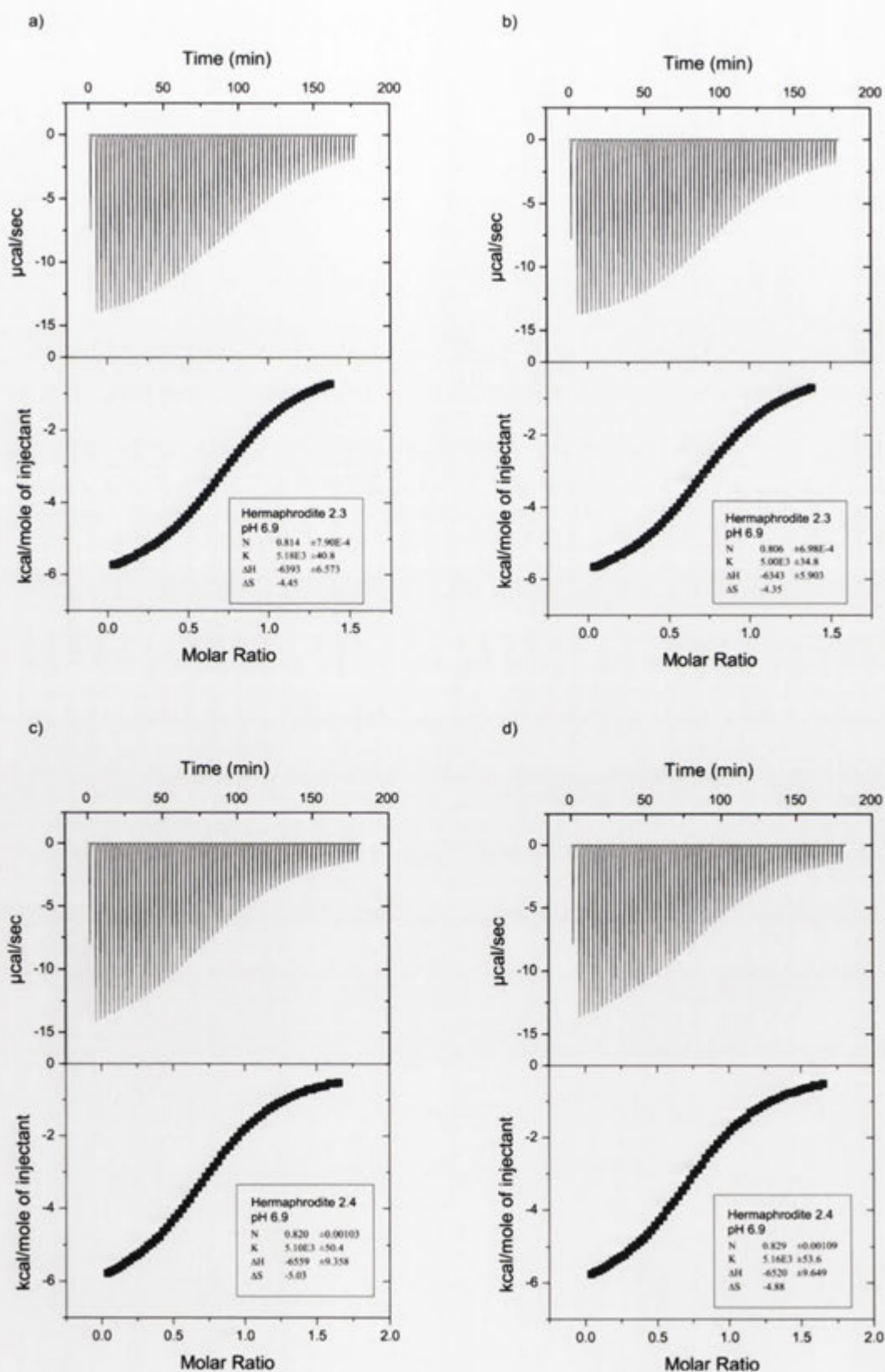
Appendix 1.1. ITC thermograms for 60 successive injections (5 µl) of 1-adamantanecarboxylate (13.28 mM) in 0.05 M NaH_2PO_4/Na_2HPO_4 buffer (pH 6.9) at 25 °C into cells containing (a,b) hermaphrodite **2.3** (2.16 mM); (c,d) hermaphrodite **2.4** (1.84 mM).
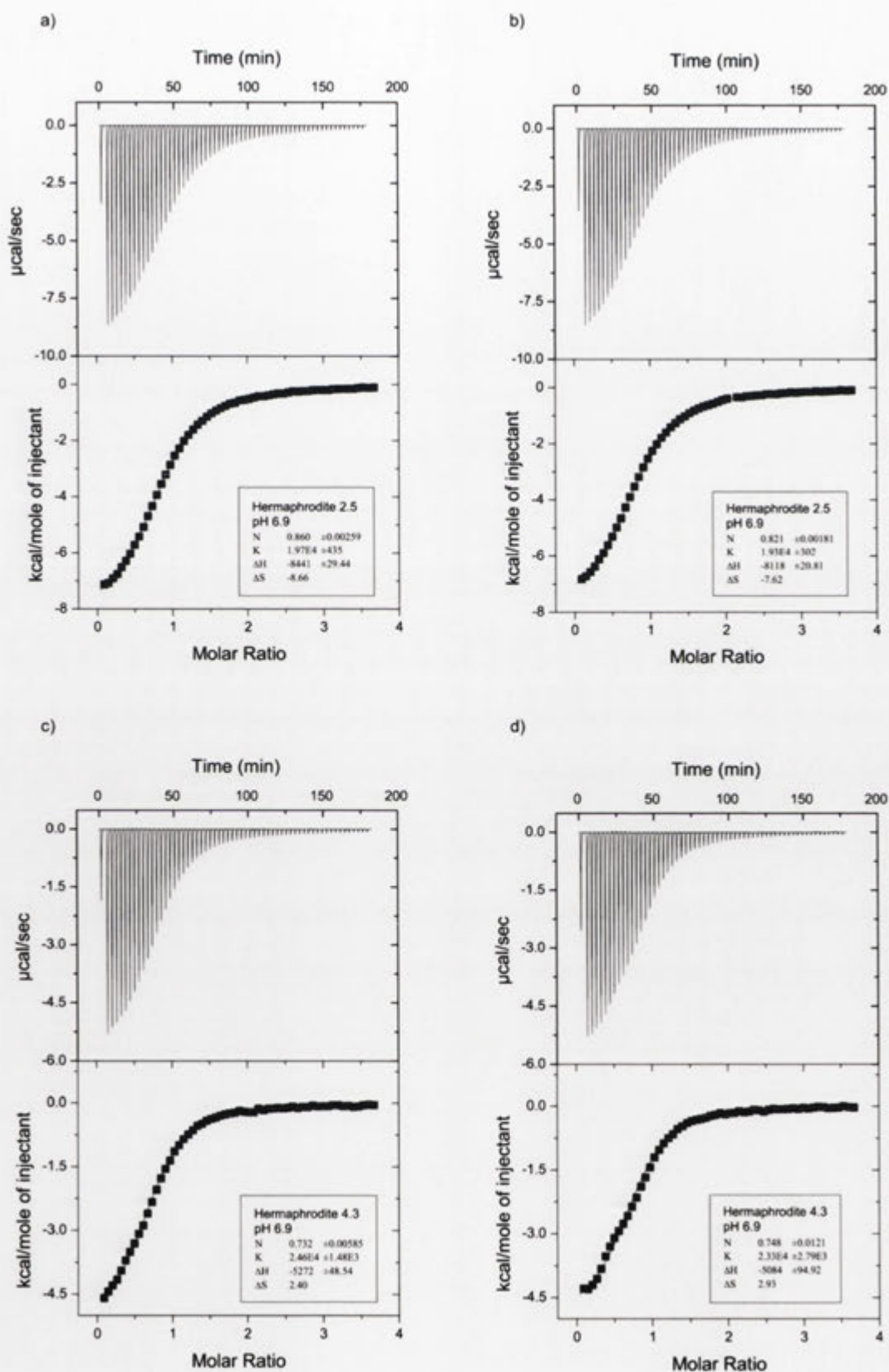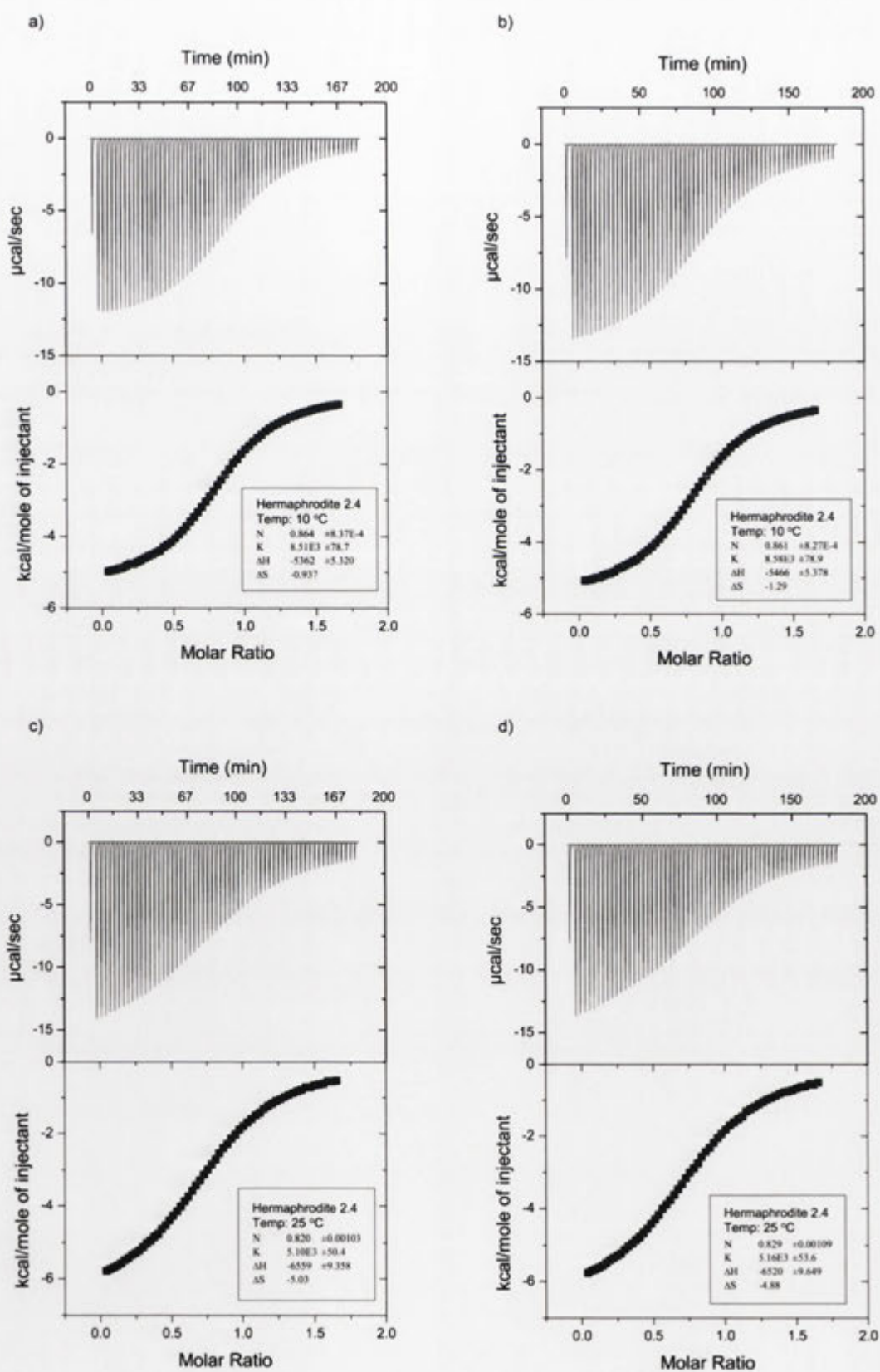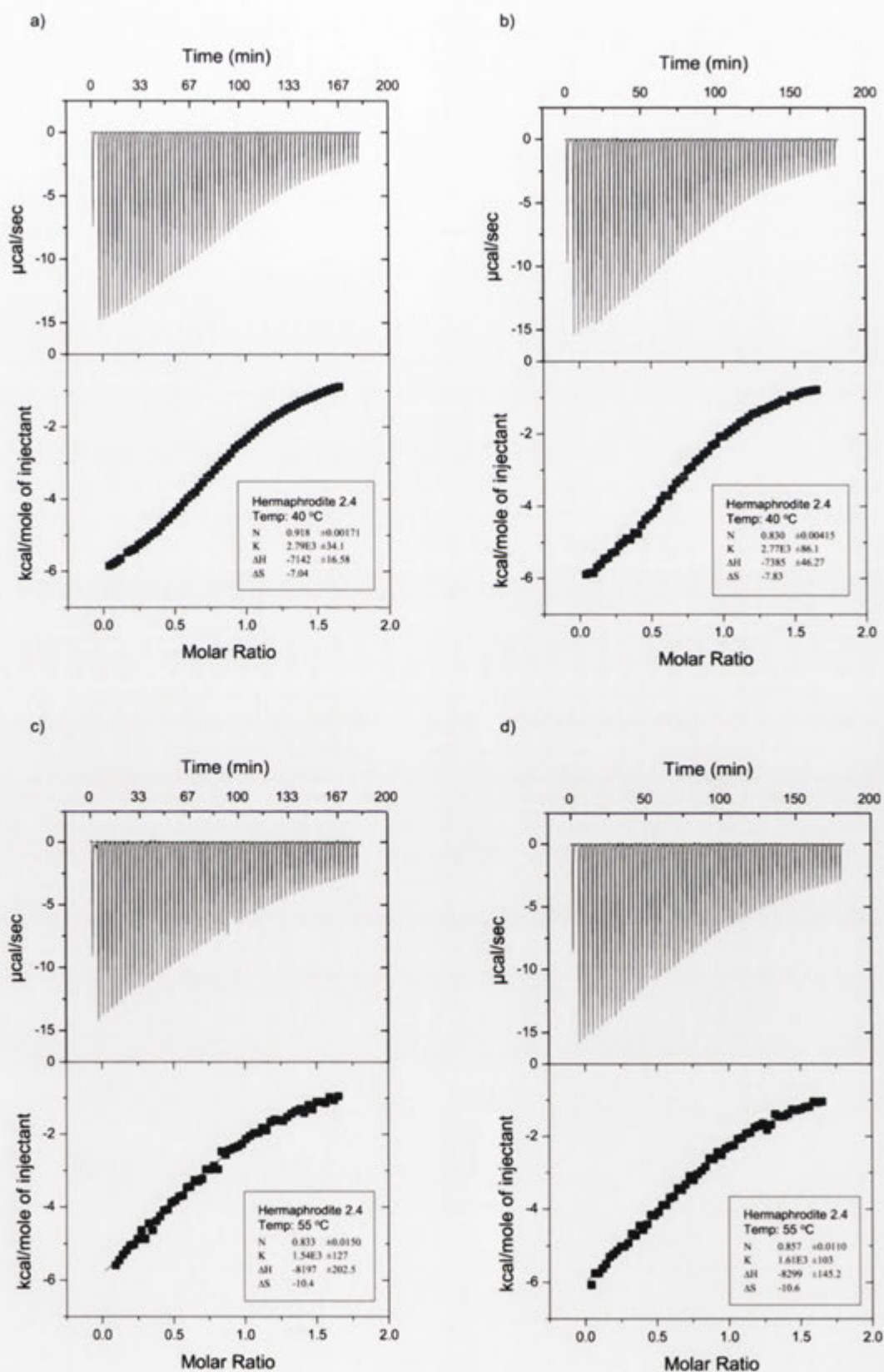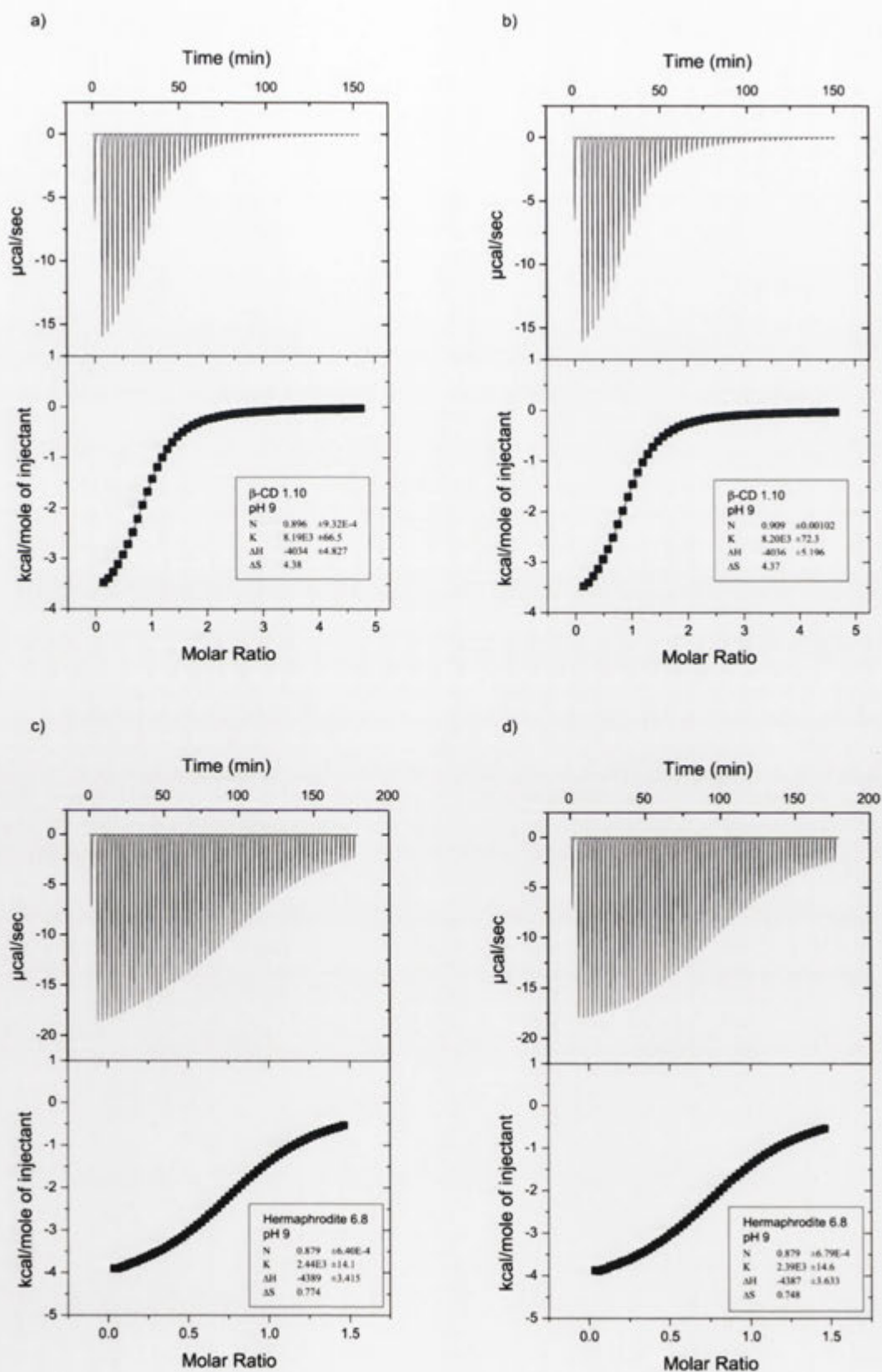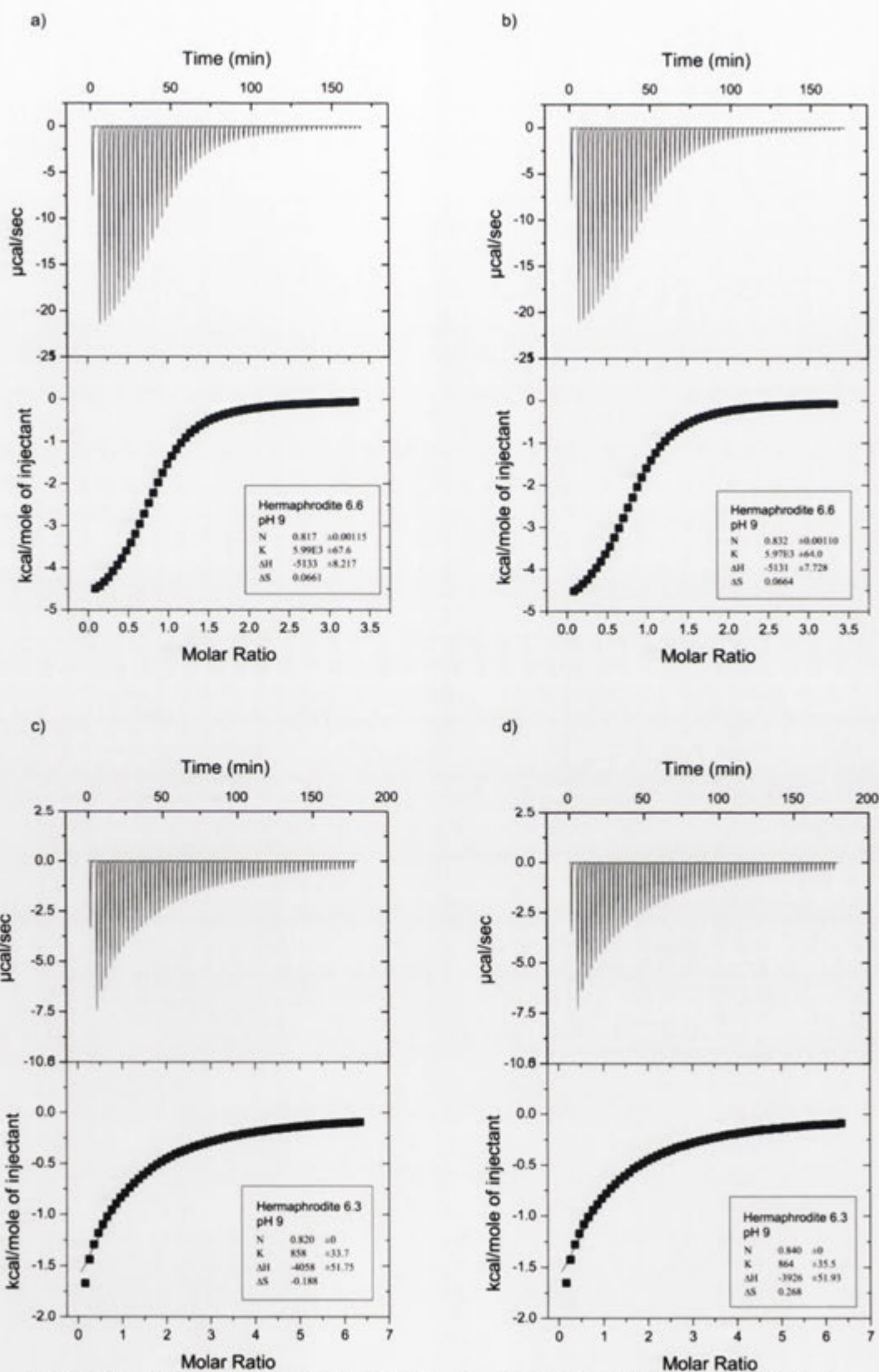
Appendix 1.2. ITC thermograms for 60 successive injections (5 μl) of 1-adamantanecarboxylate (6.5 mM) in 0.05 M NaH_2PO_4/Na_2HPO_4 buffer (pH 6.9) at 25 °C into cells containing (a,b) hermaphrodite **2.5** (0.40 mM); (c,d) hermaphrodite **4.3** (0.40 mM).
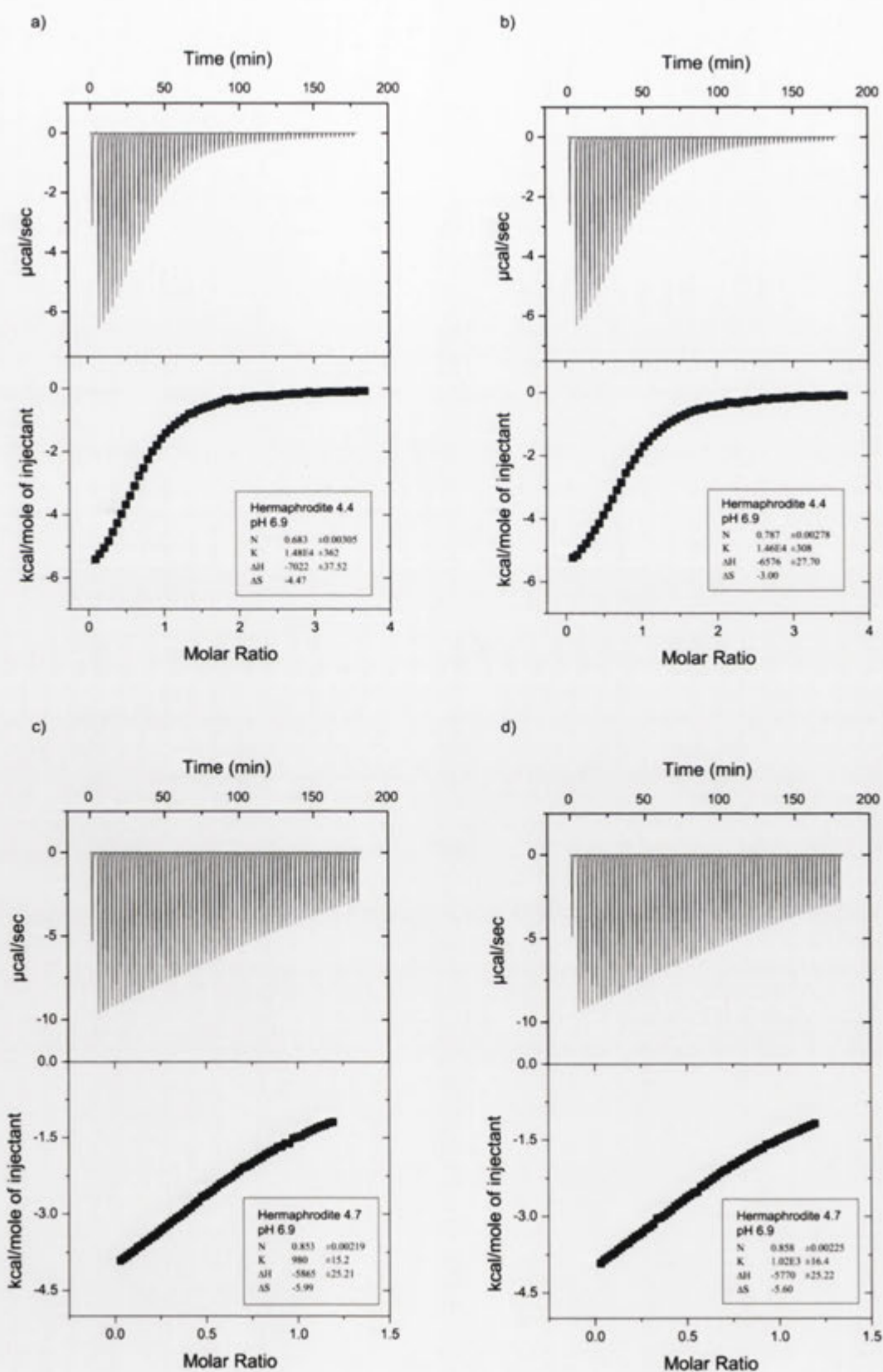
Appendix 1.3. ITC thermograms for 60 successive injections (5 µl) of 1-adamantanecarboxylate (6.5 mM a,b or 13.28 mM c,d) in 0.05 M NaH$_2$PO$_4$/Na$_2$HPO$_4$ buffer (pH 6.9) at 25 °C into cells containing (a,b) hermaphrodite **4.4** (0.40 mM); (c,d) hermaphrodite **4.7** (2.50 mM).

a)

b)
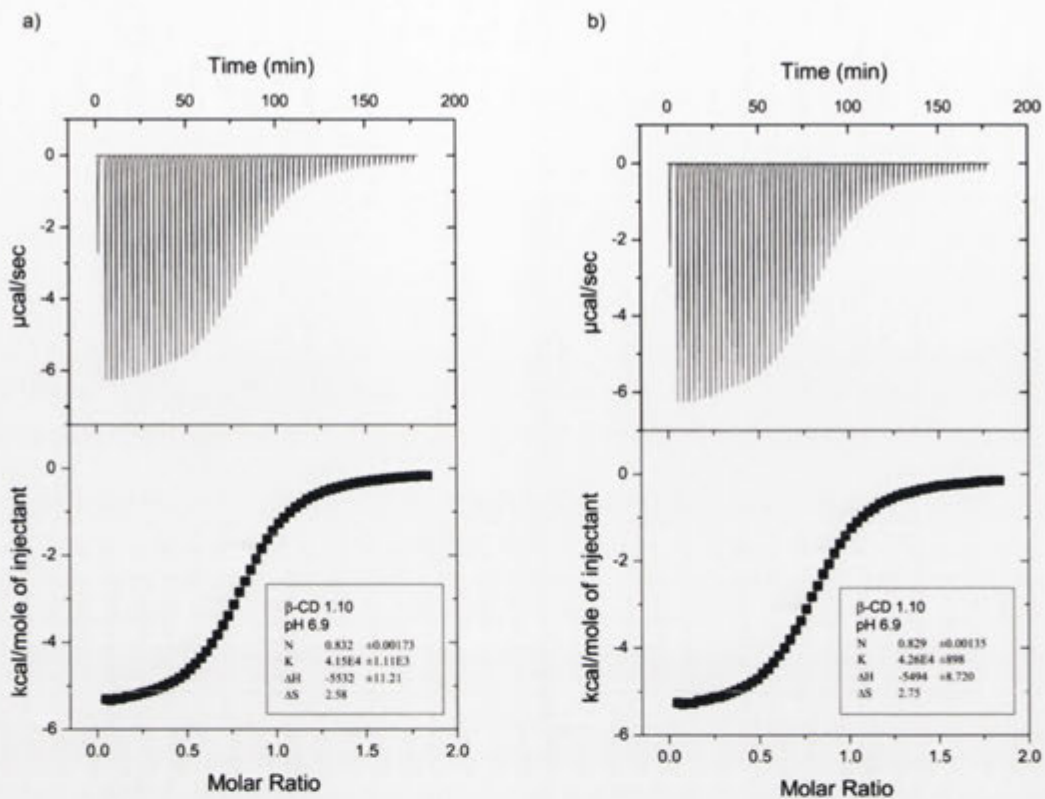
Appendix 1.4. ITC thermograms for 60 successive injections (5 µl) of 1-adamantanecarboxylate (6.5 mM) in 0.05 M NaH₂PO₄/Na₂HPO₄ buffer (pH 6.9) at 25 °C into cells containing (a,b) β-CD **1.10** (0.795 mM).

213

Appendix 1.5. ITC thermograms for 60 successive injections (5 µl) of 1-adamantanecarboxylate (13.28 mM) in 0.05 M NaH$_2$PO$_4$/Na$_2$HPO$_4$ buffer (pH 6.9) into cells containing hermaphrodite **2.4** (1.84 mM) (a,b) 10 °C; (c,d) 25 °C

Appendix 1.6. ITC thermograms for 60 successive injections (5 µl) of 1-adamantanecarboxylate (13.28 mM) in 0.05 M NaH_2PO_4/Na_2HPO_4 buffer (pH 6.9) into cells containing hermaphrodite **2.4** (1.84 mM) (a,b) 40 °C; (c,d) 55 °C

a)

b)

c)

d)

Appendix 1.7. ITC enthalpograms for 60 successive injections (5 µl) of 1-aminoadamantane.hydrochloride (26 mM) in 0.05 M $Na_2B_4O_7 \cdot 10H_2O$ buffer (pH 9) at 25 °C into cells containing (a,b) β–CD **1.10** (1.05 mM); (c,d) hermaphrodite **6.8** (4.0 mM).

Appendix 1.8. ITC enthalpograms for 60 successive injections (5 µl) of 1-aminoadamantane.hydrochloride (26 mM) in 0.05 M $Na_2B_4O_7 \cdot 10H_2O$ buffer (pH 9) at 25 °C into cells containing (a,b) hermaphrodite **6.6** (1.66 mM); (c,d) hermaphrodite **6.3** (1.84 mM).
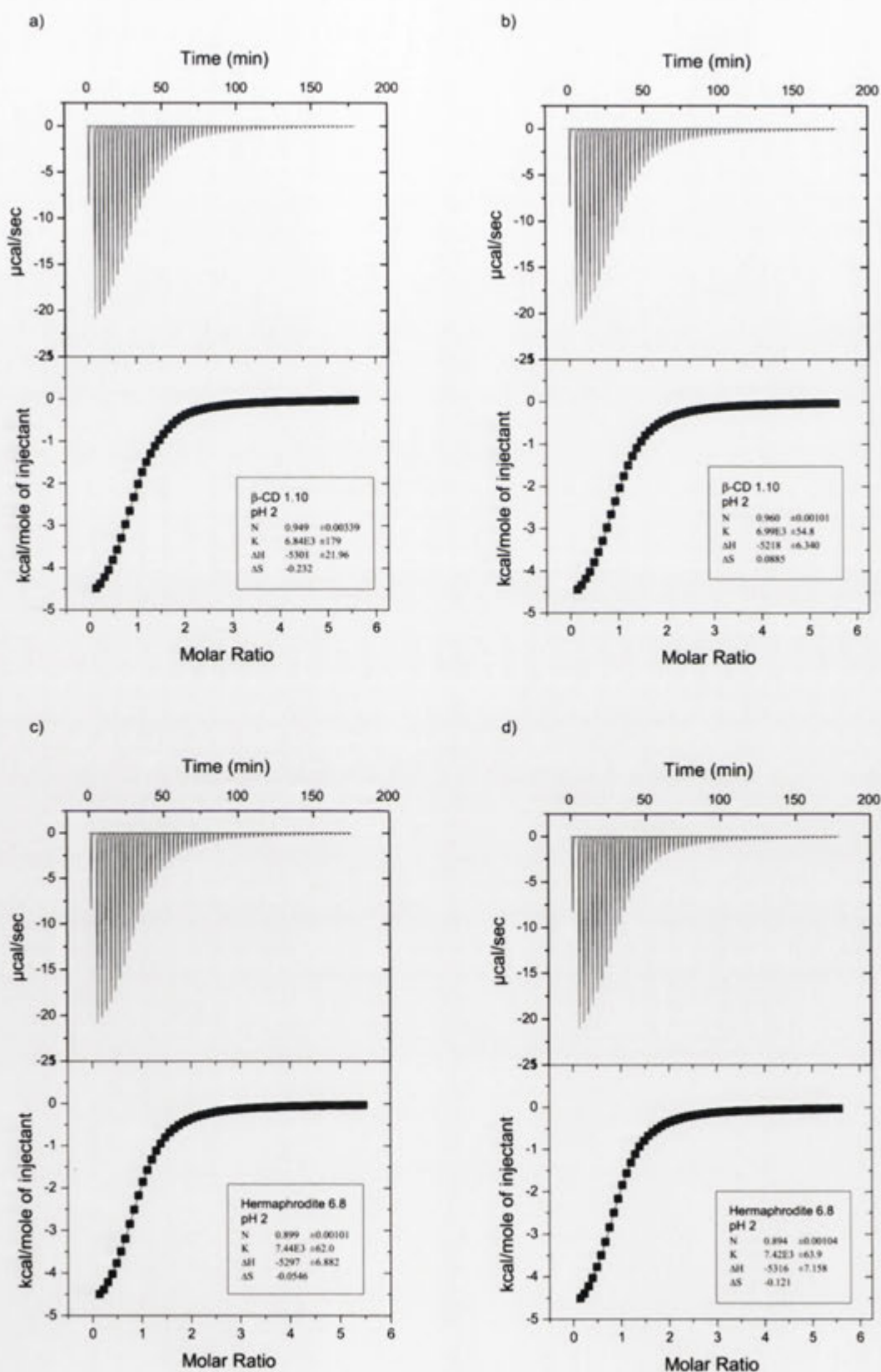
Appendix 1.9. ITC enthalpograms for 60 successive injections (5 µl) of 1-aminoadamantane.hydrochloride (26 mM) in 0.05 M NaH_2PO_4 buffer (pH 2) at 25 °C into cells containing (a,b) β-CD **1.10** (1.05 mM); (c,d) hermaphrodite **6.8** (1.05 mM).
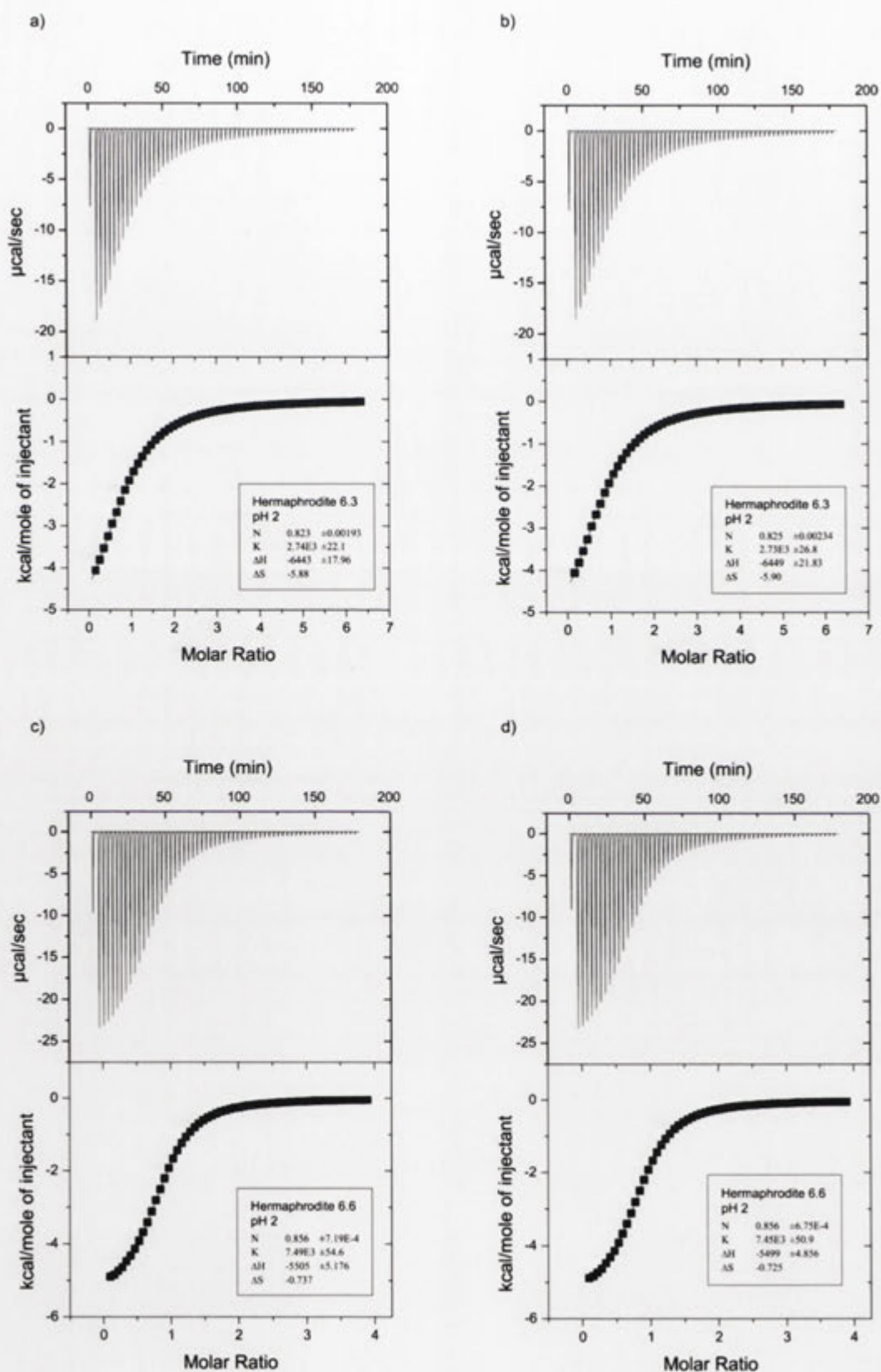
Appendix 1.10. ITC enthalpograms for 60 successive injections (5 µl) of 1-aminoadamantane.hydrochloride (26 mM) in 0.05 M NaH$_2$PO$_4$ buffer (pH 2) at 25 °C into cells containing (a,b) hermaphrodite **6.3** (0.92 mM) (c,d) hermaphrodite **6.6** (1.50 mM).
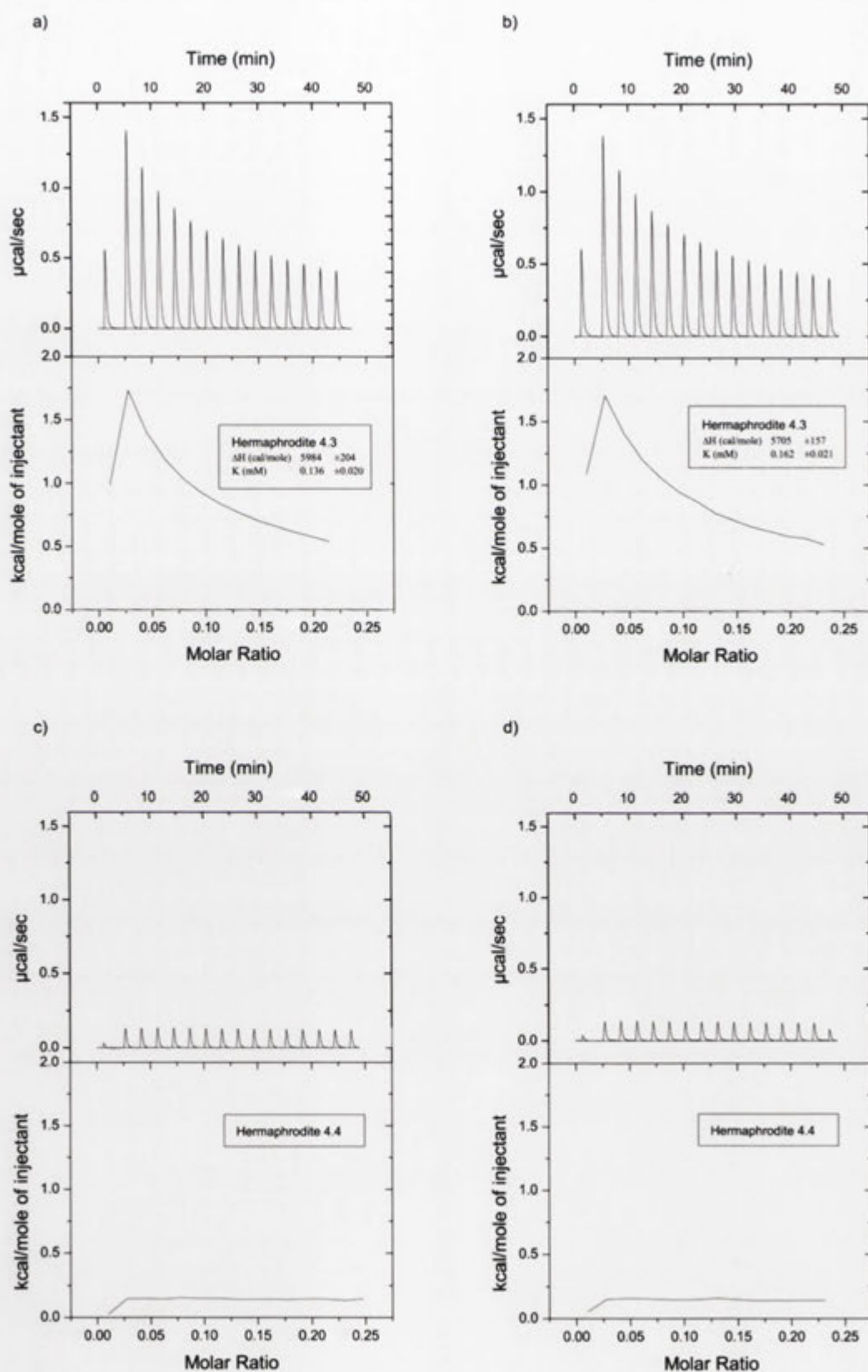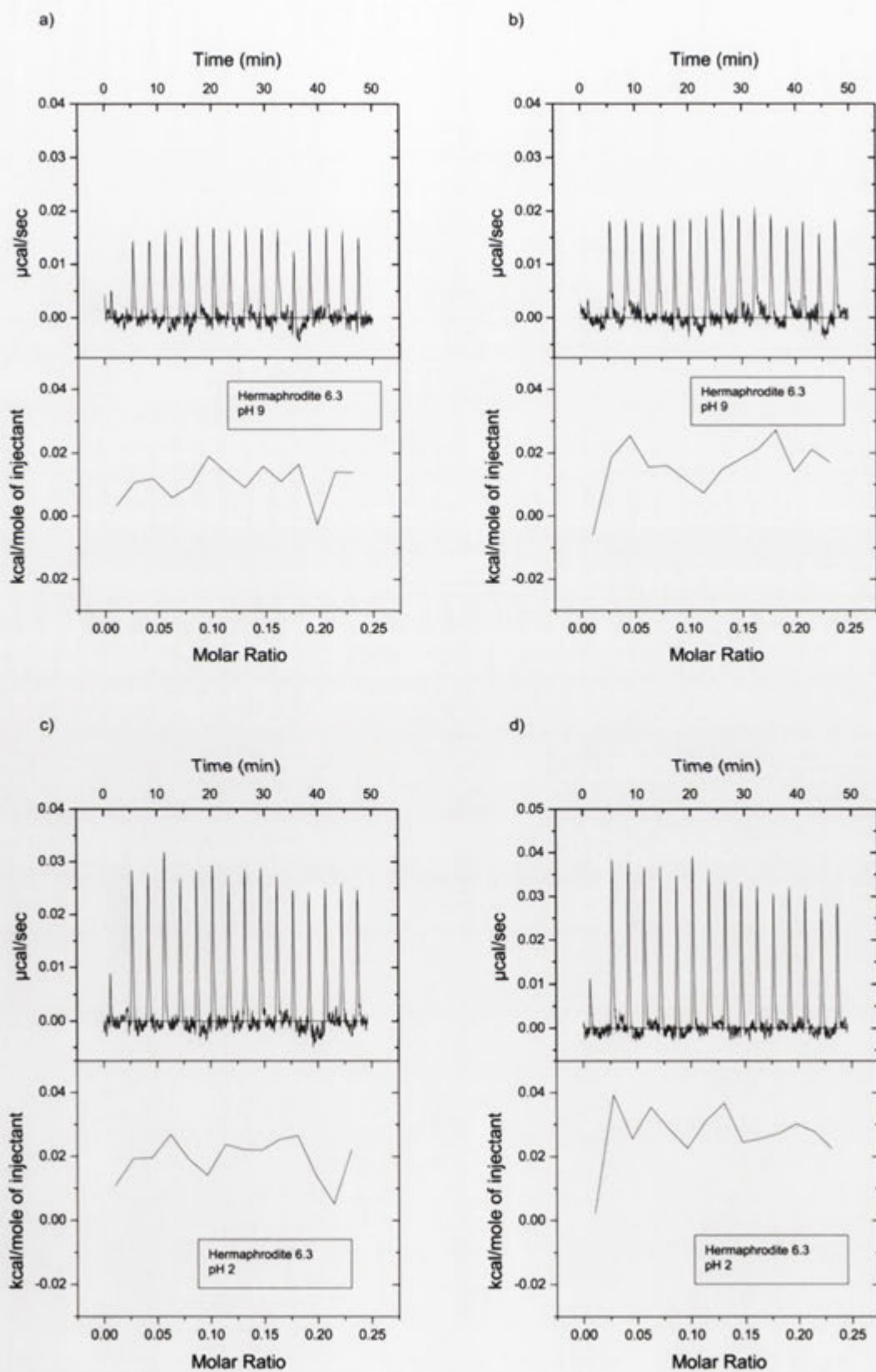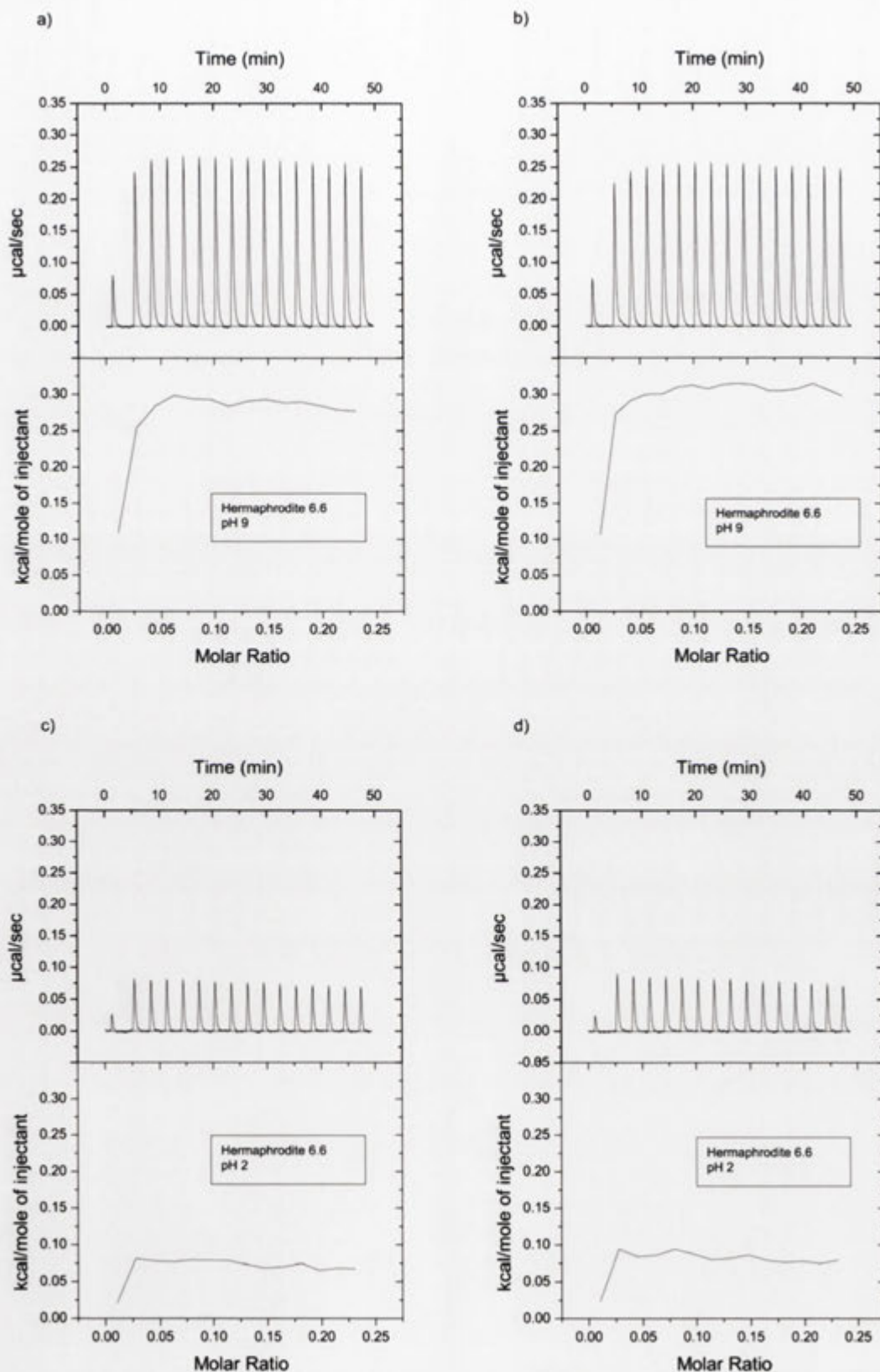
Appendix 1.11. ITC thermograms for 15 successive injections (5 μl) of either the (a,b) hermaphrodite **4.3** (5 mM) or (c,d) hermaphrodite **4.4** (5 mM) in 0.05 M NaH$_2$PO$_4$/Na$_2$HPO$_4$ buffer (pH 6.9) into cells containing identical buffer.
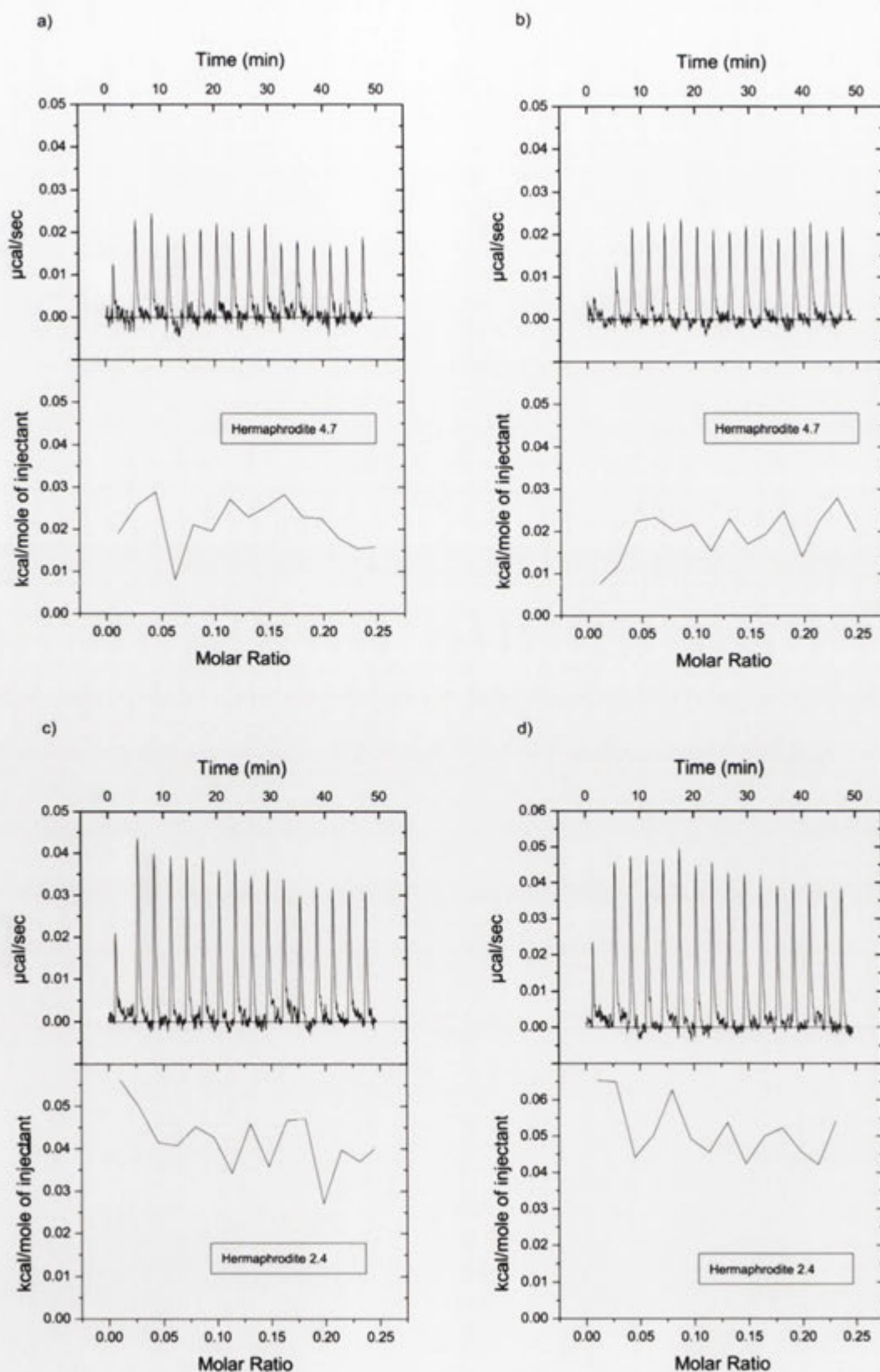
Appendix 1.12. ITC thermograms for 15 successive injections (5 μl) of either the (a,b) hermaphrodite **4.7** (5 mM) or (c,d) hermaphrodite **2.4** (5 mM) in 0.05 M NaH_2PO_4/Na_2HPO_4 buffer (pH 6.9) into cells containing identical buffer.
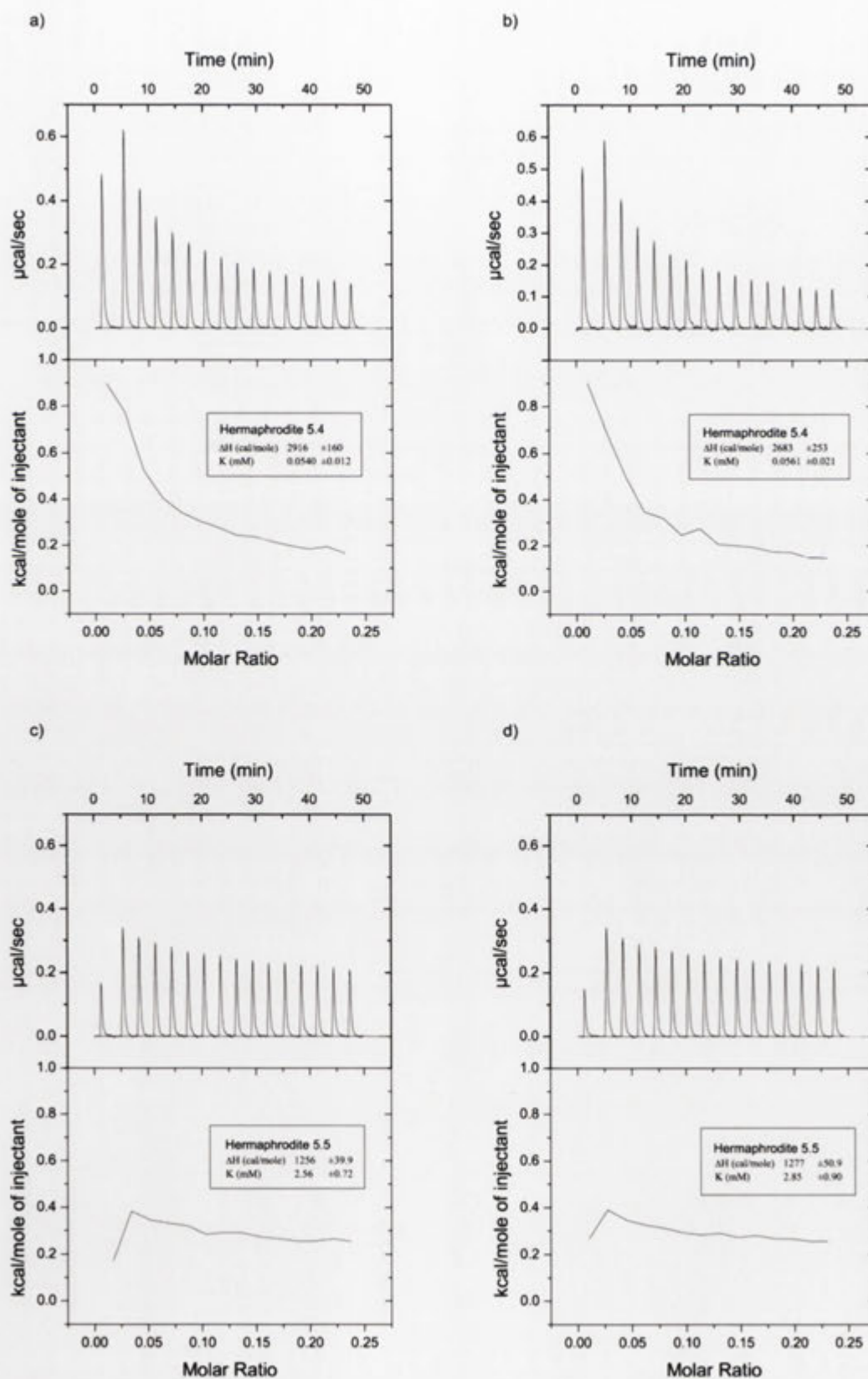
Appendix 1.13. ITC thermograms for 15 successive injections (5 μl) of either the (a,b) hermaphrodite **5.4** (5 mM) or (c,d) hermaphrodite **5.5** (5 mM) in 0.05 M NaH$_2$PO$_4$/Na$_2$HPO$_4$ buffer (pH 6.9) into cells containing identical buffer.
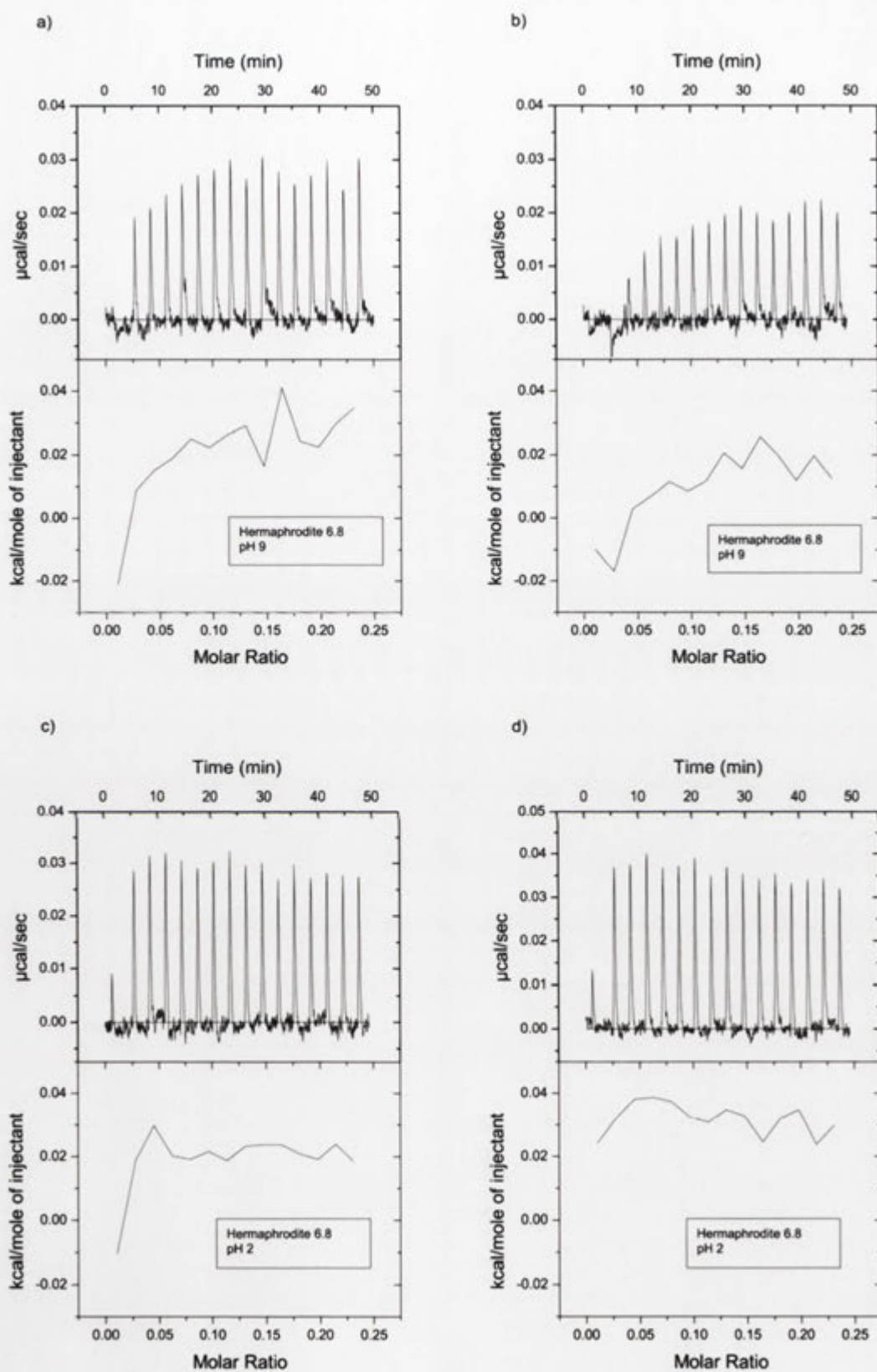
Appendix 1.14. ITC thermograms for 15 successive injections (5 µl) of the hermaphrodite **6.3** (5 mM) at (a,b) pH 9 in 0.05 M $Na_2B_4O_7 \cdot 10H_2O$ buffer or (c,d) pH 2 in 0.05 M NaH_2PO_4 buffer into cells containing identical buffer.

Appendix 1.15. ITC thermograms for 15 successive injections (5 µl) of the hermaphrodite **6.6** (5 mM) at (a,b) pH 9 in 0.05 M $Na_2B_4O_7 \cdot 10H_2O$ buffer or (c,d) pH 2 in 0.05 M NaH_2PO_4 buffer into cells containing identical buffer.

Appendix 1.16. ITC thermograms for 15 successive injections (5 µl) of the hermaphrodite **6.8** (5 mM) at (a,b) pH 9 in 0.05 M $Na_2B_4O_7 \cdot 10H_2O$ buffer or (c,d) pH 2 in 0.05 M NaH_2PO_4 buffer into cells containing identical buffer.